

https://dspace.org/

Statistical modelling of the leaching of Polycrystalline Diamond Compacts (PDCs) for integration into the product design process

Ndlovu, Andrew

2025
University of the Witwatersrand, Johannesburg
https://hdl.handle.net/10539/50049
Ndlovu, Andrew. (2025). Statistical modelling of the leaching of Polycrystalline Diamond Compacts (PDCs) for integration into the product design process. [PhD thesis, University of the Witwatersrand, Johannesburg]. WIReDSpace. https://hdl.handle.net/10539/50049

Downloaded from a DSpace repository. https://dspace.org/

Statistical modelling of the leaching of Polycrystalline Diamond Compacts (PDCs) for integration into the product design process



UNIVERSITY OF THE
WITWATERSRAND,
JOHANNESBURG

Submitted by
Andrew Ndlovu

A thesis submitted thesis submitted to the Faculty of Engineering and the Built Environment, University of the Witwatersrand, Johannesburg, in fulfilment of the requirements for the degree of Doctor of Philosophy

August 2025

Declaration

I hereby declare that the work presented in this thesis has not been submitted for any other degree or professional qualification, and that it is the result of my own independent work.

(Signature of candidate)

Date

Abstract

This thesis investigated the optimisation of the high-pressure high-temperature (HPHT) sintering process for manufacturing polycrystalline diamond compacts (PDCs) with enhanced leachability and performance. A primary focus was the precise control of the key sintering parameters: pressure, temperature and holding time. The research addressed the challenges of accurate parameter measurement under extreme HPHT conditions by developing and validating a novel *in situ* pressure calibration method using a cubic press. The method, based on real-time volume change measurements of the PDC sample and the Murnaghan equation of state, gave improved accuracy and material specificity than conventional fixed-point techniques. Furthermore, the study examined the influence of thermocouple placement on temperature measurement accuracy, demonstrating the critical importance of optimal positioning for reliable temperature monitoring.

The individual and combined effects of pressure, temperature and holding time on PDC leach rate were extensively analysed. Experiments showed that increased pressure significantly reduced leach rate, attributed to enhanced densification, reduced porosity and smaller cobalt pools. Similarly, higher sintering temperatures decreased leachability due to greater densification and altered pore morphology. Holding time also played a role, with longer durations promoting densification and thus reducing leach rate, particularly at lower temperatures. Statistical models, including linear and polynomial regression, were developed and validated to predict leach rate based on individual parameter variations.

To further understand the complex interaction between the sintering parameters, a multiple regression model was developed, revealing a significant interaction between holding time and temperature. Dominance analysis was employed to establish a hierarchy of parameter importance, identifying pressure as the most influential factor in controlling leach rate, followed by temperature, with holding time having a lesser, yet significant, indirect effect. The developed models coupled with the insights into parameter interactions and relative importance provided a comprehensive framework for optimizing the HPHT sintering process of PDCs.

Publications associated with this research

A. Ndlovu, L.A. Cornish, H.S.L. Sithebe, Relationship between sintering pressure and leach rate of polycrystalline diamond compacts (PDCs) using central composite design (CCD) modelling, Int. J. Refract. Hard Met. 124 (2024) 106854.

A. Ndlovu, L.A. Cornish, H.S.L. Sithebe, Investigating the relative importance of the sintering variables of leachability of polycrystalline diamond compacts (PDCs) using the dominance analysis (DA) model, about to be submitted.

A. Ndlovu, L.A. Cornish, H.S.L. Sithebe, Regression Model of Holding Time on Leach Rate of Polycrystalline Diamond Compacts (PDCs) during HPHT Sintering, draft.

A. Ndlovu, L.A. Cornish, H.S.L. Sithebe, Cubic Press Pressure Calibration for Polycrystalline Diamonds (PDCs) Sintering via *in situ* Volume Change and Murnaghan Equation of State, draft.

A. Ndlovu, L.A. Cornish, H.S.L. Sithebe, Effect of Thermocouple Placement on Temperature Measurement in a Cubic Press for Polycrystalline Diamond Compact (PDC) Sintering, draft.

Acknowledgements

The successful completion of this research project was made possible by the invaluable contributions, support, and guidance of numerous individuals and organisations. I would like to express my sincere gratitude to each of them.

Firstly, I am deeply indebted to my supervisor, Professor L.A Cornish, for her insightful supervision, unwavering support and expert guidance throughout this project. Her mentorship has been instrumental in shaping this research.

I extend my sincere thanks to Dr. H.S.L. Sithebe for his invaluable help, suggestions, and for facilitating this project at Element Six (Pty) Ltd - Diamond Research Laboratory.

My deepest appreciation goes to Element Six (Pty) Ltd - Diamond Research Laboratory for their generous financial support and for providing access to their state-of-the-art facilities.

Financial support from the NRF-DSI Centre of Excellence in Strong Materials (CoE-SM) is gratefully acknowledged. Their contribution was crucial for the funding of this research.

Thank you, my family, from the bottom of my heart. During this demanding period, your constant love, support and understanding, and the sacrifices you've made for me, mean the world.

Table of contents

Declaration ..... **i**

Abstract ..... **ii**

Publications associated with this research ..... **iii**

Acknowledgements ..... **iv**

List of figures ..... **v**

List of tables ..... **xiii**

Chapter 1: Introduction **1**

1.1 Background 1

1.2 Problem Statement 2

1.3 Research Questions 3

1.4 Research Objectives 3

1.5 Significance of the Research 4

1.6 Thesis Outline 5

Chapter 2: Literature review **6**

2.1 Introduction 6

2.2 HPHT Sintering of PDCs 6

2.3 Effects of Sintering Parameters on PDC Properties 12

2.3.1 Pressure 12

2.3.2 Temperature 13

2.3.3 Holding time 15

2.3.4 Interactions between Parameters 15

2.3.5 Sintering mechanisms 16

2.4 Leachability of PDCs 19

2.5 Pressure Calibration in High-Pressure Press 26

2.6 Temperature Measurement in HPHT Press 28

2.7 Statistical Modelling 30

2.8 Research Gaps and Justification 35

Chapter 3: Materials and methods 37

3.1 Materials 37

3.2 Sample Preparation 37

3.3 HPHT Sintering 37

3.3.1 Cubic Press 37

3.3.2 Cubic press calibration 38

3.3.3 Temperature Measurement 41

3.3.4 Sintering Parameters 43

3.4 Leaching 43

3.5 Characterisation Techniques 44

3.5.1 Sample Preparation 44

3.5.2 Scanning Electron Microscopy (SEM) 44

3.5.3 X-ray Diffraction (XRD) 45

3.5.4 Image analysis 45

3.5.5 X-ray Tomography (XRT) 45

3.5.6 Wear Testing 46

3.5.7 Density Determination using Geometric Method 46

3.6 Data analysis 47

3.6.1 Multiple Regression Analysis 47

3.6.2 Dominance Analysis (DA) 48

3.6.3 ImageJ Analysis 48

3.6.4 Statistical analysis 49

Chapter 4: Results 50

4.1 Leach rate data 50

4.2 SEM-BSE images of pre-leached samples....53

4.3 SEM-BSE images of leached samples....57

4.4 SEM-BSE images for unleached and leached samples....59

4.5 XRD results....60

4.6 RIR results....60

4.7 XRF results....61

4.8 EDX results....61

4.9 Density measurements results....63

Chapter 5: Challenges and Advances in Accurate Process Parameter Control....64

5.1 *Ex Situ* Pressure Calibration....64

5.1.1 Introduction....64

5.1.2 Methodology....65

5.1.3 Results....65

5.2 Temperature Measurement and the Effect of Thermocouple Placement....68

5.2.1 Introduction....68

5.2.2 Methodology....69

5.2.3 Results....69

Chapter 6: Optimising Leachability by Parameter Control: Individual Effects....74

6.1 Effect of Holding Time on Leach Rate....74

6.1.1 Introduction....74

6.1.2 Methodology....74

6.1.3 Results....74

6.2 Effect of Temperature on Leach Rate....76

6.2.1 Introduction....76

6.2.2 Methodology....76

6.2.3 Results....77

6.3 Effect of Pressure on Leach Rate 78

6.3.1 Introduction 78

6.3.2 Methodology 79

6.3.3 Results 79

Chapter 7: Integrated Parameter Optimization: Interactions and Relative Importance 81

7.1 Multiple Regression Analysis of Sintering Parameters on Leachability 81

7.1.1 Introduction 81

7.1.2 Methodology 81

7.1.3 Results 82

7.2 Dominance Analysis and the Hierarchy of Parameter Importance 88

7.2.1 Introduction 88

7.2.2 Experimental procedure 89

7.2.3 Results 89

Chapter 8: Overall Discussion 93

8.1 Detailed Discussion of Experimental Results 93

8.1.1 Advances in Accurate Process Parameter Control 93

8.1.2 Optimising Leachability by Parameter Control: Individual Effects 106

8.1.3 Integrated Parameter Optimization: Interactions and Relative Importance 125

8.2 Synthesis of Key Findings 141

8.3 Optimisation Strategies and Practical Implications 152

8.4 Limitations 153

8.5 Future Research Directions 154

Chapter 9: Overall Conclusions 156

9.1 Summary of the research 156

9.2 Main Findings and Contributions 156

9.3 Significance and Implications 158

References 159

Appendix A: X-ray tomography images. 174

Appendix B: Published paper 206

Appendix C: Sintering conditions calibration 215

List of figures

Figure 2.1: Diamond powder and WC substrate placed inside the sample assembly [23] 6

Figure 2.2: (a) HPHT press, (b) sample assembly [23] 7

Figure 2.3: Cobalt binder migration [23] 7

Figure 2.4: SEM-BSE image showing diamond-to-diamond bonding in PDC, showing cobalt pools (medium grey contrast), diamond (dark contrast) and tungsten carbide (light grey contrast) [28] 8

Figure 2.5: Sintering map for a cobalt based PDC [148] 10

Figure 2.6: Sintering mechanisms for joining of two particles [32] 16

Figure 2.7: TEM micrographs showing: (a) stacking faults; (b) micro-twinning and (c) low dislocation density of diamond intergrowth [145] 18

Figure 2.8: TEM image showing degraded cobalt pools after exposure to 700 °C for 2 h, with graphite outlined by red circles [28] 20

Figure 2.9: SEM-SE images of heat treted PDC at 900°C showing: (a) Co distribution, (b) micro-cracking, (c) Co_3O_4 confirmed by (d) EDX analysis of cobalt [61] 22

Figure 2.10 Wear behaviour for leached and non-leached PDCs subjected to a VTL test [66] 24

Figure 3.1: A cubic press capsule [22] 38

Figure 3.2: Schematic diagram of the sample assembly in the capsule with an S-type thermocouple inserted into the drilled hole on the side of the capsule 42

Figure 3.3: Leaching images showing: (a) X-ray tomography image of a leached sample and (b) Scanning electron microscope (SEM) image of the measured leached layer [13] 44

Figure 3.4: Typical image of a wear scar of the PDC after VTL test for the experimental run conditions: 5 GPa, 1500°C and 25 minutes 46
Figure 4.1: SEM-BSE images showing the effect of sintering variables on the microstructures of the diamond layer, showing: cobalt pools (medium grey contrast), diamond (dark contrast) and tungsten carbide (light grey contrast) 54
Figure 4.2: SEM-BSE images of leached and polished samples from nine experimental runs, showing: diamond (medium grey contrast), porosity (dark contrast) and tungsten carbide (light contrast) 57
Figure 4.3: SEM-BSE images of the sintered PDC samples showing: (a) unleached and (b) leached, with cobalt pools (light contrast), porosity (dark contrast) and diamond (medium dark contrast). Experimental run conditions: 5 GPa, 1500°C and 25 minutes 60
Figure 4.4: XRD patterns for the unleached and leached diamond layer samples. 60
Figure 4.5: unleached sample: (a) SEM-BSE image showing diamond (dark), cobalt (medium grey) and tungsten (light) and (b) X-ray map showing cobalt (blue), tungsten (orange) and diamond (purple) 62
Figure 5.1: Relationship between sample pressure, calculated from the Murnaghan equation of state (EOS), and measured relative volume (V/V_o) for the PDC samples. The dashed line is a linear fit to the calculated data 66
Figure 5.2: Comparison of the pressure calibration curve with reported values for fixed-point pressure transitions [18] 67
Figure 5.3: Comparison of VTL wear test results for PDC Samples: current data and values from Jivanji et al. [3], Dai et al. [4] and Zhao et al. [2] 68
Figure 5.4: Effect of sample-thermocouple proximity on temperature measurement reliability 70
Figure 5.5: X-ray radiographic image of the sample assembly with a thermocouple inserted, showing heater (light line contrast), PDC sample (dark contrast), and hot junction (black line). (Figure3.6 shows a line drawing of this sample assembly) 71
Figure 5.6: SEM-BSE images of the PDC samples sintered with two different thermocouple positions: (a) inside the heater (b) outside the heater, showing well-defined grain boundaries (red arrows), showing diamond (dark contrast), tungsten carbide (light contrast) and cobalt (medium grey contrast). The sintering conditions were 6 GPa, 1500°C and 20 minutes 72

Figure 6.1: Wear scar areas of leached PDC cutters sintered at different holding times. Sintering pressure and temperature were fixed at 7 GPa and 1500°C.....75
Figure 6.2: Boxplot analysis on the effect of holding time on leachability after 96 h leaching in HCl acid 76
Figure 6.3: Wear scar area of leached PDC cutters sintered at different sintering temperatures 78
Figure 6.4: Effect of sintering temperature on leachability after 96 h leaching in HCl acid 78
Figure 6.5: Relationship between leachability (leach rate) and sintering pressure after 96 h leaching in HCl acid 80
Figure 7.1: Main effects plot for leach rates of PDCs for pressure, holding time and temperature, horizontal dashed lines represent overall mean leach rate.....85
Figure 7.2: Interaction plot for holding time and temperature on leach rate 85
Figure 7.3: Correlation matrix showing the relationships between pressure (GPa), temperature (°C), holding time (minutes) and leach rate (µm/h), with Pearson correlation coefficients (r) and their 95% confidence intervals (CI) for each pair 86
Figure 7.4: Contour plot for effect of pressure (GPa) and temperature (°C) on leach rate (µm/h) at a fixed holding time 87
Figure 7.5: Optimisation plot showing the predicted leach rate (µm/h) as a function of pressure (GPa) and temperature (°C), showing maximum leachability achievable under the experimental boundary conditions tested, where: high = maximum value of the pressure and temperature, low = lowest value of the pressure and temperature and current = current value of the pressure and temperature 88
Figure 7.6: Venn diagram showing the complete dominance weights for the effect of sintering variables on the leachability of PDC 90
Figure 7.7: Conditional dominance weights for the of sintering variables at different subset size models 91
Figure 7.8: Percentage general dominance weights for the sintering variables 92
Figure 8.1: SEM-BSE images of PDC samples produced at: (a) calibrated pressure of 7 GPa, 1500°C and 20 minutes, (b) 5.5 GPa and 1450°C by Westraadt et al. [107], showing cobalt pools (medium grey contrast), diamond (dark contrast) and tungsten carbide (light grey contrast).....98

Figure 8.2: High-pressure phase diagram of titanium [108].....102
Figure 8.3: Ti–Pt phase diagram by Murray [141] 103
Figure 8.4: SEM-BSE images of PDC samples, taken from the bottom of the diamond layer near the interface, sintered for: (a) 20 minutes and (b) 30 minutes, showing cobalt pools (medium grey contrast), diamond (dark contrast) and tungsten carbide (light grey contrast). Red lines show interfaces between diamond grains. Sintering pressure and temperature were 7 GPa and 1500°C (Figure 4.1) 108
Figure 8.5: Relationship between leachability (leach rate) and sintering pressure after 96 h leaching in HCl acid 113
Figure 8.6: SEM-BSE images of PDC samples, taken from the middle of the diamond layer, sintered for: (a) 1500°C and (b) 1700°C, showing cobalt pools (medium grey contrast) and diamond (dark contrast) with well-defined grain boundaries (red arrow). Sintering pressure and holding time were 7 GPa and 20 minutes (Figure 4.1).....116
Figure 8.7: Relationship between leachability (leach rate) and sintering temperature after 96 h of leaching in HCl acid 119
Figure 8.8: SEM-BSE images of PDC binder pools, taken from the middle of the diamond layer, sintered at different pressures: (a) 5 GPa and (b) 7 GPa, showing cobalt pools (light contrast), tungsten (grey contrast) and diamond (dark contrast). Sintering were 1500°C and 20 minutes (Figure 4.1) 121

List of tables

Table 4.1: Leach rate data for data points 1 – 30 51
Table 4.2: Leach rate data for data points 31 – 64 52
Table 4.3: Reference Intensity ratio (RIR) values for the leached and unleached diamond layer samples. 61
Table 4.4: XRF results showing the cobalt to tungsten ratio (Co/W) between leached and unleached samples. 61
Table 4.5: EDX results of unleached sample. 62
Table 4.6: Density measurements of sintered PDC samples under varying conditions . 63
Table 5.1: Effect of thermocouple position on measured temperature with measuring thermocouples in a cubic press 72
Table 5.2: Wear scar areas of PDC samples sintered with the thermocouple positioned at 1 mm and 6 mm from the sample 73
Table 6.1: Microstructural parameters of leached PDC cutters with varying sintering holding times 75
Table 6.2: Microstructural parameters of leached PDC cutters with varying sintering temeprature 77
Table 6.3: Average cobalt pool size and shape at different pressures 79
Table 6.4: VTL measurements of the area of the wear scars on the sintered samples.. 79
Table 7.1:Variance iInflation factors (VIFs) for sintering variables 82
Table 7.2: Results of multiple regression analysis for leach rate 84
Table 8.1: Curve fits for the relationship between holding time and leachability 113
Table 8.2: Validation of the modelled data for the leach rates against the experimental data after 96 h leaching 114
Table 8.3: Curve fits for the relationship between sintering temperature and leachability 119
Table 8.4: Validation of the modelled data against the experimental data after 96 h leaching 120
Table 8.5: Curve fits for the relationship between pressure and leachability..... 124
Table 8.6: Validation of the modelled data against the experimental data after 96 h leaching 125

Chapter 1: Introduction

1.1 Background

Polycrystalline diamond compacts (PDCs) are advanced composite materials of diamond (C), cobalt (Co) and tungsten carbide (WC-Co) [1–4]. A PDC compact is composed of two key parts: a layer of polycrystalline diamond and a WC-Co substrate. These are bonded together to create a cutting tool with exceptional hardness, wear resistance, and thermal stability [1–4]. These properties make them indispensable tools in many industries, particularly oil and gas drilling, where they are used as cutting elements in drill bits [4–6]. The performance of PDC cutters directly affects drilling efficiency, bit lifespan and overall cost-effectiveness [7,8]. The PDCs are typically manufactured by a high-pressure, high-temperature (HPHT) sintering process, where micron-sized synthetic diamond grains are bonded together using a cobalt binder under extreme conditions [1–4]. This process creates a dense, intergrown diamond structure that provides the material's exceptional properties [1–4] .

With advances in high-pressure, high-temperature (HPHT) sintering technology, it is now possible to achieve a much wider operating range of the process variables, which creates opportunities to improve the conventionally-made PDCs [9]. The process variables include high sintering pressures, high sintering temperatures and shorter sintering cycle times [9]. While advances in manufacturing technology play a key role in improving PDC performance, there is also a need to advance the fundamental understanding of how changes to these process variables affect leachability.

A critical factor influencing the performance and longevity of PDC cutters is their thermal stability [7,10–12]. During drilling operations, PDCs experience significant frictional heating, which can lead to thermal damage and premature failure [7,10–12]. To combat thermal degradation and extend tool life in PDCs [7,8,12], the industry commonly employs leaching. This process selectively removes the cobalt binder from the diamond layer using strong acids, like hydrochloric acid [13-17]. Removing a layer of about 200 µm thickness from the diamond layer using acid mixtures greatly increases the thermal resistance and hence improves the PDC life [13–17]. This creates an "engineered porosity" (where the leached-out cobalt creates pores) within the PDC structure, which improves heat dissipation and reduces the risk of thermal damage

[13–17]. A leached PDC can then be heated to much higher temperatures without the diamond graphitising or cracking, so preventing premature failure [13–17]. Thermal resistance is improved because the leached layer is only composed of diamond, so heat transmission away from the tip of the working layer becomes more efficient [13–17]. The rate at which cobalt is removed during leaching, referred to as "leachability," is therefore a crucial parameter that needs to be carefully controlled during PDC manufacturing. Therefore, a study of the relationship between processing variables and leachability in a systematic way becomes necessary because it can aid in the understanding and design of PDCs with extended thermal stability. Understanding this relationship mathematically is better because mathematical models can be used to predict leachability during product design.

1.2 Problem Statement

The leachability of PDCs is significantly affected by the parameters used during the HPHT sintering process, primarily pressure, temperature and holding time. Achieving the desired microstructure and leachability requires precise control of these parameters. However, the extreme conditions within the HPHT apparatus present significant difficulties for accurate measurement and control of both pressure and temperature [18]. Conventional pressure calibration methods often rely on room-temperature phase transitions of reference materials [18], which can introduce significant errors when extrapolated to high-temperature sintering conditions. Similarly, accurate temperature measurement is complicated by steep temperature gradients within the cubic press and potential reactions between the thermocouple and the sample environment [18].

Additionally, the industry trend towards deeper leaching, well beyond a millimetre, to maximize thermal stability benefits has introduced new manufacturing challenges [8,12]. While deeper leaching enhances thermal performance, it necessitates significantly extended leaching durations, increasing processing time and costs. Therefore, the ability to accurately predict and control leachability is no longer a secondary concern but a primary determinant of PDC performance and manufacturing efficiency. Developers need to determine the leachability of new cutters early in the development cycle to optimize leaching processes and avoid costly trial-and-error approaches. This requires a comprehensive understanding of how sintering

parameters affect leachability and the development of reliable predictive models. These difficulty of accurately controlling the sintering parameters can lead to inconsistencies in PDC microstructure, variations in leachability, and ultimately, compromised performance. Therefore, there is a critical need to develop improved methods for process parameter control and to understand the interactions between sintering parameters, microstructure, and leachability to optimise the HPHT sintering process for manufacturing high-performance PDCs.

1.3 Research Questions

This research aimed to address the problems described above by investigating the following research questions:

1. How can pressure be accurately calibrated in a cubic press at the actual sintering temperatures used for PDC fabrication?
2. What is the influence of thermocouple placement on the accuracy of temperature measurement during HPHT sintering, and how does this affect PDC properties?
3. How do the individual sintering parameters (holding time, temperature and pressure) affect the leach rate of PDCs?
4. What is the combined effect of these parameters on leach rate, and how do they interact?
5. What is the relative importance of each sintering parameter in determining the leachability of PDCs?
6. Can statistical models be developed to predict leach rate based on sintering parameters, and can these models be used to optimize the sintering process?

1.4 Research Objectives

The primary objectives of this research are to:

1. Develop and validate a novel *in situ* pressure calibration method for a cubic press that provided accurate and material-specific pressure determination at sintering temperatures.

2. Investigate the influence of thermocouple placement on temperature measurement accuracy and determine the optimal placement strategy for reliable temperature monitoring.
3. Quantify the individual effects of holding time, temperature and pressure on the leach rate of PDCs.
4. Develop a multiple regression model to quantify the combined effects of sintering parameters, including interactions, on leach rate.
5. Employ dominance analysis (DA) to determine the relative importance of each sintering parameter in controlling leach rate.
6. Develop and validate predictive models for leach rate based on the individual and combined effects of sintering parameters.
7. Utilise the developed models and insights to propose strategies for optimising HPHT sintering to achieve desired PDC leachability and performances.

1.5 Significance of the Research

This research made significant contributions to the field of PDC manufacturing and applications. By developing and validating a novel *in situ* pressure calibration method, this work addressed a critical limitation in conventional HPHT sintering techniques. The improved accuracy in pressure determination, coupled with a better understanding of temperature measurement difficulties, enabled more precise control of sintering. Furthermore, the detailed investigation of the individual and combined effects of sintering parameters on leach rate, using advanced statistical modelling techniques, provided a comprehensive framework for optimising the sintering process. The findings of this research have the potential to:

- Improve the consistency and reliability of PDC manufacturing,
- Reduce manufacturing costs by optimising process parameters and minimizing material waste,
- Enable the development of tailored PDCs with specific leachability characteristics for different drilling applications,
- Advance fundamental understanding of HPHT sintering and the relationships between process parameters, microstructure and properties of PDCs.

1.6 Thesis Outline

The remainder of this thesis is structured as follows:

- **Chapter 2: Literature Review:** This chapter provides a comprehensive review of the relevant literature on HPHT sintering of PDCs, focusing on the effects of sintering parameters on microstructure and properties. It also describes various pressure calibration and temperature measurement techniques, as well as statistical modelling approaches used in materials science.
- **Chapter 3: Materials and Methods:** This chapter describes the experimental procedures employed in this research, including materials used, sample preparation, sintering process, leaching process, characterisation techniques and data analysis methods.
- **Chapter 4: Challenges and Advancements in Accurate Process Parameter Control:** This chapter presents the novel *in situ* pressure calibration method developed in this research and discusses the difficulties associated with accurate temperature measurement, including the effect of thermocouple placement.
- **Chapter 5: Optimising Leachability by Parameter Control: Individual Effects:** This chapter investigates the individual effects of holding time, temperature and pressure on the leach rate of PDCs, presenting experimental results and developing quantitative models for each parameter.
- **Chapter 6: Integrated Parameter Optimisation: Interactions and Relative Importance:** This chapter focuses on the combined effects of sintering parameters, employing multiple regression analysis to model their interactions and dominance analysis (DA) to determine their relative importance in controlling leach rate.
- **Chapter 7: Overall Discussion:** This chapter provides a comprehensive discussion and interpretation of the research findings, connecting the results from all chapters and demonstrating the significance of the work.
- **Chapter 8: Conclusions:** This chapter summarises the key findings and contributions of the research, discusses limitations and suggests directions for future research.

Chapter 2: Literature review

2.1 Introduction

This chapter provides a comprehensive review of the relevant literature on the high-pressure high-temperature (HPHT) sintering of polycrystalline diamond compacts (PDCs), focusing on the effects of sintering parameters on their microstructures and properties. The chapter begins with an overview of HPHT sintering and the key parameters that influence PDC fabrication. It then describes the specific effects of pressure, temperature and holding time on the resulting material characteristics, drawing on existing research to identify the known relationships and mechanisms. The critical importance of accurate pressure calibration and temperature measurement in HPHT processes is addressed, reviewing both conventional and alternative methods. Additionally, the chapter discusses the significance of leachability in enhancing PDC performance and examines the factors that affect this important property. Finally, an overview of relevant statistical modelling techniques commonly used in materials science is presented, followed by an identification of research gaps in the current literature that this thesis aimed to address.

2.2 HPHT Sintering of PDCs

High-pressure high-temperature (HPHT) sintering is the main method for manufacturing PDC cutters used in the oil and gas drilling industry [19–22]. This process typically involves subjecting a mixture of micron-sized synthetic diamond powder (Figure 2.1) and a cobalt binder to extreme pressures (5-10 GPa) and temperatures (1450-1900°C) for a specific duration, known as the holding time [3,23,24].

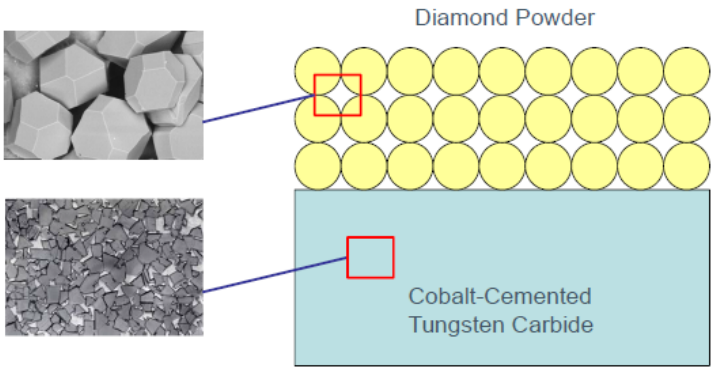


Figure 2.1: *Diamond powder and WC substrate placed inside the sample assembly [23]*

The HPHT process (Figure 2.2) consolidates the diamond particles, creating a dense, intergrown diamond structure with exceptional hardness and wear resistance [3,23,24]. The cobalt binder, which melts during the process (Figure 2.3), facilitates liquid phase sintering (LPS), a key mechanism that promotes densification and bonding between the diamond grains [25,26].

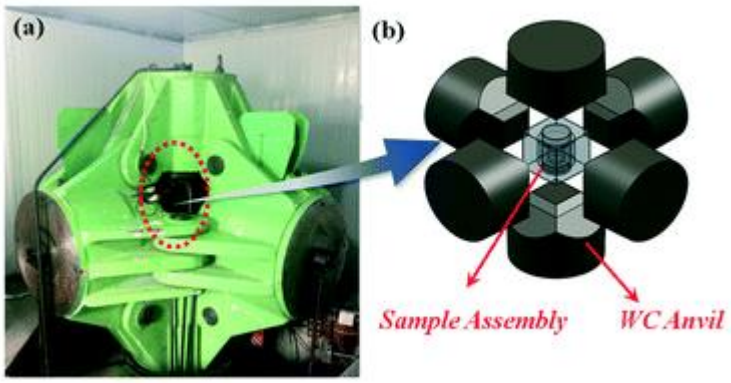


Figure 2.2: *(a) HPHT press, (b) sample assembly* [23]

The fundamental mechanisms involved in LPS, as described by German et al. [32], include particle rearrangement, solution-reprecipitation and grain shape accommodation. Initially, capillary forces exerted by the liquid cobalt draw the diamond particles closer together, leading to particle rearrangement and a reduction in porosity [32]. As the temperature increases, the cobalt dissolves diamond at points of high contact stress and facilitates its reprecipitation in regions of lower stress, leading to neck formation between particles and further densification [32]. This process is further enhanced by the application of high pressure, which increases the solubility of diamond in cobalt and promotes diamond-diamond bonding [32].

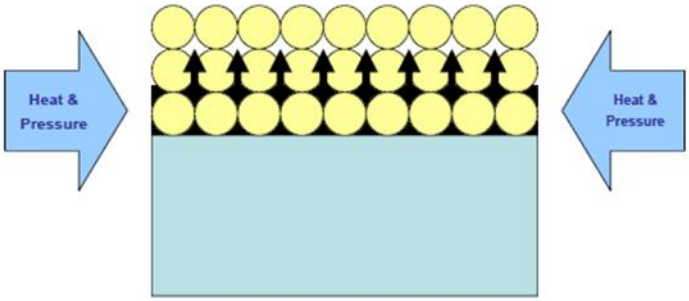


Figure 2.3: *Cobalt binder migration* [23]

Diamond-to-diamond bonding is a mechanism of PDC sintering that introduces new diamond particles between the diamond grains by re-precipitation as shown in Figure 2.4 [27,28]. Diamond-to-diamond bonding is a quantitative parameter usually measured from scanning electron microscopy (SEM) images using image analysis software (IA) and is related to the mechanical properties of the PDC [28]. Diamond-to-diamond bonding results in an intergrown diamond structure which gives excellent mechanical properties such as superior hardness and wear resistance [25].

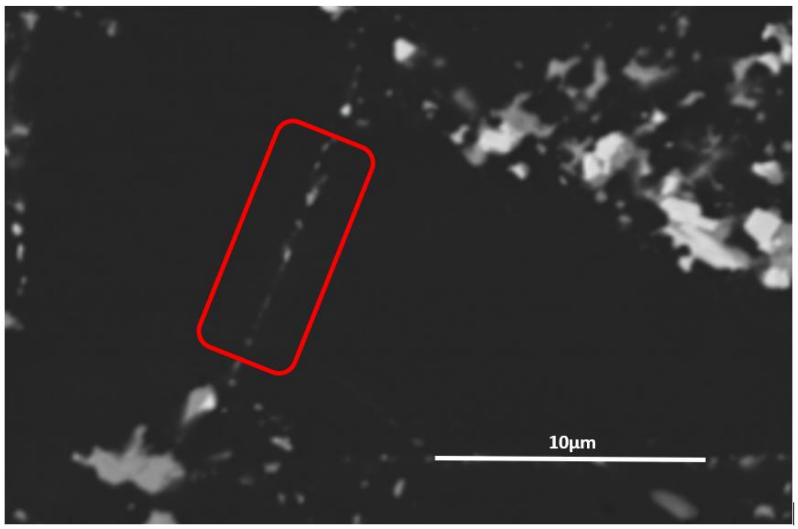


***Figure 2.4**: SEM-BSE image showing diamond-to-diamond bonding in PDC, showing cobalt pools (medium grey contrast), diamond (dark contrast) and tungsten carbide (light grey contrast) [28]*

Ozbayraktar [143] categorised the processes during polycrystalline diamond manufacturing into three stages:

(1) cold compaction,

(2) hot compaction, and

(3) liquid phase sintering.

Cold compaction

Cold compaction in PDC materials, as showed by the transition from Step A to Step B in Figure 2.5, occurs under steadily increasing pressure up to a nominal level of 5.5 GPa without the application of heat. Ozbayraktar [144] identified of PDC material three distinct processes under pressure in cold compaction: particle rearrangement,

diamond particle crushing and the filling of pores with the resulting fine particles. Initially, the applied pressure forces the particles to rearrange as they push against one another. This rearrangement leads to high stresses at the contact points between the diamond grains, ultimately causing them to fracture and result in finer particles. Ozbayraktar [142] determined that fracturing occurred due to localised contact pressures exceeding the compressive strength of diamond (>13 GPa). The threshold for diamond grain fracture was 69.5 GPa, and since stresses at diamond particle contacts can be 30 times the applied pressure, fracturing can begin with an applied pressure as low as 2.3 GPa. Furthermore, Ozbayraktar [142] observed that coarser, irregularly-shaped diamond particles were more prone to crushing than finer ones. Contact between a diamond particle with truncated corners and one with a flat face can generate pressure exceeding the strength of diamond, leading to crushing. Importantly, fracture at contact points mostly occurs below 1000°C due to the brittle nature of diamond. Above this temperature, plastic deformation occurs. In summary: The cold compaction of PDC material involves a complex interaction of particle rearrangement, crushing driven by localized high stress at contact points and pore filling [142]. This process is heavily affected by the applied pressure and the morphology of the diamond particles, with significant fracturing occurring well below the nominal compaction pressure and at temperatures below 1000°C [142].

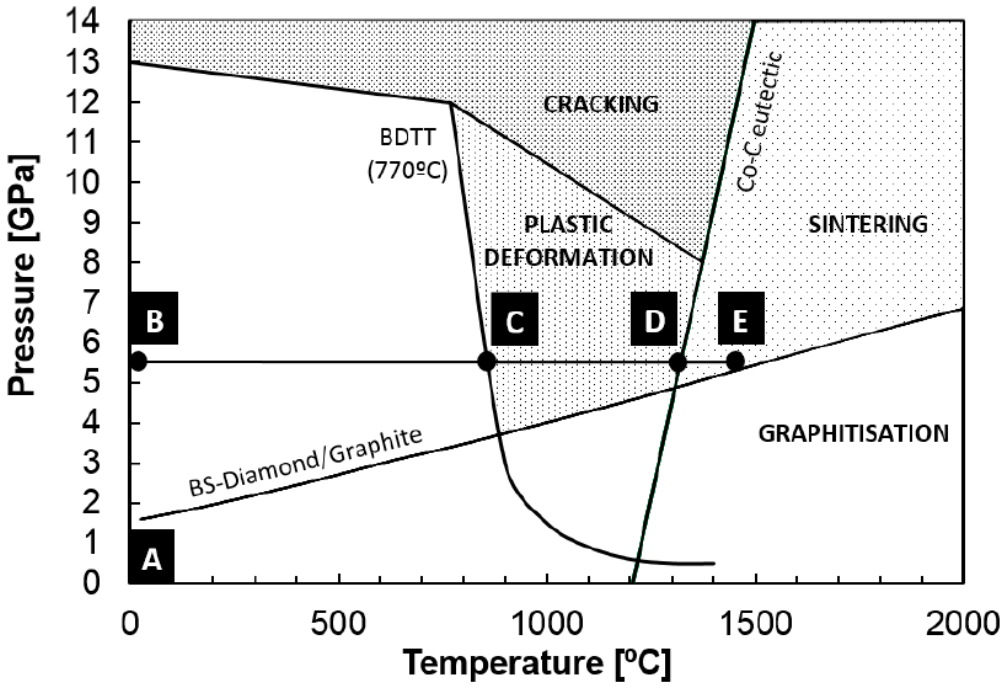


***Figure 2.5**: Sintering map for a cobalt based PDC [148]*

Hot compaction

The hot compaction stage is crucial for PDC sintering, as illustrated by the transition from Step B to Step D in Figure 2.5 and explained by several researchers [142, 144, 147, 148]. This stage is initiated by the introduction of heat, although temperatures remain below the threshold for binder infiltration. During hot compaction, driven by the simultaneous application of high pressure and temperature, the primary processes are graphitisation of diamond surfaces adjacent to pores, plastic deformation of diamond grains in contact zones and further densification of the compact by pore shrinkage. According to Brookes et al. [147], the initial application of heat promotes further densification primarily by continued crushing and rearrangement of the previously crushed particles. Brookes et al. [147] attributed this to the low pressure within the pores, which allows for the conversion of diamond to graphite. However, this graphitisation diminishes with increasing pressure as the conditions approach the diamond stable region above the Berman-Simon (BS) line, as depicted in Figure 2.2. Above 800°C, densification proceeds via plastic deformation [147, 148], where diamond grains are in direct contact. This plastic deformation is affected by both temperature and pressure, increasing at higher temperatures. Hot compaction of PDC materials causes continuous densification driven by a combination of particle

rearrangement and plastic deformation. While graphitisation occurs at lower pressures and temperatures around 800°C, it is suppressed at higher pressures. The dominant mechanism at temperatures exceeding 800°C is plastic deformation within diamond-diamond contact zones, facilitated by the elevated temperature and pressure.

Liquid phase sintering

Liquid phase sintering of PDC formation, represented by steps D to E in Figure 2.5, is primarily driven by the melting and infiltration of cobalt [144]. When temperatures exceed 1300°C, cobalt begins to melt and permeates the diamond layer. This cobalt infiltration provides two key advantages for sintering: lowering the required sintering temperatures and pressures and facilitating the dissolution of graphite from the diamond particle surfaces. For effective liquid phase sintering, Ozbayraktar [144] stated that the cobalt binder must fulfil several criteria:

- **High Carbon Solubility:** The molten cobalt must be able to dissolve a significant amount of carbon.
- **High Carbon Diffusivity:** The dissolved carbon should be able to diffuse rapidly through the molten cobalt.
- **Low Wetting Angle:** The cobalt should exhibit a low wetting angle with the diamond grains, promoting spreading and infiltration.
- **Low Interfacial Energy:** Low interfacial energy between the cobalt and diamond is desirable for effective bonding.
- **High Adhesion Energy:** Strong adhesion between the cobalt and diamond is necessary for bonding.

Ozbayraktar [144] described the infiltration stage of liquid-phase sintering. During this stage, the elevated temperatures cause the cobalt binder, which is typically present as a separate layer or pre-mixed with the diamond powder, to melt. This molten cobalt then infiltrates the porous diamond layer. Dissolved tungsten and carbon from the substrate, are also present in the molten cobalt, particularly at the interface between the diamond layer and the substrate. The excessive carbon at the interface changes the composition of the Co-W melt. The resulting molten cobalt then infiltrates the porous diamond structure, driven by the high-pressure gradients between the

diamond layer and the solid interface. As the molten cobalt fills the gaps between the diamond grains, dissolved carbon reprecipitates as diamond, effectively bonding the grains together and forming a continuous, intergrown diamond network. Simultaneously, the cobalt binder begins to infiltrate the diamond compact, again driven by pressure gradients. This mass transfer of cobalt gradually diminishes as the pressure gradient decreases, ceasing entirely once the pores are completely filled and the pressure gradient is eliminated. In summary, liquid phase sintering of PDCs involves the melting and infiltration of cobalt into the porous diamond compact. The cobalt acts as a sintering aid, facilitating the formation of strong, covalent diamond-diamond bonds. The success of this process depends on the cobalt's ability to wet the diamond surface, its solubility for carbon, and the capillary forces that draw the molten cobalt into the inter-particle spaces [29]. This infiltration, combined with the applied pressure, leads to densification and the formation of intergrown diamond with cobalt filling the remaining spaces.

2.3 Effects of Sintering Parameters on PDC Properties

The properties of the final PDC product are highly dependent on the sintering parameters employed during the HPHT process [9,30,31]. Optimising these parameters is crucial for achieving the desired microstructure, mechanical properties and leachability.

2.3.1 Pressure

Pressure plays a critical role in densification during HPHT sintering. Increased pressure promotes particle rearrangement and reduces porosity, resulting in a denser microstructure [9,19,32]. Tank et al. [33] observed a 4% increase in diamond content when sintering pressure was increased from 4.5 GPa to 7.5 GPa, demonstrating the significant effect of pressure on densification. Corrigan et al. [34] found that increasing pressure from 6 GPa to 7.5 GPa achieved the highest densification (98.22 ± 0.42 %) with negligible open porosity. The increased pressure gave better compaction and deformed and fractured the diamond grains, forming new, smaller gains, which rearranged themselves to fill the pores between larger particles leading to higher densification. Liu et al. [35] increased pressure from 5 to 7 GPa ± 0.3 GPa achieving increased densification (99.15 ± 0.42 %) and hardness (57.5 ± 0.3 GPa). Katzman et al.

[36] sintered at 7.7 GPa to increase hardness to 57 - 61 GPa and electrical resistivity to 1.3 x 10^8 Ω.cm, compared to commercial PDC compacts (52.2 ± 2 GPa) [37], which are typically sintered at 6 GPa. Yahiaoui et al. [38] used photoluminescence spectroscopy to examine PDC samples sintered at 2.6 GPa, 4.6 GPa and 9.9 GPa and observed that photoluminescence increased with pressure. In cold compaction of diamond powder [29], pressure variations significantly affect the packing density of diamond particles. The initial densification of the diamond particles was substantial due to accelerated pore shrinkage rates under applied pressure. Minnaar et al. [29] proposed that higher pressures induce deformation and fracture of diamond grains, generating smaller particles that rearrange and fill the voids between larger particles, consequently enhancing densification. Thus, pressure is a dominant factor governing densification, microstructure, and ultimately, the performance of PDCs. The consistent mention of enhanced densification, increased hardness, and altered properties with increasing sintering pressure demonstrates the need to optimise this parameter to achieve desired PDC performance for specific applications.

Ozbayraktar [144] indicated the challenges associated with achieving consistent density in sintered PDC samples, particularly when using geometric methods for density estimation. Variability in density measurements is often attributed to microstructural inconsistencies such as inhomogeneous particle packing, differential shrinkage during sintering, and localised porosity, all of which can significantly affect the final material properties. These inconsistencies are exacerbated when samples deviate from ideal geometries, as surface irregularities and non-cylindrical shapes introduce errors in volume estimation, thereby affecting calculated density values. The geometric method, while convenient, is sensitive to such deviations and may not accurately reflect true bulk density, especially in materials with complex sintering behaviour.

2.3.2 Temperature

Temperature is another crucial parameter that affects the kinetics of sintering and the resulting microstructure. During sintering, elevated temperatures drive mass transport, grain boundary migration and particle growth [39–41]. The effects of sintering temperature on the final microstructure and properties vary depending on

the material and the specific sintering technique employed. Careful control of temperature is crucial for achieving the desired properties. Sintering temperature strongly affects the microstructures of ceramics. Higher temperatures enhance the sintering process within the diamond layer. This leads to increased diffusion and bonding between diamond particles, reducing porosity and increasing the overall density of the layer. For example, Fan et al. [39] observed a significant increase in the relative density of zirconia-toughened alumina (ZTA) from approximately 93.38 ± 0.23% when sintered at 1100°C to over 98.13 ± 0.04% when sintered at 1450°C. However, excessive temperatures can also lead to exaggerated grain growth, which may negatively impact certain properties [39]. The average grain size increased from 348.28 ± 2.23 nm at 1200°C to 468.98 ± 2.19 nm at 1450°C [39]. The optimal sintering temperature for achieving the desired microstructure depend on the specific material and application.

Li et al. [40] demonstrated that sintering temperature effectively controlled the microstructure of Ti_2AlNb-based composites. The compressive strength of a Ti_2AlNb-based composite increased from 4.12 ± 0.1 GPa at 1250°C to 5.8 ± 0.2 GPa at 1350°C, although there can be an optimal temperature range for optimising mechanical properties, beyond which further increases may be detrimental. The compressive strength of the composite decreased to 4.23 ± 0.15 GPa when the sintering temperature was increased to 1400°C [40]. In contrast, Leszczyńska-Madej et al. [41] found that varying the sintering temperature during spark plasma sintering (SPS) of Al-SiC composites between 580°C and 600°C had a minimal effect on the microstructure. However, the higher sintering temperature increased hardness from 1050 ± 50 HV to 1180 ± 60 HV. While these studies were not for PDCs, they demonstrate the general principles governing sintering behaviour in ceramic materials. Since PDCs are a type of advanced ceramic composite, it is reasonable to infer that sintering temperature will similarly play a crucial role in determining their final microstructure and, consequently, their mechanical properties, such as hardness, wear resistance and compressive strength. Therefore, investigating the effects of sintering temperature on PDCs is important to achieve desired PDC performance for specific applications.

2.3.3 Holding time

Holding time is a critical sintering parameter that significantly affects microstructural evolution of ceramic materials during sintering, directly affecting mass transfer, grain boundary migration and particle growth, ultimately shaping the final properties of the sintered product [42–47]. Liu et al. [46] investigated the effect of holding time on the sintering of dense yttria-doped zirconia ceramics. They found that a modest increase in holding time from 5 minutes to 10 minutes gave a slight improvement in density, approximately 1.5%. Yang et al. [42] focused on calcium oxide-based ceramics, determining that an optimised holding time of 90 minutes yielded a flexural strength of 20.7 ± 1.8 MPa and a hardness of 17.6 ± 2.8 GPa. Extending the holding time to 150 minutes resulted in increased average grain size, approximately 220% (from 25 ± 3 µm to a larger, unspecified size), attributed to reduced porosity. Zang et al. [44] found that Ti185 alloy samples sintered at 1350°C with a 30-minute hold exhibited the highest compressive strength (1931 ± 80 MPa) and the lowest friction coefficient (0.47 ± 0.02). Although these studies focused on different materials, they collectively demonstrated the significant effect of holding time on the densification, grain growth and resulting mechanical properties of the sintered materials. As PDCs are a specialised form of ceramic composite, it is likely that the holding time during sintering will similarly strongly affect their microstructures, particularly the degree of diamond-diamond bonding, cobalt distribution and ultimately, properties like wear resistance and fracture toughness. Therefore, a thorough understanding of the effect of holding time is crucial for optimising the sintering process and achieving desired performance characteristics in PDCs.

2.3.4 Interactions between Parameters

While pressure, temperature and holding time each individually affect sintering and the resulting properties of materials like PDCs, it is crucial to recognise their interdependent effects. The optimal value for one parameter often depends upon the chosen values of the other parameters. For example, the ideal holding time may vary significantly depending on the applied pressure and temperature. German et al. [9] demonstrated that holding time and temperature interact significantly during sintering, highlighting that these parameters cannot be optimized independently. Therefore, a holistic and integrated approach to process optimisation is essential,

considering the combined and synergistic effects of pressure, temperature and holding time to achieve the desired microstructure and performance of PDCs. Understanding the interaction between the parameters is important for tailoring the properties of PDCs for specific applications and achieving optimal performance.

2.3.5 Sintering mechanisms

Sintering, particularly for polycrystalline diamond compacts, is a complex interaction of various mechanisms, significantly influenced by temperature. German et al. [32] proposed a model based on the joining of two spherical particles to explain these mechanisms (Figure 2.6).

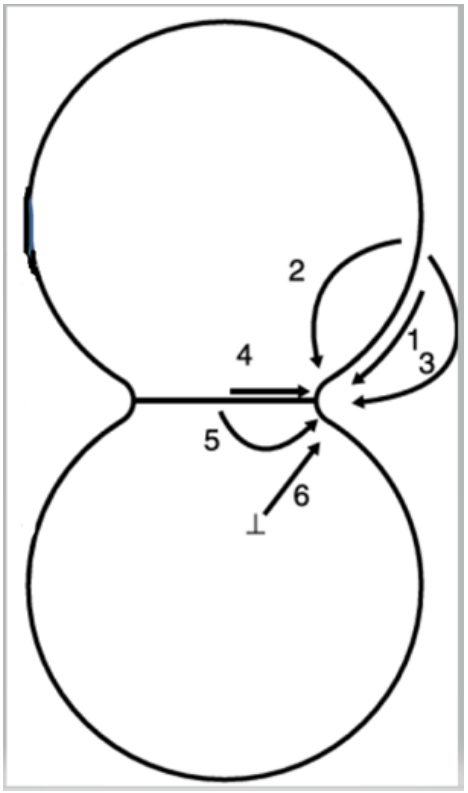


***Figure 2.6**: Sintering mechanisms for joining of two particles [32]*

This model identifies six primary transport mechanisms: (1) surface diffusion, (2) lattice diffusion from the surface, (3) vapour transport (evaporation/condensation), (4) grain boundary diffusion, (5) lattice diffusion from the grain boundary and (6) plastic flow by dislocation motion [32]. These mechanisms can be broadly categorised as either densifying (4, 5 and 6), which contribute to shrinkage by removing material from the grain boundary, or non-densifying (1, 2 and 3), which promote neck growth and particle coarsening without shrinkage. However, for PDC sintering, German et al. [32]

found that only mechanisms 3 and 6 are directly relevant. Mechanism 3, for PDCs, is redefined as "cobalt binder phase transport". This involves the dissolution of graphite (formed on diamond surfaces) into the cobalt binder and its subsequent reprecipitation as diamond, forming diamond-to-diamond bonds – a process distinct from simple evaporation-condensation. Mechanism 6 is the plastic deformation of diamond grains under the applied heat and pressure during hot compaction.

German et al. [32] described the cobalt binder phase transport as a key mechanism in liquid phase sintering. The molten cobalt facilitates the solution-reprecipitation process, where less stable carbon (graphite or strained diamond) dissolves in the cobalt and reprecipitates as more stable, well-formed diamond, leading to diamond-diamond bonding. This process is driven by the reduction in overall free energy of the system. Carbon preferentially diffuses from high-energy locations, such as diamond grain surfaces or in solution within the binder, to lower-energy sites at neck or grain boundary junctions. This leads to the deposition of carbon onto existing diamond grains, forming the crucial diamond-to-diamond bonds. This process is enhanced by increased sintering temperature and time, slowing down as the available graphite is consumed. The presence of liquid cobalt is crucial for facilitating the carbon transport. Insufficient binder can lead to non-uniform diamond intergrowth due to poor binder distribution. Minnaar et al. [29] recognises diamond grain deformation as another key densification mechanism, strongly affected by both temperature and pressure. Above a certain temperature threshold, the applied pressure causes the contact points between diamond grains to deform plastically, resulting in the movement and multiplication of dislocations within the grains. This plastic deformation leads to pore shrinkage and, consequently, densification. Pioneering work by Wamsley [145, 146] using transmission electron microscopy (TEM) revealed that in sintered PDCs, most of the original diamond grains exhibited significant deformation. In contrast, newly formed intergrowth regions showed minimal deformation. Wamsley [145. 146] observed dislocation networks and micro twinning above 700°C (Figure 2.7), with dislocations in the intergrown diamond formed low angle boundaries. The common deformation defects in PDCs included stacking faults, micro twinning, and a low dislocation density in the intergrowth regions (Figure 2.7).

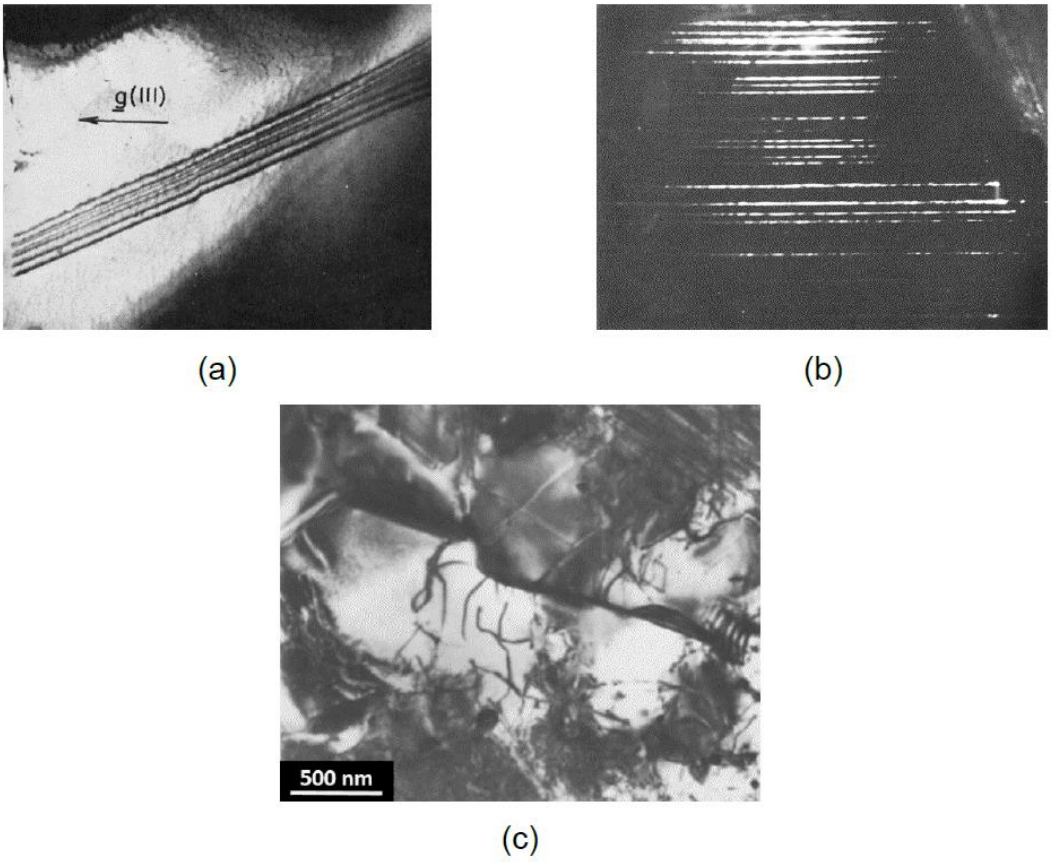


Figure 2.7: *TEM micrographs showing: (a) stacking faults; (b) micro-twinning and (c) low dislocation density of diamond intergrowth [145]*

In conclusion, the HPHT sintering of PDCs is a complex process governed by several temperature-sensitive mechanisms, including plastic deformation, grain boundary migration and diamond-to-diamond bonding via solution-reprecipitation. During the initial stages of sintering, plastic deformation of diamond grains becomes significant, particularly above 1000°C, allowing for particle rearrangement and initial densification. As the temperature increases, grain boundary migration becomes increasingly important. In this process, boundaries between adjacent diamond grains move, driven by the reduction in overall grain boundary energy. This can lead to the consumption of smaller grains by larger grains (grain growth) and the formation of direct, covalent diamond-diamond bonds where grains of similar crystallographic orientation meet. This grain boundary migration and resulting neck formation between diamond particles are illustrated by German et al. [9,32]. Finally, the cobalt binder facilitates diamond-to-diamond bonding by a solution-reprecipitation mechanism, where less

stable carbon dissolves in the molten cobalt and reprecipitates as more stable diamond at points of contact between grains. The interaction and temperature dependence of these mechanisms (plastic deformation, grain boundary migration, and solution-reprecipitation) are crucial in determining the final microstructure, and consequently, the mechanical properties and overall performance of the sintered PDC. A thorough understanding of these mechanisms is therefore essential for optimising the sintering process and tailoring PDCs for specific applications.

2.4 Leachability of PDCs

Leaching, the selective removal of cobalt from the diamond layer using strong acids, is a critical post-sintering process that significantly enhances the thermal stability and performance of PDC cutters [13,48–51]. The removal of cobalt creates the "engineered porosity" that improves heat dissipation and reduces the risk of thermal damage during drilling operations [13,48–51]. Leaching is the current industry standard [13,48–51] used to overcome thermal degradation in PDCs and extend the tool life. Cobalt is recognised as the preferred binder in PDC sintering [1, 20, 36, 50, 58], facilitating the dissolution of graphite from diamond grain surfaces and its reprecipitation as diamond, forming diamond-to-diamond bonds through intergrowth.

However, as Gou et al. [58] found, thermal resistance is inversely proportional to binder amount; lower cobalt content leads to higher thermal resistance. This is because, at the elevated temperatures experienced at the rock contact point during operation, the cobalt binder undergoes several detrimental changes, collectively referred to as cobalt degradation. These changes include promoting the graphitization of diamond, contributing to thermal stresses due to cobalt's higher thermal expansion coefficient compared to diamond, and potentially oxidizing [28]. These degradation processes diminish tool performance. Westraadt [28] identified graphitisation (Figure 2.8) as the primary cause of PDC thermal degradation, occurring at approximately 700°C when diamond is in contact with cobalt, which facilitates the conversion of diamond to graphite under low-pressure conditions. Graphite is weaker and softer than PDC, creating localised weak points that lead to fracture, chipping, or spalling and accelerating wear [28].

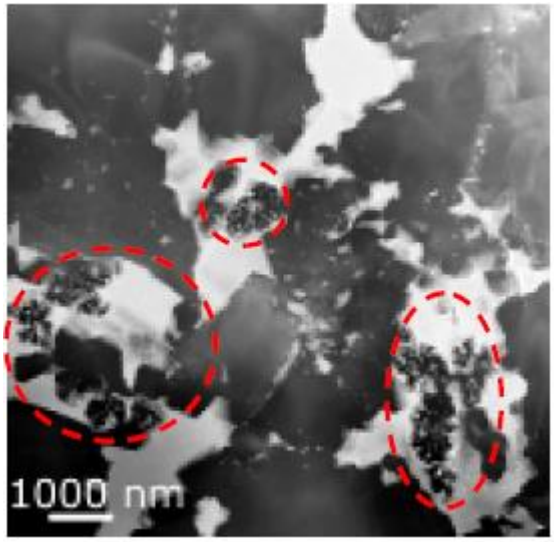


Figure 2.8: *TEM image showing degraded cobalt pools after exposure to 700 °C for 2 h, with graphite outlined by red circles* [28]

Several studies [20,28,29,58,59] investigated the thermal degradation mechanisms of PDC materials. Westraadt [28] observed micro-cracks in samples heated to 800°C in air, attributing them to graphitisation and stress-induced micro-cracking. Westraadt [28] found that these micro-cracks initiated at diamond grain edges and developed into transgranular cracks. This pattern of cracking suggested graphitisation as the likely cause. The transformation of diamond to graphite, particularly at grain boundaries where cobalt is present, results in a significant volume increase and a weaker, less dense material. This creates internal stresses and weakens the grain boundaries, making them preferential sites for crack initiation and propagation. Gou et al. [58] observed accelerated wear in a PDC with ~10 µm grain size annealed at 600°C in air, also attributing it to rapid graphitisation. Similarly, Akhaishi et al. [59] found that wear resistance was compromised above 500°C due to graphitisation. Gu et al. [20] observed transgranular cracking during wear tests, finding that temperatures at the wear surface were high enough for cobalt to facilitate diamond-to-graphite conversion, causing internal crack formation. Gu et al. [20] further investigated thermal degradation, observing degraded cobalt pools after heat treatment at 800°C, with graphite identified within the pools. Gu et al. [20] linked PDC failure to the presence of graphite in cobalt pools, noting a 54% volume increase associated with diamond-to-graphite conversion. This expansion induces lattice strain, increasing internal stress and potentially leading to micro-cracking. Katzman [36] observed a sharp increase in wear rate and reduced hardness in PDCs used for rock cutting at 700-

750°C and attributed the increased wear rate to graphite formation at the cutting edge. The high-temperature performance of PDCs is limited by the oxidation of both diamond and cobalt in oxygen-containing environments [36]. While thermodynamically unstable at ambient conditions, diamond's conversion to graphite is kinetically slow at room temperature. However, at elevated temperatures in the presence of oxygen, diamond readily oxidises to CO and CO_2. Cobalt can also oxidise, forming Co_xO_y which can be Co_3O or CoO [36], although this is often less of a direct performance limitation than diamond oxidation in typical drilling applications [60].

Francis [60] observed mass loss in PDC samples heated in air at 800°C due to the exothermic conversion of diamond to CO and CO_2, and mass gain due to the formation of CoO and Co_3O_4. However, Lin et al. [61] indicated that micro-cracking (Figure 2.9) is due to induced thermal expansion, since cobalt and diamond lattices expanded at different rates due to the significant differences in their coefficients of thermal expansion (α): cobalt ($\alpha = 13 \times 10^{-6}\ °C^{-1}$) and diamond ($\alpha = 1.0 \times 10^{-6}\ °C^{-1}$).

Lin et al. [61] indicated that micro-cracking (Figure 2.9) is attributed to differential thermal expansion, as cobalt and diamond exhibit significantly different temperature-dependent coefficients of thermal expansion (α). At room temperature, cobalt has a coefficient of approximately $13 \times 10^{-6}\ °C^{-1}$, while diamond is $1.0 \times 10^{-6}\ °C^{-1}$. However, these values increase with temperature, increasing mismatch in lattice expansion during thermal cycling. This disparity induces internal stresses at the interface, promoting micro-crack formation.

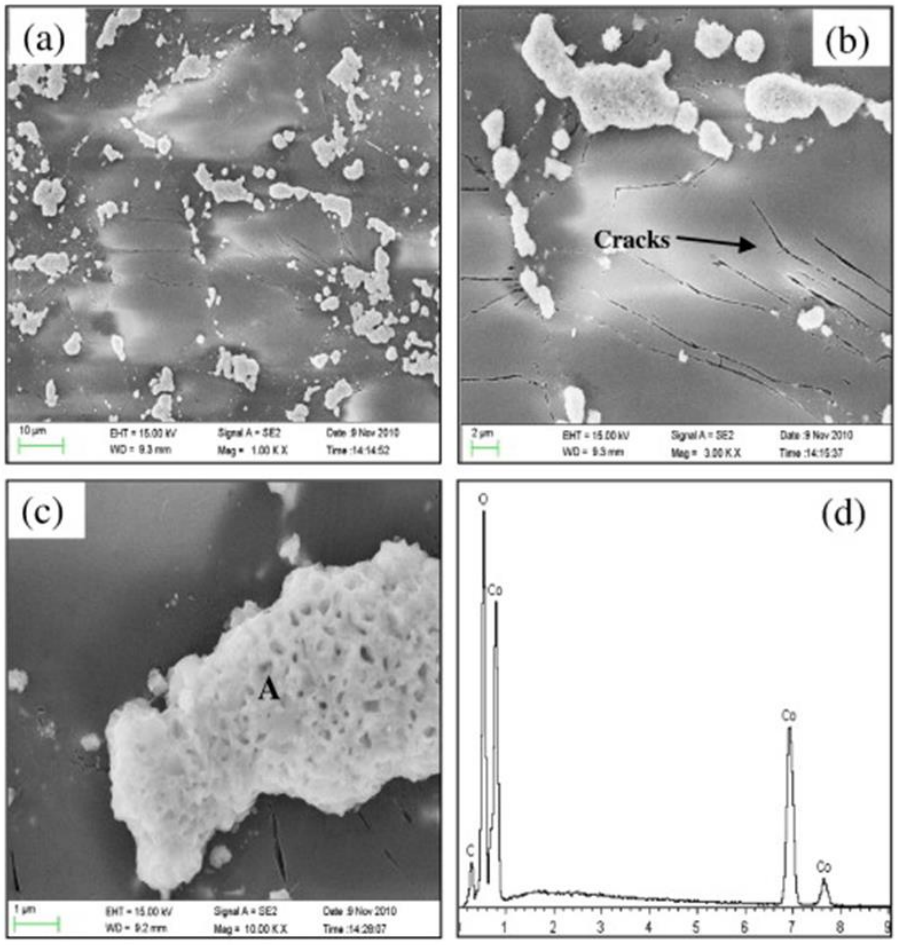


Figure 2.9: *SEM-SE images of heat treted PDC at 900°C showing: (a) Co distribution, (b) micro-cracking, (c) Co_3O_4 confirmed by (d) EDX analysis of cobalt* [61]

The induced significant internal stress due to the formation of Co_xO_y such as Co_3O_4 [61], generates micro-cracks within the polycrystalline diamond layer, greatly reduced wear resistance of the PDC cutting tool during service. Thermal stability is improved by minimising or eliminating cobalt in the diamond layer [10,62]. Alternative approaches include using ultrahigh pressures for sintering or non-cobalt binders. Thus, Shin [63] sintered PDCs at 7.7 GPa and 2000°C, achieving 1.5 vol.% cobalt and improved hardness. Yamaoka [64] used TiC as a binder but did not achieve a well-sintered PDC. However, they successfully sintered PDC with TiB_2, because a protective B_4C layer around diamond grains prevented direct contact with cobalt and stopped graphitisation. Westraadt [65] found improved wear resistance and thermal stability with $MgCO_3$ and $CaCO_3$ as binders, although extreme sintering conditions were required, increasing manufacturing costs and hindering commercial availability. More recently, Jivanji [4] demonstrated that sintering PCD with ZrB_2 yielded excellent performance in vertical turret lathe (VTL) applications, even outperforming leached

PCD cutters processed under the same conditions, demonstrating the potential of ZrB_2 as a thermally stable binder.

Currently, the industry standard for improving thermal stability and extending PDC life is acid leaching to remove cobalt [13,48,49,51]. Bellin et al. [12] of General Electric patented this process, demonstrating improved wear resistance in leached PDCs than standard PDCs in vertical turning lathe (VTL) tests (Figure 2.10). However, it must be recognised that Shumburger [149] of National Oilwell Varco (NOV) holds the primary intellectual property rights related to the leaching of PDC cutters, and they have earned billions of dollars in patent royalties. A VTL is a machine tool that rotates a rock workpiece against a stationary PDC tool, allowing for controlled and repeatable testing of PDC wear and performance under simulated drilling conditions. Corrigan [34] defines thermal degradation as accelerated wear or premature fracture due to stress-induced cracking, graphitisation, and/or oxidation at high service temperatures. Lin et al. [66] and Yahiaoui [38] recognised the VTL test as the primary method for evaluating thermal stability, as it combines all degradation mechanisms. In essence, the thermal stability of PDCs is complex affected by several factors, including the presence and amount of the cobalt binder (which catalyses graphitisation and contributes to thermal expansion mismatch) and the oxidation of diamond at elevated temperatures. While alternative binders and sintering methods exist, acid leaching to remove cobalt remains a common industry practice for improving thermal stability and extending PDC lifespan. The VTL testing is a primary method for evaluating thermal stability under simulated service conditions.

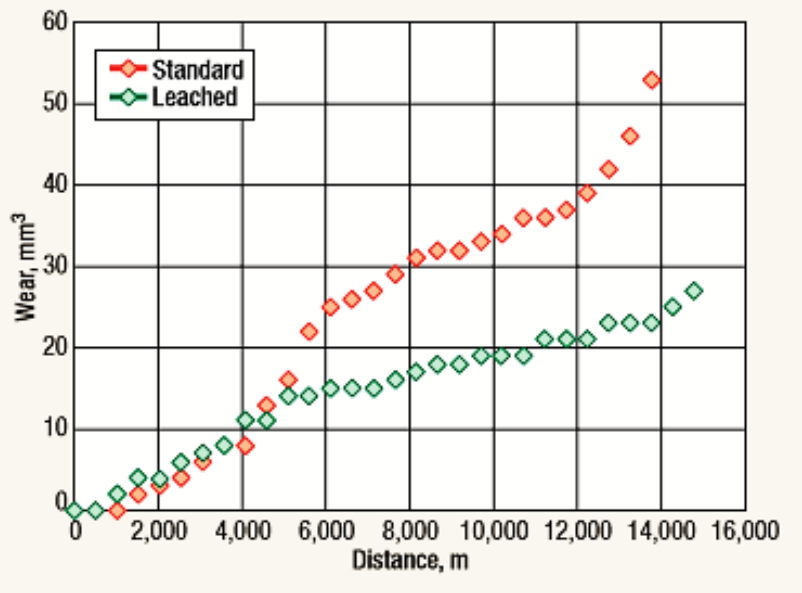


Figure 2.10 *Wear behaviour for leached and non-leached PDCs subjected to a VTL test [66]*

The chemical process underlying the leaching of the cobalt binder in PDC compacts exposed to HCl is fundamentally an acid dissolution reaction. Given that cobalt is the metallic binder phase, the main reaction expected is its dissolution in hydrochloric acid [13]:

$$\boldsymbol{Co(s) + 2HCl(l) \rightarrow CoCl_2(l) + H_2(g)}\textbf{.....Equation 1}$$

This reaction results in the formation of soluble cobalt chloride and the evolution of hydrogen gas. The liberation of hydrogen gas can contribute to the formation and propagation of pores, facilitating further acid ingress and accelerating the leaching process. Tungsten, present as inclusions or dissolved within the binder, is generally considered more resistant to non-oxidizing acids like HCl than cobalt [48]. However, its presence and distribution within the cobalt matrix can significantly affect the overall leaching kinetics. While bulk elemental tungsten is largely unreactive with HCl [48,49], any WC in the diamond layer can alter the binder's susceptibility to attack.

Several general principles govern the rate of chemical leaching of PDCs. A larger accessible surface area of the dissolvable phase (cobalt) directly leads to a faster leaching rate [13, 49]. Furthermore, the kinetics of the reaction are typically enhanced by higher acid concentrations and elevated temperatures [13, 49, 51]. The transport of reactants to the reacting surface and the removal of products away from it can also become rate-limiting factors. Crucially, differences in electrochemical potentials

between the various phases present (cobalt, tungsten and diamond) can induce galvanic corrosion effects, where the more active metal (cobalt) preferentially dissolves, accelerating its degradation and removal [51].

The processing parameters employed during PDC synthesis dictate the final microstructure, the material's susceptibility to acid leaching. The selection of processing variables (pressure, temperature and holding time) was driven by their well-established effect on the microstructure of PDCs [2,9,29,32], as described below.

Pressure (processing variable): Increasing the sintering pressure during fabrication of PDC compacts is well-known to lead to higher densification and a significant reduction in total porosity [29,32,52]. Critically, higher pressures also promote more effective diamond-diamond and diamond-binder bonding, leading to a denser, more consolidated structure. Mechanistically, this high degree of densification is expected to result in a reduction in the accessible surface area for HCl, as fewer open pores and channels are available for acid ingress. Furthermore, higher pressures reduce the open interconnectivity of the cobalt binder network [29,32]. This means a larger proportion of the cobalt is entrapped within isolated pockets, making it less accessible to the acid and therefore slows the leaching rate.

Temperature (processing variable): The sintering temperature exerts a complex and critical effect on both densification and diffusion of binder. Similar to pressure, higher temperatures generally promote greater densification, which reduces overall porosity [29,32,52] and therefore is expected to slow leaching rate. Elevated temperatures facilitate the formation of WC within the cobalt binder, which can precipitate out from the supersaturated liquid during cooling [29,32]. The presence and characteristics of WC phase are expected to significantly alter the binder's reactivity with HCl, since it can act as a barrier to acid attack. During high-temperature sintering, tungsten atoms can dissolve into the cobalt lattice. As tungsten is comparatively inert to HCl [48,49], any dissolved tungsten within the cobalt solid solution would increase the corrosion resistance of the binder.

Holding Time (processing variable): The holding time of the PDC compact at the sintering temperature is linked to the extent of densification and, more importantly, diffusion [29,32,52]. Longer holding times increase the concentration of WC within the

diamond layer, which reduces the reactivity of cobalt with chloride ions, diminishing the overall leaching efficiency.

Porosity (microstructural variable): Porosity, particularly open porosity and interconnected pores, is a direct pathway for HCl ingress. Higher total porosity, and especially a higher volume fraction of interconnected pores, provides greater accessible surface area for the HCl to react with the cobalt binder [50]. Thus, higher porosity promotes significantly faster leaching rates.

Binder Interconnectivity (open vs closed) (microstructural variable): The morphology and continuity of the cobalt binder network are important [29]. If the cobalt binder forms a continuous, interconnected pathway throughout the compact (open interconnectivity), the acid can readily permeate and dissolve it efficiently. Conversely, if the binder phase is largely isolated into discrete, closed pockets within the diamond matrix, it becomes significantly less accessible to the acid. Therefore, a high degree of open interconnectivity of the binder promotes a faster leaching rate, whereas isolated or “closed” binder regions slow the leaching rate.

Secondary Phases (W-Co-C) in the Binder (microstructural variable): The presence and distribution of WC within the diamond layer can affect the leaching of PDCs as stated above [49]. However, its increased concentration due to diffusion during longer holding times or increased temperature would alter the local microstructure. This alteration may reduce the binder’s reactivity with chloride ions, thereby slowing the leaching rate.

Solid Solutions in the Cobalt Binder (microstructural variable): The dissolution of tungsten and carbon atoms into the cobalt lattice to form a solid solution modifies the intrinsic chemical reactivity and electrochemical potential of the binder [48]. Given tungsten's inherent inertness to non-oxidizing acids [48], dissolved tungsten in the cobalt reduces the leachability of cobalt in acid.

2.5 Pressure Calibration in High-Pressure Press

High-pressure, high-temperature (HPHT) synthesis of polycrystalline diamond compacts requires precise control of pressure within a cubic press. The applied pressure directly affects densification, grain growth and the bonding between diamond particles and the cobalt binder [25, 26]. However, accurately determining the pressure

experienced by the sample within the cubic press is a significant challenge. This requires determining the actual pressure within the sample chamber as a function of applied load (or ram force), a procedure to establish the precise relationship between these two parameters within the sample chamber This relationship can serve as a means of pressure determination for future experiments, analogous to a calibration curve.

Conventionally, pressure calibration in cubic presses relies on fixed-point transitions of standard materials [18]. This method utilises materials, such as bismuth (Bi), thallium (Tl), and barium (Ba), that undergo well-characterised phase transitions at specific pressures and temperatures [18, 68]. By monitoring changes in electrical resistance, volume, or crystal structure, the pressure at which these transitions occur can be identified, providing calibration points [18]. Ono et al. [68] investigated the Bi-III to Bi-V transition using *in situ* X-ray diffraction, providing valuable data for calibration within the pressure and temperature ranges relevant to PDC sintering.

Despite the widespread use of fixed-point methods, several inherent difficulties limit their accuracy:

(1) Non-Hydrostaticity: Pressure gradients and deviatoric stresses within the sample chamber create non-hydrostatic conditions. These conditions can significantly alter the pressure at which phase transitions occur, leading to calibration errors [69, 70]. Careful sample assembly and selection of appropriate pressure-transmitting media are crucial to minimise non-hydrostaticity, but complete elimination is difficult.

(2) Temperature Gradients: Variations in temperature within the sample chamber introduce significant errors, particularly for calibration methods relying on temperature-sensitive phase transitions. If the temperature is not uniform, the phase transition will be broadened, making it difficult to pinpoint the transition pressure accurately from the known P-T phase diagram [69, 70]. Precise temperature control and measurement are, therefore, essential.

(3) Sample-Medium Interactions: Chemical reactions or diffusion between the sample (or calibrant) and the pressure-transmitting medium can alter the actual pressure experienced by the sample and its composition. This is not merely a calibration issue, it

fundamentally changes the sintering environment. Careful selection of chemically compatible materials is crucial to minimise these interactions [18].

(4) Material-Specificity: Traditional fixed-point calibrations may not accurately indicate the pressure by the PDC. This is caused by differences in material compressibility.

To address these limitations, the present study introduced a novel *in situ* pressure calibration method for cubic presses used in PDC synthesis. This method, building upon established principles [18, 137, 138, 139], utilises the PDC sample itself as the pressure sensor. By directly measuring the volume change of the PDC during sintering and applying the Murnaghan equation of state [140], a material-specific and more accurate pressure calibration is achieved. This improved accuracy is crucial for optimising the microstructure and performance of PDCs, leading to greater control and reproducibility in manufacturing. This method was used for all sintering experiments in this study.

2.6 Temperature Measurement in HPHT Press

Accurate temperature control during sintering of PDC cutters is important due to its large effect on the final material properties and, ultimately, the cutter performance. The optimal temperature profile ensures the formation of a desired microstructure, while deviations lead to significant inconsistencies in the material properties of the PDC cutter [9]. These inconsistencies primarily manifest in variations in hardness, wear resistance and impact toughness. For example, if the sintering temperature is too low, the cobalt binder for bonding the diamond particles within the PDC cutter will not melt completely or infiltrate fully [9]. The incomplete melting and infiltration result in a weakly bonded structure, significantly reducing the wear resistance of the PDC cutter. Conversely, if the sintering temperature is too high, the diamond surface within the PDC cutter tends to undergo graphitisation, the transformation of diamond into graphite, a much softer and less wear-resistant form of carbon [9]. This transformation weakens the diamond structure, reducing the wear resistance and hardness of the PDC. Furthermore, prolonged exposure to high temperatures can lead to abnormal grain growth of the diamond grains, further weakening the diamond and reducing its hardness and wear resistance [71].

The critical importance of precise temperature control is shown by the concept of a "sintering window" – a precise combination of pressure and temperature required for optimal densification and bonding of diamond particles, as defined by German et al. [9]. Deviations from this window, including temperature variations, can lead to incomplete sintering or graphitisation, both of which negatively affect hardness and wear resistance. A delicate balance is required in controlling both temperature and pressure during sintering to achieve the desired material properties in PDCs. Further research reinforced the significance of temperature control throughout sintering. Kanyanta et al. [72] showed how temperature variations during the cooling stage of sintering can induce significant stress transients within the PDC, which can lead to micro-cracks and delamination, that affect hardness and impact toughness of the PDC cutter. Westraadt et al. [5] studied the mechanisms of thermal degradation in PDCs, finding that high sintering temperatures can induce graphitisation of the diamond, weakening the material and causing cracking, ultimately reducing hardness and wear resistance. Scott et al. [11] reviewed the effect of PCD microstructures and mechanical properties, showing that grain size and binder content, affected by sintering temperature, can affect strength, toughness and wear resistance. McKie et al. [71] studied the abnormal grain growth (AGG) during HPHT sintering of fine-grained PDCs. Temperature variations can lead to non-uniform grain growth, potentially weakening the material and affecting its mechanical properties. Accurate temperature measurement within high-pressure, high-temperature (HPHT) apparatus, such as cubic presses, is crucial for controlling the sintering process and achieving desired material properties. However, the extreme conditions and complex geometry of these high pressure presses present significant challenges [73, 74]. Thermocouples are typically employed for temperature monitoring, but their accuracy can be compromised by several factors. Steep temperature gradients exist within the pressure cell, particularly outside the heater assembly, due to heat loss to the surrounding pressure-transmitting medium [73, 74]. Furthermore, high pressure itself can alter the electromotive force (emf) output of thermocouples, causing deviations from standard calibration curves [73]. The placement of the thermocouple relative to the sample is critical. Ideally, the thermocouple should be as close as possible to the sample. However, the physical constraints of the cubic press cell often necessitate less-than-ideal positioning. This

necessitates careful consideration of thermocouple type, calibration under pressure, and optimal placement within the cell assembly to minimise measurement errors.

Thermocouples, the most common temperature sensors in HPHT experiments, operate based on the thermoelectric effect [73], specifically the combination of the Thompson effect and the Peltier effect [73,75]. The Thompson effect describes the electric potential difference generated along a single conductor subjected to a temperature gradient, while the Peltier effect refers to the electric potential difference that arises across the junction of two dissimilar metallic wires. A thermocouple is formed by joining two dissimilar metallic wires at one end, creating a "hot" junction [73,75]. The electromotive force (emf) or voltage measured at the open ends of the thermocouple wires can be expressed as an integral over a given temperature interval, Equation 2.2 [73]:

$$\Delta e_{0J} = \int_{T_0}^{T_J} \alpha(x, P, T, \dots)\, \mathrm{d}T$$

……Equation 2.2

where α = coefficient of thermal expansion, T_0 = reference temperature at the open end of the thermocouple (usually at room temperature), T_J = unknown temperature at the junction, ≤ = Seebeck coefficient, a function of composition (x), pressure (P) and temperature (T). The Seebeck coefficient is the magnitude of the induced thermoelectric voltage in response to a temperature difference [75].

2.7 Statistical Modelling

Statistical modelling plays an increasingly important role in materials science research, enabling researchers to analyze complex datasets, quantify relationships between variables and optimise processes. There are several different techniques.

Regression Analysis: Regression analysis is a widely used technique for modelling the relationship between a dependent variable and one or more independent variables [76–78]. The fundamental multiple regression equation, as described by Hadi et al. [79], can be expressed as:

$$Y = a + bX$$

…… Equation 2.3

where *Y* = the dependent variable, leachability, and *X* = sintering variables, and *a* and *b* are the regression coefficients. Equation 2.2 was expanded to show an interaction term *XY a*nd a power term X^2 as expressed in Equations 2.3 and 2.4 [80–84].

$$\sum Y = an + b\sum X \quad \textbf{..... Equation 2.4}$$

$$\sum XY = a\sum X + b\sum X^2 \quad \textbf{..... Equation 2.5}$$

The regression model that expressed more than one sintering variable is shown in Equation 2.5, where X_1 and X_2 are the sintering variables [80–84].

$$Y = a + b_{1X_1} + b_{2X_2} \quad \textbf{..... Equation 2.6}$$

Equation 2.5 was also expanded to include interaction terms *XY* and a power terms X^2 in a regression equation that had two sintering variables (Equations 2.6, 2.7 and 2.8) [85].

$$\sum Y = an + b_1\sum X_1 + b_2\sum X_2 \quad \textbf{..... Equation 2.7}$$

$$\sum X_1 Y = a\sum X_1 + b_1\sum X_1^2 + b_2\sum X_1 X_2 \quad \textbf{.....Equation 2.8}$$

$$\sum X_2 Y = a\sum X_2 + b_1\sum X_1 X_2 + b_2\sum X_2^2 \quad \textbf{..... Equation 2.9}$$

The coefficients of the sintering variables, a_x and b_x, are given by Equation 2.9 and equation 2.10. They are used to assess the adequacy of the regression model [85].

$$b_X = \frac{n\sum XY - \sum X\sum Y}{n\sum X^2 - \left(\sum X\right)^2} \quad \textbf{.....Equation 2.10}$$

$$a_X = \frac{\sum Y}{n} - \frac{b_{X\sum X}}{n} \quad \textbf{..... Equation 2.11}$$

The correlation coefficient (*r*), which indicates how well the model equation fits the data is given by Equations 2.11 and 2.12 [85].

$$r_X = \frac{n\sum XY - \sum X \sum Y}{\sqrt{n\sum X^2 - (X)^2} \times \sqrt{n\sum Y^2 - \left(\sum Y\right)^2}}$$ ***……. Equation 2.12***

$$R^2 = \frac{a\sum Y + b_1 \sum X_{1Y+b_2} \sum X_{2Y} - \frac{\left(\sum Y\right)^2}{n}}{\sum Y^2 - \frac{\left(\sum Y\right)^2}{n}}$$ ***……. Equation 2.13***

In summary, regression analysis, with its ability to handle multiple variables and incorporate interaction and power terms, power terms, provides a robust framework for modelling complex relationships in materials science, particularly valuable for PDC sintering, where multiple interdependent parameters affect the final product's properties.

Dominance Analysis (DA): Dominance Analysis is a statistical method for determining the relative importance of variables in a regression model [84,86–88]. It divides the overall model R^2 into contributions attributable to each variable, considering all possible subset models [84,86–88]. Cancado et al. [89] defined relative importance as the contribution each independent variable made to the overall regression fit *(R^2)* of the linear model, taking into consideration both its individual effect and its effect when shared with the other independent variables in a regression equation. The R^2 is a statistical measure used in regression analysis to quantify the proportion of variance in the leachability (the variable being predicted) that can be explained by the sintering variables (those used for prediction) [89]. It is derived from a linear model [90–94]:

$$\boldsymbol{y_i = \beta_0 + x_{i1}\beta_1 + \cdots + x_{iP}\beta_P + e_i}$$ ***……Equation 2.14***

where the dependent variable y_i is modelled as a linear function of independent variables with values $x_{i1}, \ldots\ldots\ldots, x_{iP}$, with unknown coefficients $\beta_1, \cdots\cdots, \beta_P$, and e_i representing the unexplained variation. The coefficients $\beta_k, k = 0, \ldots, p$, are estimated by minimising the sum of squared unexplained variation. If the estimated coefficients are $\hat{\beta}_k$ and the fitted response values are $\hat{y}_i = \beta_0 + x_{i1}\beta_1 + \cdots + x_{iP}\beta_P$, the coefficient of regression fit R^2 can be written as [90,95]:

$$R^2 = \frac{Model\ SS}{Total\ SS} = \frac{\sum_{i=1}^{n}(\hat{y}_i - \bar{y})^2}{\sum_{i=1}^{n}(y_i - \bar{y})^2}$$

…… Equation 2.15

where y = actual value of the response variable, $\hat{y}$ = predicted value of the response variable and $\bar{y}$ = the average value of the response variable. The R^2 measures the proportion of variation in y that is explained by the p independent variables in the model [90]. Every independent variable in a regression model is assumed to contribute to the overall predictive effect, R^2, by three main effect levels: direct, partial and total [86]. The direct effect is the contribution of each independent variable for predicting the dependent variable, in isolation from all other independent variables. The partial effect is the explanatory ability of each independent variable in a particular subset or subsets of independent variables (i.e., conditional on a subset of the other independent variables) [86]. Explanatory ability of a variable is how much of the change in the dependent variable can be attributed to this specific independent variable, after accounting for the effects of other independent variables. The total effect is the contribution of each independent variable in the full model (i.e., controlling for all other independent variables) [86]. Thus, relative importance shows which independent variable contributes most to R^2 so that decisions using the relative contribution of each independent variable can be made and the explanatory power of the model can be evaluated.

Several methods for studying relative importance have been used [76,78,85,96,97], such as standardised regression coefficients. However, they often fall short due to limitations in handling moderately correlated independent variables or failing to consider all variable effects (direct, partial and total) [87,98,99]. Dominance analysis (DA), a statistical model for determining the relative importance of independent variables in a regression model, was developed by Budescu et al. [84] and divides the overall model fit R^2 into contributions attributable to each independent variable, so that the independent variable with the largest share is considered more important.

Dominance analysis uses R^2 and p predictors of a linear model to partition independent variables [84]. It uses the "all subset models" approach where each possible combination of the predictors from the (full) model is considered as a subset model, and the measure of model fit R^2 is recorded for each model. For p independent

variables, the number of possible subset models is 2^P. A subset model has size k which is the number of independent variables. Therefore, there will be $\binom{p}{k} = \frac{P!}{k!(P-k)!}$ models of size k. For example, with a total of $p = 3$ independent variables, x_1, x_2 , and x_3 , $2^P = 2^3 = 8$ subset models need to be estimated [86,89]:

$k = 0 \rightarrow \binom{3}{0} = 1$ null/empty model;

$k = 1 \rightarrow \binom{3}{1} = 3$ models with 1 independent variable: $[x_1], [x_2], [x_3]$;

$k = 2 \rightarrow \binom{3}{2} = 6$ models with 2 independent variables: $[x_1x_2], [x_1x_3], [x_2x_3]$;

$k = 3 \rightarrow \binom{3}{3} = 1$ full model with all 3 independent variables: $[x_1x_2x_3]$.

The incremental contribution an independent variable makes to a subset model, ΔR^2, is defined as the difference between the value of the measure of model fit R^2 for a model that includes the independent variable and R^2 for the same model excluding the independent variable [86,89]. Thus, the additional contribution that x_1 makes to model $[x_2x_3]$ is calculated as [86,89]:

$$\boldsymbol{\Delta R^2[x_1|x_2x_3] = R^2[x_1x_2x_3] - R^2[x_2x_3]} \text{.....} \textbf{\textit{Equation 2.2.16}}$$

The DA calculates weights on three levels (complete dominance, conditional dominance and general dominance) within a given number of independent variables p [89]. For example, if x is the number of indpendent variables, where each variable, x_i, is compared in a pairwise fashion to every other indpendent variable, x_j (where $i, i = 1, \dots, p-1$ and $i \neq j$), for their additional contribution to the measure of model fit R^2 [89]. Also, R_q^2 is the fit value for the model M_q which does not include x_i, where $q = \text{model } 1, 2, \dots, 2^p$ and R_{iq}^2 is the change in R_q^2 when x_i is added to M_q. If x_i contributes more than x_j to all M_q models that do not include both x_i and x_j, then x_i shows complete dominance over x_j. Conditional dominance is determined by first calculating the measure $\overline{\Delta R_{iq|k}^2}$ for an independent variable x_i by averaging its additional contribution to subset models of a given model size *k* [86,89]:

$$\boldsymbol{\overline{\Delta R_{iq|k}^2} = \frac{\sum \Delta R_{iq|k}^2}{\binom{p}{k}}} \text{.....} \textbf{\textit{Equation 2.2.17}}$$

where *k* (which is ≤ P) = number of independent variables in the subset model (model size) and $\binom{p}{k}$ = number of models of size k. Conditional dominance of x_i over x_j is

measured by the difference between their conditional measures at each model size. If the average additional contribution of x_i is larger than the average additional contribution of x_j for all model sizes (i.e., all k), then conditional dominance is established.

The general dominance value associated with x_i, G_i, is an average of all conditional contributions over all model sizes [86,89]:

$$G_i = \frac{\sum_{k=1}^{p} \overline{\Delta R^2_{iq|k}}}{p} \quad \text{.....Equation 2.2.18}$$

An independent variable shows general dominance if it has the highest overall average incremental validity across regression sub-models of sizes 0 to $k-1$ [84,89].

In summary, Dominance Analysis provides a robust and insightful method for identifying the relative importance of independent variables in complex regression models. By considering all possible subset models and evaluating contributions at multiple levels, DA offers a more nuanced understanding of variable influence compared to conventional methods. This is particularly valuable in fields like materials science, where multiple interacting factors often govern material properties and process outcomes. For example, in the study of processes like sintering, DA can be used to determine the relative importance of parameters like pressure, temperature and time on key properties of the final product. By identifying the most dominant factors, researchers can optimise processes more effectively and develop a deeper understanding of the underlying mechanisms.

2.8 Research Gaps and Justification

Despite the significant body of research on HPHT sintering of PDCs, several knowledge gaps remain:

- **Accurate High-Temperature Pressure Calibration:** While *ex situ* pressure calibration methods have been proposed [18, 100, 137, 138, 139], there is still a need for reliable techniques that can be readily implemented in HPHT presses used for PDC manufacturing.
- **Comprehensive Understanding of Parameter Interactions:** While individual effects of sintering parameters have been studied [13,48,51], a more

comprehensive understanding of their combined effects and interactions is needed, particularly for optimising leachability.

- **Quantitative Models for Leachability:** While some studies [9,32,111–115] have explored the qualitative effects of sintering parameters on leachability, there is a lack of quantitative models that can accurately predict leach rate based on a combination of parameters.
- **Optimisation of Leachability for Enhanced Thermal Stability:** The current industrial trend towards deeper leaching requires a more thorough understanding of how to optimise the sintering process to achieve desired leachability while maintaining mechanical integrity. This thesis addressed this gap by providing a framework for optimizing sintering parameters to tailor PDC properties for specific applications.

Chapter 3: Materials and methods

3.1 Materials

The materials used in this research for fabricating polycrystalline diamond compact (PDC) cutters were synthetic diamond powder, a cobalt binder, and cemented tungsten carbide (WC-Co) substrates. Synthetic diamond powder with an average particle size of 16 µm was used as the primary material for the diamond layer of the PDCs. The mixture consisted of a tri-modal feed of individual diamond grits added in different ratios. The composition of this powder mixture is not disclosed because it is a trade secret of Element Six. A cobalt powder with an average particle size of 6 µm was employed as the binder material to facilitate the sintering process and provide bonding between the diamond particles. Cemented tungsten carbide (WC-12%Co) substrates were used as the supporting component for the PDC cutters.

3.2 Sample Preparation

The green body was made by placing the diamond powder into a metal cup and inserting a WC-Co substrate. The green body was then outgassed in a vacuum furnace at ~10-5 bar and ~1100°C for 30 minutes to eliminate adsorbed gases and surface impurities, which can be detrimental to sintering. Next, the green body was put in additional metal cups to prevent re-absorption of gases prior to sintering. The green body was subsequently assembled into a pyrophyllite capsule.

3.3 HPHT Sintering

3.3.1 Cubic Press

A 6×32,000 kN hinge-type cubic hydraulic press was employed for both the calibration and sintering experiments. This press (Figure 3.1), with six hydraulic cylinders each capable of generating 32,000 kN force, provided a total potential force of 192,000 kN. The system comprised a hydraulic pump driven by an electric motor to pressurise hydraulic fluid stored in an oil tank. The pressurised fluid was then directed to the cylinders via a booster and a directional control valve. A pressure relief valve ensured the system remained within safe operating pressures, while a pressure gauge provided real-time monitoring. Each cylinder housed a ram that transmitted the force to an anvil, which in turn applied pressure to the sample.

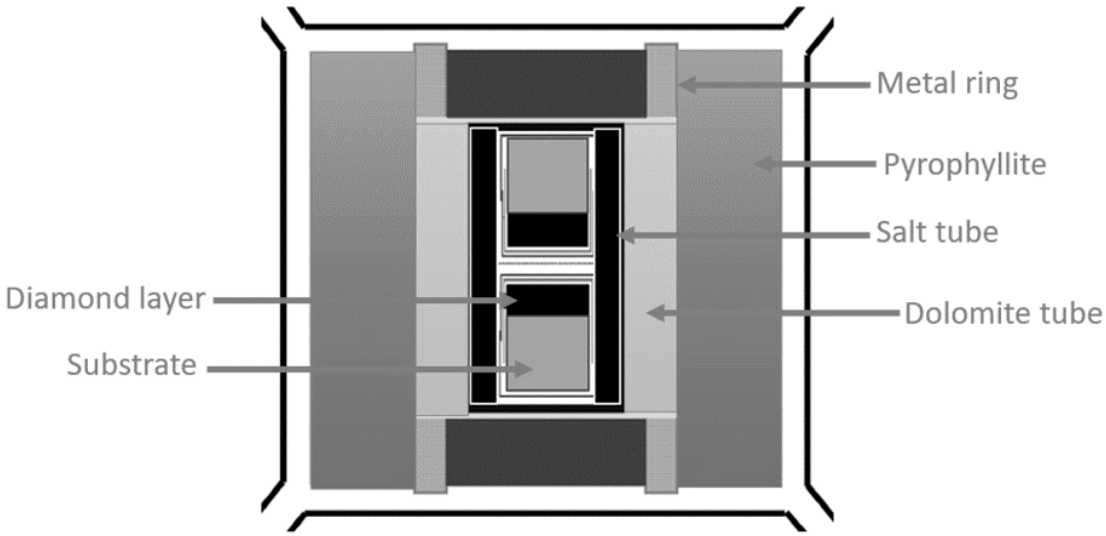


Figure 3.1: *A cubic press capsule* [22]

To investigate the individual effects of pressure, temperature and holding time on leach rate, three sets of experiments were conducted. Samples were housed within a cubic press capsule for all sintering runs (Figure 3.1). The experiments were conducted in three sets, systematically varying one parameter while holding the others constant:

- **Pressure Variation:** Pressure was varied between 5 GPa and 7 GPa, while holding temperature and time constant at 1600°C and 20 minutes.
- **Temperature Variation:** Temperature was varied between 1500°C and 1700°C, while holding pressure and time constant at 6 GPa and 20 minutes.
- **Holding Time Variation:** Holding time was varied between 5 and 30 minutes, while holding pressure and temperature constant at 6 GPa and 1600°C.

Additional samples were sintered at combinations of 1550°C or 1750°C, 26 minutes or 33 minutes holding time, and 6.8 GPa or 8 GPa pressure to validate the predictive models.

3.3.2 Cubic press calibration

The sintering conditions within the cubic press were characterised using an approach that correlated the applied ram load with the densification of the PDC sample. This approach aimed to establish a practical “sintering conditions calibration” for this specific press and material, rather than providing an absolute, fundamental pressure calibration. Experiments were carried out at different setpoint ram loads (3300 kN,

6610 kN, 8800 kN, and 10800 kN) and a fixed temperature of 1500°C. These selected ram loads were chosen to be within the typical pressure range of 5-8 GPa associated with successful PDC sintering [5]. This method relies on direct measurements of the volume change of a PDC sample during sintering. Here, V was the volume of the sample at a given applied pressure, and V_o was the initial volume of the sample prior to the application of pressure (i.e., at ambient conditions). The ratio of V and V_o is the relative volume. This method was based on measuring the *ex situ* volume change of the PDC sample after sintering and then utilising the Murnaghan equation of state [106] as an empirical fitting function to describe this observed densification. The process involved:

- **Initial Volume Determination (V_o):** The initial volume (V_o) of the cold-pressed diamond powder compact prior to sintering was determined by weighing 5g of diamond powder and calculating its volume based on a previously determined powder packing density of 3.52 g/cm³ [72] using Archimedes' method. The diamond powder was then placed in a niobium container and encapsulated within a pyrophyllite block, which served as both the pressure-transmitting medium (PTM) and gasket material. Pyrophyllite was selected for its balance of compressibility for pressure transmission and chemical inertness at experimental temperatures.
- ***Ex situ* Final Volume Measurement (V):** After each sintering cycle, the pyrophyllite block was carefully disassembled to extract the niobium container. The resulting cylindrical diamond compact was removed from the niobium container. The dimensions of the compact were then measured using a digital micrometer (Mitutoyo (400-162-40), precision ± 0.001 mm). To ensure accuracy, the diameter (d) and height (h) were measured at three different locations, and average values were used to calculate the final volume (V) using the formula for the volume of a cylinder:

$V = \pi(d/2)^2h$

where:

V = volume of the cylinder,

π = mathematical constant pi (approximately 3.14159),

d = average diameter of the cylinder,

h = average height of the cylinder.

- **Empirical Densification Modeling using Murnaghan EOS:** EosFit (Version 7.6) software was used to analyze the experimental data by performing a curve fit using the Murnaghan equation of state:

$$P(V) = \frac{K_0}{K_0'}\left[\left(\frac{V}{V_0}\right)^{-K_0'} - 1\right] \quad \textbf{.....Equation 3.1}$$

where:

P = pressure,

V_o = initial volume,

V = volume at pressure P,

K_o = bulk modulus at zero pressure,

K_o' = pressure derivative of the bulk modulus at zero pressure.

where P is the calculated effective compaction pressure, V_o is the initial volume, V is the final volume at a given ram load, K_o is the bulk modulus at zero pressure, and K_o' is the pressure derivative of the bulk modulus at zero pressure.

It is important to clarify the application of the Murnaghan equation in this context: while describing the elastic compression of bulk materials; here it was used as a phenomenological model to describe the non-linear relationship between the applied ram load and the observed *ex situ* volume reduction of the porous diamond compact. The input for EosFit included the applied ram load (or its nominal pressure calculated as P=F/A) and the corresponding measured initial (V_o) and final (V) volumes. The software was used to determine the optimal empirical coefficients (K_o and K_o') that best represented this densification under the experimental conditions. These empirically derived coefficients became the calibration parameters for characterising the compaction effectiveness of the press set-up for the PDC material studied.

The “calculated effective compaction pressure” obtained from this empirical fit (Figure 5.1) shows the increasing resistance of the diamond compact to further densification as porosity is eliminated and plastic deformation of diamond particles occurred. This approach thus provided a continuous relationship that describes how the material responds to increasing ram load, effectively serving as a “sintering conditions calibration” curve for the current system, relevant to the bulk volume change of the PDC sample during sintering.

3.3.3 Temperature Measurement

The Experiments used a 6x32,000 kN hinge-type cubic press at a fixed pressure of 6 GPa. The sample assembly consisted of a cylindrical pyrophyllite capsule with the PDC sample placed inside as shown in Figure 3.6. The PDC sample was inserted in a titanium cup (99.5% purity). A cylindrical graphoil was used to generate the high temperatures required for PDC sintering. In a cubic press, the precise distance between the sample and the thermocouple is important for accurate temperature measurement. This is because the cubic press lacks direct thermocouple control. Instead, the user inputs a desired power level on the control panel, and then inserts a thermocouple to measure the resulting temperature. If the distance between the sample and the thermocouple varies, the temperature readings will be inconsistent and unreliable.

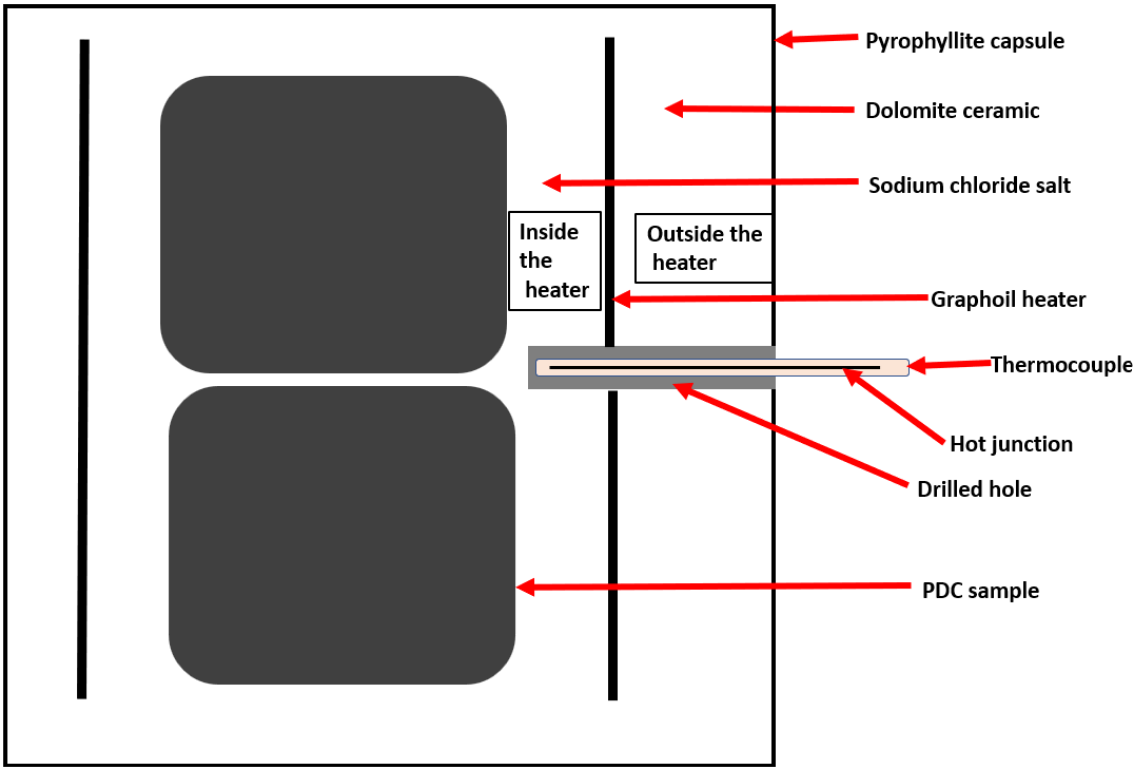


Figure 3.2: *Schematic diagram of the sample assembly in the capsule with an S-type thermocouple inserted into the drilled hole on the side of the capsule*

A Type S (Platinum-10% Rhodium) thermocouple was used for temperature measurements. While Type S thermocouples are generally recommended for continuous use up to 1600°C [109], their short-term exposure is up to 1750°C [109]. Given the relatively short sintering times used in this study (maximum 30 minutes), and the careful positioning of the thermocouple to minimize temperature gradients, it was deemed that a Type S thermocouple would provide sufficient accuracy. However, it is acknowledged that operating the thermocouple near its upper temperature limit is a potential source of error. A hole was drilled on the side of the pyrophyllite capsule, Figure 3.2 and the thermocouple was inserted into the hole in the pyrophyllite capsule. To investigate the effect of the thermocouple position, temperature measurements were taken at six different locations described below.

Inside of the heater: the thermocouple hot junction was positioned between the PDC sample and the graphite heater at distances of 1 mm (Temperature 1), 2 mm (Temperature 2) and 3 mm (Temperature 3) away from the sample.

Outside of the heater: the thermocouple hot junction was positioned outside the graphite heater at distances of 4 mm (Temperature 1), 5 mm (Temperature 2) and 6 mm (Temperature 3) away from the sample.

The entire capsule assembly was then carefully placed within the cubic press. Temperature readings were recorded using a Pico TC-08 data logger connected to the thermocouple.

3.3.4 Sintering Parameters

Three primary sintering parameters were selected as independent variables to study their influence on the dependent variable, PDC leachability. These were: pressure, temperature and holding time. Each independent variable was assigned three levels, representing the minimum and maximum values achievable within the operational range of the cubic press, based on prior experience and preliminary testing, as well as the midpoint. These levels were:

- **Sintering Pressure:** 5 GPa, 6 GPa and 7 GPa
- **Sintering Temperature:** 1500°C, 1600°C and 1700°C
- **Sintering Holding Time:** 20 minutes, 25 minutes and 30 minutes.

A full 2^3 factorial design was implemented using Minitab 21 software, providing a total of 64 experimental runs. This design allowed for the investigation of the individual effects of each parameter, as well as their interactions. To ensure statistical validity and assess the repeatability of the experiments, three replicates were performed for each unique combination of pressure, temperature and holding time. The experiment varied the sintering pressure, temperature and holding time to assess how each factor, and their combinations, affected the leach rate of the PDC. Data for run orders (sequence of experimental runs) were recorded.

3.4 Leaching

The sintered PDC samples were subjected to leaching to assess their cobalt binder removal rate. This involved immersing the samples in a 0.2 M hydrochloric acid (HCl) solution maintained at a constant temperature of 110°C for 96 hours. Following leaching, the depth of cobalt removal was measured (Figure 3.7) using X-ray

tomography (XRT) with an X-TEK XTV160 instrument (Nikon Metrology, United Kingdom). This non-destructive technique allowed accurate quantification of the leach depth. Three measurements were taken per sample, and the average and standard deviation of these measurements were calculated.

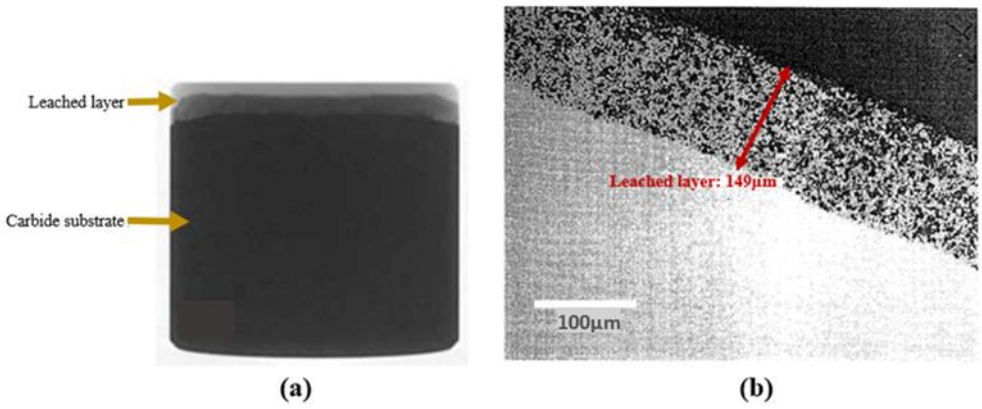


Figure 3.3: *Leaching images showing: (a) X-ray tomography image of a leached sample and (b) Scanning electron microscope (SEM) image of the measured leached layer [13]*

3.5 Characterisation Techniques

3.5.1 Sample Preparation

The sintered PDC samples were sectioned using a Struers Secotom-10 precision cutting machine with a 12 cm diameter diamond-coated wheel. A radial cut was made through the centre of each sample to expose a cross-section for microstructural analysis and leach depth measurement. The cutting parameters were: 3500 rpm wheel speed, 0.02 mm/s feed rate, and water as a coolant. One half of each sectioned sample was mounted in Struers PolyFast conductive resin using a Struers CitoPress-10 at 180°C and 250 bar. The mounted samples were ground using silicon carbide papers (220 and 1200 grit) and polished using diamond suspensions (9 µm, 3 µm, and 1 µm) on polishing cloths. A final polishing step using 0.05 µm colloidal silica was performed. Samples were thoroughly cleaned with isopropanol and dried between each grinding and polishing step. Microstructural analysis and leach depth measurements were performed across the cross-sections.

3.5.2 Scanning Electron Microscopy (SEM)

The microstructure of the sintered and leached PDC samples was examined using a a Zeiss Evo15 scanning electron microscope (SEM) equipped with a backscattered electron (BSE) detector. SEM-BSE images were obtained (Appendix A) at an

accelerating voltage of 10 keV to analyse the morphology sintered samples as well as the porosity distribution of the leached samples.

3.5.3 X-ray Diffraction (XRD)

X-ray diffraction (XRD) analysis was performed using a PANalytical X'Pert3 diffractometer equipped with a Cu Kα radiation source (λ = 154.18 pm), operated at 45 kV and 40 mA. The XRD patterns were collected to identify the phases present in the leached and unleached PDC samples. PANalytical HighScore Plus (version 3.0) and the ICSD database (Version 1.5) were used to identify the phases present in the samples. The Reference Intensity Ratio (RIR) method was used to calculate relative phase proportions. This was semi-quantitative and was suitable for assessing the relative proportions of cobalt-based and tungsten-based phases in the unleached and leached PCD samples.

3.5.4 Image analysis

The porosity, aspect ratio (AR) and Feret diameter (FD) of the leached microstructures were obtained from the SEM-BSE micrographs using ImageJ software (Version 1.46) on 16 images for each specimen at 1000x magnification and SIS-pro software. The aspect ratio (AR) gave an indication of cobalt pool shape, while the FD gave an indication of cobalt pool size. The AR was the ratio of the length to the width of the particle and was derived from the ratio of the major and minor axis of a fitted ellipse. The Feret diameter (FD) was the distance between two parallel tangents of the particle at different arbitrary angles and was derived from the longest distance between any two parallel points of the particle. Calculations of the microstructural parameters were done using MathConnex 2000 with MathCad 2000 Professional. For each specimen, 16 SEM-BSE micrographs were analysed. Means and standard deviations were calculated for porosity, aspect ratio, and Feret diameter, as shown in Tables 6.1, 6.2 and 6.3.

3.5.5 X-ray Tomography (XRT)

X-ray tomography was employed to measure the leach depth in the PDC samples after leaching. Two measurements per sample were taken. An X-TEK XTV160 system (United Kingdom) was used with a VJ Technologies P051 X-ray source operated at 80 kV and 2 mA to capture a radiographic image of the leach depth.

3.5.6 Wear Testing

To assess the wear resistance of PDC samples, the vertical turning lathe (VTL) operated at a spindle speed of 200 rpm, resulting in an infeed rate of 0.54 metres per revolution under a cutting speed of 1.8 m/s and a normal load of 5000 N; testing was stopped after 30 passes. Two wear scars per sample were produced and hence two measurements per sample were taken. A ZEISS ZEN optical profilometer and ZEN Core software measured the resulting wear scars.

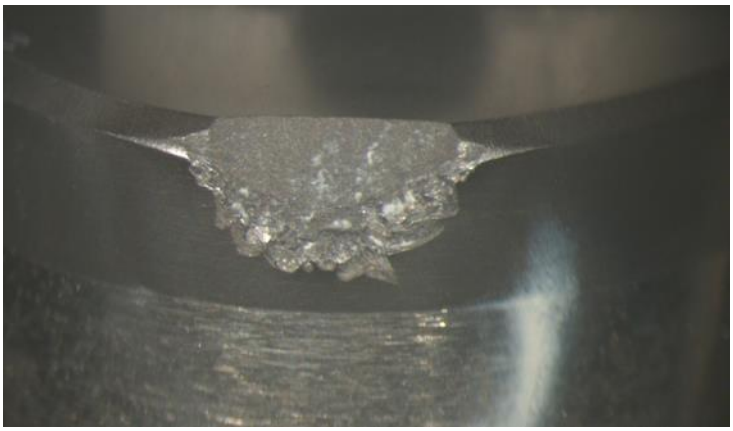


Figure 3.4: *Typical image of a wear scar of the PDC after VTL test for the experimental run conditions: 5 GPa, 1500°C and 25 minutes*

3.5.7 Density Determination using Geometric Method

To estimate the density of the sintered polycrystalline diamond compacts (PDCs), a geometric approach was employed. This method assumed the sample geometry to be a cylindrical disk.

The procedure involved the following steps:

- Mass Measurement

The substrate portion of the PDC composite was removed using EDM cutting and each mass of the diamond table samples was measured using a digital mass balance (Kern analytical balance (Z741081)).

- Dimensional Measurement

The radius and height of each disk-shaped sample were measured using a digital calliper (Mitutoyo 500-171-30).

- Volume Calculation

The volume of each sample was calculated using the formula for a cylinder:

$V=\pi r^2 h$

where r is the radius and h is the height of the sample

- Density Calculation

Density was then computed using the standard formula:

$\rho=\text{Mass}/\text{Volume}$

It is acknowledged that this method may introduce variability due to geometric variations and measurement precision. Surface irregularities, non-uniform thickness, and deviations from ideal cylindrical geometry could give inconsistencies in the calculated density values.

3.6 Data analysis

3.6.1 Multiple Regression Analysis

Multiple regression analysis was performed using Minitab 21 software to establish the relationship between the independent variables (sintering pressure, temperature and holding time) and the dependent variable (leach rate). The leach rate (µm/h) was obtained from X-ray tomography measurements of the leached PDC samples.

3.6.2 Dominance Analysis (DA)

Dominance analysis was employed to determine the relative importance of the sintering parameters (pressure, temperature and holding time) affecting the leach rate. The leach rate data were analysed using dominance analysis using Minitab 21 software.

3.6.3 ImageJ Analysis

The SEM images were processed using a median filter with a radius of 2 pixels in ImageJ software (Version 1.46) to enhance contrast and reduce noise. The image brightness and contrast were adjusted to optimise feature visibility. A thresholding procedure was then applied to segment the images into pores (dark regions) and the solid matrix (bright regions). Manual thresholding was performed based on visual inspection. Manual thresholding was chosen rather than automatic thresholding in ImageJ for the following reasons:

- Visual Accuracy and Control: Manual thresholding allowed inspection and fine-tuning of the segmentation of pores (dark regions) and the solid matrix (bright regions) across varying image conditions. This was particularly important given the heterogeneity in contrast and brightness across samples, which could lead to inconsistent results with automatic methods.
- Avoiding Misclassification: Automatic thresholding algorithms (e.g., Otsu, Triangle, etc.) can sometimes misclassify regions due to noise, uneven illumination, or subtle grayscale variations. Manual adjustment ensured that only true pore regions were segmented, improving the reliability of porosity and pore morphology measurements.

It is acknowledged that automatic thresholding can be useful in certain contexts, but in the case of this study, manual thresholding provided greater precision and consistency for the specific characteristics of the PDC images. After thresholding, ImageJ was used for quantitative analysis of porosity and pore morphology (aspect ratio and Feret diameter).

3.6.4 Statistical analysis

The statistical analysis in this study was carried out using Minitab 21 software. Analysis of Variance (ANOVA) was performed to evaluate the significance of each term ($\alpha = 0.05$). Model adequacy was evaluated using R-squared test.

Chapter 4: Results

This chapter presents the findings derived from the data collected as described in Chapter 3.

4.1 Leach rate data

Tables 4.1 and 4.2 show the average leach rate for each unique combination of sintering parameters for all 64 individual experimental runs. These leach rate data were derived from the leach depth measurements in Appendix A. Table 4.1 shows the leach rate data for data points 1 – 30 and Table 4.2 shows the leach rate data for data points 31 – 64. The experiments had three levels of pressure (5, 6 and 7 GPa), three levels of temperature (1500, 1600 and 1700 °C), and three levels of holding time (20, 25 and 30 minutes), resulting in 27 unique combinations. To assess experimental variability and improve the reliability of the results, replicate experiments were added at several combinations of these parameters, leading to a total of 64 experimental runs. Replicate experiments (i.e., repeating an experimental run with a specific pressure, temperature, and holding time) were done to estimate inherent random variation due to uncontrolled factors, measurement errors, slight differences in material preparation, or instrument fluctuations.

Initially I listed all 64 individual runs to show the raw data from 3^3 factorial design experiments.

***Table 4.1**: Leach rate data for data points 1 – 30*

	Independent variables			Response variable
	x_1	x_2	x_3	y
Run order	**Pressure (GPa)**	**Temperature (°C)**	**Holding time (min)**	**Leach rate (μm/h)**
1	6	1600	25	3.69 ± 0.02
2	5	1500	30	6.98 ± 0.03
3	7	1700	20	1.15 ± 0.01
4	7	1700	30	0.72 ± 0.02
5	5	1500	20	10.14 ± 0.08
6	7	1500	30	3.16 ± 0.02
7	6	1600	25	4.61 ± 0.03
8	6	1600	25	4.74 ± 0.01
9	5	1700	20	5.22 ± 0.04
10	5	1700	30	4.85 ± 0.02
11	7	1500	20	3.56 ± 0.03
12	5	1700	20	5.20 ± 0.02
13	7	1500	30	3.47 ± 0.07
14	6	1600	25	4.64 ± 0.06
15	7	1700	30	0.68 ± 0.02
16	6	1600	25	4.72 ± 0.07
17	6	1600	25	4.75 ± 0.01
18	5	1700	30	4.84 ± 0.04
19	7	1700	20	1.17 ± 0.02
20	5	1500	20	10.29 ± 0.06
21	5	1500	30	7.05 ± 0.07
22	7	1500	20	10.24 ± 0.09
23	6	1600	25	4.71 ± 0.08
24	5	1700	20	5.21 ± 0.02
25	6	1600	25	4.61 ± 0.04
26	6	1600	25	4.73 ± 0.06
27	7	1500	30	3.49 ± 0.02
28	5	1700	30	4.86 ± 0.05
29	7	1700	20	1.16 ± 0.01
30	5	1500	30	7.06 ± 0.09

***Table 4.2**: Leach rate data for data points 31 – 64*

	Independent variables			Response variable
	x_1	x_2	x_3	y
Run order	**Pressure (GPa)**	**Temperature (°C)**	**Holding time (min)**	**Leach rate (µm/h)**
31	7	1500	20	3.55 ± 0.06
32	5	1500	20	10.32 ± 0.09
33	7	1700	30	0.69 ± 0.03
34	7	1700	30	0.74 ± 0.01
35	5	1500	30	7.08± 0.02
36	7	1700	20	1.18 ± 0.04
37	7	1500	30	3.48 ± 0.02
38	6	1600	25	4.64 ± 0.03
39	6	1600	25	4.76 ± 0.02
40	5	1600	30	4.90 ± 0.03
41	7	1500	20	3.56 ± 0.05
42	5	1500	20	10.44 ± 0.08
43	6	1600	25	4.66 ± 0.03
44	5	1700	20	4.70 ± 0.05
45	7	1700	30	0.92 ± 0.01
46	5	1700	30	4.89 ± 0.01
47	7	1500	30	3.45 ± 0.04
48	6	1600	25	4.63 ± 0.02
49	5	1500	30	7.05 ± 0.07
50	5	1500	20	10.30 ± 0.09
51	7	1500	20	3.60 ± 0.03
52	5	1700	20	4.85 ± 0.02
53	6	1600	25	4.64 ± 0.05
54	7	1700	20	1.17 ± 0.01
55	6	1600	25	4.61 ± 0.01
56	5	1600	25	6.94 ± 0.03
57	6	1600	20	5.80 ± 0.06
58	6	1600	30	4.57 ± 0.02
59	6	1700	25	5.21 ± 0.04
60	6	1600	25	4.86 ± 0.07
61	7	1600	25	3.65 ± 0.04
62	6	1500	25	4.58 ± 0.03
63	6	1600	25	4.85 ± 0.03
64	6	1600	25	5.89 ± 0.06

4.2 SEM-BSE images of pre-leached samples

Figure 4.1 shows SEM-BSE images of the pre-leached diamond layer of the 27 experimental runs, excluding replicate runs. These micrographs were taken from the top of the diamond layer. Temperature changes reading across the page and pressure changes reading down the page. Holding time changes when turning over the pages (with pressure and temperature staying in the same place).

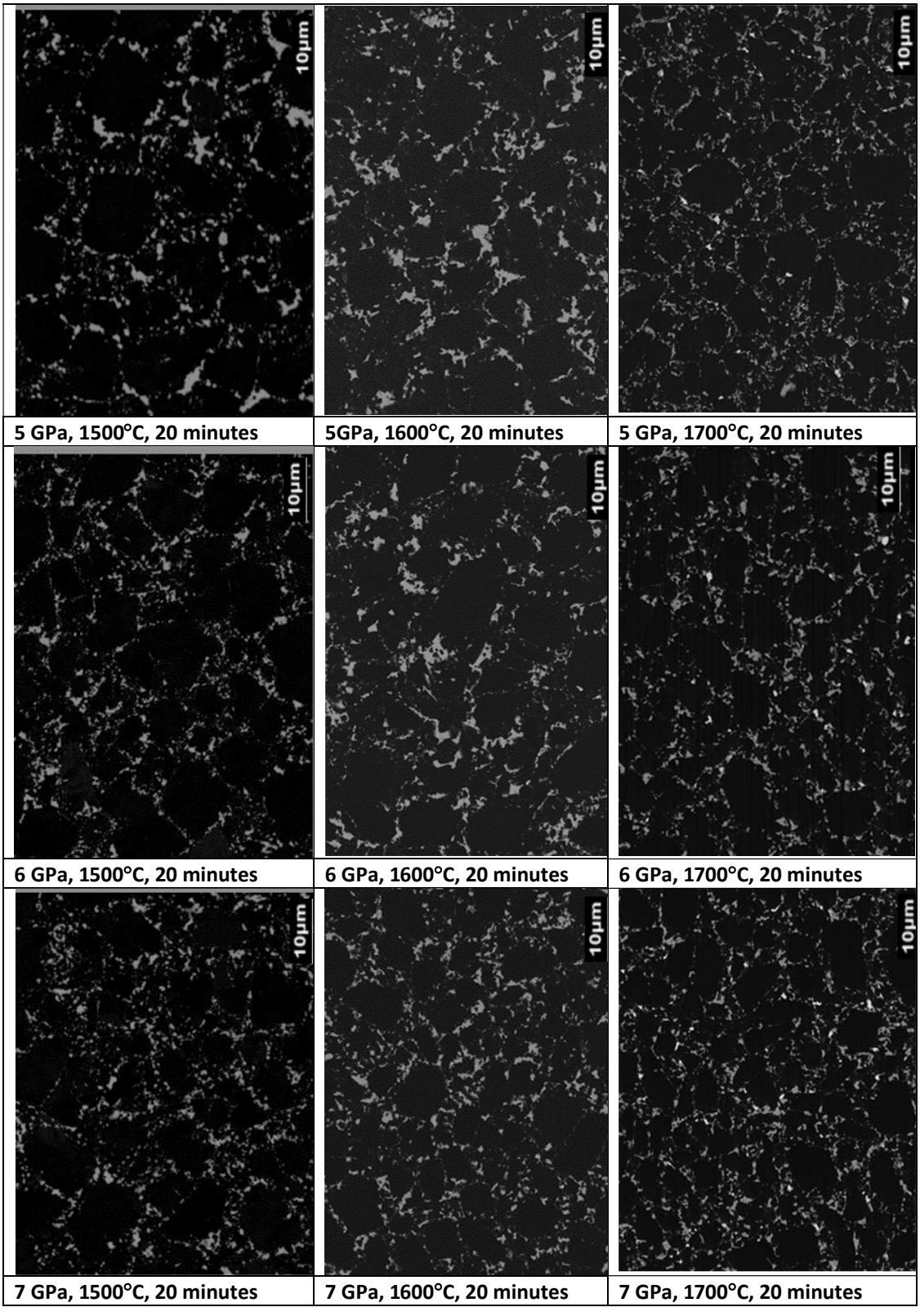


Figure 4.1: *SEM-BSE images showing the effect of sintering variables on the microstructures of the diamond layer, showing: cobalt pools (medium grey contrast), diamond (dark contrast) and tungsten carbide (light grey contrast)*

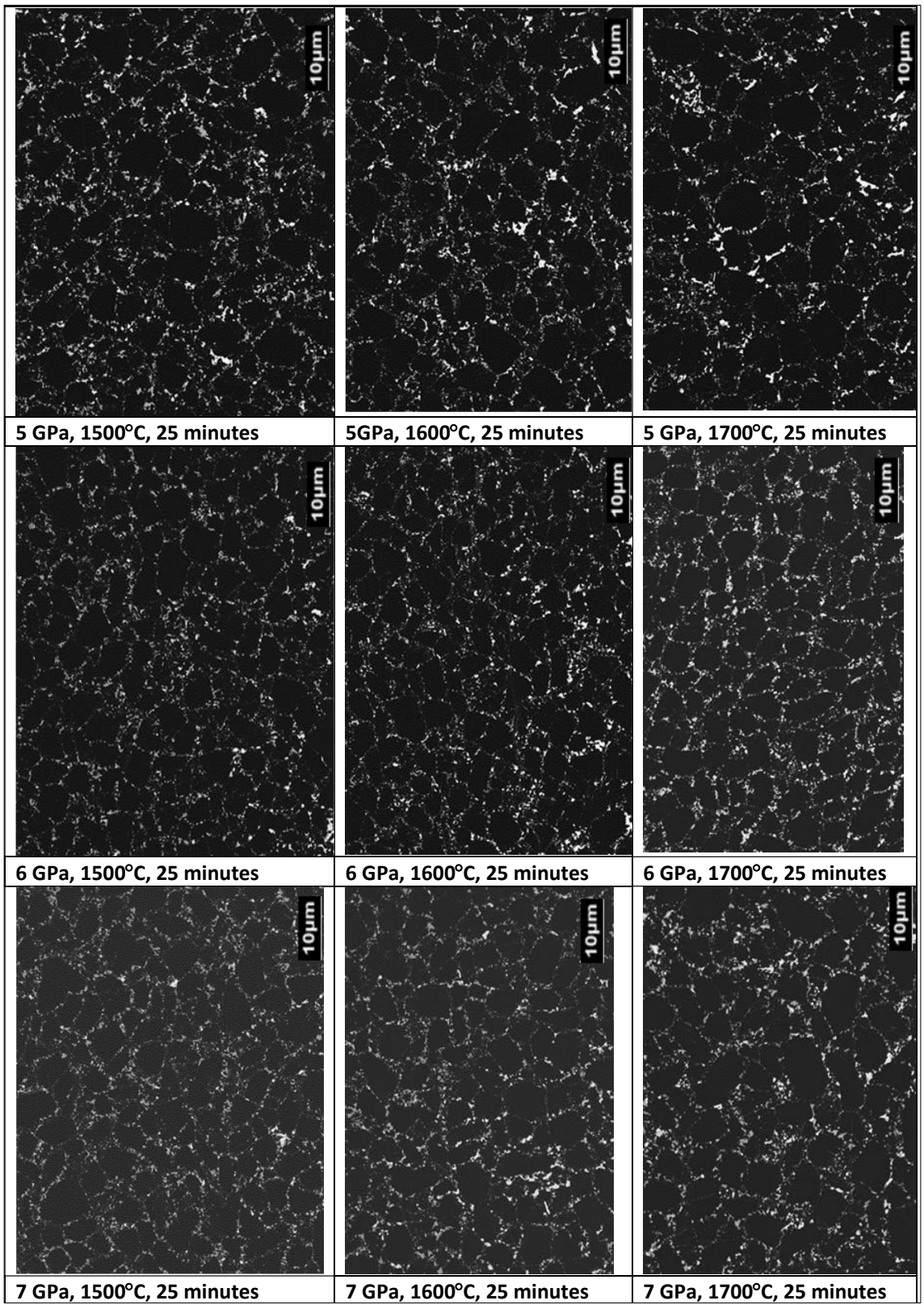


Figure 4.1 (continued): *SEM-BSE images showing the effect of sintering variables on the microstructures of the diamond layer, showing: cobalt pools (medium grey contrast), diamond (dark contrast) and tungsten carbide (light grey contrast)*

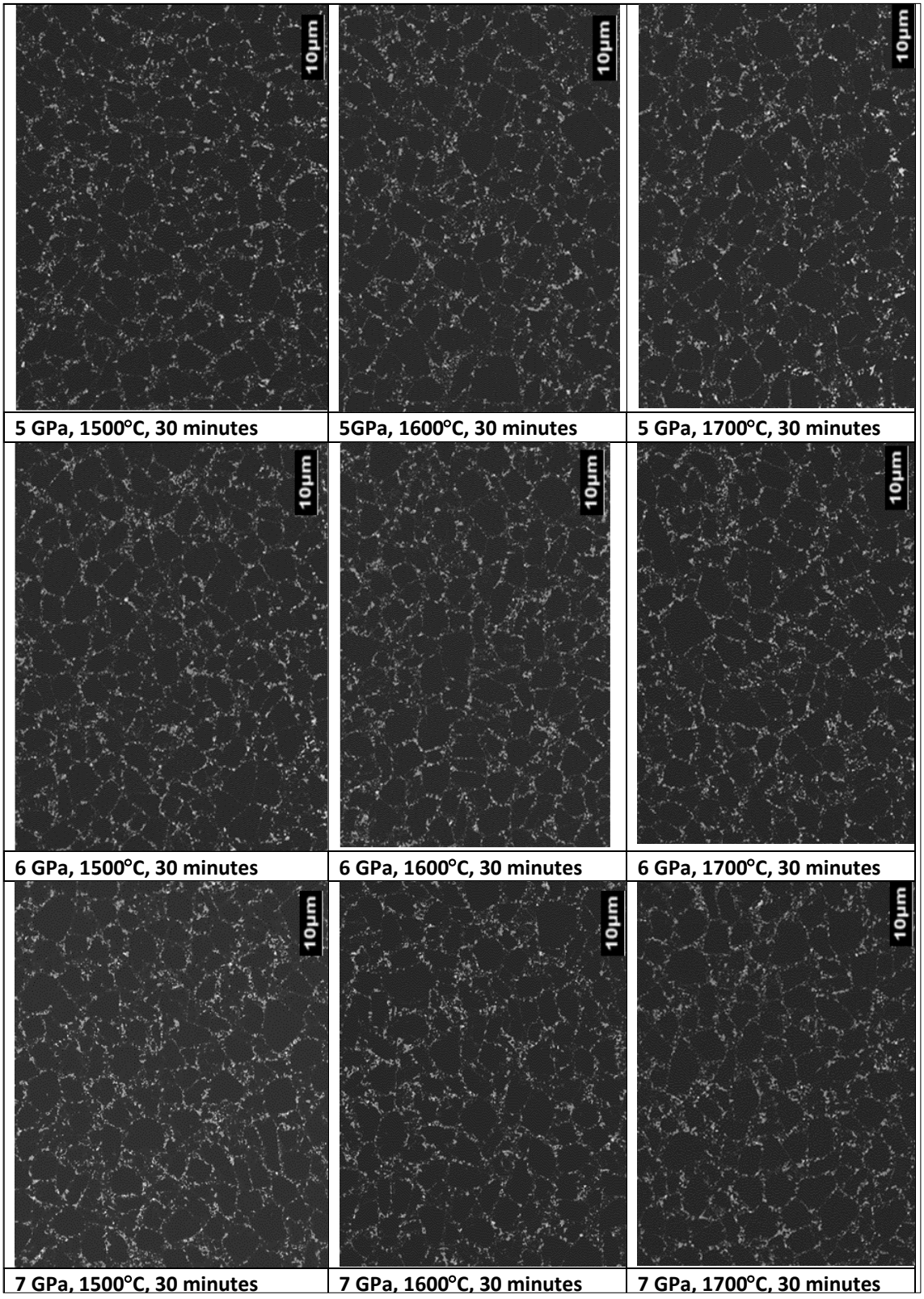


Figure 4.1 (continued): *SEM-BSE images showing the effect of sintering variables on the microstructures of the diamond layer, showing: cobalt pools (medium grey contrast), diamond (dark contrast) and tungsten carbide (light grey contrast)*

4.3 SEM-BSE images of leached samples

From the 27 leached experimental runs, excluding replicates, samples from nine runs were studied on an SEM. Figure 4.2 shows SEM-BSE images of the laser cut, leached and polished samples from nine experimental runs. The samples had porosity and a continuous network of diamond with tungsten carbide particles. However, there was a possible removal of some of the Co and WC phases during sample preparation because the pores are located close to the WC grains and the dark contrasts are interconnected and are not spherical.

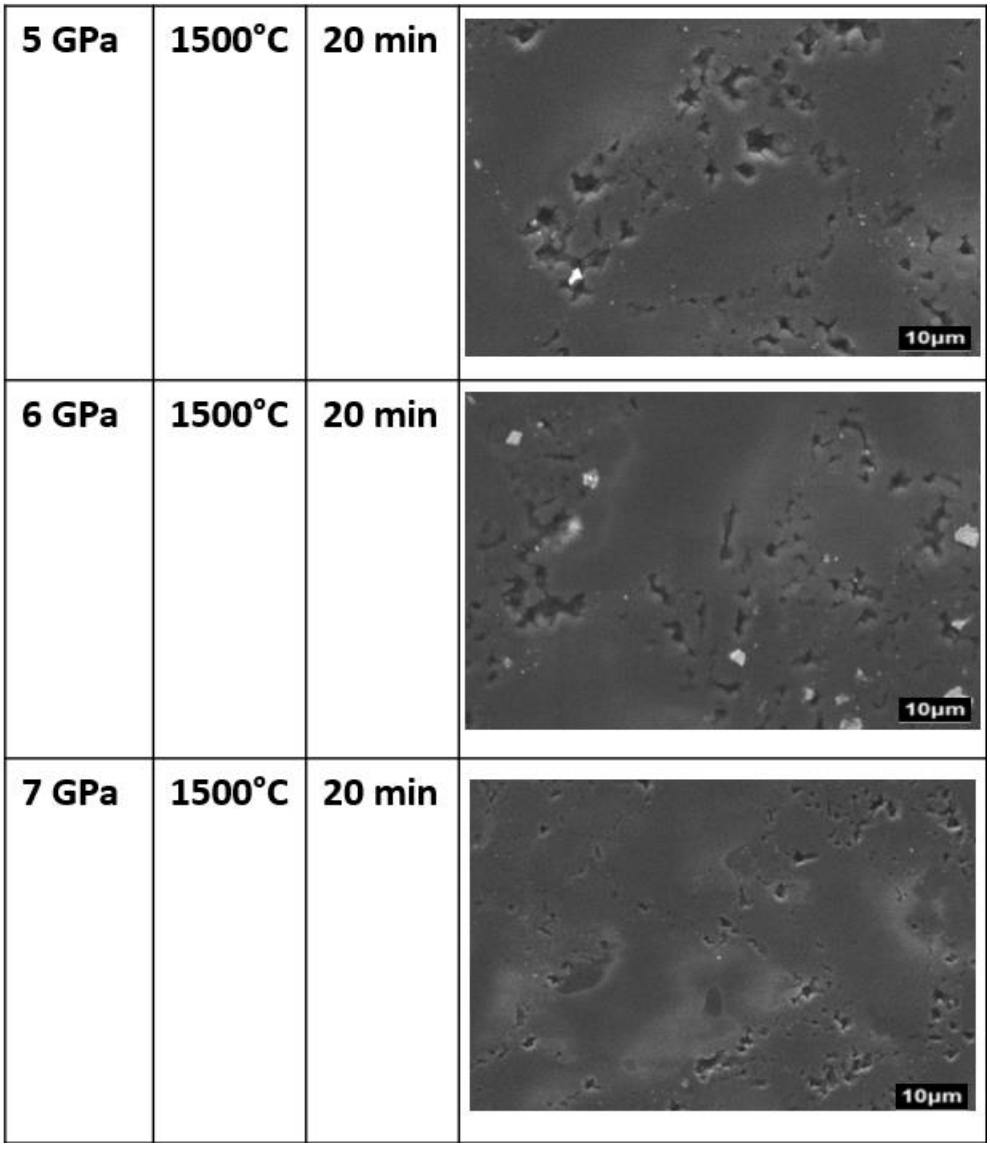


Figure 4.2: *SEM-BSE images of leached and polished samples from nine experimental runs, showing: diamond (medium grey contrast), porosity (dark contrast) and tungsten carbide (light contrast)*

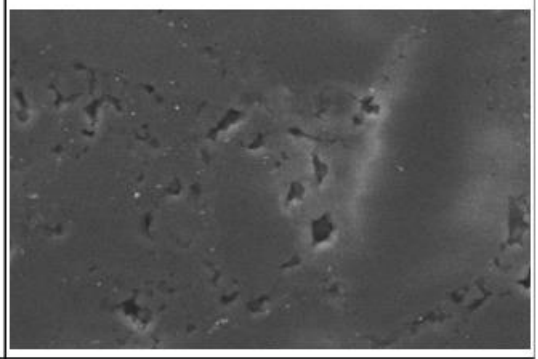
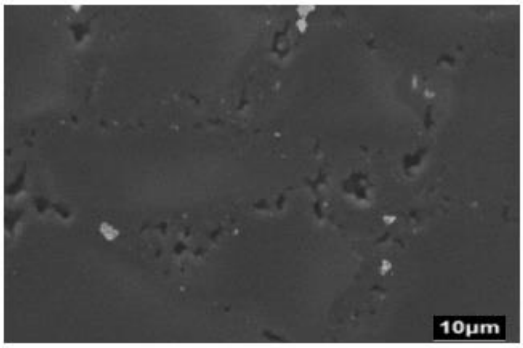
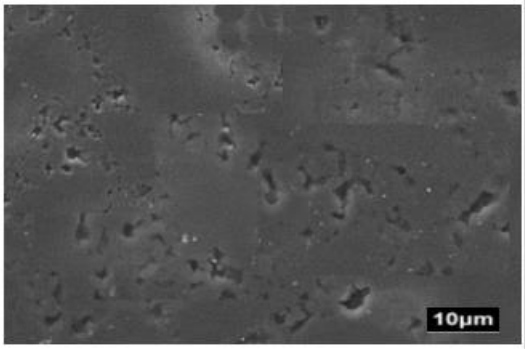
5 GPa	**1500°C**	**20 min**	
5 GPa	**1600°C**	**20 min**	
5 GPa	**1700°C**	**20 min**	

Figure 4.2 (continued): *SEM-BSE images of leached and polished samples from nine experimental runs, showing: diamond (medium grey contrast), porosity (dark contrast) and tungsten carbide (light contrast)*

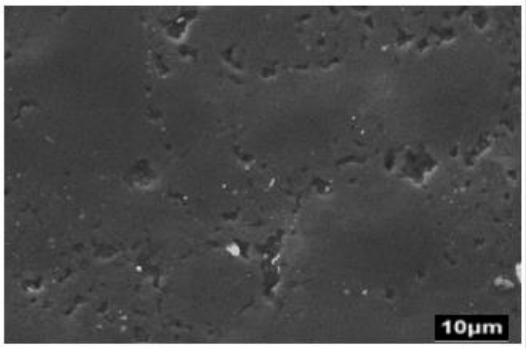
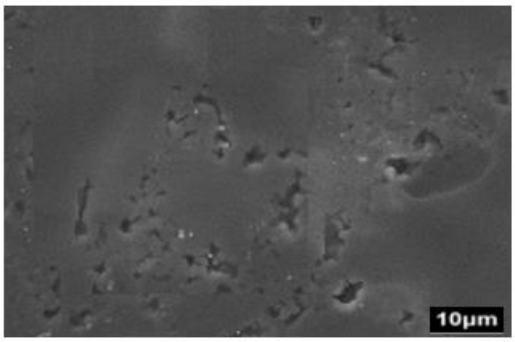
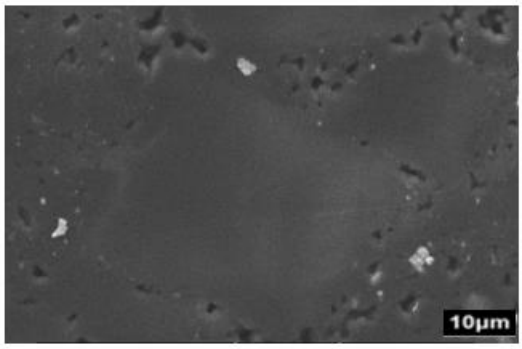
5 GPa	1500°C	20 min	
5 GPa	1500°C	25 min	
5 GPa	1500°C	30 min	

Figure 4.2 (continued): *SEM-BSE images of leached and polished samples from nine experimental runs, showing: diamond (medium grey contrast), porosity (dark contrast) and tungsten carbide (light contrast)*

4.4 SEM-BSE images for unleached and leached samples

From the 27 experimental runs, one unleached sample and one leached sample were analysed on SEM. Figure 4.3 shows SEM images of both unleached and leached PDC samples, demonstrating the cobalt removal during leaching. The unleached sample had cobalt pools distributed within the diamond matrix, and in the leached sample, the cobalt pools had been removed, leaving porosity that characterises the leached microstructure similar to leached samples in Figure 4.2.

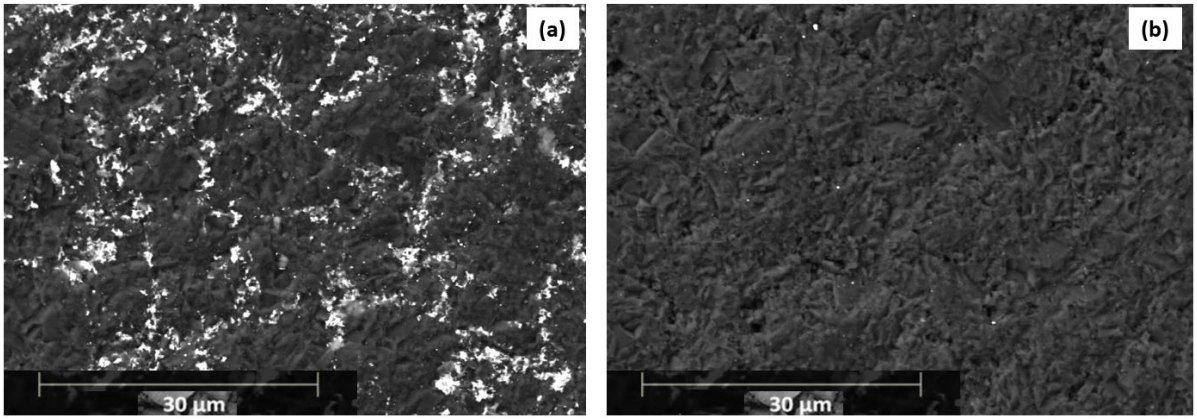


Figure 4.3: *SEM-BSE images of the sintered PDC samples showing: (a) unleached and (b) leached, with cobalt pools (light contrast), porosity (dark contrast) and diamond (medium dark contrast). Experimental run conditions: 5 GPa, 1500°C and 25 minutes*

4.5 XRD results

The one unleached sample and one leached sample (Figure 4.3) were also analysed by XRD. Figure 4.4 shows the effectiveness of leaching in removing cobalt from the PDC cutters. Both XRD patterns indicated tungsten carbide (WC), Co_3W and carbon (C), as expected. The intensity of the Co_3W peak at 59° was lower in the leached sample, indicating less of this phase after leaching. The peak at 51° is a combination of peaks from two phases, C (diamond, the major component of PCD) and Co_3W. The diamond signal overshadowed the decrease from Co_3W peak, making the 51° peak unreliable for assessing Co_3W reduction.

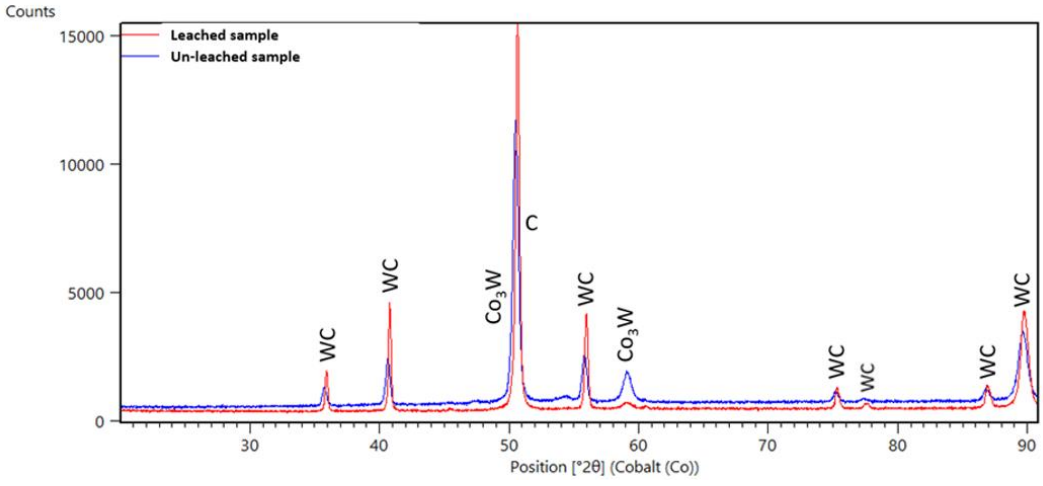


Figure 4.4*: XRD patterns for the unleached and leached diamond layer samples.*

4.6 RIR results

Reference intensity ratio (RIR) analysis was performed on one leached and one unleached PDC sample (Figure 4.3). The relative amounts of cobalt and tungsten

phases in these samples were determined using RIR quantitative phase analysis, as shown in Table 4.3.

Table 4.3: *Reference Intensity ratio (RIR) values for the leached and unleached diamond layer samples.*

RIR	Leached PCD	Unleached PCD
Cobalt (Co_3W)	0.20 ± 0.01	0.91 ± 0.03
Tungsten carbide (WC)	1.11 ± 0.02	1.21 ± 0.01

4.7 XRF results

X-ray fluorescence (XRF) analysis was performed on one leached and one unleached PDC sample (see Figure 4.3). The cobalt-to-tungsten (Co/W) ratios for these samples are listed in Table 4.4.

Table 4.4*: XRF results showing the cobalt to tungsten ratio (Co/W) between leached and unleached samples.*

Parameter	Leached PCD	Unleached PCD
Co/W Ratio	0.23 ± 0.01	0.46 ± 0.03

4.8 EDX results

The one unleached sample (Figure 4.3) was analysed by EDX. This sample was sintered with the sintering conditions of 5 GPa, 1500 °C and 20 minutes. The EDX results corroborate the XRD findings, confirming that the samples used in this study contained diamond, cobalt, and tungsten. Table 4.5 shows the quantitative EDX results, showing the weight percentages of diamond, cobalt, and tungsten. While tungsten was clearly present in the sample as shown by both EDX and the X-ray map, the bulk EDX analysis presented in Table 4.5, including regions of both diamond and tungsten carbide, cannot definitively quantify the presence of tungsten carbide due to the large carbon signal from the diamond including matrix. Additionally, there is a large standard deviation for the small value of W and even a large standard deviation for Co (Table 4.5), showing that there was variation in the results. Figure 4.5 shows inconsistencies

between its two parts, showing that there were problesm with data capture: a) indcated small regions of a higher atomic number region (either WC or W) than Co, while b) indicated that nearly all of the same region was tungsten. Additionally, light elements such as carbon can be overrepresented in compositional analysis due to matrix effects or limitations in detection techniques [150].

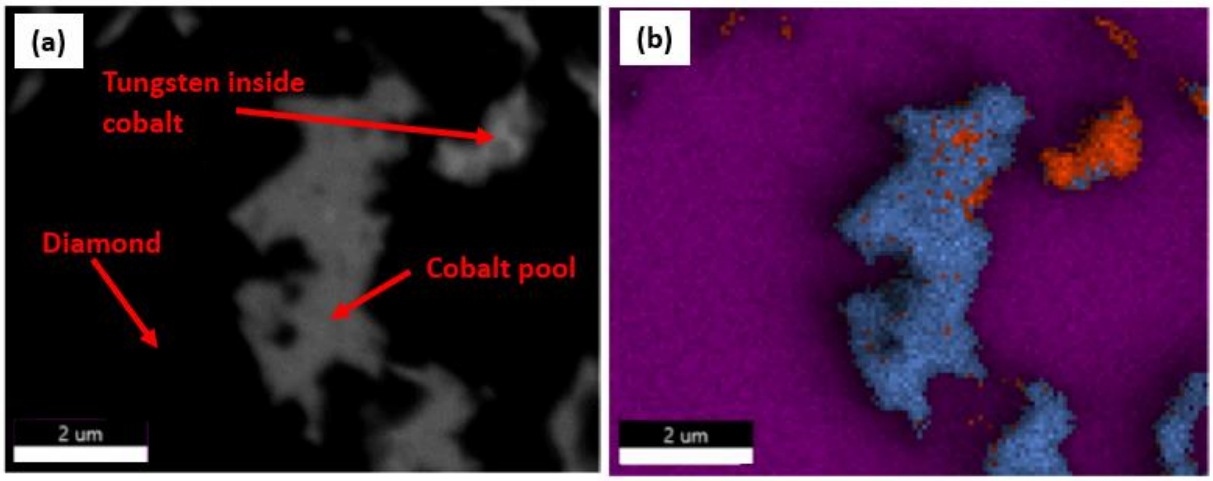


***Figure 4.5**: unleached sample: (a) SEM-BSE image showing diamond (dark), cobalt (medium grey) and tungsten (light) and (b) X-ray map showing cobalt (blue), tungsten (orange) and diamond (purple)*

***Table 4.5:** EDX results of unleached sample.*

Sample	Diamond (wt%)	Cobalt (wt%)	Tungsten (wt%)
Unleached sample	88.8 ± 0.9	9.1 ± 2.0	2.1 ± 1.2

4.9 Density measurements results

Table 4.6 shows the density measurements of sintered PDC samples under varying pressure, temperature, and holding time conditions. Taking the standard deviations into account, there was no significant variation across the tested ranges.

Table 4.6: Density measurements of sintered PDC samples under varying conditions

Effect of Pressure (GPa)	**5**	**6**	**7**
Density (g/cm^3)	3.1 ± 0.2	3.3 ± 0.1	3.2 ± 0.2
Temperature (°C)	**1500**	**1600**	**1700**
Density (g/cm^3)	3.3 ± 0.3	3.4 ± 0.1	3.1 ± 0.2
Time (Minutes)	**20**	**25**	**30**
Density (g/cm^3)	3.3 ± 0.1	3.1 ± 0.3	3.4 ± 0.3

Chapter 5: Challenges and Advances in Accurate Process Parameter Control

The successful synthesis of PDCs by HPHT sintering relies heavily on precise control of the process parameters, particularly pressure and temperature. Accurate measurement and control of these parameters is crucial for achieving the desired microstructure, phase compositions and ultimately, the mechanical properties of the final product. However, the extreme conditions within the HPHT apparatus present significant challenges for accurate parameter determination. This chapter explores these challenges and describes the investigation undertaken made in this research towards achieving more accurate and reliable pressure and temperature control during PDC sintering.

5.1 *Ex Situ* Pressure Calibration

5.1.1 Introduction

Precise pressure management is critical during the sintering of PDCs to achieve targeted material properties. Therefore, accurate pressure measurement is essential for both research and industrial HPHT processes. Conventional pressure calibration techniques in high-pressure equipment, like cubic presses, often utilise fixed-point phase transitions of known materials, usually measured at ambient temperature [18,100]. However, these established methods suffer from several drawbacks. Firstly, they are susceptible to non-hydrostatic stress states within the pressure cell. Secondly, the pressure-transmitting medium can affect the actual pressure experienced by the sample, introducing uncertainty, so the medium choice is important. Thirdly, precisely detecting phase transitions can be challenging [18]. Factors such as the press setup itself, the high temperatures involved and large sample size, interfering with measurements can complicate the interpretation of results. Fourthly, extrapolating room-temperature calibration data to the elevated sintering temperatures can lead to significant inaccuracies, as material properties and behaviour change with temperature. This section introduces a novel real-time pressure calibration method designed to overcome these limitations, providing more accurate and material-specific pressure determination directly during PDC sintering.

5.1.2 Methodology

The *ex situ* pressure calibration method was based on direct measurements of the volume change of a PDC sample (diamond powder with cobalt) during sintering, coupled with the Murnaghan equation of state [140] for a more direct and relevant calibration compared to conventional fixed-point methods. The experimental set-up and procedure are described in detail in Chapter 3.

5.1.3 Results

To quantify the observed densification of the diamond powder compacts during sintering, an empirical fitting approach based on the Murnaghan equation of state was utilised [140]. While its fundamental application is for elastic compression, here it served as an expression to relate the applied conditions to the relative volume change (V/V_o) and a calculated effective “resistance to compaction”. This allowed the establishment of a practical “sintering conditions calibration” for the cubic press used. Figure 5.1 illustrates this relationship, plotting the derived “sample pressure” (calculated from the Murnaghan EOS, representing the effective pressure required for the observed densification) against the measured *ex situ* relative volume (V/V_0) for the PDC sample. The data show the progressive plastic deformation and porosity reduction occurring within the compacts.

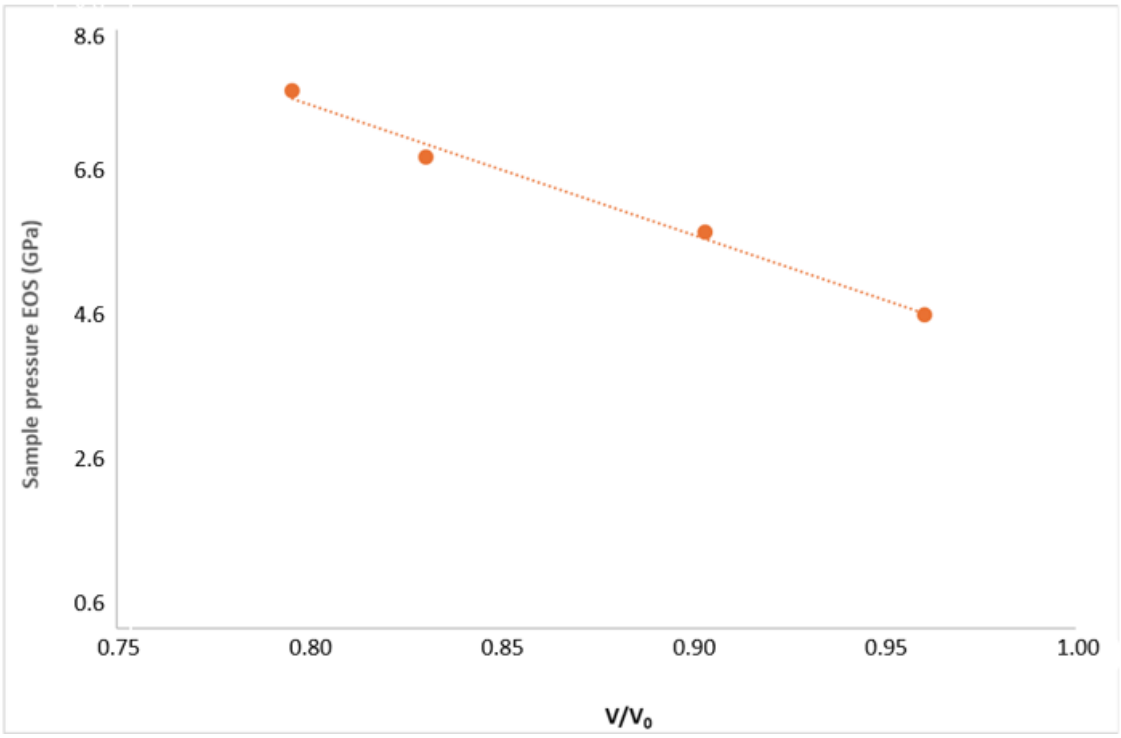


***Figure 5.1**: Relationship between sample pressure, calculated from the Murnaghan equation of state (EOS), and measured relative volume (V/V_o) for the PDC samples. The dashed line is a linear fit to the calculated data*

To provide a baseline for understanding the applied conditions, Figure 5.2 shows the calculated nominal pressure (P = F/A) applied by the rams of the cubic press as a function of ram load. This nominal pressure was determined directly from the applied ram force (F) and the ram face area (A). To assess the accuracy and inherent limitations of this simple calculation for determining the actual sample pressure within the cell, this nominal pressure curve was compared against the internationally recognised pressure values for several fixed-point phase transitions [18, 137-140]. These reported pressure values for these transitions, as reviewed and recommended as standard values by Decker et al. [18], were obtained from Bridgman [137] for Bi I-II (25.5 kbar), Kennedy et al. [138] for Tl II-III (36.7 kbar), Drickamer [139] for Ba I-II (55 kbar) and Haygarth et al. [140] for Bi III-V (77 kbar). The measured pressures deviated from the values of Decker et al. [18], with the largest discrepancy observed near the Ba I-II and Bi III-V transitions.

The "'Measured pressure" data points represent the nominal pressures calculated from P=F/A corresponding to the ram loads at which these fixed-point transitions (Bi I-II, Tl II-III, Ba I-II, Bi III-V) were observed in this cubic press. The data points represent

known absolute pressure values for these transitions and are plotted against their corresponding ideal ram loads [18].

Figure 5.2 shows a significant deviation between the nominal pressure calculated by P=F/A and the actual, independently established fixed-point pressures. This discrepancy, particularly noticeable near the Ba I-II and Bi III-V transitions, demonstrates the limitations of using a simple P=F/A calculation for determining the true pressure within a cubic press. Factors such as friction between the rams and dies, friction within the gasket assembly, and pressure gradients within the cell significantly reduce the actual pressure experienced by the sample compared to the nominal applied pressure. Therefore, while P=F/A provided a reference for the applied ram load, it did not represent an accurate sample pressure calibration for the system used.

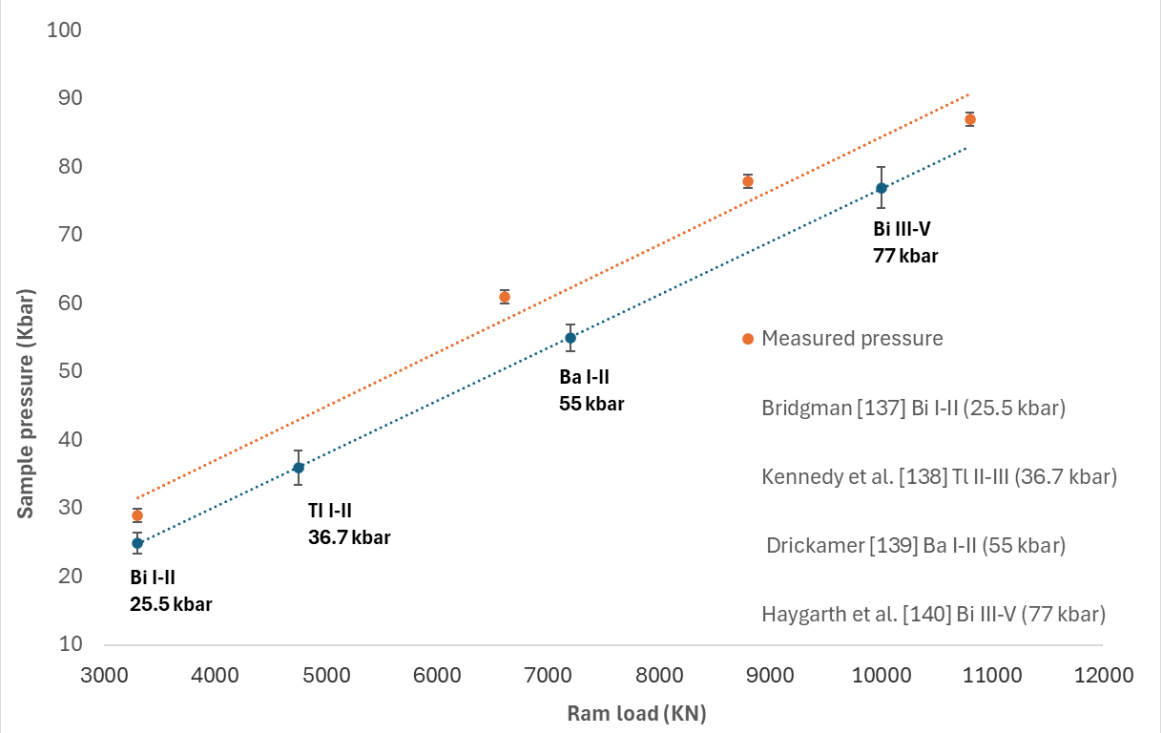


Figure 5.2: *Comparison of the pressure calibration curve with reported values for fixed-point pressure transitions [18]*

The wear resistance of the sintered PDC samples was evaluated by the VTL (Vertical Turret Lathe) wear test method [2,3,4] to assess their tribological properties under application-relevant conditions. Figure 5.3 compares the wear scar area of a PDC sample sintered from this study with PDC samples of Jivanji et al. [3], Dai et al. [4] and Zhao et al. [2]. The wear scar area was used to assess wear resistance, with smaller values indicating better wear performance [4]. Zhao et al. [2] did not report the

starting grain size. While direct comparison of absolute pressure values between different high-pressure systems can be difficult (as shown in Figure 5.2), this comparison demonstrated the similar wear resistance of the current material and the effectiveness of the current sintering conditions in producing functional PDCs.

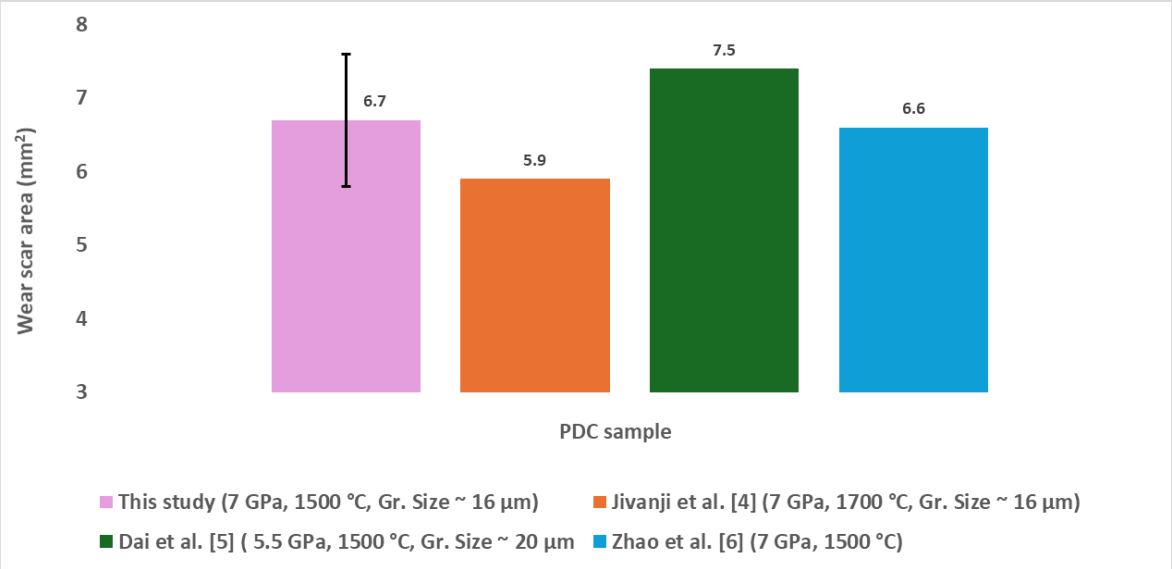


Figure 5.3: *Comparison of VTL wear test results for PDC Samples: current data and values from Jivanji et al. [3], Dai et al. [4] and Zhao et al. [2]*

5.2 Temperature Measurement and the Effect of Thermocouple Placement

5.2.1 Introduction

Accurate temperature measurement during high-pressure, high-temperature sintering is important for controlling the sintering process and achieving the desired properties in PDCs. However, the extreme conditions within the cubic press present difficulties for accurate temperature monitoring. Steep temperature gradients, the effect of pressure on thermocouple output and potential chemical reactions between the thermocouple and surrounding materials can all contribute to measurement errors [73, 75]. In a cubic press, which lacks direct thermocouple control, the precise distance between the sample and the monitoring thermocouple is important. The user inputs a desired power level on the control panel, and a thermocouple is then inserted to measure the resulting temperature. Since there is no independent temperature regulation by the thermocouple, any variation in the distance between the sample and the thermocouple will lead to inconsistent and unreliable temperature readings. This

section describes the effect of thermocouple placement on temperature measurement accuracy during PDC sintering in a cubic press, indicating a key source of potential error, and discusses the implications for process control and product quality.

5.2.2 Methodology

The experimental set-up for investigating the influence of thermocouple placement is described in detail in Chapter 3 (Materials and Methods).

5.2.3 Results

Figure 5.5 compares the temperature readings from two Type S thermocouples during a sintering run, where the sample was contained in a titanium cup. One thermocouple was in direct contact with the sample (and thus the titanium cup, 0 mm gap), while the other was positioned with a 1 mm gap. Figure 5.5 shows the temperature readings from thermocouples at 0 mm and 1 mm separation from the titanium cup. While both thermocouples recorded similar temperature profiles up to approximately 1400°C, the 0 mm thermocouple began to exhibit increasingly erratic readings, including sharp spikes, above this temperature. Despite the instability, the 0 mm thermocouple reached a similar peak temperature to the 1 mm thermocouple, but at a slightly earlier time.

This failure was unexpected, as Type S thermocouples are rated for short term use up to 1750°C, significantly higher than the temperature at which the thermocouple failed. The premature failure was well below the expected temperature limits, indicating that factors other than simply exceeding the rated temperature were responsible. Subsequent examination of the failed thermocouple revealed localised melting at the point of contact with the titanium cup. In contrast, the thermocouple positioned 1 mm away from the sample maintained stable temperature readings throughout the experiment and did not fail, demonstrating the localised issue at the point of contact for the failed thermocouple.

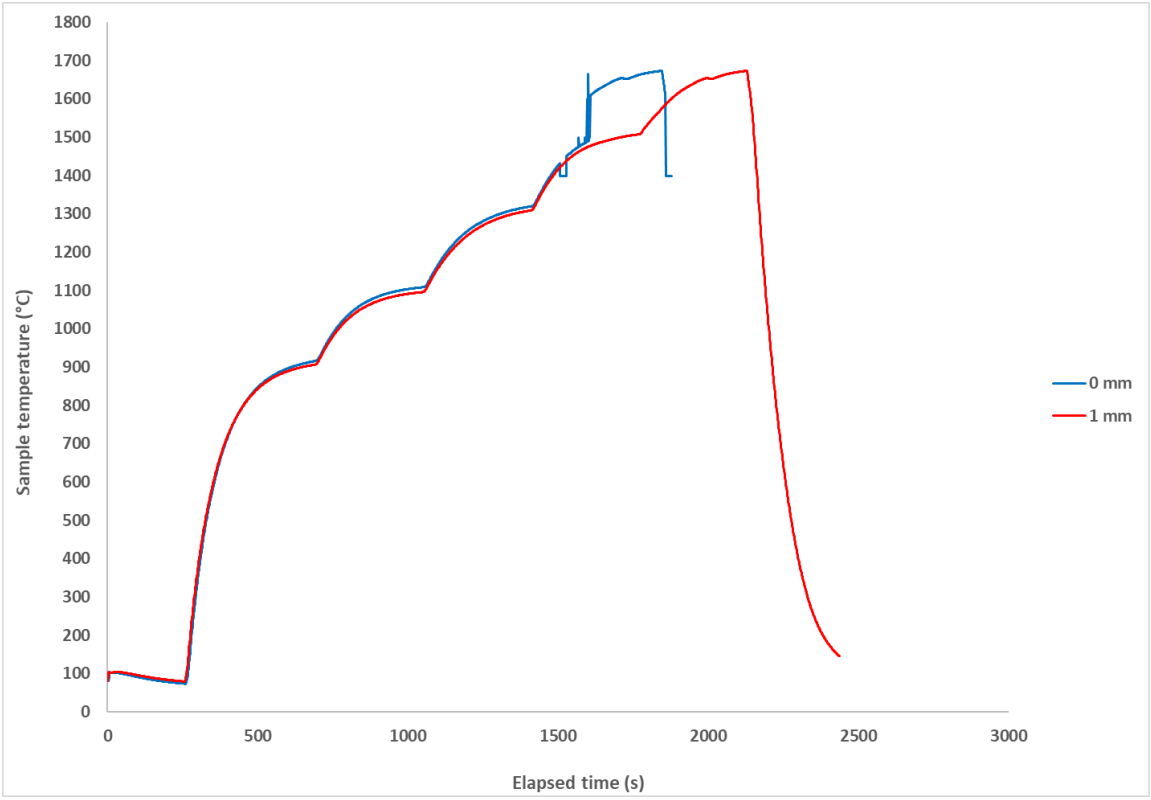


Figure 5.4: *Effect of sample-thermocouple proximity on temperature measurement reliability*

Figure 5.6 shows an X-ray radiographic image of the experimental set-up with a thermocouple inserted inside the capsule, with the PDC sample, heater, thermocouple, and the hot junction positioned within the pyrophyllite capsule. This image shows the accurate placement of the thermocouple within the capsule, ensuring that the hot junction was very near the PDC sample, positioned between the sample and the graphoil heater, for reliable temperature measurement.

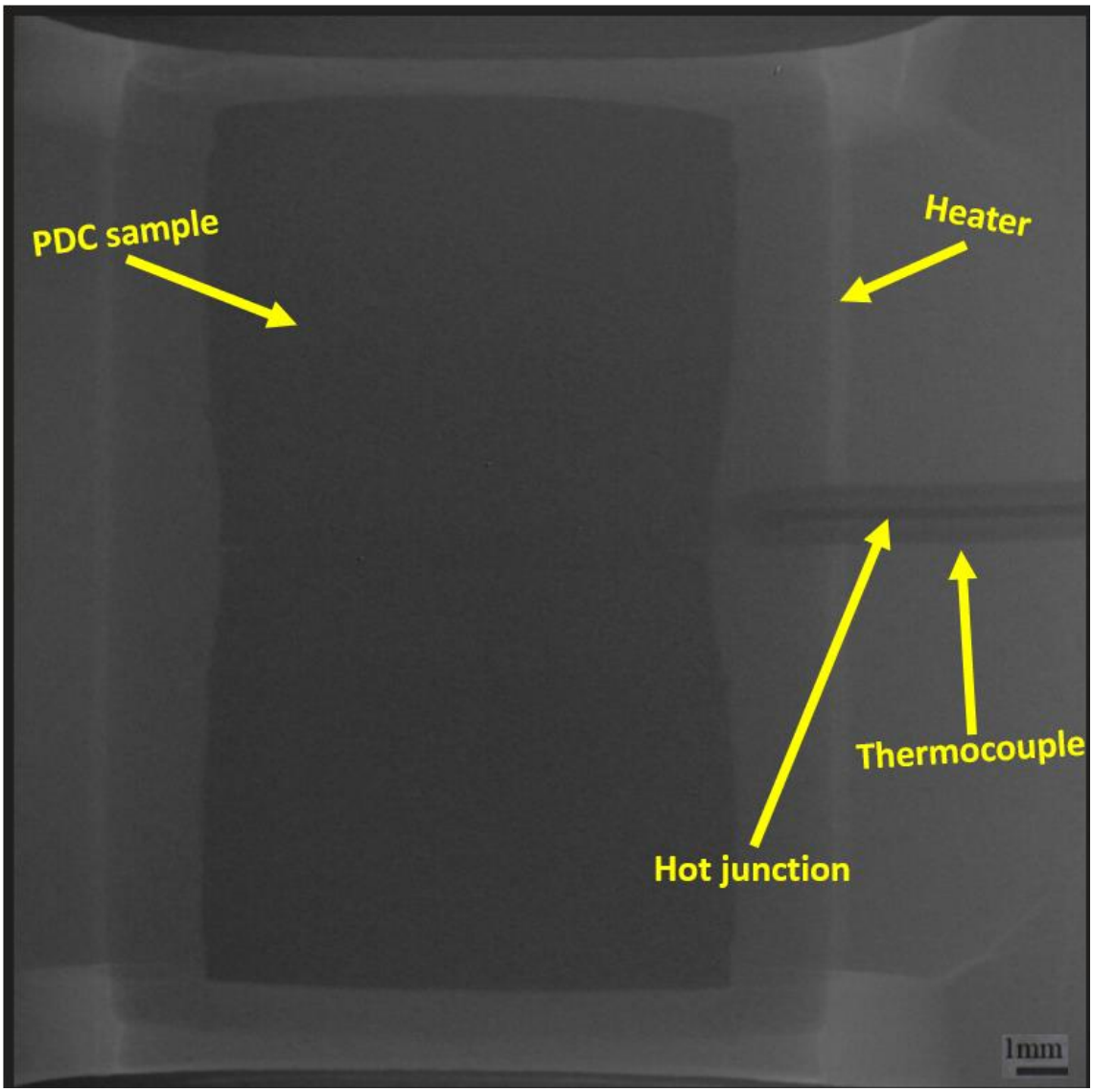


Figure 5.5: *X-ray radiographic image of the sample assembly with a thermocouple inserted, showing heater (light line contrast), PDC sample (dark contrast), and hot junction (black line). (Figure3.6 shows a line drawing of this sample assembly)*

Table 5.1 shows the PDC sample temperature measurements, indicating that as the thermocouple was moved further away from the sample (and especially when moved outside the heater), the measured temperature decreased. There were large temperature differences between measurements taken inside and outside the heater as expected. A relatively small temperature gradient was observed inside the heater, with a difference of only about 3°C between 1 mm and 3 mm away from the sample. Conversely, a much steeper gradient was observed outside the heater, with a temperature drop of approximately 35°C between 4 mm and 6 mm. Table 5.1 shows that the overall temperature decrease was about 50°C between 1 mm and 6 mm distance. The overall average gradient from 1 mm to 6 mm was approximately

10°C/mm, while the gradient outside the heater, between 4 mm and 6 mm, was steeper, at around 17.5°C/mm.

***Table 5.1**: Effect of thermocouple position on measured temperature with measuring thermocouples in a cubic press*

Thermocouple position	Temperature 1 (°C)	Temperature 2 (°C)	Temperature 3 (°C)
Inside the heater	1510.3 ± 3.1	1511.7 ± 3.3	1509.5 ± 3.2
Outside the heater	1495.2 ± 3.4	1481.9 ± 3.8	1459.1 ± 3.5

Figure 5.6 shows SEM-BSE images of the PDC samples sintered with two different thermocouple positions. The sample sintered with the thermocouple placed inside the heater (Figure 5.6a) had a well-developed microstructure characterised by extensive neck formation between diamond grains. The grain boundaries were well-defined, indicating good bonding. The diamond grains were well-sintered, with a relatively uniform distribution of cobalt and tungsten carbide. In contrast, the PDC sample sintered with the thermocouple placed outside the heater (Figure 5.6b) shows that the necks between diamond grains were less developed and, in some areas, appeared to be absent. Figure 5.6b shows more precipitation of tungsten carbide at the grain boundaries and triple junctions.

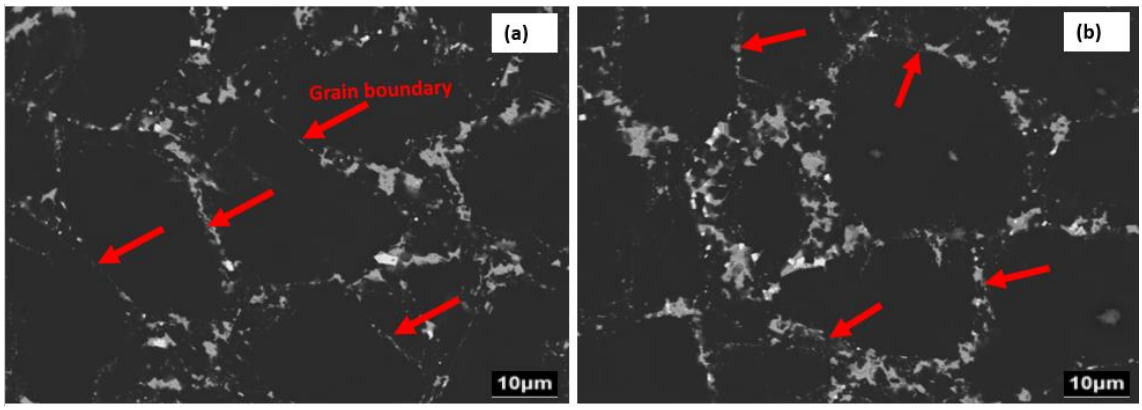


***Figure 5.6**: SEM-BSE images of the PDC samples sintered with two different thermocouple positions: (a) inside the heater (b) outside the heater, showing well-defined grain boundaries (red arrows), showing diamond (dark contrast), tungsten carbide (light contrast) and cobalt (medium grey contrast). The sintering conditions were 6 GPa, 1500°C and 20 minutes*

Table 5.2 shows that the PDC sample sintered with the thermocouple placed inside the heater had smaller wear scar area than the sample sintered with the thermocouple placed outside the heater, having better wear resistance. The difference in wear scar area between the two samples was statistically significant because the standard deviations did not overlap. It is important to note that the 1 mm position in Table 5.2 corresponds to a location inside the heater, as indicated in Table 5.1, while the 6 mm position corresponds to a location outside the heater.

Table 5.2: *Wear scar areas of PDC samples sintered with the thermocouple positioned at 1 mm and 6 mm from the sample*

Thermocouple position	**Wear scar area (mm^2)**
1 mm (inside the heater)	6.7 ± 0.5
6 mm (Outside the heater)	8.9 ± 0.4

Chapter 6: Optimising Leachability by Parameter Control: Individual Effects

This chapter investigated the individual effects of the important sintering parameters, holding time, temperature and pressure, on the leach rate of polycrystalline diamond compacts (PDCs). Understanding how each parameter individually affected leach rate is crucial for optimising the sintering process. The insights gained from the individual parameter analysis formed the foundation for the integrated parameter optimisation described in Chapter 6, where the combined effects and interactions of these parameters were explored. By examining the relationship between each parameter and leach rate, this chapter developed quantitative models to predict leachability under different sintering conditions. Each section focused on one of the key sintering parameters (pressure, temperature, or holding time), presenting the experimental results, analysing the underlying mechanisms affecting the PDCs.

6.1 Effect of Holding Time on Leach Rate

6.1.1 Introduction

This section investigated the influence of sintering holding time on the leach rate of PDCs. Holding time, a crucial parameter in HPHT sintering, was expected to affect the microstructure and, consequently, the leachability of PDCs. Previous research [42–47] had shown that holding time affects the densification of ceramic materials by mechanisms such as mass transfer, grain boundary migration and particle growth.

6.1.2 Methodology

The experimental data used in this section were obtained from a series of sintering experiments conducted using a 6x32,000 kN hinge-type cubic press, described in detail in Chapter 3 (Materials and Methods).

6.1.3 Results

Table 6.1 shows that increasing the holding time by 10 minutes decreased porosity, pore aspect ratio and pore Feret diameter of the leached microstructure. These data, presented in Table 6.1, were derived from image analysis of the leached samples shown in Figure 4.2

***Table 6.1**: Microstructural parameters of leached PDC cutters with varying sintering holding times*

Holding time	Porosity (Vol.%)	Pore aspect ratio	Pore Feret diameter (µm)
20 minutes	8.1 ± 0.4	0.7 ± 0.2	2.70 ± 0.38
30 minutes	6.3 ± 0.2	0.4 ± 0.1	1.63 ± 0.15

Figure 6.1 shows the wear resistance of PDC cutters with different holding times. Despite a slight decrease in wear scar area with increased holding time, the large and overlapping standard deviations indicate that there was no statistically significant difference in wear resistance. Even with three samples tested, there were still large standard deviations.

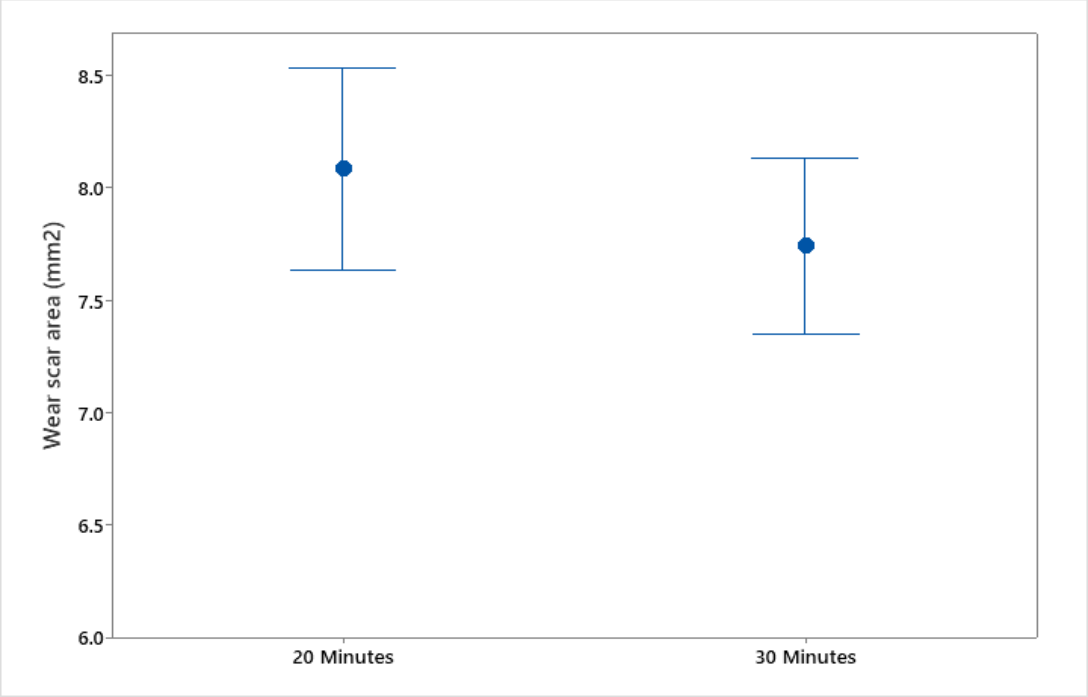


***Figure 6.1**: Wear scar areas of leached PDC cutters sintered at different holding times. Sintering pressure and temperature were fixed at 7 GPa and 1500°C*

Figure 6.2 shows that leachability was reduced with increased holding time. The leach rate data were derived from Tables 4.1 and 4.2. The median leachability for the 20-minute sample was 5.12 ± 0.19 µm/h, whereas the median leachability for the 30-minute sample was 4.14 ± 0.17 µm/h. The boxplots also show variability in leachability within each holding time group. The interquartile range (IQR), represented by the box

length, indicated the spread of the middle 50% of the data. Both the 20-minute and 30-minute holding time averages had similar standard deviations, although the IQR for the 20-minute group was slightly larger.

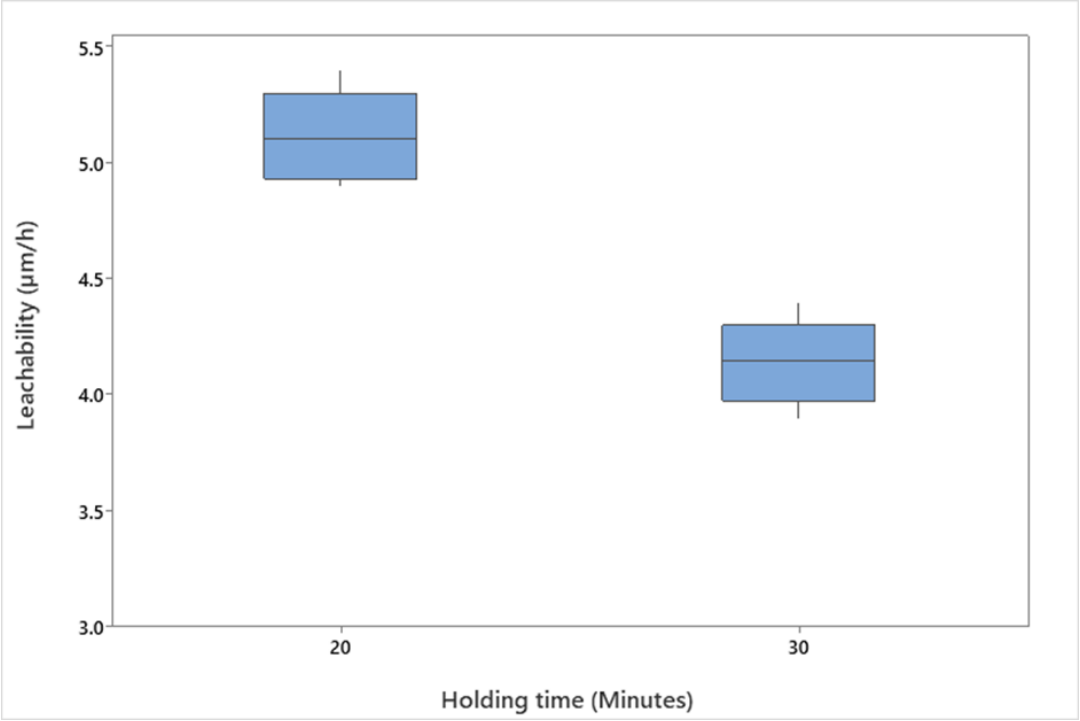


***Figure 6.2**: Boxplot analysis on the effect of holding time on leachability after 96 h leaching in HCl acid*

6.2 Effect of Temperature on Leach Rate

6.2.1 Introduction

This section describes the effect of sintering temperature on the leach rate of polycrystalline diamond compacts (PDCs). Temperature is a critical parameter in HPHT sintering, governing the kinetics of densification, phase transformations [9,32], and ultimately, the microstructure and properties of the final product [9,32]. Previous research [40,42,44,45,117–119] demonstrated the significant effect of temperature on the sintering behaviour of various ceramic materials, and this section describes the effect on the leach rate of PDCs.

6.2.2 Methodology

The experimental data used in this section were obtained from sintering experiments conducted using a 6x32,000 kN hinge-type cubic press. The details of the experimental

set-up, materials and sample preparation are provided in Chapter 3 (Materials and Methods).

6.2.3 Results

Table 6.4 shows the results obtained for samples sintered at 1500°C and 1700°C and the sample sintered at 1500°C had higher porosity. The data in Table 6.4 were derived from image analysis of the leached samples shown in Figure 4.2. This indicated that lower sintering temperatures resulted in a higher volume of pores after leaching. Furthermore, the pore aspect ratio was higher for the 1500°C sample, indicating that the pores in the sample sintered at the lower temperature were more equiaxed, whereas the pores in the sample sintered at the higher temperature were more elongated. Finally, the pore Feret diameter was slightly larger for the 1500°C sample than the 1700°C sample, indicating that sintering at 1500°C promoted the formation of larger and more rounded pores after leaching than at 1700°C.

***Table 6.2**: Microstructural parameters of leached PDC cutters with varying sintering temeprature*

Temperature (°C)	Porosity (Vol.%)	Pore aspect ratio	Pore Feret Diameter (µm)
1500	8.7 ± 0.3	0.8 ± 0.1	1.90 ± 0.38
1700	5.9 ± 0.2	0.4 ± 0.1	1.44 ± 0.35

Figure 6.5 shows the wear resistance of the leached PDC cutters for samples sintered at 1500°C and 1700°C. Three samples each from the experimental runs in Tables 4.1 and 4.2 were taken and analyzed on VTL testing for wear resistance. The PDC cutter sintered at 1700°C had smaller wear scar area. Since the error bars for the two samples do not overlap, the difference in wear scar area was statistically significant, and indicated that the higher sintering temperature had improved wear resistance.

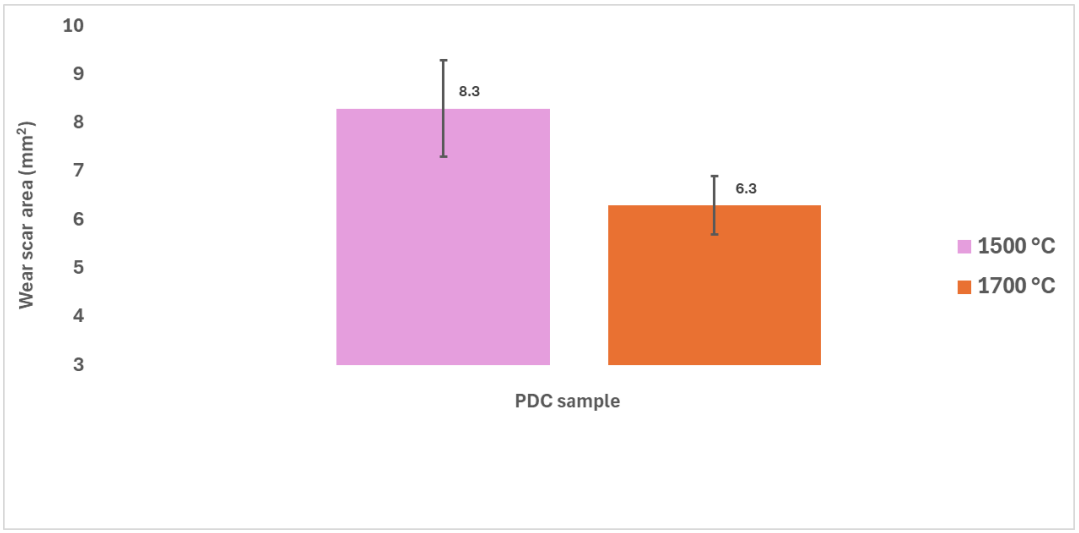


Figure 6.3: *Wear scar area of leached PDC cutters sintered at different sintering temperatures*

The leach rates of the PDC samples after 96 hours of leaching in HCl acid are shown in Figure 6.6. The leach rate data were derived from Tables 4.1 and 4.2. The leach rate decreased as the sintering temperature increased. The non-overlapping error bars showed that the difference was statistically significant.

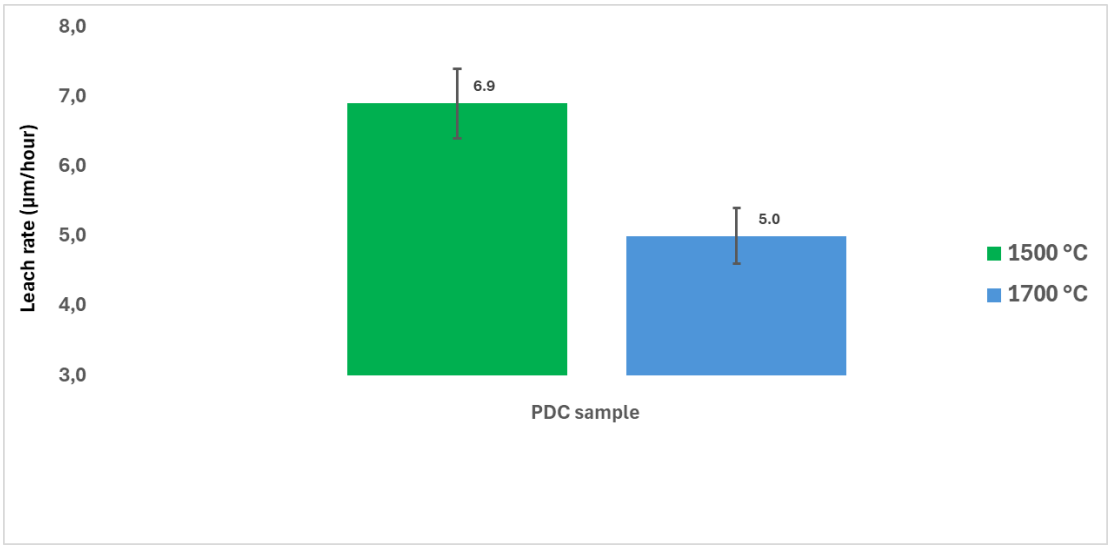


Figure 6.4: *Effect of sintering temperature on leachability after 96 h leaching in HCl acid*

6.3 Effect of Pressure on Leach Rate

6.3.1 Introduction

This section investigated the effect of sintering pressure on the leach rate of polycrystalline diamond compacts (PDCs). Pressure is a critical parameter in HPHT sintering, significantly affecting the densification, microstructure, and resulting

properties of PDC materials. This section investigated the effects of pressure on leach rate and presents a quantitative model to describe this relationship.

6.3.2 Methodology

The experimental data used in this section were obtained from sintering experiments conducted using a 6x32,000 kN hinge-type cubic press, as detailed in Chapter 3 (Materials and Methods).

6.3.3 Results

The derived cobalt pool sizes (FD) and shapes (AR) are presented in Table 6.3. The data in Table 6.3 were derived from image analysis of the leached samples shown in Figure 4.2. The FD of the cobalt pools decreased with increased sintering pressure, as did the AR, although the standard deviations were quite large, as shown in Figure 6.3.

***Table 6.3**: Average cobalt pool size and shape at different pressures*

Sample	Cobalt pool aspect ratio (AR)	Cobalt pool feret diameter (μm)
5 GPa	9.1 ± 2.2	2.36 ± 0.16
7 GPa	4.9 ± 2.7	1.06 ± 0.09

***Table 6.4:** VTL measurements of the area of the wear scars on the sintered samples*

Pressure	Wear scar area (mm^2)	Minimum	Maximum
5 GPa	12.7 ± 1.5	11.0	14.1
7 GPa	3.1 ± 1.0	1.9	4.0

Table 6.4 shows the wear scar measurements of the samples: the 5 GPa sample had the largest wear scar. Higher pressures have more densification and better abrasive wear performance. However, the leaching rate is lower. Three samples each from the experimental runs in Tables 4.1 and 4.2 were taken and analyzed on VTL testing for wear resistance. The 7 GPa sample had the lowest standard deviation. The variability in wear test results for hard materials such as polycrystalline diamond compacts (PDC) often has several origins. Microstructural heterogeneity is a primary cause, where even

well-produced samples can exhibit localised variations in diamond particle packing, binder phase distribution, or the presence of microscopic defects (like porosity or binder pools) at the point of wear contact. Additionally, small differences in surface finish across samples can significantly influence initial wear [21]. Wear tests are very variable, as wear is a complex phenomenon which is highly sensitive to localised material properties and specific contact conditions. Finally, when dealing with a small sample size (e.g., only three samples), any inherent material variability or minor experimental fluctuations can be significantly amplified, leading to larger standard deviations.

Figure 6.5 shows the relationship between the leach rate and pressure for determining the mathematical model to predict the leachability as function of pressure.

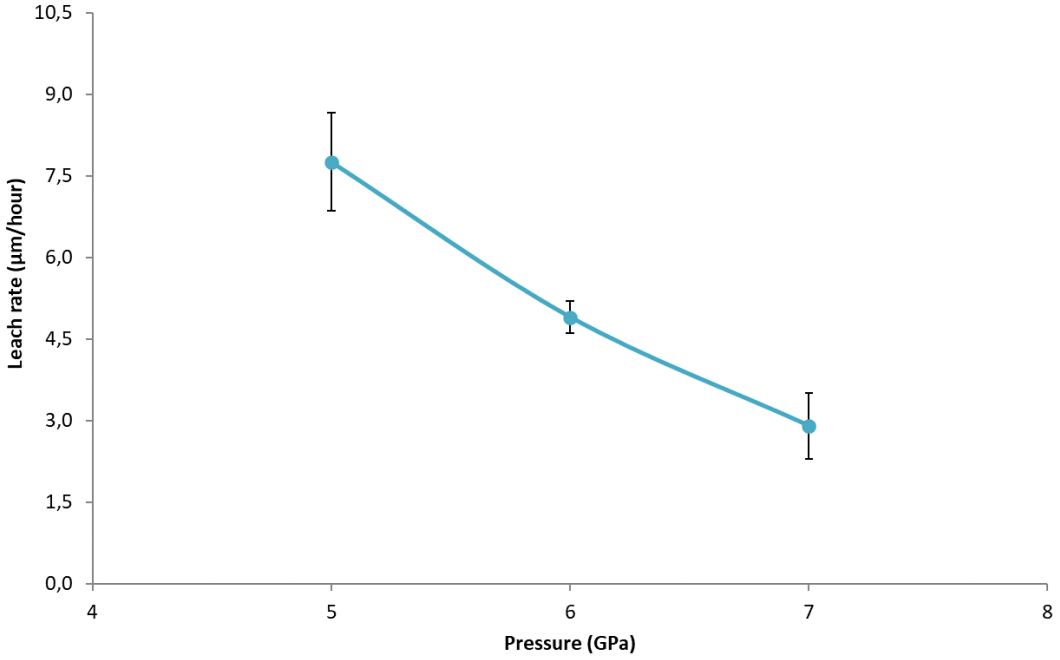


Figure 6.5: *Relationship between leachability (leach rate) and sintering pressure after 96 h leaching in HCl acid*

Chapter 7: Integrated Parameter Optimization: Interactions and Relative Importance

This chapter moved beyond the individual parameter effects explored in Chapter 6 to investigate the combined influence of pressure, temperature and holding time on the leach rate of polycrystalline diamond compacts (PDCs). Recognising that these parameters often interact in complex ways during HPHT sintering, this chapter employed advanced statistical techniques to analyse their combined effects and establish their relative importance to determine leachability. Section 7.1 focused on the development and application of a multiple regression model to quantify the relationships between the sintering parameters, including a significant interaction term between holding time and temperature. Building upon the multiple regression analysis, Section 7.2 utilised Dominance Analysis (DA) to determine the relative importance of each parameter, to providing a hierarchical understanding of their effects on leach rate.

7.1 Multiple Regression Analysis of Sintering Parameters on Leachability

7.1.1 Introduction

This section focused on the development and analysis of a multiple regression model to quantify the combined effects of sintering pressure, temperature and holding time on the leach rate of PDC cutters. Previous chapters explored the individual effects of these parameters, this chapter investigated their interactions and developed a predictive model that captures their relationships with leachability. Understanding these combined effects is crucial for optimising the sintering process and tailoring PDC properties for specific applications.

7.1.2 Methodology

A multiple linear regression model was developed using the leach rate data in Tables 4.1 (run orders 1 to 30) and 4.2 (run orders 31 to 64). The experimental design, materials, sample preparation, sintering procedures, leaching process and leach rate measurements are described in Chapter 3 (Materials and Methods).

The independent variables were:

- X1: Holding Time (minutes)
- X2: Sintering Temperature (°C)
- X3: Sintering Pressure (GPa)

The dependent variable was:

- Y: Leach Rate (μm/h).

7.1.3 Results

To assess multicollinearity among the predictor variables, variance inflation factors (VIFs) were calculated using Minitab software. VIF values greater than 10 indicate potential multicollinearity issues, which can affect the stability and interpretation of regression coefficients [90,95]. The VIF values are presented in Table 7.1. The VIF value for the interaction term between holding time and temperature was above 10, indicating some multicollinearity.

Table 7.1*:Variance iInflation factors (VIFs) for sintering variables*

TERM	**VIF**
Holding time	5.65
Temperature	4.93
Pressure	1.05
Holding time*temperature	10.70

The results of the multiple regression analysis are summarised in Table 7.2. The model provided a good fit to the data, explaining 86.4% of the variability in leach rate (R^2 = 0.864). The analysis revealed that sintering pressure had a significant negative effect on leach rate ($p < 0.001$), indicating that higher pressures lead to lower leach rates. Temperature also had a significant negative effect on leach rate ($p < 0.001$). The

interaction between holding time and temperature was statistically significant ($p < 0.01$), suggesting that the effect of holding time on leach rate depended on the temperature, and vice-versa. Holding time, individually, also had a significant effect on the leach rate.

- Coefficients: These are the estimated coefficients for each sintering variable in the regression equation. They indicate the strength and direction of the relationship between each variable and the leach depth [90,92,95]. A positive coefficient for pressure means that as pressure increases, leach depth also tends to increase.
- DF: This stands for "degrees of freedom." For regression analysis, it is the number of independent pieces of information available to estimate a parameter [124–126]. For individual coefficients, it is usually 1 [124–126]. For the regression model and error, it shows the sample size and the number of variables in the model [124–126].
- t-value: This is the test statistic calculated to assess the statistical significance of each coefficient [85,127]. It is calculated by dividing the coefficient by its standard error [85,127].
- p-value: This is the probability of observing the obtained t-value (or a more extreme value) if there was no real relationship between the sintering variable and leach depth. A low p-value (typically less than 0.05) indicates that the variable has a statistically significant effect on leach depth [92–94,128].
- F-value: This is the test statistic for the overall significance of the regression model [124,125]. It assesses whether the model explains a significant amount of variability in the dependent variable [124,125].

***Table 7.2**: Results of multiple regression analysis for leach rate*

	Coefficients	DF	t-value	Standardised coefficients	p-value	F-value
Regression model	-	4	-	-	0.00	4.37
Intercept	56.72	1	6.34	-	0.01	-
Holding time	-1.02	1	3.18	-0.13	0.01	-
Temperature	-0.02	1	7.02	-0.41	0.00	-
Pressure	-2.11	1	10.25	-0.65	0.00	-
Holding time*temperature	0.01	1	2.65	-	0.01	-
Error	-	40	-	-	-	-

Figure 7.1 shows the main effects of each sintering variable on the leach rate, while holding other variables constant. Increasing sintering pressure led to decreased leach rate. Similarly, increased holding time and temperature also decreased the leach rate. These trends were consistent with the results of the multiple regression analysis (Table 7.2, i.e., sintering pressure, holding time and temperature negatively affected the leach rate.

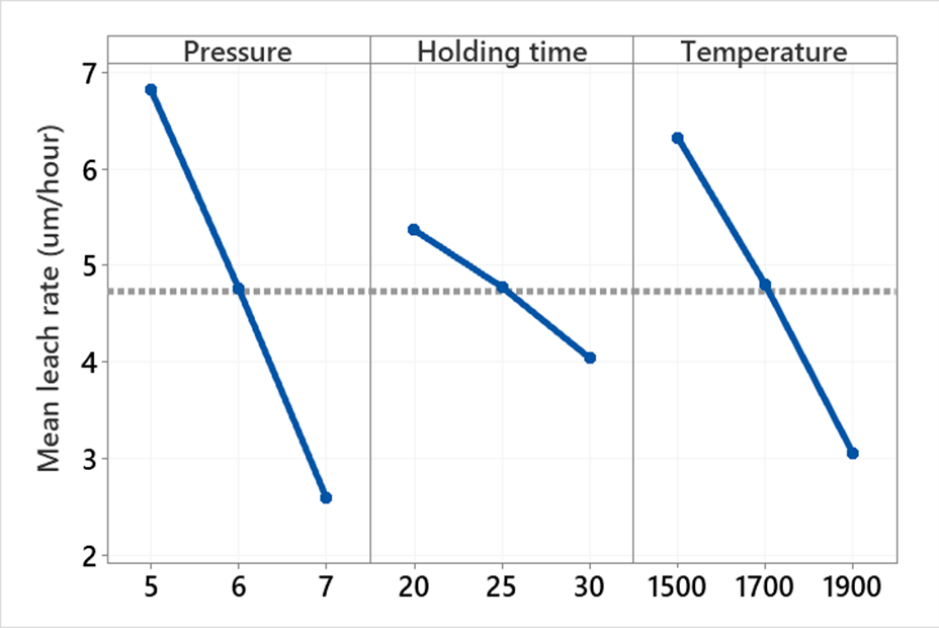


***Figure 7.1**: Main effects plot for leach rates of PDCs for pressure, holding time and temperature, horizontal dashed lines represent overall mean leach rate*

An interaction effect occurs when the effect of one variable on the leach rate depends on the level of another variable. The interaction plot in Figure 7.2 shows that the effect of holding time on the leach rate differs depending on the temperature. At the lowest temperature (1500°C), increased holding time led to greater decreased leach rate than the highest temperature (1900°C). This confirmed the significant interaction between holding time and temperature shown by multiple regression analysis (Table 7.2) and VIFs (Table 7.1).

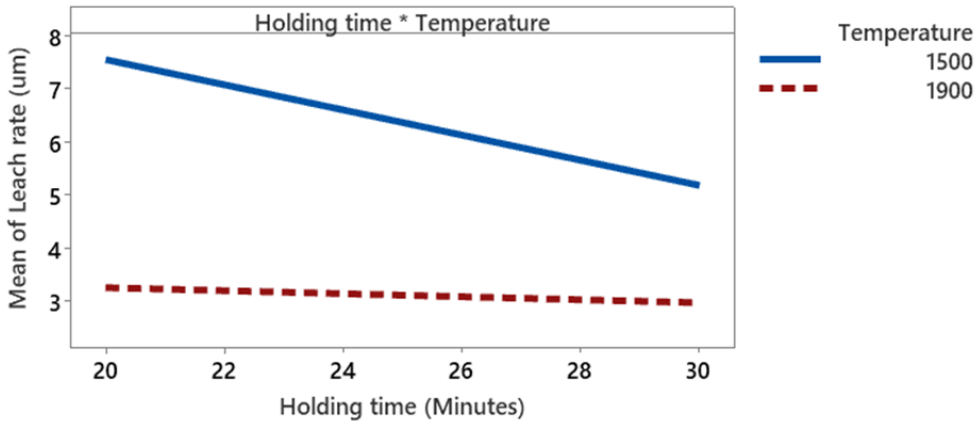


***Figure 7.2:** Interaction plot for holding time and temperature on leach rate*

Figure 3.3 shows the correlation matrix, which is a quantitative assessment of the relationships between the individual sintering parameters (pressure, temperature and holding time) and the leach rate. Each scatter plot displays the relationship between two variables. The Pearson correlation coefficients (r) and their associated confidence intervals (CI) reveal the strength and direction of these relationships. A strong negative correlation was derived between pressure and leach rate (r = -0.700, 95% CI [-0.807, -0.548]), indicating that higher pressures were associated with lower leach rates. Similarly, temperature exhibited a statistically significant negative correlation with leach rate (r = -0.543, 95% CI [-0.696, -0.343]), indicating that increased temperatures corresponded to decreased leach rates. In contrast, holding time displayed a weak and non-significant negative correlation with leach rate (r = -0.221, 95% CI [-0.442, 0.027]). No significant correlations were found between the sintering parameters themselves (pressure and temperature, pressure and holding time, temperature and holding time).

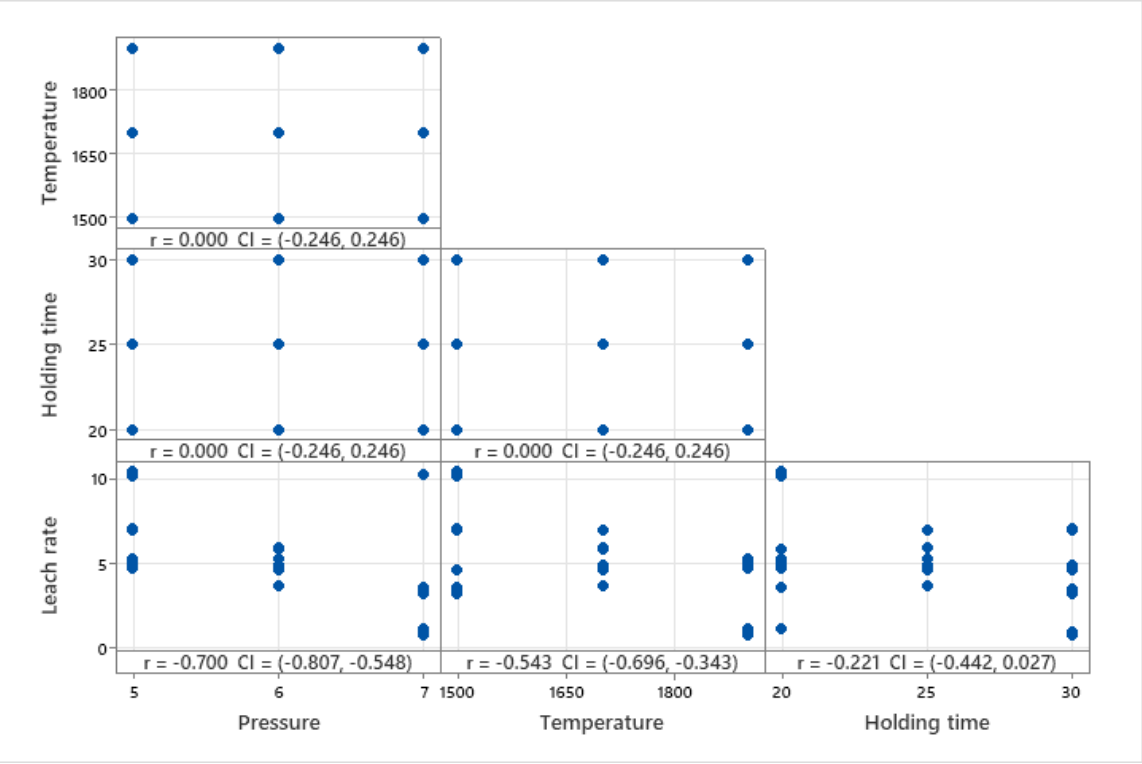


***Figure 7.3**: Correlation matrix showing the relationships between pressure (GPa), temperature (°C), holding time (minutes) and leach rate (µm/h), with Pearson correlation coefficients (r) and their 95% confidence intervals (CI) for each pair*

Figure 7.4 illustrates the combined effect of pressure and temperature on leach rate as a contour plot, with a fixed holding time. Holding time was chosen as constant due to its minimal influence on leach rate as shown in Figure 7.4. Higher leach rates were

generally achieved at lower pressures (<~6.0 GPa) and lower temperatures (<~1650°C) within the investigated range. Conversely, increasing both pressure and temperature tended to decrease the leach rate.

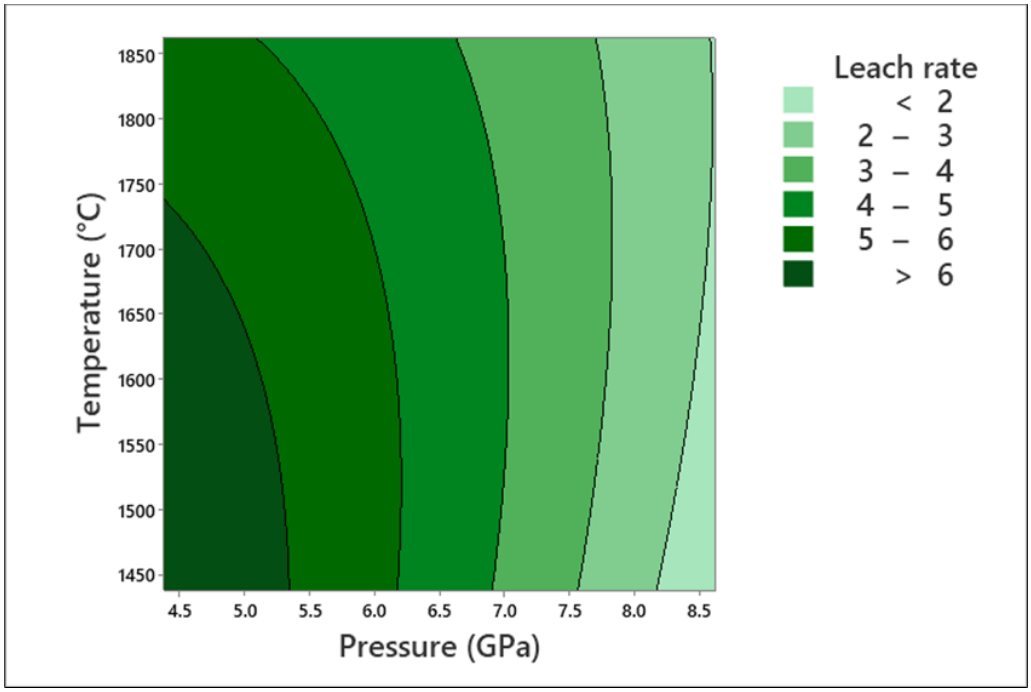
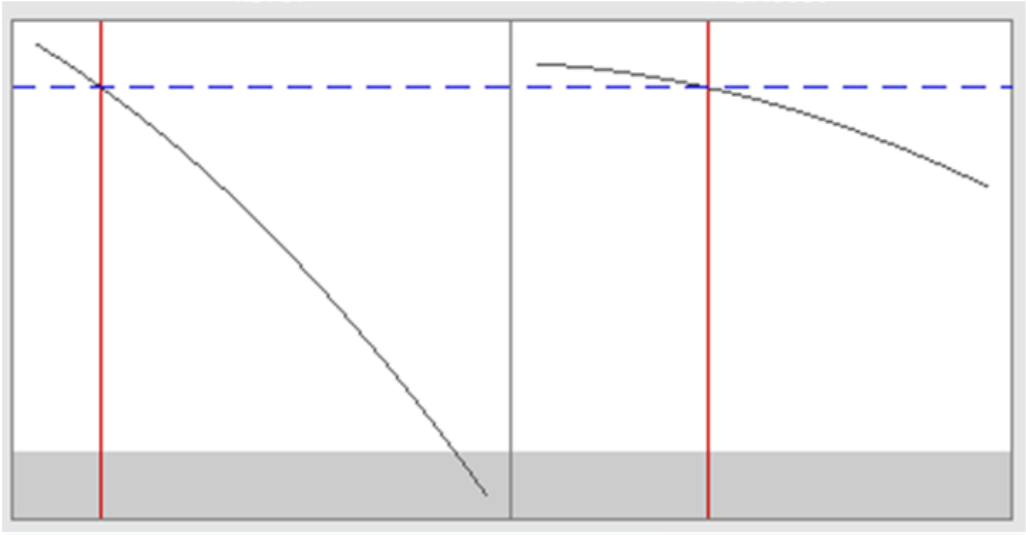


Figure 7.4: *Contour plot for effect of pressure (GPa) and temperature (°C) on leach rate (µm/h) at a fixed holding time*

To determine the optimal conditions for maximizing leach rate, an optimisation plot was generated (Figure 7.5). The analysis indicated that a pressure of 5.0 GPa and a temperature of 1437.9°C predicted a maximum leach rate of 6.1 µm/h. The individual desirability (d) for this maximum leach rate was 0.85, and the composite desirability (D) was 0.85, These optimised settings are consistent with the trends in Figures 7.1 and 7.3, where lower pressures and lower temperatures were associated with higher leach rates.



	Pressure	Temperature	Maximum leach rate
High	8.6	1862.1	D: 0.85
Current	5.0	1600.0	d: 0.85
Low	4.3	1437.9	Y= 6.1

Figure 7.5: *Optimisation plot showing the predicted leach rate (µm/h) as a function of pressure (GPa) and temperature (°C), showing maximum leachability achievable under the experimental boundary conditions tested, where: high = maximum value of the pressure and temperature, low = lowest value of the pressure and temperature and current = current value of the pressure and temperature*

7.2 Dominance Analysis and the Hierarchy of Parameter Importance

7.2.1 Introduction

To understand the relative importance of the sintering parameters (pressure, temperature and holding time) on the leachability of PDCs, a statistical technique known as dominance analysis (DA) was employed. Dominance analysis is a powerful method for dividing the variance explained by a regression model (R^2) into contributions attributable to each predictor variable, thus allowing for a determination of their relative importance in predicting the dependent variable [84,99]. Unlike conventional regression coefficients, which only reflect the unique contribution of a variable while holding all other predictors constant, Dominance Analysis provides a more comprehensive assessment of variable importance by considering all possible subset models [88, 89, 135], and examines the contribution of each variable, both individually and in all possible combinations with other predictors. This approach provides a more robust measure of importance, even with some correlation among the independent variables, as often occurs for process parameters like those involved

in HPHT sintering. The DA is based on the "all subset models" approach, where each possible combination of predictors is considered as a subset model. The incremental contribution of a variable to a given subset model is defined as the difference in the model fit (R^2) when that variable is included versus when it is excluded [86,87]. By examining these incremental contributions across all possible subsets, DA allows for the assessment of complete, conditional and general dominance, providing a comprehensive understanding of the direct, partial and total effects of each variable [87,88].

7.2.2 Experimental procedure

In this study, DA was applied using the experimental data generated from the full 2^3 factorial design with three replicates (64 runs in total), as described in Chapter 3 (Materials and Methods).

7.2.3 Results

The Venn diagram (Figure 7.6) shows the complete dominance weights for each sintering variable and their combinations. Pressure had the highest individual dominance weight (0.49), significantly larger than temperature (0.29) or holding time (0.05). This indicated that pressure had the most substantial impact on leachability when considered in isolation. Furthermore, pressure demonstrated high dominance weights in combination with other variables: Pressure + Temperature (0.78), Pressure + Time (0.54), and Pressure + Temperature + Time (0.84). These results clearly demonstrated pressure's strong individual effect and its synergistic interactions with other variables in influencing PDC leachability.

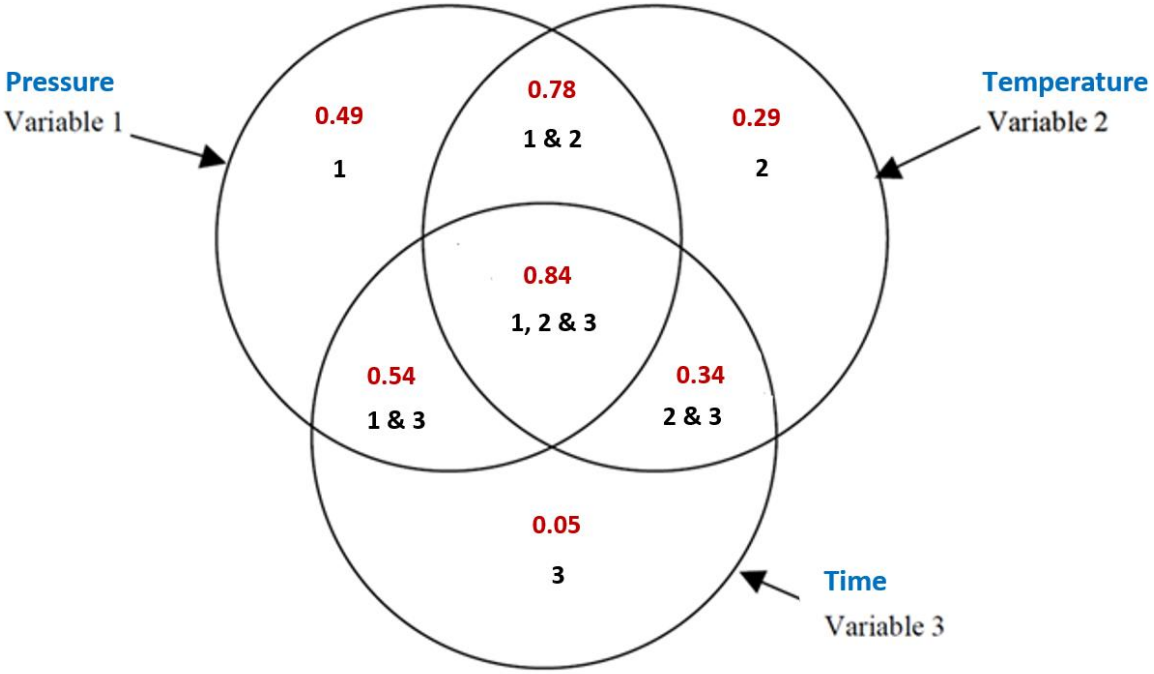


***Figure 7.6**: Venn diagram showing the complete dominance weights for the effect of sintering variables on the leachability of PDC*

Figure 7.7 displays the conditional dominance weights for each parameter across different subset sizes (K values). The K value represents the number of variables considered simultaneously in a subset model (K=0: overall average dominance; K=1: individual effects; K=2: pairwise interactions; K=3: combined effect and all interactions). Across all subset sizes, pressure consistently had the highest dominance weight, followed by temperature, and then holding time. This shows the hierarchy of influence: Pressure > Temperature > Holding Time. Notably, the dominance weight of holding time increased with increasing subset size, indicating the presence of a suppressor effect [76].

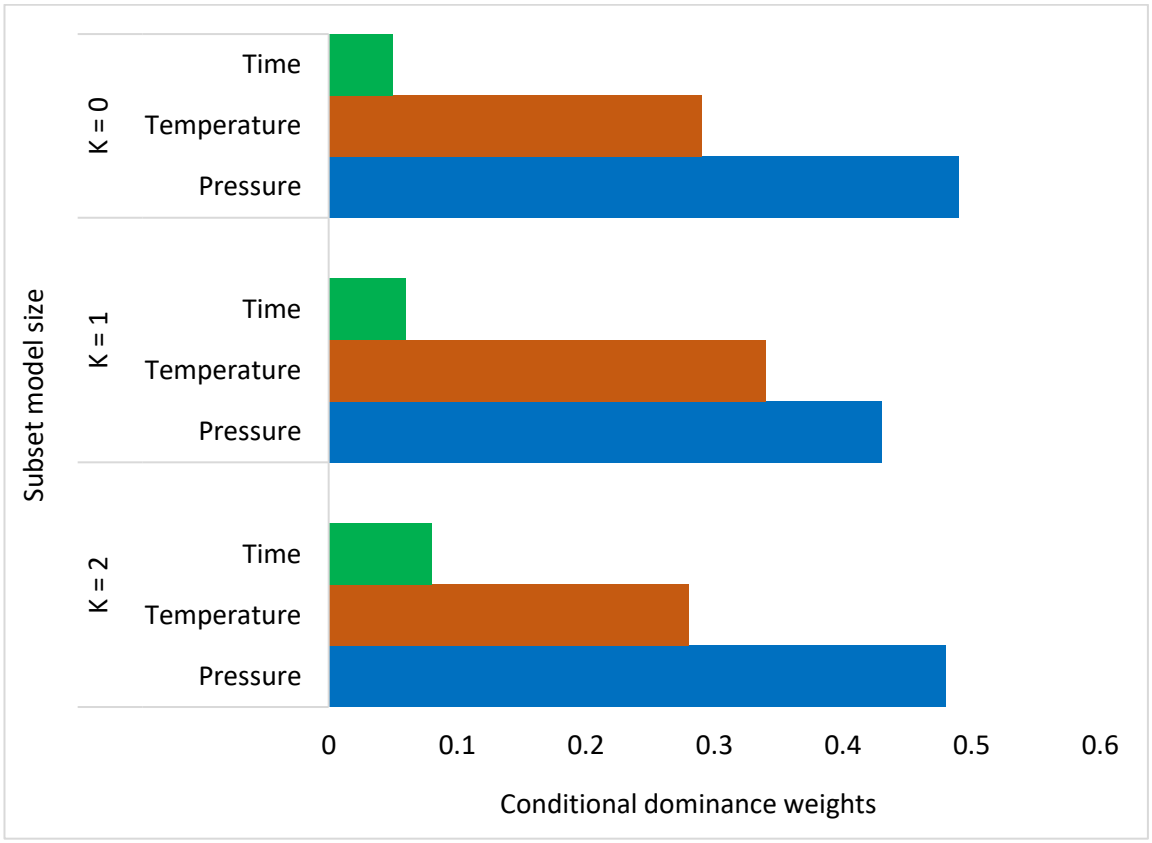


Figure 7.7: *Conditional dominance weights for the of sintering variables at different subset size models*

Figure 7.8 shows the general dominance weights, representing the relative contribution of each variable to the total variation in leachability, as follows: Pressure (56%), Temperature (37%) and Holding Time (7%). Figure 7.8 confirms Figures 7.6 and 7.7 that pressure was the most important factor in determining leachability, followed by temperature, with holding time having a relatively minor contribution.

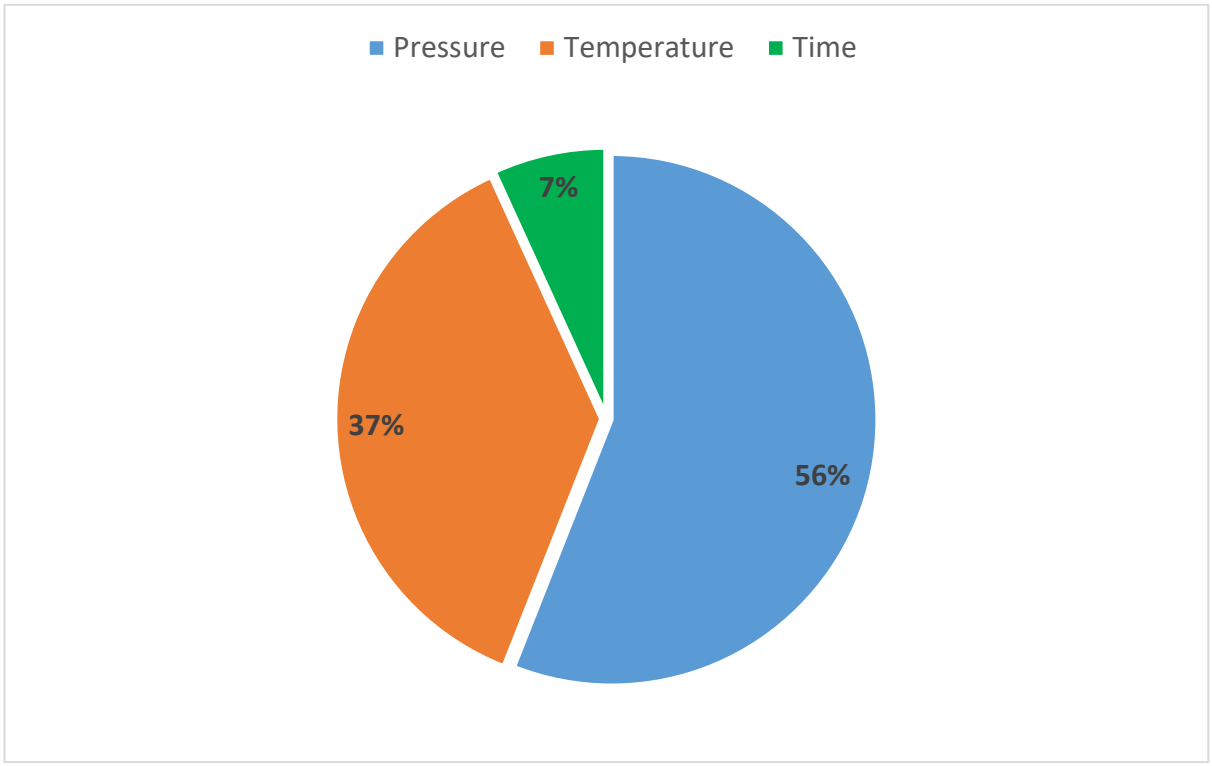


***Figure 7.8**: Percentage general dominance weights for the sintering variables*

Chapter 8: Overall Discussion

This chapter discusses the individual experimental results, followed by the synthesis of the key findings of the research presented in the preceding chapters, providing a comprehensive discussion and interpretation of the results in the context of HPHT sintering of PDCs. The research investigated the critical roles of pressure, temperature and holding time on the microstructure, leachability, and ultimately, the performance of PDC cutters. This chapter analyses the interaction of these parameters, discuss the underlying mechanisms governing their effects, and discusses the implications of these findings for optimising the sintering process. Furthermore, the limitations of the study are acknowledged, and directions for future research are presented.

8.1 Detailed Discussion of Experimental Results

8.1.1 Advances in Accurate Process Parameter Control

8.1.1.1 Pressure Calibration

Figure 5.1 characterizes the densification behaviour of the PDC sample, showing a strong correlation between the calculated effective compaction pressure (derived from an empirical Murnaghan-like fit to the *ex situ* relative volume measurements, V/V_o) and the observed volume reduction. A linear fit to the data yielded:

$$Y = -17.414X + 21.544 \quad \textbf{Equation 8.1}$$

where Y represents the calculated effective compaction pressure (GPa) and X is the measured relative volume (V/V_o).

The high R^2 value of 0.9894 indicated that this empirical linear relationship provided a very good fit to the experimental densification data within the investigated range. This fit mathematically described how the diamond compact resisted further compression as its porosity was progressively eliminated by plastic deformation under increasing applied load. The negative slope of -17.414 in Equation 8.1 confirmed the expected inverse relationship (as the effective compaction pressure [increasing resistance to compaction] increased, the relative volume (V/V_o) of the compact decreased). The *y*-intercept of 21.544 is a theoretical extrapolation beyond the physical limits of the experiment (as V/V_o cannot reach zero). It must be emphasised that this empirical fit described the plastic deformation and porosity reduction of the porous diamond compact, and the “effective compaction pressure” obtained should not be interpreted

as the intrinsic elastic bulk modulus of 100% dense diamond, as described in the introduction to this section. This empirical relationship is valid only within the specific range of ram loads and temperatures tested.

There were significant and systematic deviations between the calculated nominal pressure and the actual fixed-point transition pressures (Figure 5.2). The differences near the Bi III-V transition could be due to larger uncertainties associated with higher-pressure calibrations [18]. Accuracy of pressure measurements at 50 kbar could be ~2%, and ~4% at 100 kbar, which is consistent with the magnitude of the deviation's pressures >50 kbar in this study. At the Bi III-V transition (77 kbar), the measured pressure deviated from the reported value [18] by approximately 10 kbar, which is significantly greater than the expected uncertainty of ~3 kbar based on the cited accuracy. This non-ideal relationship demonstrated that the P=F/A calculation did not accurately give the true pressure within the sample cell. The use of pyrophyllite as a pressure transmitting medium (PTM), while chemically inert and machinable, can introduce non-hydrostatic stresses that cause deviations between nominal and true sample pressures.

Figure 5.1 provides a practical calibration for sintering conditions by linking ram load settings to densification outcomes, enabling reproducible diamond sintering in the cubic press. In contrast, Figure 5.2 shows the discrepancy between calculated and actual pressures [18], demonstrating the value of empirical calibration over precise pressure measurements.

While fixed-point methods are necessary for establishing absolute pressure scales, and interpolation techniques are needed between them [18], this study took a different approach. Recognising the difficulties in obtaining precise *in situ* absolute pressure values with a simple P=F/A calculation, especially for a complex system like a cubic press, this method used the densification of PDCs directly under controlled ram loads at sintering temperatures. The empirical application of the Murnaghan equation of state (Figure 5.1) to *ex situ* volume change measurements provided a continuous description of densification behaviour, which is useful for optimizing PDC sintering parameters.

The systematic overestimation of pressure by the P=F/A method was consistent with other cubic press calibrations, such as Wang et al. [70] who found that pressures determined by their DTA-based method (with the aluminium fusion curve) in a cubic press were higher than those derived from conventional fixed-point calibrations. They attributed this to non-hydrostatic stresses and limitations of the fixed-point method [70]. Fixed-point calibrations, while standard [18], rely on detecting phase transitions in reference materials that may experience different pressures than the sample due to non-hydrostatic stresses within the pressure chamber [70]. Despite its non-ideal pressure transmission characteristics, pyrophyllite was used as the PTM due to its compatibility with the cubic press set-up and its widespread use in similar high-pressure experiment.

The choice of pressure transmitting medium (PTM) significantly affects the actual sample pressure, as demonstrated by Walker et al. [106] who showed varying pressure transmission efficiencies for different castable ceramics. Pyrophyllite, utilized as PTM in this study due to its practical advantages, possesses distinct compressibility and shear strength characteristics compared to media used in standard fixed-point calibrations [106]. These properties, coupled with friction within the cell assembly, influence the complex relationship between applied ram load and the true pressure experienced by the PDC sample. This complex pressure transmission, where the actual pressure is lower than the nominal P=F/A value, contributes to the observed systematic discrepancy between our P=F/A nominal pressures and the fixed-point values in Figure 5.2.

The more pronounced deviations observed in Figure 5.2, particularly around the Ba I-II and Tl I-II transitions, are likely a consequence of several interacting factors inherent to solid-media high-pressure systems:

- **Non-Hydrostatic Stress:** In a cubic press, even with a well-designed pressure-transmitting medium, achieving perfectly hydrostatic pressure (equal pressure in all directions) is extremely difficult. The solid pressure-transmitting medium transmits pressure through a combination of flow and deformation. As the pressure increases, different parts of the medium and sample assembly may experience different stress states. This non-hydrostaticity is often exacerbated

around phase transitions of materials within the assembly (including the pressure medium and the sample itself). The Ba I-II and Tl I-II transitions, occurring in the intermediate pressure range, could significantly alter the stress distribution, leading to a larger deviation from the ideal hydrostatic pressure.

- **Pressure Medium Compressibility Changes:** The pressure-transmitting medium's compressibility (how much its volume changes under pressure) is not constant. It can change gradually with increasing pressure, and, crucially, it can change abruptly at phase transitions. If the pressure medium undergoes a phase transition or a significant change in compressibility in the pressure range of the Ba I-II and Tl I-II transitions, this will affect how pressure is transmitted to the sample. This can lead to a localized increase or decrease in the actual pressure experienced by the sample, compared to what's calculated based on an average compressibility or a linear fit.
- **Sample Assembly Arrangement and Pressure Distribution:** The specific geometry of the sample assembly (the arrangement of the sample, pressure medium, gaskets, and other components within the cubic press) plays a significant role in how pressure is distributed. Friction between the different components, and the deformation of these components under pressure, can create pressure gradients. These gradients might be more pronounced in certain pressure ranges, particularly if the pressure medium or other assembly components are undergoing phase transitions or significant changes in their mechanical properties.

Another discrepancy in Figure 5.2 was the significant temperature difference between the sintering experiments (1500°C) of this study and the typical room-temperature (25°C) condition under which many standard fixed-point transitions were reported [18]. While PDC densification measurements (Figure 5.1) were conducted at the actual sintering temperature, the phase transition pressures used for comparison in Figure 5.2 were mainly based on room temperature data [18].

Phase transition pressures are temperature-dependent [68]. For example, Ono et al. [68] investigated the high-pressure, high-temperature behaviour of bismuth, including the Bi-III to Bi-V transition, using *in situ* X-ray powder diffraction. They found a negative temperature dependence for this transition (pressure decreased with

increasing temperature), with a phase boundary described by P (GPa) = 12.4 - 0.016 × T(K). Extrapolating this to the current sintering temperature of 1500°C gave a Bi-III to Bi-V transition pressure significantly lower than the commonly-used 7.7 GPa room temperature value [18]. The equation would yield a transition pressure around 1.6 GPa at 1500°C, demonstrating that a fixed point like 7.7 GPa (room temperature) [18] would underestimate the actual pressure at 1500°C.

While *in situ* X-ray diffraction, as used by Ono [68], provided valuable temperature-dependent phase boundary data, its practical implementation for routine pressure calibration in large-volume cubic presses designed for bulk sample synthesis is difficult due to the complexity of the experimental set-up and the physical inaccessibility of the press chamber during operation. Thus, the *ex situ* volume change method (Figure 5.1) is a complementary approach that directly characterises the bulk densification of PDC samples under actual sintering temperatures and applied ram loads, making it particularly suitable for guiding PDC synthesis, even if it cannot provide absolute *in situ* pressure values.

Figure 8.1(a) shows the microstructure of a PDC sample sintered in this study at 1500°C and a ram load corresponding to a calculated nominal pressure of approximately 7 GPa. As previously discussed, (Figure 5.2), this 7 GPa value is a nominal estimate, and the true in-situ pressure may differ. For comparison, Figure 8.1(b) displays a representative microstructure of a PDC sample sintered by Westraadt et al. [107] at their reported conditions of 5.5 GPa and 1450°C. Both microstructures clearly exhibit the characteristic features of well-sintered PDC, including a dense network of intergrown diamond grains, a uniformly distributed metallic cobalt binder, and the presence of some residual tungsten carbide.

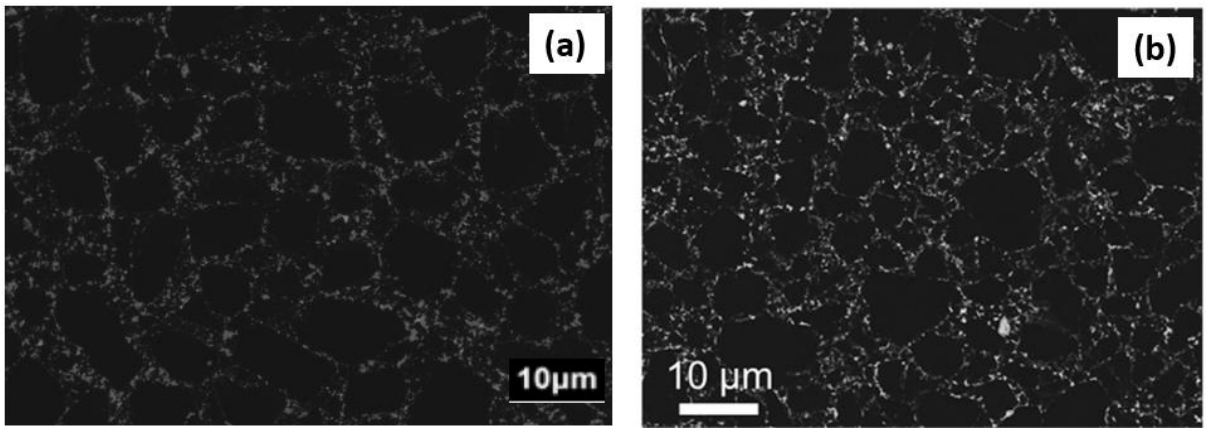


Figure 8.1: *SEM-BSE images of PDC samples produced at: (a) calibrated pressure of 7 GPa, 1500°C and 20 minutes, (b) 5.5 GPa and 1450°C by Westraadt et al. [107], showing cobalt pools (medium grey contrast), diamond (dark contrast) and tungsten carbide (light grey contrast)*

In both samples, the cobalt binder distribution appears largely uniform. Despite variations in specific sintering parameters and potentially starting materials, both this study and Westraadt et al. [107] successfully achieved well-sintered PDC microstructures characterized by effective diamond-diamond bonding.

The ability to produce high-quality sintered PDC at the conditions determined by this experimental approach (specifically, ram loads corresponding to the optimal densification range identified in Figure 5.1) supports the efficacy of the 'sintering conditions calibration' for cubic presses. While microstructural differences (e.g., related to diamond grain size, as seen in Figure 8.1) and precise pressure comparisons remain complex, the successful sintering achieved at our operational conditions demonstrates a robust process. The chosen ram load, which translates to a calculated nominal pressure of 7 GPa, resulted in successful sintering, similar to Westraadt et al. [107] who used 5.5 GPa, indicating that various pressure/temperature combinations can lead to effective consolidation.

To evaluate the wear performance of the PDC using the calibration method in the current study, Figure 5.3 compares the VTL wear test results of the PDC sample of the current study to those of Dai et al. [4], Zhao et al. [2] and Jivanji et al. [3]. The PDC sample of the current study, sintered at 7 GPa and 1500°C, exhibited comparable wear resistance to PDC samples from the other studies, although it had a large error bar.

Figure 5.3 shows the VTL wear test results for the PDC sample in this study (mean wear scar area of 6.7 mm²). The large error bar indicated variability in the wear performance of the PDC samples examined in this study. Due to this large error bar, the results from this study showed overlap with, and were broadly comparable to, values reported by Zhao et al. [2], Jivanji et al. [3], and Dai et al. [5], even when considering that those studies were obtained under similar processing conditions and testing methodologies.

Jivanji et al. [3] reported a lower wear scar area (5.9 ± 0.4 mm²) compared to this study. The variation is in the samples from this study which could have originated from the non-homogeneous samples (microstructure and analyses of phases (Table 4.3). This shows that a statistically significant difference cannot be established. However, potential contributing factors to their [3] improved wear resistance could include their higher sintering temperature (1700°C vs. 1500°C) and the presence of ZrB_2 in their samples.

Compared to the PDC samples of Dai et al. [5], which was sintered at 5.5 GPa with a grain size of ~20 μm and showed a wear scar area of 7.5 mm² ± 0.6, the sample of the current study (sintered at 7 GPa with a grain size of ~16 μm) exhibited a lower wear scar area. Similarly, the variation was in the samples from this study, although the higher sintering pressure in this study (7 GPa vs 5.5 GPa [5]) likely resulted in a denser microstructure and enhanced diamond-diamond bonding, which significantly contributed to improved wear performance [32].

Thus, this experimental approach, based on *ex situ* volume change measurements of the PDC sample, empirically fitted with the Murnaghan equation (Figure 5.1), enabled the successful and reproducible sintering of PDC materials. The achieved microstructures (Figure 8.1) and wear resistance (Figure 5.3) are broadly comparable to those reported in the literature, demonstrating the practical efficacy of this method in identifying suitable sintering parameters in a cubic press. This approach serves as a practical 'sintering conditions calibration' for a specific press, allowing to correlate controllable ram loads directly with the resulting densification and material properties.

While acknowledging the complexities and uncertainties in determining absolute in-situ pressure (as highlighted by the discrepancies in Figure 5.2, stemming from the

P=F/A nominal calculation and temperature effects on fixed points), this method offers distinct advantages for PDC synthesis. Unlike conventional fixed-point calibrations or DTA-based methods [18, 70] which can be equipment-intensive and require external reference materials, this approach utilizes readily available equipment to directly monitor the material's compaction response during processing. This provides a material-specific and temperature-relevant understanding of densification under the actual sintering conditions, streamlining the optimization process for industrial applications. It minimizes reliance on potentially inaccurate extrapolated data from room-temperature fixed points or calibrations obtained from different systems.

The 'sintering conditions calibration' developed here is crucial for enabling the precise control of parameters for PDC synthesis, aiding the optimization of material properties and performance by directly linking applied ram load to material response. It provides a robust, practical framework for achieving desired densification and material quality in polycrystalline diamond production.

8.1.1.2 Temperature Measurement and the Effect of Thermocouple Placement

Figure 5.6 shows SEM-BSE images of the PDC samples sintered with two different thermocouple positions. The sample sintered with the thermocouple placed inside the heater (Figure 5.6a) had a well-developed microstructure characterised by extensive neck formation between diamond grains and well-defined grain boundaries. In contrast, the PDC sample sintered with the thermocouple placed outside the heater (Figure 5.6b) showed that the necks between diamond grains were less developed and, in some areas, appeared to be absent. Thermocouple position affects sintering quality due to the following factors:

- **Lack of Independent Temperature Regulation:** Since there was no active feedback mechanism for temperature control by the thermocouple, the system did not automatically adjust power to maintain a constant temperature at the sample. Instead, the power input was fixed, and heat was generated.
- **Thermal Gradients:** Within the confined space of the cubic press, significant thermal gradients existed. The thermocouple measured the temperature only at its actual physical location. Although the overall power input remained constant, slight variations in the distance between the thermocouple and the

sample exposed the thermocouple to different temperatures within the thermal gradient. These positional differences led to inconsistent readings that, while accurate for the thermocouple's location, may not have experienced the actual temperature experienced by the sample.

Therefore, although the samples remained in the same physical position relative to the heat source for different experiments, the temperature measured by the thermocouple varied due to its actual placement within the non-uniformly heated volume. These variations in measured temperature directly corresponded to the actual thermal conditions experienced by the sample, which dictated the extent of sintering and the resulting microstructures. Figure 5.6 shows that a higher and more stable measured temperature (when the thermocouple was inside the heater) correlated with superior microstructures (better neck formation), demonstrating that thermocouple position is important for the effective sintering temperature delivered to the sample. Thus, precise thermocouple placement in a cubic press, where temperature is measured passively rather than actively controlled, is a potential measurement error and significantly affects understanding of the true process conditions, with direct implications for process control and the quality of the final product.

To understand the potential cause of the thermocouple failure, it is important to consider the behaviour of titanium at high pressures and temperatures. In this study, a titanium cup was used to contain the sample. Figure 8.2 shows the pressure-temperature phase diagram of titanium, adapted from Dewaele et al. [108], which incorporates phase boundaries determined by Zhang et al. [110] and Tonkov et al. [111]. At the experimental conditions experienced by the thermocouple (approximately 6 GPa and 1500°C) (Table 5.1), the phase diagram suggests that titanium would be in the (solid) β-Ti phase field. The localized melting observed on the failed thermocouple, along with the erratic temperature readings in Figure 5.5, indicated a possible eutectic reaction between the titanium cup and the S-type thermocouple's Inconel 600 sheath. The phase diagram of titanium (Figure 8.2) [108] shows the phase transformations at different temperatures and pressures. Although

the Ti phase diagram indicated a high melting point, it did not include the thermocouple materials.

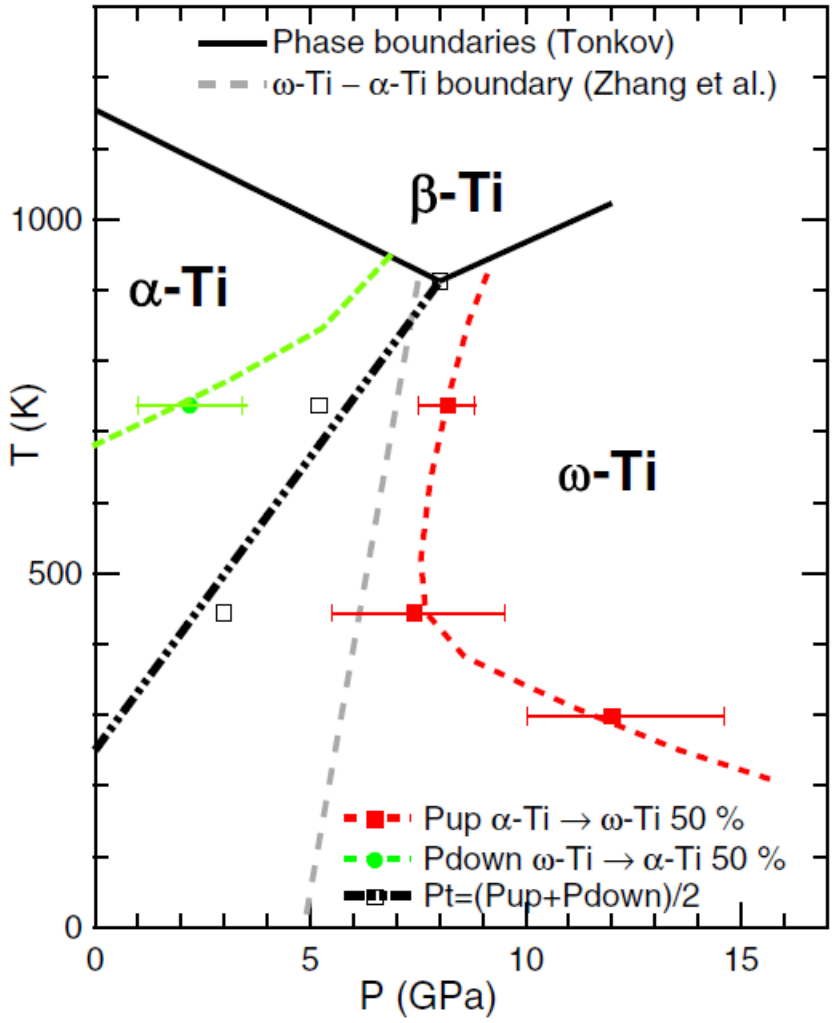


Figure 8.2: *High-pressure phase diagram of titanium [108]*

In the current study, the direct contact between the S-type thermocouple and the titanium cup at high temperature and pressure was detrimental. S-type thermocouples use a junction of platinum and a platinum-rhodium alloy 90 at. % Pt / 10 at. % Rh). At elevated temperatures, the platinum-titanium binary diagram has two low temperature eutectic reactions (1310°C and 1320°C) (Figure 8.3 [141]) below the melting points of titanium (1668°C) or platinum (1768°C) [141]. The localised melting on the failed thermocouple could be due to this. The temperature at which the thermocouple failed (~1400°C) was fairly close to the eutectic temperature of the lowest temperature and most Ti-rich eutectic in the Ti-Pt binary phase diagram [141].

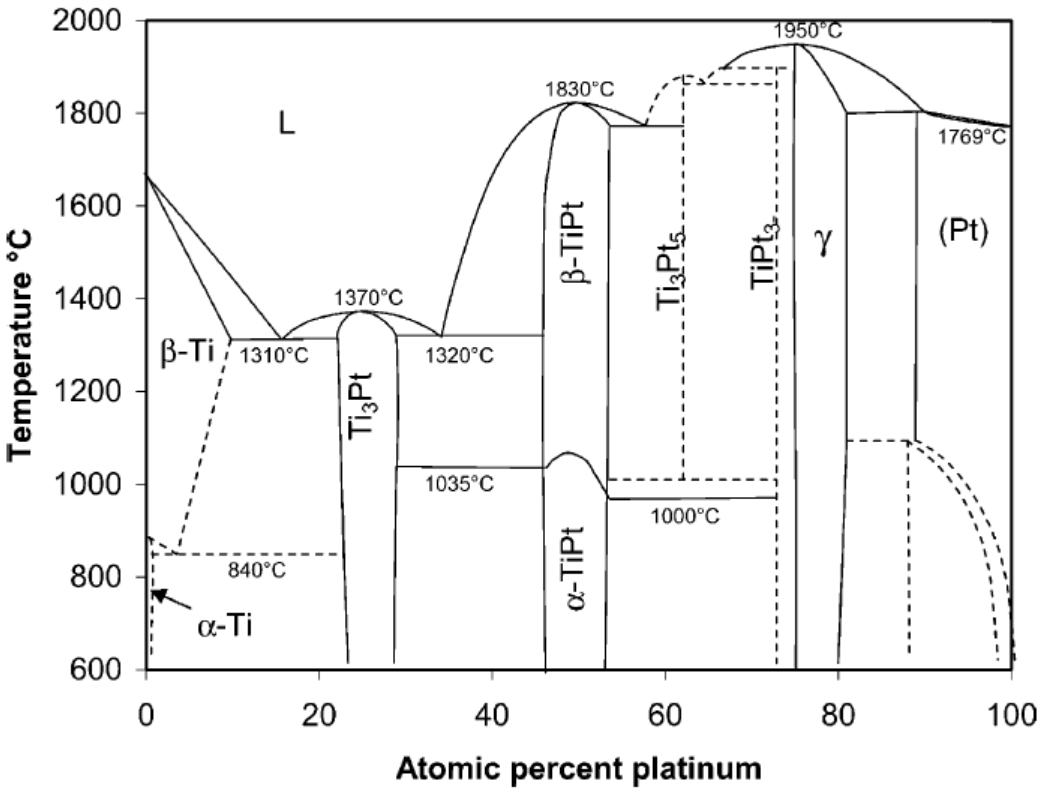


Figure 8.3: *Ti–Pt phase diagram by Murray [141]*

The thermocouple positioned 1 mm away from the sample did not experience direct contact with the titanium and did not react. Thus, this thermocouple survived and provided stable temperature readings throughout the experiment (Figure 5.5). This demonstrates the crucial role of minimising direct contact between reactive materials like titanium and platinum-based thermocouples at high temperatures and pressures.

Figure 5.6 shows the capsule assembly, showing the set up to maintain 1 mm separation between the thermocouple junction and the titanium cup containing the sample. The benefit of this configuration was supported by Figure 5.5 where direct contact between the titanium and the thermocouple materials led to failure. This physical separation proved crucial in preventing the formation of a low-melting-point eutectic, thus preserving the thermocouple's integrity and enabling continued temperature measurement throughout the experiment.

While separating the thermocouple from the reactive sample is crucial, the extent of this separation must be carefully considered to ensure accurate temperature measurement. Table 5.1 showed the effect of thermocouple position on measured

temperature within a cubic press set-up. Positioning the thermocouple outside the heater decreased measured temperatures by 50.4°C compared to inside the heater. The objective was to position the thermocouple close enough to the sample to accurately reflect its temperature, but far enough to prevent detrimental chemical interactions, such as forming of a eutectic, which occurred with direct contact. The 1 mm gap chosen for the experiment was a compromise between these two competing factors. It provided sufficient separation to prevent the eutectic reaction, shown by the stable readings (Figure 5.5) and the survival of the thermocouple, which still remained within the heated zone to provide a reasonably accurate measurement of the sample temperature. Placing the thermocouple completely outside the heater, as shown in Table 5.1, would introduce an unacceptably large error in the temperature measurement, potentially underestimating the sample temperature by 3.3%.

The observed temperature variations and the estimated thermal gradients within the cubic press were further complicated by the known effects of pressure and high temperature on thermocouple performance, as documented by Li et al. [73] and Ongrai et al. [75]. Li et al. [73] investigated thermocouple behaviour under high pressure in a multi-anvil press and found that the electromotive force (emf) versus temperature relationship of Type S thermocouples (like those used in this study) was significantly affected by pressure, and deviated, leading to temperature measurement errors. At 5 GPa, they observed a +5°C deviation, and at 15 GPa, the deviation ranged from +25°C to -35°C between room temperature and 1800°C. While the current study was conducted at 6 GPa, within this range, Li et al. [73] shows that the pressure effect alone could introduce a significant error in the temperature readings. Thus, the pressure effect on the Type S thermocouples promoted higher temperature readings than the actual sample temperature, partially explaining the temperature difference between the 'inside' and 'outside' thermocouple positions, in addition to the real thermal gradient.

Li et al. [73] also identified other significant sources of error, including uncertainties in hot junction position and geometry, pressure gradients, and non-hydrostatic stress within the high-pressure assembly. These factors likely contributed to the temperature

gradient found in this study, especially within the heater assembly. Li et al. [73] also noted that mechanical deformation of thermocouple wires can lead to large errors. In the cubic press environment, the closing and opening of the anvils can directly compress, bend, or shear the thermocouple wires and sheath, especially if the thermocouple is not carefully positioned. This deformation can affect the contact area and introduce stresses at the thermocouple junction, as well as altering the bulk thermoelectric properties of the wires, leading to inaccurate temperature measurements.

The long-term stability of thermocouples at high temperatures is also a concern. Ongrai et al. [75] demonstrated significant drift in Type R thermocouples (platinum and 13% rhodium) aged at 1350°C for 500 hours of exposure time. Given the similar compositions of the Type R and Type S thermocouples (platinum – 10 at. % rhodium), it is reasonable to expect similar drift behaviour in the Type S thermocouples used in study, especially at temperatures exceeding 1500°C. While the duration of this study was significantly shorter than Ongrai et al. [27], even short-term drift could have contributed to the uncertainty in temperature measurements of this study.

Li et al. [73] estimated an overall error of 1.6% for Type S thermocouples up to 1700°C due to the combined effects of position uncertainty, pressure gradients, and non-hydrostatic stress. Due to the potential for pressure-induced changes in thermocouple emf, long-term drift, and the inherent uncertainties in high-pressure temperature measurements, the reported temperatures should be considered as estimates with an associated uncertainty of 1.6% [73]. The combination of these factors demonstrates the difficulties of accurate temperature measurement in high-pressure, high-temperature environments and shows the need for careful thermocouple selection, placement and a thorough consideration of potential sources of error. The observed differences between 'inside' and 'outside' heater measurements, while indicating a thermal gradient, were likely also affected by these thermocouple limitations. The thermocouples were used to monitor the temperature at different locations within the sample assembly. The thermocouple positioned 1 mm from the sample recorded higher temperatures than the thermocouple at 6 mm, as shown in Table 5.1. This

temperature difference, reflecting the thermal gradient within the assembly, directly affected the sintering process and, consequently, the microstructure and wear performance of the PDC samples.

This study demonstrated the critical influence of thermocouple placement on the accuracy of temperature measurement during HPHT sintering of PDCs. Placing the thermocouple inside the heater, closer to the sample, provided a more accurate measurement of the actual sintering temperature than placing it outside the heater. However, direct contact between the thermocouple and reactive sample components must be avoided to avoid thermocouple failure. The 1 mm gap reduced thermocouple-sample reactions and enabled more stable temperature readings. There were steep temperature gradients within the cubic press, which need to be considered for assessing temperature measurements. Furthermore, the study demonstrated the significant impact of temperature gradients within the sample assembly on the resulting microstructure and wear resistance of the PDCs. While the press was operated at a constant power setting, the different thermocouple positions (1 mm vs. 6 mm) revealed significant temperature variations, indicating that the actual sintering temperature experienced by different samples varied considerably. This variation in sintering temperature directly influenced the microstructure and wear performance.

8.1.2 Optimising Leachability by Parameter Control: Individual Effects

8.1.2.1 Effect of Holding Time on Leach Rate

The decreased leach rate with increasing holding time can be attributed to the microstructural changes that occurred during sintering. Longer holding times at temperature also resulted in more diffusion of tungsten from the substrate which could have affected the chemical composition of the binder and slowed the leaching rate. A longer holding time promotes greater densification, shown by the reduced porosity in Figure 4.2 and listed in Table 6.1. Leaching intentionally introduced porosity in the leached microstructures, which is called “engineered porosity” (Figures 4.2 and 4.3). This porosity is desirable because the leached layer comprised only the interconnected diamond network, which transmits heat away from the tip of the working layer and improves wear resistance [13,48,51]. However, some of the

engineered porosity possibly came from the removal of some of the Co and WC phases during sample preparation.

Figure 4.2 indicates the densification during sintering because the number and size of the pores are related to the original cobalt pools and hence the degree of densification. This might seem counterintuitive, as removing the cobalt by leaching should decrease density. However, there are two separate densification processes. Firstly, there is the densification which occurs during initial sintering, where the material is heated to bond the cobalt and diamond particles [9,32]. Cobalt acts like a glue that holds the diamond particles together, so more cobalt leads to a denser structure before leaching [9,32]. Secondly, there is the “engineered porosity” created by leaching. When the cobalt is leached out, it leaves behind empty pores, increasing porosity, which is beneficial in this case to transmit heat away, improving wear resistance [13,48,51].

The degree of densification during sintering directly affects the final porosity after leaching [9,32,111–115]. A denser pre-leached structure, with smaller cobalt pools initially, will have smaller pores after leaching. The microstructure of a leached material depends on the initial density of its precursor. A higher density precursor, analogous to a densely packed sponge, results in a leached structure with smaller and fewer pores than one derived from a lower density precursor. While leaching inherently increases porosity due to the removal of cobalt, the initial density of the pre-leached structure plays a critical role in determining the final pore size and distribution [9,32,111–115]. This “engineered porosity” significantly affects the material's performance, particularly in applications where heat dissipation and wear resistance are crucial [9,32,111–115].

Figure 8.4 shows that the 30-minute leached sample had fewer and smaller pores than the 20-minute leached sample, indicating that the extra 10 minutes holding time during sintering reduced porosity and hence further densification as expected. The reduced leachability in 30-minute leached sample was due to the reduced porosity achieved by the longer holding time, since densification continues gradually with time [9,32].

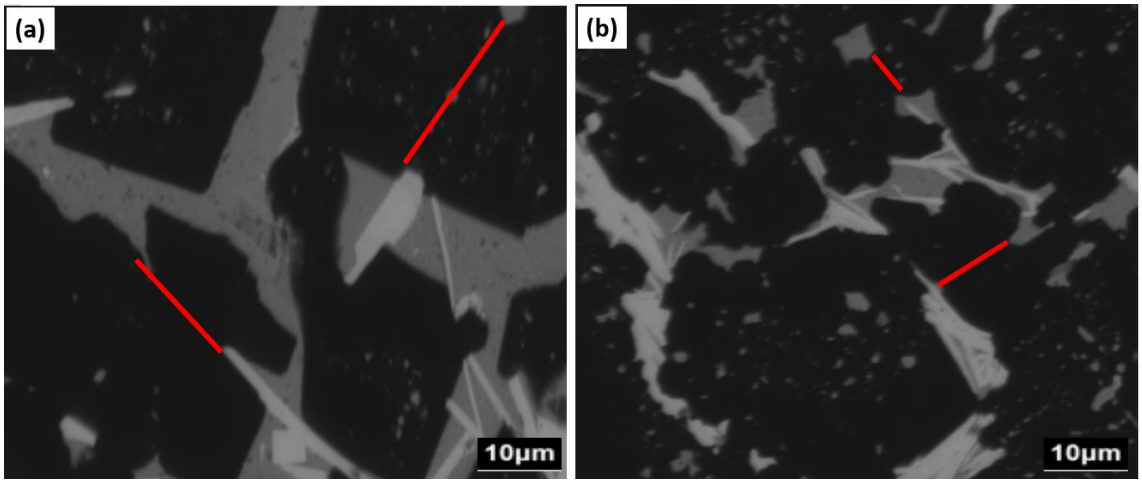


Figure 8.4: *SEM-BSE images of PDC samples, taken from the bottom of the diamond layer near the interface, sintered for: (a) 20 minutes and (b) 30 minutes, showing cobalt pools (medium grey contrast), diamond (dark contrast) and tungsten carbide (light grey contrast). Red lines show interfaces between diamond grains. Sintering pressure and temperature were 7 GPa and 1500°C (Figure 4.1)*

The longer holding time (30 minutes) in Figure 8.4(b) resulted in less Co between the diamond grains than Figure 8.4(a) (20 minutes). The increased densification is primarily attributed to the extended time available for the key sintering mechanisms to progress. These mechanisms include liquid-phase sintering facilitated by the cobalt binder. The molten cobalt wets the diamond surface and is drawn into the interparticle spaces by capillary forces [32]. It then acts as a solvent, dissolving less stable carbon (from strained diamond regions or graphite) and promoting the reprecipitation of more stable diamond at grain contact points leading to increased diamond-diamond contact. This solution-reprecipitation process, along with grain boundary migration (where boundaries between grains of similar orientation move to reduce grain boundary energy), contributes to densification. This process, along with the improved particle packing, leads to a denser material. Figure 8.4b shows this improved packing, showing how particles are better accommodated to each other and fit together more tightly. The mechanisms of solution-reprecipitation and grain boundary migration during sintering are well-documented in materials science literature [9].

Figure 8.4 does not show clear evidence of classical sintering neck formation between diamond grains, which would appear as discrete bridges of newly-formed diamond. Rather, they show varying degrees of diamond-diamond proximity. Figure 8.4(b), representing the longer sintering time, shows a more compact structure with narrower

cobalt regions. This is because the extended sintering time allowed for more complete infiltration of the cobalt and more extensive diamond-diamond contact, reducing the volume fraction of the cobalt phase [32].

Grain boundaries between diamond grains of different crystallographic orientations are present in Figure 8.4. There are areas of very close diamond-diamond contact with low remaining cobalt.

While the current study focused on achieving densification through extended sintering time, Sha et al. [116] investigated the impact of initial diamond grain size on the wear behaviour of PDC. They reported improved wear resistance with larger initial grain sizes after annealing at 700°C, attributing this to enhanced grain interlocking and densification [116]. This contrasts with the findings of the present study, where extended sintering time did not significantly improve wear resistance despite achieving a certain level of densification. Both the current study and the work by Sha et al. [116] showed densification was crucial for wear resistance. The current study achieved densification primarily through extended sintering time, promoting more complete solution-precipitation. In contrast, Sha et al. [116] observed enhanced densification with a larger initial diamond grain size. While it is generally easier to achieve full density with smaller initial particles due to shorter diffusion distances, Sha et al.'s findings likely stem from the use of a wider grain size distribution. In such distributions, larger grains can act as a rigid framework, while smaller particles fill the interstices, leading to a higher packing density even before sintering begins. This improved initial packing, combined with subsequent solution-precipitation, can result in greater final density. This study identified grain rearrangement as mechanisms driving densification during extended sintering. While Sha et al. [116] did not state the mechanism, their mention of "enhanced grain interlocking" suggested a similar process. Larger initial grain sizes might facilitate greater contact area and potentially more pronounced deformation during sintering, leading to better interlocking and ultimately densification. Thus, Sha et al. [116] stated that larger diamond grains packed tighter after annealing, while this study found that even with smaller diamond grains, given more time, they can accommodate to fit tighter. Figure 6.3 shows how the extra sintering time promoted densification:

(1) **Grain rearrangement:** The grains rearranged and interlocked more effectively. German et al. [9] explained how the liquid cobalt facilitates this, by filling the voids and preferentially dissolving low density graphite to reduce surface energy. The dissolution of graphite and the lubrication provided by the liquid cobalt allows the diamond grains to rearrange and achieve a denser packing. However, Gou et al. [50] demonstrated that reducing cobalt content by various treatments can improve the friction and wear performance of PDCs. This shows the importance of controlling cobalt content, for example by optimising sintering time as investigated in the current. Sha et al. [116] also indicated the important role of cobalt in PCD performance, observing that both insufficient and excessive cobalt negatively affected wear resistance [116]. This emphasises the need to optimise cobalt content, not only by controlling sintering time, as investigated in this study, but also by considering the initial grain size of the diamond particles. The initial grain size can influence the cobalt distribution within the microstructure, which in turn affects both densification and wear behaviour. While German et al. [9] identified the crucial role of cobalt in facilitating densification during sintering, Gou et al. [50] demonstrated that reducing cobalt content can improve the tribological properties of PDCs. Thus, while sufficient cobalt is necessary to facilitate effective densification during sintering, recognised by German et al. [9], excessive cobalt can decrease wear resistance, as observed by Gou et al. [50]. Gou et al.[50] demonstrated that leaching cobalt and annealing can improve the tribological properties by reducing graphitisation and promoting the formation of protective transfer films. These are thin material layers that transfer from one or both contacting surfaces during sliding, adhering to the surfaces and acting as barriers to reduce wear and friction. Thus, optimising sintering time and post-sintering treatments to control cobalt content and distribution is essential to achieve optimal wear resistance in PDC materials.

(2) **Plastic deformation:** While particle rearrangement is a primary contributor to pore size reduction during sintering, plastic deformation of diamond grains also plays a significant role at elevated pressures and temperatures. This deformation can lead to restrictions in pore channels, enhancing densification.

It is important to distinguish this from solution-precipitation mechanisms, which are discussed separately.

(3) **Reduced voids:** The overall porosity reduces, leading to a denser structure. This occurs by solution-precipitation [50], where the carbon-saturated liquid precipitates diamond at grain contacts to form necks, which reduces surface area and thus surface energy.

In the 30-minute leached sample (Figure 8.4 (b)), the cobalt was less accessible to the acid because of reduced pore size and fewer pores, reducing the leach rate. The trend of reduced leachability with increased holding time (Figure 6.2) was attributed to the densification, with fewer and smaller pores. Thus, less of the cobalt binder was exposed to the acid, reducing the surface area available for leaching [50].

The unexpected finding that the changes in porosity did not result in statistically significant differences in wear resistance (Figure 6.1) could indicate a complex interaction between microstructure and wear mechanisms. Alternatively, the changes made in the current study were not significant, so did not lead to changes in wear resistance. Gou et al. [50] showed that the effectiveness of microstructural changes in improving wear resistance may depend on the specific wear mechanisms involved. It was expected that the assumed denser microstructure (30-minute sample with less porosity), would have improved wear resistance (Figure 6.1).

However, while a slight decrease in mean wear scar area was observed for cutters sintered for 30 minutes compared to 20 minutes, this difference was not statistically significant (Figure 6.1), as indicated by the overlapping standard deviations.

This unexpected result questions the anticipated correlation between increased densification (reduced porosity) resulting from longer sintering times and improved wear resistance in the leached PDC cutters. It is possible that the dominant wear mechanisms in the test used were not sensitive to the degree of densification achieved by extending the sintering time from 20 to 30 minutes, or that the changes in porosity were not substantial enough to significantly impact wear resistance. For example, if abrasion was the primary wear mode, the overall hardness of the tungsten carbide inclusions might affect the wear resistance more than the effect of the porosity, and mask it [116]. Alternatively, the relatively small difference in porosity between the two

samples (Table 5.1) might not have been sufficient for a significant change in wear resistance, and measurement of the wear scar area was somewhat crude and did not consider the depth profile nor morphology of the wear scar, which could have provided more information on the wear mechanisms. Gou et al. [50] also recognised the complex interactions of wear mechanisms for PCDs, including transfer film formation, graphitisation and passivation. They [50] indicated that the effectiveness of microstructural changes in improving wear resistance may depend on the particular wear mechanisms involved. This could explain why the observed differences in porosity between the 20-minute and 30-minute sintered samples (Table 6.1) in the current work did not give a statistically significant difference in wear resistance. Sha et al. [116] observed variations in friction coefficient with different initial grain sizes, due to differences in surface residual stress and their effect on wear mechanisms [116]. Thus, the relationship between microstructure and wear resistance may be complex and affected by more than porosity and grain size. Figure 4.2 shows 2D SEM images of the leached samples, which are slices through 3D structures. In 2D images, only open pores that intersect the surface are visible, but closed pores within the sample would not be visible [116]. Leaching typically targets the interconnected cobalt network [9], so the resulting porosity is likely to be mostly open and interconnected, and some isolated cobalt pools could remain and not be accessible to the acid.

Figure 4.4 shows the XRD data, showing the effectiveness of leaching in removing the cobalt-based phase, agreeing with the SEM results in Figure 4.3. The intensity of the Co_3W peak at 59° was lower in the leached sample, indicating less of this phase after leaching. However, a small amount of the Co_3W was still present, shown by low intensity peaks in the leached sample. The duration of leaching (or holding time) plays a critical role in determining the completeness of cobalt removal [50]. A longer holding time may further reduce the residual cobalt amount.

***Table 8.1**: Curve fits for the relationship between holding time and leachability*

Mathematical model	K, slope	Fitted equation	Correlation coefficient (R^2)
Exponential	5.916	$Y = 5.916e^{-0.009x}$	0.991
Linear	-0.043	$Y = -0.043X + 5.789$	0.998
Logarithmic	-1.067	$Y = -1.067\ln(X) + 8.131$	0.997
Polynomial	0.002	$Y = 0.002X^2 – 0.124X + 6.778$	1
Power	9.707	$Y = 9.707X^{-0.226}$	0.999

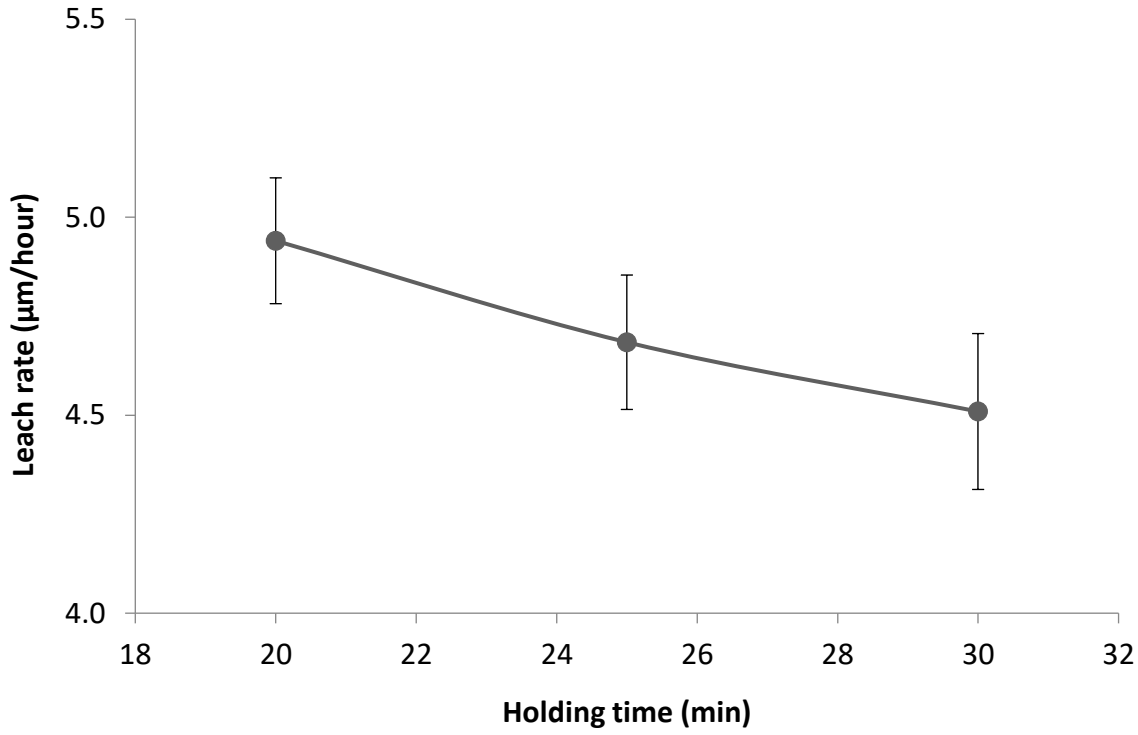


***Figure 8.5:** Relationship between leachability (leach rate) and sintering pressure after 96 h leaching in HCl acid*

Several mathematical models were considered to describe the relationship between leach rate and holding time (Figure 8.5, Table 8.1). Minitab software was used to fit these models to the data, and their goodness of fit was assessed using the correlation coefficient (R^2). R^2 values, ranging from 0 (weak relationship) to 1 (perfect relationship), indicated how well each model represented the data [76-78]. All models had R^2 values above 0.96, suggesting a strong fit to the relationship between leach rate and holding time under the experimental conditions. The polynomial model provided a perfect fit ($R^2 = 1$), indicating that it accounted for all variability in leach rate. Therefore,

the following polynomial model best describes the influence of holding time on leach rate within the tested conditions:

$$Y = 0.002X^2 - 0.124X + 6.778 \text{.....} \textbf{Equation 8.2}$$

where: X = holding time and Y = leach rate.

The value of 6.778 in Equation 8.2 is the intercept and is the leach rate when the holding time was 0 minutes. This value was ignored because holding time would never be 0 minutes since the typical time to sinter a commercial PDC starts at 20 minutes [14,16]. In addition, moving the intercept to zero would affect the accuracy of the model to predict within the boundary sintering conditions of 20– 30 minutes. To validate the mathematical model in Equation 8.2, samples sintered at 26 minutes and 33 minutes were leached for 96 hours. These two holding times were chosen because 26 minutes fell within the sintering boundary conditions tested and 33 minutes fell outside the sintering boundary conditions tested. The 26-minute sample was validating the suitability of the model to predict leach rates within the boundary conditions, while the 35-minute sample was validating the suitability of the model to predict leach rates outside the boundary conditions. Holding times less than 20 min were not validated because most products are sintered from 20 minutes and above [9].

***Table 8.2**: Validation of the modelled data for the leach rates against the experimental data after 96 h leaching*

Sintering holding time	**Modelled value (µm/h)**	**Experimental value (µm/h)**	**Variation (%)**
26 minutes	4.63	4.67 ± 0.17	4
33 minutes	3.99	4.31 ± 0.37	32

Table 8.2 compares the modelled and experimental data. For the 26-minute sample, the modelled value showed only a 4% deviation from the experimental data, demonstrating good agreement within the established boundary conditions (Equation 8.2). In contrast, for the 33-minute sample, the model overestimated the experimental value by 32%, indicating a significant limitation in its predictive accuracy when exceeding the defined holding time range (>30 minutes).

This study demonstrated that increasing sintering holding time significantly reduced the leach rate of PDCs. This effect was attributed to enhanced densification during sintering, leading to a less porous microstructure that reduced the leaching acid's accessibility to the cobalt binder. The polynomial model provides a valuable tool for predicting leach rate based on holding time within the tested range. While longer holding times improved densification, the effect on wear resistance was not statistically significant, suggesting that either the changes were insufficient or a more complex relationship between microstructure and wear mechanisms.

8.1.2.2 Effect of Temperature on Leach Rate

The significant negative correlation between sintering temperature and leach rate was a consequence of the temperature-driven microstructural changes during sintering. These changes were consistent with the principles of liquid phase sintering (LPS) [32] and mechanisms of diamond sintering described by German et al. [9]. Figure 4.2 and Figure 4.3 show the effect of leaching and the creation of “engineered porosity” in the PDC samples. In the unleached sample (Figure 4.3 (a)), cobalt pools were dispersed within the diamond matrix. They acted as a binder during initial sintering, facilitating densification by "gluing" the diamond particles together, a mechanism characteristic of liquid phase sintering [32]. The leached sample (Figure 4.3 (b)) had a distinct porous network, formed by the selective removal of these cobalt pools, which was intentionally introduced by leaching, hence "engineered porosity". The interconnected diamond structure that remained is strong and effectively transmits heat away, improving wear resistance [13,121]. The densification during initial sintering, determined by the amount of cobalt, directly affects the final porosity after leaching. Table 6.4 shows that a denser pre-leached structure with more cobalt resulted in smaller and fewer pores after leaching [9,13,32,121]. Higher sintering temperatures resulted in lower porosity and more elongated pores (Table 6.4). The porosity and pore morphology changes with sintering temperature agree with the general principles of sintering, i.e., higher temperatures gave increased densification and diamond intergrowth [32]. The microstructural changes also agreed with the mechanisms of diamond sintering described by German et al. [9], together with the importance of operating within a specific "sintering window": a combination of pressure and temperature that avoids graphitisation and ensuring cobalt melt infiltration. The

chosen sintering temperatures of 1500°C and 1700°C and 6 GPa pressure were within this optimal window, as shown by the successful densification and formation of a strong diamond network. German et al. [9] also described the sintering mechanism to involve carbon transport driven by pressure gradients, with dissolution of graphite in low-pressure regions and precipitation of diamond at high-pressure grain contacts. The interconnected diamond network observed in the leached samples (Figure 4.2) showed this, and diamond precipitation occurred preferentially at the contact points between diamond grains (Figure 8.6).

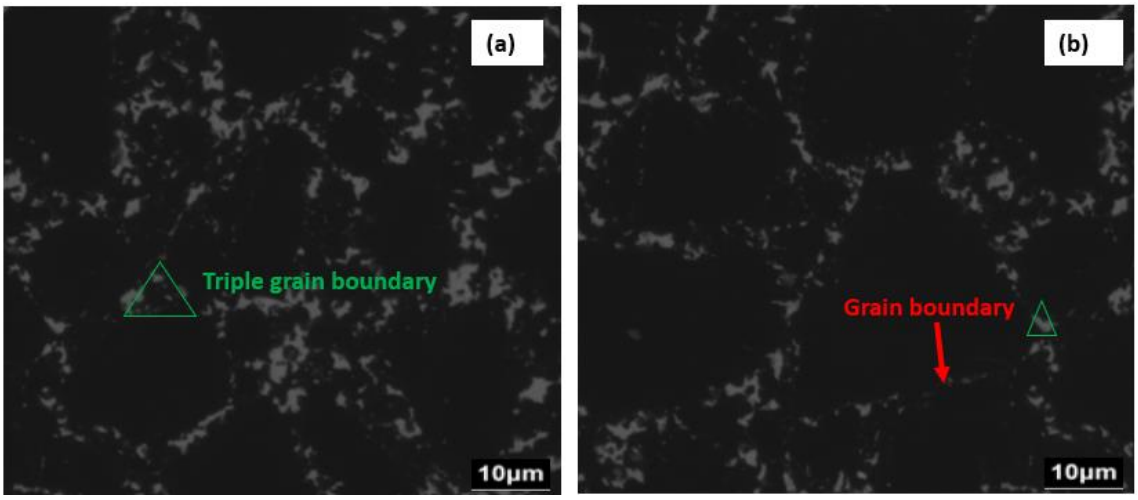


Figure 8.6: *SEM-BSE images of PDC samples, taken from the middle of the diamond layer, sintered for: (a) 1500°C and (b) 1700°C, showing cobalt pools (medium grey contrast) and diamond (dark contrast) with well-defined grain boundaries (red arrow). Sintering pressure and holding time were 7 GPa and 20 minutes (Figure 4.1)*

Figure 8.6 shows the microstructural evolution of the PDCs at different sintering temperatures. At the lower sintering temperature of 1500°C (Figure 8.6(a)), cobalt pools are visible, along with the initial formation of areas where diamond grains are touching together. German et al. [32] described this initial contact between grains as a result of capillary forces exerted by the liquid cobalt phase, initiating densification during the early stages of liquid phase sintering (LPS). The presence of these areas of contact in Figure 8.6(a) confirms that LPS was active even at this lower temperature. Additionally, Figure 8.6(a) shows diamond reprecipitation, consistent with the observations of German et al. [9], where diamond dissolves in regions of lower pressure and reprecipitates at grain contacts where the pressure is higher.

However, at the higher sintering temperature of 1700°C (Figure 8.6(b)), the cobalt pools are less prominent, and there is significantly more grain coalescence. This indicates enhanced densification and increased diamond-diamond bonding. German et al. [32] define grain coalescence as the joining of two grains through initial contact followed by grain boundary migration. This process is evident in Figure 8.6(b), suggesting its significant contribution to the microstructural evolution of PDCs at higher sintering temperatures. The more pronounced grain coalescence at 1700°C correlates with the higher wear resistance observed (Figure 6.5).

Triple grain boundaries, also visible in Figure 8.6, are a characteristic feature of LPS. German et al. [32] describe these junctions as a result of grains coming together during densification, driven by the movement of the liquid phase along grain boundaries.

Both sintering temperatures (1500°C and 1700°C) fall within the established "sintering window" [9] for diamond, as shown by the absence of graphitization (Figure 4.4) and the successful densification of the PDCs. The increased grain coalescence and reduced porosity observed at 1700°C are consistent with the lower leach rate (Figure 6.6) and higher wear resistance (Figure 6.5). The improved wear resistance at 1700°C is attributed to a combination of microstructural and phase compositional factors directly resulting from the higher sintering temperature. The improved wear resistance was due to a combination of factors related to the microstructure and phase composition, which were directly caused by the higher sintering temperature:

(1) **Enhanced Densification and Reduced Porosity:** The higher sintering temperature of 1700°C promoted greater densification during liquid phase sintering (LPS) [32] (Figure 8.6). The 1700°C sample had fewer and smaller pores than the 1500°C sample (Table 6.4). This denser microstructure with reduced porosity provided greater resistance to abrasive wear, as there were fewer voids and weak points that could initiate crack propagation and material removal.

(2) **Increased Grain Coalescence and Stronger Diamond Network:** The 1700°C sample (Figure 8.6 (b)) had greater grain coalescence than the 1500°C sample (Figure 8.6 (a)). This indicated higher diamond-diamond bonding, facilitated by the enhanced diffusion and diamond solution-reprecipitation [9]. The stronger,

more interconnected diamond network provided better resistance to the stresses encountered during wear.

(3) **Grain Size Considerations:** Dai et al. [4] showed the dependence of grain size on wear resistance, where finer-grained PDCs exhibited higher hardness and thermal resistance, while coarser-grained PDCs had better impact resistance. The higher grain coalescence in the 1700°C sample (Figure 8.6 (b)) indicates a larger grain size than the 1500°C sample, agreeing with Dai et al. [4] that coarser grains improve impact resistance and fracture toughness, which are beneficial for wear resistance (Figure 8.6 (b)).

There was a significant reduction in leach rate as the sintering temperature increased (Figure 6.6). The inverse relationship between sintering temperature and leach rate was mainly attributed to the microstructural changes during sintering, particularly porosity, pore morphology and the distribution of the cobalt binder phase.

1. **Densification and Porosity:** As discussed earlier, higher sintering temperatures promoted greater densification during liquid phase sintering (LPS) due to enhanced diffusion and atomic mobility [32]. The 1700°C sample (Figure 8.6 (b), Table 6.4) had significantly lower porosity than the 1500°C sample (Figure 8.6 (a) and Table 6.4). This denser microstructure, with fewer voids, impeded the penetration of the HCl acid during leaching. Fewer pathways ware available for the acid to access and react with the cobalt binder, resulting in a slower rate of cobalt removal.

2. **Pore Morphology and Interconnectivity:** The morphology and interconnectivity of the pores was also important. The ImageJ analysis (Table 6.4) revealed that the 1700°C sample had a lower pore aspect ratio, indicating more elongated pores. Although the slightly smaller Feret diameter suggests these pores were individually smaller, their elongated shape, compared to the more equiaxed pores in the 1500°C sample, may have led to a less efficient network for acid transport. This reduced connectivity, despite the smaller pore size, would hinder acid flow and reduce the leach rate.

3. **Cobalt Distribution:** While the XRD analysis (Figure 4.4) confirmed the effective removal of cobalt from the surface of the leached samples, the distribution of cobalt within the bulk of the PDC differed between the two sintering temperatures. The higher sintering temperature might have led to a more homogenous distribution of the

remaining cobalt (Figure 8.6), potentially within a denser network of WC and the Co_3W intermetallic phase, making it less accessible to the acid.

***Table 8.3**: Curve fits for the relationship between sintering temperature and leachability*

Mathematical model	K, slope	Fitted equation	Correlation coefficient (R^2)
Exponential	4.826	$Y = 4.826e^{-0.006x}$	0.989
Linear	-0.009	$Y = -0.009X + 21.113$	1
Logarithmic	-1.224	$Y = -1.224\ln(X) + 12.698$	0.997
Polynomial	0.006	$Y = 0.006X^2 – 0.331X + 9.115$	9.988
Power	11.321	$Y = 11.321X^{-0.116}$	0.995

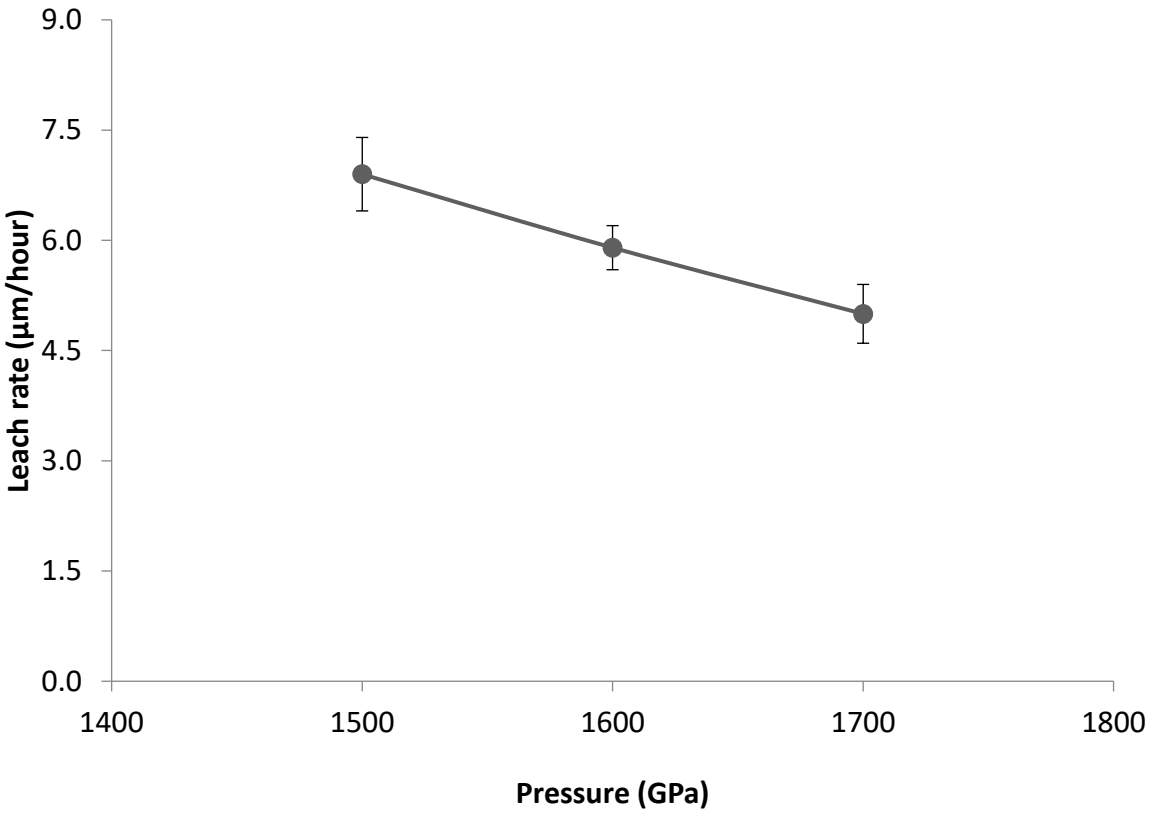


***Figure 8.7:** Relationship between leachability (leach rate) and sintering temperature after 96 h of leaching in HCl acid*

Table 8.3 shows different mathematical models that were considered suitable to describe the relationship between leach rate and temperature in Figure 8.7. All the fitted equations to Figure 8.7 (Table 8.3) had correlation coefficients greater than 0.96, indicating they all described the relationship between leach rate and holding time well under the experimental conditions used. However, the equation with a perfect fit (i.e., R^2 of 1) to the experimental data was the polynomial model, implying that 100% of the variability in leach rate was predicted by the mathematical model. Thus, under the experimental conditions tested, the effect of temperature on the leach rate was modelled by:

$$Y = -0.009X + 21.113 \quad \textbf{Equation 8.3}$$

where: X = sintering temperature and Y = leach rate.

To validate the mathematical model in Equation 8.3, samples were sintered at 1550°C and 1750°C and leached for 96 hours. These two temperatures were chosen because 1550°C fell within the sintering boundary conditions tested and 1750°C fell outside the sintering boundary conditions tested. The 1550°C sample validated the suitability of the model to predict leach rates within the boundary conditions, while the 1750°C sample validated the suitability of the model to predict leach rates outside the boundary conditions.

Table 8.4: *Validation of the modelled data against the experimental data after 96 h leaching*

Temperature (°C)	Modelled value (µm/h)	Experimental value (µm/h)	Variation (%)
1550	6.41	6.21 ± 0.15	3
1750	4.51	3.61 ± 0.41	22

Table 8.4 compares modelled and experimental data. For the 1550°C sample, the modelled value showed only a 3% deviation from the experimental value, demonstrating good agreement within the established boundary conditions (Equation 8.3). In contrast, for the 1750°C sample, the model overestimated the experimental

value by 22%, indicating a significant limitation in its predictive accuracy when exceeding the defined sintering time range (>1700°C).

Sintering temperature had a significant negative correlation with the leach rate of PDCs. Higher sintering temperatures led to reduced leach rates, primarily due to enhanced densification, altered pore morphology and achieved a more homogenous distribution of the remaining cobalt within a more consolidated diamond and WC network. The linear model (Y = -0.009X + 21.113) is a valuable tool for predicting leach rate based on sintering temperature within the tested range (1500-1700°C). The findings demonstrate the importance of carefully controlling sintering temperature to optimise the microstructure and leachability, ultimately improving performance.

8.1.2.3 Effect of Pressure on Leach Rate

The observed negative correlation between sintering pressure and leach rate was explained by the effect of pressure on the microstructure of PDCs during sintering.

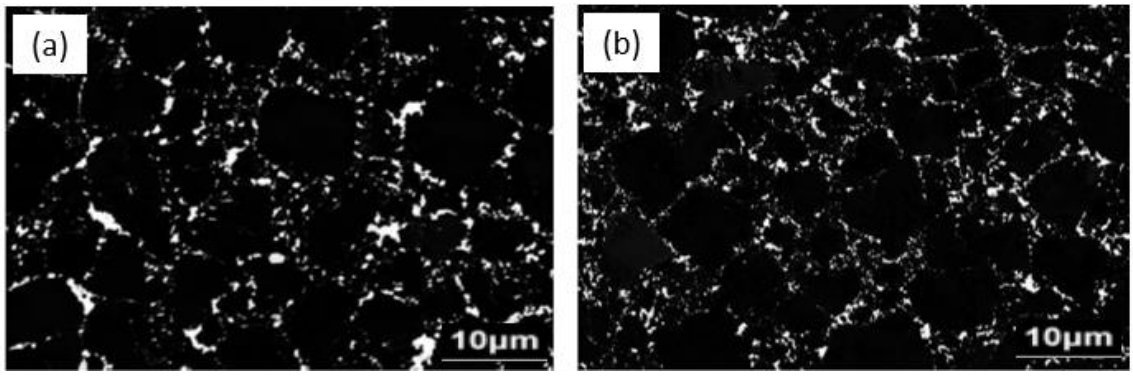


Figure 8.8*: SEM-BSE images of PDC binder pools, taken from the middle of the diamond layer, sintered at different pressures: (a) 5 GPa and (b) 7 GPa, showing cobalt pools (light contrast), tungsten (grey contrast) and diamond (dark contrast). Sintering were 1500°C and 20 minutes (Figure 4.1)*

A systematic reduction in both the average cobalt pool size (Figure 8.8, Table 6.7) occurred with increasing sintering pressure. This was attributed to rearrangement of the diamond particles at elevated pressures. This process is active during both cold and hot compaction stages and promote pore shrinkage and a reduction in the cobalt pool size [9, 29, 32], as indicated by their smaller Feret diameters. Furthermore, the diminished pore size at higher pressures restricts cobalt infiltration from the cemented carbide substrate into the diamond layer [3,5]. The 7 GPa sample, with the smallest pre-infiltration pores (Figure 8.8), allowed for minimal cobalt ingress, and thus the

smallest average cobalt pool size (smallest average Feret diameter). This showed the pressure-dependent nature of cobalt migration from the substrate to the diamond layer.

The 5 GPa sample had the highest cobalt content, 9.2 ± 0.9 vol.% (Table 4.5), agreeing with Westraadt et al. [5], who found 9.0 ± 1.0 vol.% Co for a PDC sintered at 5.5 GPa. The present findings were consistent with Dai et al. [4], who found 10.7 ± 0.1 vol.% Co for a sample sintered at 5.5 GPa. Thus, higher sintering pressures reduced pre-infiltration porosity, limiting cobalt infiltration and ultimately reducing the overall cobalt content within the diamond layer. The wear resistance of PDCs was inversely related to cobalt content, agreeing with previous results [4,38,61,66,115,123]. As expected, the sample with the highest cobalt content (5 GPa) had the poorest wear resistance (Table 6.8), agreeing with industrial experience [14,16,59], where elevated cobalt content is associated with diminished wear resistance.

Cobalt, while acting as a binder during sintering, compromises wear resistance in the final product. It facilitates the dissolution of graphite from diamond grain surfaces and its subsequent reprecipitation as diamond, leading to diamond-to-diamond bonding and intergrowth [9,32]. This creates new diamond grain connections, between the original diamond grains [9,32]. A clear correlation exists between sintering pressure and wear scar area, Table 6.8. The wear scar area of the PDC samples decreased significantly with increasing sintering pressure (Table 6.8). This inverse relationship was directly linked to the reduced porosity (Table 6.7) and reduced cobalt pool size (Figure 6.10) at higher pressures, leading to a more wear-resistant structure. However, this enhanced wear resistance was accompanied by a reduction in leaching rates (Figure 6.9). The denser, less porous material from higher pressure sintering hinders acid access to the binder during the leaching process [13,48–50]. Thus, there is an inherent trade-off in PDC manufacturing between achieving optimal wear resistance and maintaining efficient leaching characteristics.

There was substantial reduction, ~78%, in the cobalt phase in leached samples (Table 4.3). Conversely, tungsten carbide (Table 4.3) remained relatively stable, indicating that leaching (HCl acid) had a minimal effect on the tungsten carbide, because it has greater resistance to HCl [49]. Despite the substantial reduction in the cobalt phase,

the remaining 22% (Table 4.3) indicated that some of the cobalt was inaccessible to the HCl acid during leaching and was probably within closed pores or cavities [51]. Closed pores prevented the acid from reaching and dissolving the encapsulated cobalt. The closed porosity in the PCD is attributed to Ostwald ripening during sintering, where larger pores grow at the expense of smaller pores [51]. Some pores become completely enclosed within the material, resulting in closed porosity [51].

The reduction of cobalt was consistent with XRD (Figure 4.4) and XRF (Table 4.4) results and showed that leaching mainly removed Co_3W, leaving WC mostly intact. Again, leachability (ease with which cobalt can be removed) exhibited a negative correlation with sintering pressure (Figure 6.9). This is because cobalt pool size (Feret diameter) affects acid flow pathways. Larger cobalt pools (larger Feret diameters) provide wider channels for acid ingress, facilitating cobalt removal, and smaller pools (smaller Feret diameters) restrict acid flow, hindering leachability [13]. Among the investigated pressures, the 5 GPa sample exhibited the fastest leachability (Figure 6.9) and the largest cobalt pool size (Table 6.10). Thus, leachability of the cobalt binder is directly governed by the distribution and accessibility of cobalt between diamond particles [13]. Additionally, diamond grains can encapsulate cobalt pools, effectively shielding them from the acid solution.

The initial leaching reaction involves chloride anions from the HCl acid interacting with exposed cobalt pools surfaces. These anions subsequently diffuse deeper through intergranular pores, reacting with additional cobalt to form soluble cobalt chloride, which is then removed from the cutter [13,51]. As cobalt is leached, the pools become pores. Leachability is affected by the diffusion rate of anions and reaction products through the newly formed pores. Therefore, the size of the cobalt pools (Figure 6.10) dictates both the rate-limiting step of leaching and the subsequent pore size, which in turn governs acid diffusion and access to the remaining cobalt [13,51]. Smaller pools (smaller Feret diameters) restrict diffusion, decreasing the leaching rate, while larger pools (larger Feret diameters) facilitate diffusion, enhancing the leaching rate [13,51]. Figure 6.9 shows the relationship between leach rate and pressure.

Various mathematical models were evaluated using Minitab software to determine their suitability for describing the relationship between leach rate and pressure, with

the correlation coefficient (R^2) being the evaluation metric. Table 8.5 presents five models that effectively fitted the data.

***Table 8.5**: Curve fits for the relationship between pressure and leachability*

Mathematical model	K, slope	Fitted equation	Correlation coefficient (R^2)
Exponential	17.167	$Y = 17.167e^{-0.212x}$	0.9697
Linear	-1.047	$Y = -1.047X + 11.139$	0.9847
Logarithmic	-6.221	$Y = -6.221\ln(X) + 15.988$	0.9762
Polynomial	0.302	$Y = 0.302X^2 - 4.667X + 21.813$	0.9803
Power	45.745	$Y = 45.745X^{-1.263}$	0.9767

The linear model with the highest R^2 value (0.9847) had the best fit to the experimental data, while the exponential model had the lowest. This implied that 98.47% of the variability in leach rate was explained by the linear model within the tested experimental conditions. Therefore, the effect of pressure on leach rate can be effectively modelled by:

$$Y = -1.047X + 11.139 \quad \textbf{Equation 8.4}$$

where: Y = leach rate and X = sintering pressure.

The slope (K = -1.047) quantified the extent to which sintering pressure affects the leach rate. The intercept (11.139) represents the theoretical leach rate at a sintering pressure of 0 GPa, which is not useful since commercial PDC sintering typically starts at 5 GPa [14,16,30]. Shifting the intercept to zero would compromise the model's accuracy within the relevant pressure range of 5 GPa to 7 GPa. To validate Equation 8.4, samples were sintered at 6.8 GPa and 8 GPa and leached for 96 hours. The 6.8 GPa sample was chosen to test the model's predictive capability within the established boundary conditions, while the 8 GPa sample served to evaluate its performance outside this range. Pressures below 5 GPa were not considered as they are not commonly used in commercial PDC production.

***Table 8.6**: Validation of the modelled data against the experimental data after 96 h leaching*

Pressure (GPa)	Modelled value (µm/h)	Experimental value (µm/h)	Variation (%)
6.8	4.03	4.12 ± 0.44	2.4
8	2.76	1.05 ± 0.17	61.9

Table 8.6 compares the modelled and experimental leach rates. For the 6.8 GPa sample, the model deviated from the experimental value by only 2.4%, demonstrating good agreement within the established boundary conditions. However, at 8 GPa, the model significantly over-predicted the experimental value by 62%, demonstrating the inaccuracy beyond the defined pressure range (>7 GPa). This agrees with the increased standard deviations observed at the boundary limits in Figure 6.9.

Increased pressure reduced leachability, mainly due to increased densification, reduced porosity, decreased cobalt pool sizes and increased diamond contiguity. The linear model from the CCD analysis (*Y = -1.047X + 11.139*) provided a useful tool for predicting leach rate as a function of pressure within the investigated range. The findings also demonstrated the trade-off between leachability and wear resistance, with higher pressures favouring the latter. The selective nature of leaching mainly targeting the cobalt-containing phase was demonstrated by XRD and XRF.

8.1.3 Integrated Parameter Optimization: Interactions and Relative Importance

8.1.3.1 Multiple Regression Analysis of Sintering Parameters on Leachability

The multiple regression model showed the interaction of sintering parameters on PDC leachability. From Table 7.2, the regression equation to predict the leach rate of PDC based on the sintering parameters was:

$$Y = -1.02X_1 - 0.02X_2 - 2.11X_3 + 0.01X_1X_2 + 56.72 \quad \textbf{Equation 8.5}$$

where: Y = value of the leach rate, X_1 = sintering holding time (first independent variable), X_2 = sintering temperature (second independent variable), X_3 = sintering

pressure (third independent variable), X_1X_2 = interaction term: holding time*temperature.

Table 7.2 presents the core statistical results of the multiple regression model, quantifying the relationship between the sintering parameters (holding time, temperature, pressure and their interaction) and leach depth. The F-value (4.37), p-value (< 0.001), R^2 (86.4%) indicated that the overall regression model was statistically significant, i.e., sintering parameters collectively explained a significant proportion of the variability in leach depth. The R^2 value of 86.4% quantified this, i.e., the model explained 86.4% of the variance in leach depth, and a good fit for this type of data [19], demonstrating that the chosen sintering parameters were important factors affecting leachability of PDC cutters. The pressure (coefficient = -2.11, $p < 0.001$) is negative and highly significant ($p < 0.001$), indicating that higher pressure leads to lower leach depth. This is consistent with previously discussed mechanisms related to increased densification, reduced porosity and greater mechanical interlocking at higher pressures [9,32], all of which hinder the penetration and effectiveness of the leaching agent [9,32]. Equation 8.4 indicated that for every 1 GPa pressure increase, the leach depth decreases by 2.11 µm/h assuming all other variables are held constant. The temperature (coefficient = -0.02, $p < 0.001$) was also negative and highly significant ($p < 0.001$), indicating that higher temperatures led to a lower leach depth. This is consistent with several mechanisms that can occur at higher temperatures. Enhanced cobalt flow can lead to binder depletion in critical areas [9]. The formation of brittle intermetallic, such as Co_3W, at the diamond-cobalt interface can weaken the structure. Furthermore, cobalt undergoes a phase transformation from its face-cantered cubic (FCC) structure to a hexagonal close-packed (HCP) structure at elevated temperatures [88], which can alter the mechanical properties of the binder phase [9,32]. Thus, increased densification, reduced porosity, greater mechanical interlocking (all promoted by higher pressure), cobalt flow, intermetallic carbide formation and the cobalt transition (all promoted by higher temperature) contribute to more resistant microstructures, reducing the leach depth.

Increased densification, reduced porosity and greater mechanical interlocking contribute to more resistant microstructures to acid leaching, reducing the leach

depth. Equation 8.4 also indicated that for every 1°C increase in temperature, the leach depth decreased by 0.02 units, assuming all other variables were held constant. The Holding Time (coefficient = -1.02, $p < 0.01$) was negative and significant ($p < 0.01$), i.e., indicating longer holding times were associated with lower leach depths. This is consistent with mechanisms related to increased densification, enhanced binder distribution and potential stress relaxation during prolonged holding [9,32], particularly at lower temperatures [9,32]. However, the effect was less strong than pressure or temperature, as indicated by the smaller coefficient and higher p-value. This also suggests that for every 1-minute increase in holding time, the leach depth decreased by 1.02 units, assuming all other variables are held constant (Equation 8.4).

The positive and significant coefficient for the interaction term confirmed the presence of an interaction effect between holding time and temperature. This indicated that the effect of holding time on leach depth was dependent on the temperature, and *vice versa*. The positive coefficient implies that as temperature increased, the negative effect of holding time on leach depth became less pronounced. This is consistent with the interaction plot (Figure 7.2), which showed that at higher temperatures, holding time had a negligible effect on leach depth.

The results in Table 7.2 were consistent with Figures 7.1 and 7.2. For example, the negative coefficients for pressure, temperature and holding time in Table 7.2 directly correspond to the negative slopes in Figure 7.1. The significant positive interaction coefficient in Table 7.2 agreed with the non-parallel lines in the interaction plot (Figure 7.2), demonstrating the temperature-dependent effect of holding time. The microstructural differences in Figure 4.2, particularly the porosity variations, support the significant effects of pressure and temperature on leach depth in Table 7.2. The strong negative correlations between pressure and leach rate, and temperature and leach rate in Figure 7.3 agree with the significant negative coefficients for these parameters in Table 7.2. The weak correlation between holding time and leach rate was also consistent with the smaller and less significant coefficient for holding time in the regression model. Table 7.2 was consistent with the trends in Figure 7.4: negative coefficients for pressure and temperature were consistent with lower pressures and temperatures generally resulting in higher leach rates. The high VIF for the interaction

term in Table 7.1 indicated potential multicollinearity, which was established in the interaction between holding time and temperature in Table 7.2.

Table 7.1 presents the variance inflation factors (VIFs) for each predictor variable in the multiple regression model. The VIFs are used to assess the degree of multicollinearity, which occurs when predictor variables are highly correlated with each other. High multicollinearity can inflate the variance of the regression coefficients, making them unstable and difficult to interpret [80,81]. A VIF >10 is often considered an indicator of problematic multicollinearity [80], suggesting that the standard errors of the affected regression coefficients might be inflated. This is the core problem. When multicollinearity is high (VIF > 10), the standard errors of the coefficients for the correlated variables tend to be larger than they would be if the variables were uncorrelated. The model has trouble distinguishing the effects of the correlated variables, leading to more uncertainty in their individual estimates. The VIF for the interaction term (Holding time*Temperature) was 10.70 (exceeding the threshold of 10). This was due to the inherent relationship between these two parameters in sintering. It might be difficult to completely isolate the effects of holding time and temperature because they are often adjusted together to achieve desired microstructural changes. The presence of multicollinearity, particularly for the interaction term, did not diminish the importance of the interaction effect or the overall findings of this study. Instead, it demonstrated the inherent complexity of the relationship between holding time and temperature in sintering. The high VIF for the interaction term showed that the effects of holding time and temperature on leach depth are interdependent and cannot be fully separated. This is consistent with the understanding that these two parameters work together to affect densification and binder distribution [129]. This is not a flaw in the model, but rather a realisation of the inherent interdependence of these two parameters in sintering. The multicollinearity does not invalidate the significant interaction effect found in the regression analysis. Instead, it emphasised the need to consider the combined effect of holding time and temperature when optimising PDC manufacturing to achieve the desired leach rate and performance.

Figure 7.1, the main effects plot, shows how each sintering parameter (pressure, temperature and holding time) individually affected the leach rate of PDC cutters. Plotting the mean leach rate against different levels of each variable while holding the others constant, isolated the main effect of each parameter. There was a clear negative trend between pressure and leach rate. As sintering pressure increased, the mean leach rate decreased significantly. This was directly linked to the effect of pressure on densification and porosity: higher pressure gives greater densification [9,32], reducing the overall porosity and the interconnectedness of the pores within the PDC. Reduced porosity creates fewer pathways for the leaching agent to penetrate and react with the cobalt binder [13]. Higher pressures increase the mechanical interlocking between the diamond and cobalt phases, increasing the number of closed pores, and making it harder for the acid to remove the cobalt [29]. Therefore, reduced porosity and increased mechanical interlocking at higher pressures significantly hinder the leaching process, lowering leach rates.

Figure 7.1 also shows a negative trend between sintering temperature and leach rate, as sintering temperature increased, the mean leach rate decreased. This trend was consistent with established mechanisms (Section 8.1) related to cobalt distribution and diamond-to-diamond bonding [9, 32]. Higher sintering temperatures are known to enhance the diffusion and flow of the cobalt binder, leading to a more uniform distribution and greater encapsulation of the diamond particles [9]. Furthermore, higher temperatures promote reprecipitated diamond at grain boundaries, increasing the number of diamond-to-diamond bonds [32]. The resulting enhanced encapsulation and increased diamond-to-diamond bonding reduce the surface area of exposed cobalt and create a more acid-resistant microstructure, thus lowering the leach rate.

Figure 7.1 shows a negative trend between holding time and leach rate, although less pronounced than that of pressure or temperature. As holding time increased, the mean leach rate decreased. Longer holding time allows for more complete densification, particularly at lower temperatures where diffusion rates are slower [130]. It also provides more time for the cobalt binder to distribute more uniformly, leading to better encapsulation of diamond particles. Longer holding times can also

allow for stress relaxation within the PDC, potentially giving a more stable microstructure that is less prone to leaching, and hence a lower leach rate [72]. However, the effect was less pronounced because the main mechanisms are more strongly influenced by pressure and temperature. The interaction plot (Figure 6.2) also demonstrated that the effect of holding time was highly dependent on sintering temperature.

The trends in the main effects plot (Figure 7.1) were entirely consistent with the results of the multiple regression analysis (Table 7.2). The negative coefficients for pressure, temperature and holding time in the regression equation directly corresponded to the negative slopes in the main effects plot (Figure 7.1), reinforcing that each of these sintering parameters had a negative effect on leach rate. Figure 7.1 shows the individual effects of each sintering parameter on the leach rate of PDC cutters, demonstrating the dominant role of pressure and temperature in controlling the microstructure and, consequently, leachability. The main effects plot (Figure number 6.1), in conjunction with Figures 7.2, 7.3 and 7.4 and the regression analysis, Table 7.2, provides a comprehensive understanding of the interactions between sintering parameters and leach rate, which is crucial for optimising the PDC manufacturing process. By carefully controlling pressure, temperature and holding time, manufacturers can tailor the microstructure of PDC cutters to achieve the desired leach rate. For example, if a lower leach rate is desired for a particular application, the main effects plot suggests that higher pressure, higher temperature and a longer holding time would be beneficial. Conversely, if a higher leach rate is needed, lower pressure, lower temperature and a shorter holding time would be preferred.

Figure 7.2, the interaction plot, shows the effect of holding time on leach rate is moderated by temperature. It reveals that the relationship between holding time and leach rate was not constant but changed depending on the specific temperature. This dynamic interaction is necessary to understand the complex leaching behaviour of PDC cutters. The most important feature of the Figure 7.2 was that the lines representing the effect of holding time at 1500°C and 1900°C are not parallel, which is an indicator of an interaction effect [79]. Without any interaction, the lines would be parallel [79],

i.e., the effect of holding time on leach rate would be consistent across different temperatures. At 1500°C, increasing holding time decreased in the leach rate because the line had a clear negative slope. This is consistent with the principles of sintering: at lower temperatures, diffusion rates are slower [32] and longer holding times allow for more time for the cobalt binder infiltrate and fill the pores between diamond particles, reducing porosity and creating a denser microstructure [9]. Longer holding times allow more time for the cobalt to distribute more uniformly, leading to better encapsulation of the diamond particles and reduced exposed cobalt surface area [32]. Longer holding times also allows for increased mechanical interlocking because they allow diamond-to-diamond bonds to form [9,32]. The combination of these factors makes the PDC structure more resistant to leaching, hence the decreased leach rate with increased holding time at 1500°C.

At 1900°C, increased holding time had a negligible effect on the leach rate (Figure 7.2). The line is nearly horizontal, indicating almost no change in leach rate with changed holding time, which is also consistent with the principles of sintering [32]. At higher temperatures, diffusion is significantly accelerated [32]: near-maximum densification is achieved relatively quickly due to the enhanced cobalt flow. The cobalt binder distributes rapidly and uniformly, encapsulating the diamond particles effectively in a shorter time. Since these processes occur rapidly at 1900°C, extending the holding time beyond a certain point gives little additional benefit for altering the microstructure to further reduce leachability. The PDC microstructure has already reached a state where further changes in holding time have a minimal impact on the leach rate. There is also the potential of diamond degradation or unwanted grain growth if the holding time is excessive at high temperatures [71,131]. The interaction plot (Figure 7.2) confirmed the significant interaction effect that was statistically identified by multiple regression analysis (Table 7.2) and indicated by the high VIF for the interaction term (Table 7.1). The regression coefficient for the interaction term (0.01) was positive, indicating that the negative effect of holding time on leach rate became less pronounced as temperature increased, agreeing with the interaction plot, Figure 7.2.

Figure 7.3 shows strong negative correlation between pressure and leach rate (r = -0.700, 95% CI [-0.807, -0.548]), i.e., as sintering pressure increased, the leach rate decreased significantly. The narrow confidence interval suggests a high degree of certainty in this relationship. Figure 7.3 also shows a significant negative correlation between temperature and leach rate (r = -0.543, 95% CI [-0.696, -0.343]), i.e., higher sintering temperatures are associated with lower leach rates. Again, the relatively narrow confidence interval reinforced the reliability of this finding. Furthermore, higher temperatures form WC precipitates [32] at the diamond-cobalt interface [32], creating a diffusion barrier that further hinders leaching. Figure 7.3 also shows a weak and non-significant negative correlation between holding time and leach rate (r = -0.221, 95% CI [-0.442, 0.027]), suggesting that holding time, on its own, has a minimal effect on the leach rate than pressure and temperature. The dominant processes affecting microstructure and leachability (densification, binder flow, carbide formation) [9,32] were more strongly influenced by pressure and temperature. While holding time did play a role in allowing these processes to occur, its effect became less pronounced at higher temperatures where these processes were accelerated. The interaction plot (Figure 7.2) also supported this by showing that the effect of holding time is largely dependent on temperature.

Figure 7.4 summarises the interaction between pressure and temperature on leach rate. The contour plot demonstrates that lower pressures and lower temperatures were conducive for higher leach rates. The different regimes are:

1. **Lower Pressure Regime (below 6.0 GPa):**
    - Higher Leach Rate (darker green): This region has conditions that favour more porous microstructures, since lower sintering pressures result in less densification [29].
    - Mechanism: Increased porosity and resulting larger surface area of exposed cobalt facilitate faster leaching.
2. **Lower Temperature Regime (below 1650°C):**
    - Higher Leach Rate (darker green): This region has conditions where cobalt diffusion and flow during sintering are less pronounced.

- Mechanism: Reduced cobalt flow and WC formation at the diamond-cobalt interface increase cobalt exposure to the acid.

3. **Higher Pressure and Temperature Regime (top right):**
    - Lower Leach Rate (lighter green): This region has conditions that promote a denser microstructure with minimal porosity.
    - Mechanism: High pressure and temperature enhance densification and mechanical interlocking, while cobalt flow and carbide formation create barriers, all hindering acid penetration and protecting the cobalt binder.
4. **Holding Time as constant:**
    - Holding time was held constant in this analysis because its influence on leach depth was smaller than pressure and temperature, especially at the higher temperatures investigated.
    - Mechanism: Densification and cobalt redistribution reach near-completion quickly at higher temperatures used in this study, limiting the effect of holding time on leachability.

Figure 7.4 combines the statistical findings (regression analysis) in Table 7.2, the microstructural changes in Figure 4.2 and the theoretical understanding of sintering mechanisms [9,32]. It shows how sintering parameters affect the microstructure and, consequently, the leachability of PDC cutters, which is crucial for optimising the manufacturing process to achieve the desired balance between leach rate and wear resistance of PDC cutters. The contour plot predicts the leach rate under different sintering conditions, enabling manufacturers to tailor the process to meet specific application requirements. For example, if a higher leach rate is desired to create a more aggressive cutting microstructure, the plot indicates that lower pressures and temperatures are necessary. Conversely, if a lower leach rate is needed for enhanced durability, higher pressures and temperatures should be used.

Figure 7.5, the optimisation plot, provided parameters to maximise the leach rate of PDC cutters. The identified optimal settings of 5.0 GPa and 1437°C are from the fundamental leaching mechanisms discussed throughout the study and are consistent with the trends in Figures 7.3 and 7.4:

1. **Optimised Pressure (5.0 GPa):**
    - Rationale: This pressure was within the lower end of the investigated range and is in the region associated with higher leach rates in Figure 7.4.
    - Mechanism: At 5.0 GPa, sintering results in a microstructure that retains the interconnected porosity, giving the necessary pathways for the leaching agent to effectively penetrate the PDC structure and react with the cobalt binder, and giving a higher leach rate. Lower pressures also reduce the mechanical interlocking of the diamond and cobalt phases, making it easier for the acid to attack and remove the cobalt.
2. **Optimised Temperature (1437°C):**
    - Rationale: The temperature of 1437°C falls within the lower end of the investigated temperature range, which is consistent with the trend in Figure 7.4.
    - Mechanism: At 1437°C, diffusion and flow of the cobalt binder during sintering are limited. Consequently, the cobalt does not fully encapsulate the diamond particles, leaving a larger surface area exposed to the leaching agent. Additionally, 1437°C is less likely to promote the formation of extensive, continuous tungsten carbide layers at the diamond-cobalt interface, which would hinder leaching. There is also less diamond degradation at lower temperatures.
3. **Maximum Leach Rate (6 µm/h):**
    - Rationale: The predicted 6 µm/h leach rate was the highest achievable under the experimental conditions tested, signifying a microstructure conducive to efficient cobalt removal.
    - Mechanism: This leach rate is from the optimised microstructure achieved at 5.0 GPa and 1437°C. The interconnected porosity, less extensive cobalt encapsulation and likely absence of significant interfacial carbide barriers all contribute to this maximised rate of cobalt removal.

4. **Desirability (d = 0.84, D = 0.84):**
    - Rationale: The 'd' is the desirability of a single response variable, while 'D' is the combined desirability across multiple response variables. The high desirability values, which range from 0 to 1 with 1 representing the most desirable outcome, indicate that the optimised settings were highly favourable for achieving the desired maximised leach rate. In this study, optimisation targeted only the leach rate as the response variable and resulted in a desirability value of (d = D = 0.84).
5. **Practical Implications:**

The optimisation plot provided actionable information for manufacturers of PDC cutters. By sintering at the recommended pressure and temperature, they can achieve a microstructure that maximises leach rate, leading to cutters with enhanced performance for specific drilling applications. This could allow faster drilling rates, improved bit life and reduced drilling costs. For example, a higher leach rate can be used to create cutters with more aggressive cutting profiles, making them ideal for applications requiring high rates of penetration. The optimisation plot, which suggests operating at the lower end of the tested pressure and temperature ranges to maximise leach rates in PDC cutters, is consistent with broader industrial practices [66] aimed at enhancing manufacturing efficiency and product performance. In many industrial processes [66], operating at lower energy inputs (lower temperatures and pressures) is generally favoured for several reasons:

- Energy Efficiency: Lower temperatures and pressures typically require less energy, leading to reduced operational costs. This is a common principle in manufacturing where energy consumption is a significant portion of the operating budget [132,133].
- Equipment Longevity: Operating equipment at lower pressures and temperatures can reduce wear, prolonging the life of manufacturing equipment and reducing maintenance costs. This is because extreme conditions can accelerate material degradation, leading to more frequent repairs or replacements [133,134].

- Safety: Lower operating pressures reduce the risk of catastrophic failure of the WC anvils used in the high-pressure cubic press, enhancing safety during PDC sintering [134]. Such failures can result in high-energy ejection of WC fragments, posing a significant hazard to personnel and equipment.
- Environmental Impact: Reduced energy consumption also reduces carbon footprints, aligning with global trends towards more sustainable and environmentally-friendly manufacturing practices.
- Cost of Production: Apart from energy savings, operating under milder conditions can reduce the need for highly specialised, expensive materials for withstanding extreme pressures and temperatures.
- Material Properties: In some manufacturing processes, lower temperatures and pressures can help achieve desirable material properties. For example, in sintering of ceramics or metals, avoiding extreme conditions can prevent unwanted phase transformations, grain growth, or thermal stress that can compromise the quality of the final product [71].

Thus, the optimisation plot's recommendation to use lower pressure (5.0 GPa) and lower temperature (1437°C) to maximise leach rate is therefore not only beneficial for achieving the desired leachability in PDC cutters but also aligns with these broader industrial benefits. It suggested a manufacturing approach that is potentially more energy-efficient, cost-effective and environmentally sustainable, while still achieving the desired product performance. This approach aligns with the general trend in industrial manufacturing towards optimising processes for both product quality and operational efficiency. However, this apparent benefit has a disadvantage. Wear resistance is reduced when sintering at lower pressures and temperatures. Conversely, achieving higher material densification and superior abrasive wear performance necessitates higher sintering pressures, which unfortunately correspond to lower leaching rates. This presents a balance in process optimisation, as the enhancement of one desirable parameter occurs at the expense of another.

The core objective of acid leaching in PDC cutters is to ultimately improve the material's performance: durability and wear resistance during drilling. Thus, the recommendation to utilise sintering conditions that reduce initial wear resistance,

even to facilitate more efficient leaching, needs careful consideration. If leaching is an additional processing step intended to enhance wear, then the starting material's intrinsic wear characteristics, influenced by sintering conditions, must be considered.

While leaching adds cost and time, production expenses must be weighed against the PDC cutter’s performance requirements. Industrial interest is the performance : cost ratio, which encompasses both the achieved product quality and the associated manufacturing cost. The Value per Length of Tool-life" (VLT) data also needs to be considered, as it directly quantifies the economic value derived from a cutter`s lifespan in operational settings.

The optimal manufacturing strategy for PDC cutters is contingent upon the specific application. Drilling in highly abrasive formations demands maximising wear resistance, potentially justifying higher sintering costs and slower leaching rates. Conversely, less demanding applications might prioritise lower overall production costs, even with a slight reduction in wear performance. This demonstrates that a single, universally optimal set of processing parameters is improbable; rather, a tailored approach based on the intended end-use and its associated performance requirements is necessary. In essence, achieving an industrially viable PDC cutter requires an understanding of the trade-offs between sintering conditions, leaching and the final operational performance (VLT), allowing for a data-driven approach to optimise the performance/cost ratio for diverse drilling applications.

The multiple regression analysis quantified the combined effects of pressure, temperature and holding time on the leach rate of PDC cutters. The model, which explained a substantial proportion, 86.4%, of the variance in leach rate, revealed the dominant role of pressure, the significant influence of temperature and the important interaction between holding time and temperature. These findings, supported by microstructures, correlation analysis, contour plot of leachability, and an optimisation plot, provided a valuable framework for optimising sintering to achieve desired leachability characteristics in PDC cutters. The model can be used to predict leach rates under different combinations of parameters, allowing for a more targeted approach to PDC manufacturing.

8.1.3.2 Dominance Analysis and the Hierarchy of Parameter Importance

Dominance analysis clearly established pressure as the most dominant factor influencing the leach rate of PDCs within the investigated parameter range. Sintering pressure had complete dominance over both sintering temperature and holding time (Figure 7.6) within the studied range. This is consistent with Figure 7.1 and agreed with previous studies [9,32,136] where higher pressure improved densification [136]. For example, Montross et al. [136] observed a 4% increase in diamond content in PDCs when the sintering pressure was increased from 4.5 GPa to 7.5 GPa.

While pressure undeniably plays a critical role, it is important to recognise the interaction between the sintering parameters. Firstly, sintering temperature governed the diffusion kinetics of atoms, which is fundamental to the sintering process [136]. Elevated temperatures enhanced atomic mobility, facilitating material transport and promoting neck formation and grain growth, all contributing to densification. Secondly, holding time at the sintering temperature allows for the microstructure to be closer to equilibrium and bearer completion of diffusion and microstructure rearrangements. Insufficient holding time may hinder complete densification, even under high pressure, which indicated that the interaction between pressure and holding time existed. Although Figure 7.6 shows the significant effect of sintering pressure on densification, it is important to consider the synergy between pressure, temperature and holding time. Figures 7.7 and 7.8 demonstrate the dominance of sintering pressure on the leach rate of PDCs, but it is important to realise that this does not imply pressure acted in isolation. Dominance analysis here demonstrated the combined effects and interactions of all sintering parameters, including temperature and holding time. Pressure affected densification [9,32], bringing particles closer together, while temperature facilitated the necessary atomic diffusion for bonding [9], and holding time ensured the nearer completion of these processes [9]. The resulting leach rate was a consequence of this interaction.

Figure 7.7 shows an interesting trend in the dominance analysis. While the weights of sintering pressure and temperature had no clear pattern across different model subset sizes, the weight of holding time consistently increased with increasing subset size. This behaviour indicated the presence of a suppressor variable, described by Braun et

al. [26]. The negligible contribution of sintering holding time in Figure 7.7 indicated that it had a weak independent relationship with leachability, identifying it as a suppressor variable [136]. A suppressor variable may exhibit a weak correlation with the dependent variable in isolation but can be strongly correlated with other independent variables that are themselves correlated with the dependent variable. Thus, the suppressor variable "cleans up" the noise in other variables, ultimately leading to a more substantial contribution to the dependent variable. While the suppressor variable itself may not have a strong direct effect, it indirectly influences the dependent variable by its suppressive effect on other variables. Darlington et al. [90] demonstrated the importance of including suppressor variables in a model because exclusion can lead to underestimating the suppressed variable's weight, which inflates model error and reduces predictive power. While including suppressor variables can introduce multicollinearity—a situation where predictor variables are highly correlated with each other—and consume degrees of freedom, which reduces the statistical power of the analysis and makes it harder to find statistically significant results, the risk of excluding a relevant variable (leading to omitted variable bias) generally outweighs these potential disadvantages [90].

The concept of suppressor variable agrees well with PDC sintering. The suppressor effect of sintering time on leachability can amplify the effects of pressure and temperature. For example, longer sintering times, while not directly influencing leachability, allow for greater densification under high pressure [90]. This densification can lead to a more compact microstructure with reduced porosity, making it harder for leaching agents to penetrate and extract soluble components [90]. Thus, the suppressor effect of time amplified the effect of pressure in hindering leachability. In addition, extended sintering times under pressure can cause grain growth, further reducing porosity and limiting the pathways for leaching [90].

Another example is that prolonged sintering at high temperatures can cause phase transformations within the PDC [10], such as the formation of the intermetallic compound Co_3W and the ceramic WC in the diamond layer. The WC phase plays a similar role as an intermetallic compound in affecting leachability as Co_3W. Both compounds exhibit lower solubility in leaching agents [7,8,9,10] and help densify the PDC, which hinders leaching because they make it more difficult for the acid to

dissolve and extract the binder. This further strengthens the effect of temperature on reducing leachability with time. The formation of these phases, particularly at grain boundaries, can alter the microstructure of the PDC, potentially making the grain boundaries less permeable to the leaching agents [10]. This reduced permeability further restricts the access of the acid to the cobalt binder, limiting the effectiveness of leaching. The presence of Co_3W and WC can contribute to increased densification of the PDC during sintering [10]. A denser microstructure has fewer pores and defects, which limits the pathways for the leaching agent to penetrate and access the cobalt binder [7].

The established hierarchy (Figures 7.6, 7.7 and 7.8) of parameter importance (Pressure > Temperature > Holding Time) provides valuable guidance for optimising the sintering process. Manipulating pressure is the most effective means of controlling leachability. The dominance of pressure can be attributed to its significant effect on densification during sintering. As discussed in Chapter 6, higher pressure enhances particle rearrangement, reduces porosity and promotes diamond-diamond bonding [16]. These microstructural changes directly hinder acid penetration during leaching, resulting in lower leach rates. Furthermore, higher pressure can lead to a reduction in the overall cobalt content in the diamond layer (discussed in Chapter 6), further contributing to reduced leachability. However, the significant interaction between holding time and temperature, coupled with the suppressor effect of holding time, demonstrates the need for a holistic approach that considers the synergistic effects of all three parameters.

Dominance analysis provided a quantitative assessment of the relative importance of pressure, temperature and holding time for determining the leachability of PDCs. The results indicated pressure as the most dominant factor, followed by temperature, with holding time having a smaller, although significant, indirect effect by its interactions with pressure and temperature.

These findings have important practical implications for the manufacturing of PDC cutters. They show that controlling pressure and temperature, is crucial for achieving the desired microstructure and leach rate. This knowledge can be used to optimise sintering, to tailor PDC cutter properties for specific drilling applications, and

ultimately improve drilling performance and efficiency. Dominance analysis provided a more nuanced understanding of the relative importance of each parameter, which can be used to prioritise optimisation efforts. Thus, focusing on optimising pressure and temperature is likely to yield the greatest improvements in leachability, while manipulating holding time can be used to further refine the microstructure.

8.2 Synthesis of Key Findings

A fundamental challenge in HPHT sintering of PDCs is the accurate determination and control of the key process parameters: pressure and temperature. This thesis addressed this challenge through two significant methodological advancements. Firstly, Chapter 5.1 developed a novel *in situ* pressure calibration method based on the volume change of the PDC sample. This approach overcame limitations of conventional fixed-point calibrations [18,68], which are often performed at room temperature and can be affected by non-hydrostatic stresses and variations in pressure-transmitting media. The novel *in situ* pressure calibration method yielded consistently larger pressure values than the fixed method, indicating that previous studies [18, 137, 138, 139] which relied on fixed-point calibrations may have underestimated the actual pressures involved in PDC sintering. This finding is consistent with Wang et al. [70], who also observed higher pressures using a differential thermal analysis (DTA) method.

Secondly, Chapter 5.2 found that direct contact between commonly used S-type thermocouples and the titanium sample container led to thermocouple failure due to the low temperature eutectic between Pt and Ti [142]. This problem was resolved by introducing a 1 mm gap between the thermocouple and the sample, preventing the reaction while maintaining sufficient proximity for accurate readings. This finding demonstrated the need for careful consideration of thermocouple placement in HPHT experiments, especially when using titanium as the sample container. While thermocouples remain a standard tool, their inherent limitations at high pressures and temperatures, including potential drift and pressure-induced emf changes [73; 75], should be considered. Furthermore, as indicated by the absence of graphitisation in Figure 4.4, the sintering temperatures and pressures remained within the appropriate "sintering window" for diamond as recommended by German et al. [32]. The XRD analyses of both leached and unleached samples showed no significant peak around 26 degrees 2-theta, the position of a strong graphite peak in PDC materials [5,10]. This

absence confirmed that substantial graphitisation of the diamond did not occur during the sintering of the samples used in this study, validating the selected sintering conditions.

Chapters 6 investigated the individual and combined effects of pressure, temperature and holding time on the leachability and microstructure of PDCs. All three parameters, holding time, temperature and pressure, when increased during sintering of PDCs, led to a more compact, less porous microstructure and hence increased densification. Section 6.1 showed that increased holding time resulted in less porous microstructures (Figure 4.2 and Table 6.1). This was further corroborated by Figure 8.4, which shows a tighter, more compact microstructure in the sample subjected to extended holding. Section 6.2 showed that increasing the sintering temperature resulted in less porous microstructures and hence increased densification (Figure 4.2. and Table 6.4). Figure 8.6 shows reduced porosity, more pronounced grain coalescence, and small cobalt pools at 1700°C than at 1500°C. Table 6.4 lists quantitative data, showing lower porosity for the sample sintered at 1700°C than at 1500°C. Section 6.3 showed that higher sintering pressures reduced pre-infiltration porosity, limiting cobalt infiltration and ultimately reducing the overall cobalt content and average cobalt pool size within the diamond layer (Figure 6.10, Table 6.7). Smaller cobalt pools are a direct indicator of greater densification, as the diamond grains are packed more tightly.

A key aspect of understanding PDC behaviour is identifying the mechanisms responsible for densification during sintering. While holding time, temperature and pressure resulted in reduced porosity and increased densification, the emphasis on the specific underlying mechanisms differ between them. Holding time allows more time for these mechanisms to occur. Temperature affects how fast these mechanisms occur, particularly diffusion and coalescence. Pressure affects the compaction and reduction in pores between the diamond grains. Grain coalescence, solution-precipitation and pore shrinkage are mechanisms that occur during the liquid phase sintering (LPS) of PDCs, contributing to densification and the development of the final microstructure [9,32]. However, they are distinct processes with different driving forces and effects:

- **Solution-Precipitation Mechanism:** The solution-precipitation mechanism, primarily explained by German et al. [9,32], involves the preferential dissolution of diamond in the non-contact regions and depositing in the neck regions. The dissolved carbon then diffuses through the liquid cobalt binder and re-precipitates onto diamond surfaces in lower-stress regions like developing necks and existing pores. This net transport promotes neck growth between diamond grains, thereby reducing surface energy, shrinking pores, and significantly contributing to overall densification [9,32].
  Concurrently, grain rearrangement, facilitated by liquid cobalt acting as a lubricant, allows diamond grains to shift into a denser packing, filling voids [9]. The dissolution of low-density graphite can further aid this rearrangement. The combined effect of solution-precipitation and grain rearrangement is a substantial reduction in porosity, a defining characteristic of increased densification [9].

  Evidence of solution-precipitation mechanism is shown in Figure 8.6, with the solid necks – bridges of diamond connecting adjacent diamond grains. These diamond necks provided direct evidence of solution-precipitation, where diamond dissolved in the non-contact regions and depositing in the neck regions. These necks were much clearer in the sample sintered at 1700°C (Figure 8.6 (b)) than at 1500°C (Figure 8.6 (a)). This is because temperature is extremely important for solution-precipitation [9]. Higher temperatures increase the solubility of diamond in cobalt which is a major factor because it determines how much diamond can dissolve and be available for re-precipitation. Higher temperatures also increase the diffusion rate of carbon atoms through the liquid cobalt [9]. This is important for transporting the dissolved carbon from high-stress to low-stress regions. Pressure also has a significant, but generally less direct effect than temperature, on solution-precipitation. The high pressure applied during sintering enhances the solubility of diamond in cobalt, which is a thermodynamic effect, further promoting this solution-precipitation process [9]. High pressures also create the stress

gradients that drive the process from high stress at contact points to lower stress in pores/necks.

Figure 8.6 shows WC precipitates at the diamond-cobalt interfaces. The increase in WC at the diamond-cobalt interface in the sample at 1700°C (Figure 8.6) provides indirect support for the occurrence of enhanced diamond solution-precipitation at higher temperatures. The formation of WC requires a source of carbon, which here, is mainly the diamond particles [32]. The increased WC at the interface indicated that more diamond dissolved into the cobalt at higher temperatures, making more carbon available for reaction with tungsten. This is consistent with the increased neck formation and reduced porosity observed at higher temperatures (Figure 8.6), which are direct consequences of diamond solution-precipitation. However, it is important to note that WC formation is a separate chemical reaction and, on its own, is not definitive proof of diamond reprecipitation. This increased dissolution is consistent with the observed neck formation and pore rounding (Figure 8.4), further supporting the role of solution-precipitation. The pores within the sintered sample for 30 minutes (Figure 8.4 (b)) were more rounded than in the sample sintered for 20 minutes. This indicated that solution-precipitation occurred because it tends to round out sharp features and create more rounded pores, as material is deposited in areas of low stress/curvature [9,32].

- **Grain Coalescence Mechanism:** In addition to solution-precipitation, grain coalescence also plays a significant role in the microstructural evolution of PDCs during sintering. Grain coalescence is the process by which two or more adjacent diamond grains, in direct contact, merge to form a single, larger grain [9,32]. This occurs by migration of the grain boundary separating the grains, driven by the reduction in total grain boundary area and, consequently, the overall grain boundary energy. The presence of the liquid cobalt phase enhances atomic mobility at the grain boundaries, facilitating this migration [9,32]. The result is an increase in the average diamond grain size, a reduction

in the number of grains, and a contribution to overall densification, particularly if there are pores on the grain boundaries that are removed [9,32].

This is evident in Figure 8.6 (b), where the sample sintered at 1700°C shows significantly more grain coalescence than the sample sintered at 1500°C (Figure 8.6 (a). This because temperature is generally the more dominant factor for the grain coalescence mechanism. Higher temperatures increase the atomic mobility at grain boundaries, which is essential for grain boundary migration. Grain boundary migration is fundamentally a thermally activated process, so temperature has a very strong effect on the rate of coalescence [9,32]. In Figure 8.6 (a), the diamond grains appear more distinct, with a higher proportion of cobalt separating them. In Figure 8.6 (b), the diamond regions appear larger and less distinct, with several areas showing close contact between diamond grains and reduced intervening cobalt (indicated by red arrows). These features suggest that some grain coalescence occurred, contributing to the increased diamond-diamond bonding. However, it is important to note that solution-precipitation can also lead to close diamond-diamond contact [9].

- **Particle Rearrangement Mechanism**: The particle rearrangement mechanism is dominant in the initial stages of sintering. High applied pressure forces diamond particles to shift and pack more closely [9]. The liquid cobalt binder significantly facilitates this rearrangement by acting as a lubricant, reducing friction and allowing particles to slide past each other, while capillary forces also draw them together [9,32]. This initial rearrangement substantially reduces the size and number of pores. Subsequently, solution-precipitation and grain coalescence, both enhanced by the applied pressure and liquid cobalt, further contribute to pore shrinkage and overall densification. High pressure increases diamond solubility, promotes atomic mobility, and increases the driving force for grain boundary migration, ultimately leading to a final microstructure with significantly reduced porosity [9,32].

Pressure is the dominant factor influencing particle rearrangement. The applied force directly pushes the diamond particles closer together, overcoming frictional resistance and initiating the rearrangement process. Figure 8.8 shows the PDC binder pools, provided indirect evidence of enhanced particle rearrangement at higher sintering pressures. In the sample sintered at 5 GPa (Figure 8.8 (a)), the cobalt pools were relatively large and irregularly shaped, suggesting that the diamond particles had undergone less rearrangement and compaction. As the sintering pressure increased to 6 GPa (Figure 8.8 (b)), the cobalt pools appeared smaller and more rounded. At 7 GPa the cobalt pools were smaller and more rounded, indicating more particle rearrangement and densification. This trend was consistent with the expectation that higher pressure forces the diamond particles into a tighter packing arrangement, reducing the overall porosity and altering the distribution of the remaining cobalt [4,29].

For all three parameters (increased holding time, temperature and pressure), the consistent result of increased densification and reduced porosity was decreased leach rate and overall leachability (Figures 5.7, 5.11 and 5.14). The mechanisms responsible for the reduced leach rate and overall leachability are fundamentally the same, regardless of whether increased holding time, temperature, or pressure is the primary driver of densification. These mechanisms are all consequences of the reduced porosity and increased density. The reduction in both leach rate and overall leachability in denser, less porous PDCs is a result of several interconnected mechanisms, all depending on the altered microstructure. These mechanisms, while working together, can be distinctly identified:

- **Reduced Cobalt Accessibility:** If the cobalt binder forms a continuous, interconnected network throughout the PDC, with a high degree of exposure to the surface and internal pores, the acid can easily penetrate and dissolve the cobalt. This results in high leachability. However, if the cobalt binder is less exposed, either because it is surrounded by more diamond (higher diamond density) or trapped within a less porous structure (higher overall density), the acid has a greater difficulty reaching and reacting with the cobalt. This leads to reduced leachability. In Figure 8.4 (b), the 30-minute sample had fewer and

smaller pores than the 20-minute sample in Figure 8.4 (a). This indicated that the cobalt in Figure 4.2 (b) was less accessible to the acid. The smaller pores in Figure 4.2 (b) are where the cobalt used to be. The fact that there are fewer of them, and they are smaller, means the acid had a greater difficulty reaching and removing the cobalt. Therefore, the smaller size and reduced number of pores in the longer-sintered sample directly corroborated the mechanism of reduced cobalt accessibility and increased densification.

- **Restricted Acid Penetration:** This mechanism focuses on the geometry of the porosity. Fewer pores, smaller pores, and, crucially, reduced interconnectivity between pores, create a more difficult and constricted path for the acid to follow. This hinders the diffusion of fresh acid into the material and the diffusion of dissolved cobalt reaction products out of the material, significantly slowing the leaching process. The porosity in Figure 8.4 (b) were the pathways the acid took to remove the cobalt. The shape, size, and interconnectedness of that porosity showed how easily the acid could penetrate. The fewer and smaller pores in Figure 8.4 (b) were important, because they were a more restricted pathway for the acid to penetrate the material. This supports that a denser microstructure with smaller, potentially less interconnected pores, hinders acid diffusion and slows down the leaching process (Figure 4.2).

- **Reduced Reactive Surface Area:** Leaching is inherently a surface reaction. The rate of cobalt removal is directly proportional to the amount of cobalt surface area exposed to the acid [13, 16,17]. Increased densification, and the resulting reduction in porosity, decrease cobalt surface area available for reaction. This is a fundamental limitation to the reaction rate. The increased WC precipitates (Figure 5.2 (b)) created a more twisting path for the acid to penetrate the material. The acid had to navigate around the WC particles to reach the cobalt. Thus, the reactive surface area involves both the size of the pores, and whether their openings are obstructed.

- **Increased Cobalt Encapsulation:** This mechanism addresses overall leachability. As the material densifies, there is a higher probability that some cobalt pools will become completely surrounded by the diamond, forming closed pores [9,32]. The acid cannot access the cobalt within these isolated pockets, preventing the acid to remove it. This limits the total amount of cobalt that can be leached, regardless of how long the leaching process continues. The process of Ostwald ripening, as described by German et al. [9], is important for this phenomenon. During sintering, larger pores tend to grow at the expense of smaller pores, driven by a reduction in overall surface energy [9,32]. As this process continues, some pores can become completely pinched off and enclosed within the surrounding diamond and tungsten carbide matrix, resulting in closed porosity. This creates isolated pockets within the diamond layer that are inaccessible to the acid. The quantitative evidence for this encapsulation is in Table 5.10 which shows the RIR values for the cobalt and tungsten carbide phases before and after leaching. While the tungsten carbide RIR remained relatively stable (decreasing only slightly from 1.2 to 1.1), indicating its resistance to the HCl acid [49], the cobalt RIR showed a large reduction from 0.9 in the unleached sample to 0.2 in the leached sample. This represented an approximate 78% reduction in the cobalt phase. Importantly, despite this substantial removal of cobalt, a significant 22% remained after leaching. This residual cobalt was strong evidence that a portion of the cobalt was inaccessible to the acid. Given the mechanism of Ostwald ripening [32]and closed pore formation, the residual cobalt is located within these closed pores or cavities. Therefore, the sintering process, by Ostwald ripening, created the conditions for cobalt encapsulation, directly affecting the effectiveness of subsequent leaching.

These four distinct, yet interconnected, mechanisms work synergistically to explain why denser, less porous PDCs exhibit both a slower leach rate and a lower overall leachability.

Chapter 6 also investigated the individual effects of pressure, temperature and holding time by simple linear regression models (Equations 8.2, 8.3 and 8.4). To determine which sintering variable most strongly influenced leach rate, these three simple linear

regression models were evaluated. Since the sintering variables studied were measured in different units. Pressure was measured in Giga Pascals, temperature in Celsius, and holding time in hours, and their coefficients were not directly comparable. Therefore, standardised coefficients were used to make a comparison of their effects. The standardised coefficients indicated that pressure had the strongest negative effect on leach rate than temperature and holding time (Table 7.2). Thus, the standardised coefficient for pressure was -0.65 ($p < 0.05$), while the coefficient for temperature was 0.41 ($p < 0.05$) and for holding time was -0.13 ($p < 0.05$) (Table 7.2). This indicated that a 1 standard deviation increase in pressure was associated with a 0.65 standard deviation decrease in leach rate. The negative signs for all coefficients indicated that increases in all three sintering variables were associated with decreases in leach rate. Although the R^2 value was also highest for the pressure model (R^2 = 86%), the standardised coefficients provided the most direct comparison of effect size. However, because simple linear regression models hold other variables constant, they cannot account for interaction effects between the sintering variables studied. The effect of pressure on leach rate is independent of the values of temperature and holding time. This means that increasing pressure always decreases leach rate by a consistent amount, no matter the temperature or holding time. Each parameter acts in isolation.

Unlike Chapter 6 which investigated the individual effects of pressure, temperature and holding time by simple linear regression models, Chapter 7 investigated the combined effects of pressure, temperature, and holding time using multiple regression and dominant analysis (Figures 7.1, 7.2, 7.3, 7.4, 7.6, 7.7). The R^2 value for the multiple regression model was 86% which indicated that the model explained a substantial portion of the variance in leach depth. The 86.4% of the variability in the leach rate can be attributed to the sintering parameters included in the model (holding time, temperature, pressure and their interaction). However, it is important to acknowledge that 13.6% of the variance in leach depth could not be explained by this model. This is a non-negligible portion that was not accounted for by the sintering holding time, temperature, pressure or their interaction. This unexplained variance demonstrates the inherent complexity of the PDC leaching process and several potential contributing factors, which can be broadly categorised as:

- **Variations in raw material composition:** Variations in the composition of the starting powders (e.g., trace impurities, particle size distribution of the diamond powder) can affect the microstructure of the sintered PDC, especially in the binder which might affect the cobalt pools that could change the leach rate [5,13]. These variations, not captured in the model's independent variables, could significantly affect leachability.
- **Microstructural inhomogeneities:** Sintering might not produce a perfectly uniform microstructure. Local variations in density, grain size, or the distribution of the binder within the PDC compact can lead to differences in leaching behaviour. For example, there was a large standard deviation for the small value of tungsten and even a large standard deviation for Co (Table 4.5), showing that there was variation in the results. Another example is the high standard deviation in the density measurements (Table 4.6), which may be attributed to similar microstructural inconsistencies. Inhomogeneous packing, uneven shrinkage, or localized porosity during sintering could result in density fluctuations across samples. Additionally, the geometric method used to estimate density, which was based on mass and dimensional measurements, may have introduced further variability, especially if the samples deviated from ideal cylindrical shapes or had surface irregularities. Furthermore, it is important to consider that EDS (observed anomalies in Figure 4.5) typically overestimates lighter elements such as carbon (diamond) and underestimates heavier elements like cobalt and tungsten, unless specific calibration samples and procedures are employed. This analytical bias can contribute to microstructural inhomogeneities.
- **Presence of defects:** Micro-cracks, porosity introduced during sintering or prior processing steps [19] can act as preferential pathways for leaching, leading to increased leach rates in localized areas. The model did not account for the presence or distribution of these defects.
- **Equipment-specific variations:** Minor differences in the sintering cubic press (e.g., temperature gradients within the furnace, variations in applied pressure) could introduce variability that is not captured by the nominal settings.

- **Leaching solution consistency**: The changes in the concentration, pH, or temperature of the leaching solution can affect the leach rate. While these factors are ideally kept constant, small fluctuations could contribute to the unexplained variance. In this study, HCl was used to leach out cobalt. While stronger acids might offer higher overall extraction rates, the primary goal of this study was to examine the relationship between sintering variables and leachability, not to maximize cobalt recovery. Although other acids such nitric acid could lead to more cobalt extraction, HCl presents a good balance of availability for testing, and safety for handling, while also being cost-effective.
- **Inherent Variability in Measurement:** All measurements inherently possess some degree of error. While efforts were made to minimise inaccuracies during the measurement of sintering parameters and leach depth, small errors can inevitably contribute to the unexplained variance. The leach depth was measured using X-ray tomography, a technique with its own limitations and potential for error. For example, as shown in Appendix A, sample 42 displayed curvature of the interface which could mean that the depth could have been measured inaccurately. Due to limited equipment availability, only a single measurement was performed for each data point sample. Although multiple measurements would have reduced uncertainty, the single measurement provided a reasonable measurement, particularly at low leach depths. The assumption of perfectly flat interfaces, which would theoretically make a single measurement sufficient, was not accurate because data point 42 in Appendix A, showed interface curvature. Curved interfaces could introduce significant uncertainty to the measurement, particularly at larger leach depths, exceeding 800 µm.

Figure 7.1 shows pressure's dominant effect, with a significant negative coefficient indicating that increased pressure strongly reduced leachability. Temperature also exhibited a significant negative effect, while holding time's effect, although statistically significant, was less pronounced (Figure 7.1). Importantly, the model showed a significant interaction between holding time and temperature (Figure 7.2), indicating that holding time's effect on leachability depends on the sintering temperature (Figure 7.2). At lower temperatures, longer holding times are necessary for sufficient

densification and reduced leachability, but at higher temperatures, these processes occur much more rapidly, diminishing the effect of extended holding times (Figure 7.2). Dominance analysis (DA) further supported the interaction between holding time and temperature (Figure 7.7), with holding time acting as a suppressor variable. This means that while holding time may not have a strong direct effect on leachability, it enhances the effects of temperature (Figure 7.7).

The interaction term (X_1X_2) in a subsequent regression model (Equation 7.1) provided further statistical evidence of this, with a positive coefficient demonstrating that the negative effect of holding time on leach rate was lessened at higher temperatures. This is demonstrated by the non-parallel lines in the interaction plot (Figure 7.2). Thus, the effect of pressure on leachability was not entirely independent and can be modified by the values of temperature and holding time. However, even with these modifications, pressure maintained the largest overall influence

Recognising the interactions between the parameters is crucial for accurate modelling of leach rate; ignoring them would lead to inaccurate predictions and suboptimal sintering parameters. The interconnected and interdependent nature of the sintering mechanisms, revealed by this deeper understanding of interactions, is not simply additive. Understanding these interactions is also important for more precise process optimisation, offering opportunity to fine-tune the PDC microstructure and properties by optimising the combined values of pressure, temperature and holding time. Thus, for PDCs, pressure's dominance persists due to its fundamental role in mechanical compaction and limiting cobalt infiltration. Temperature and holding time modify the microstructure by diffusion, but they do not negate pressure's initial impact. The interactions refine the current understanding that is optimal, indicating temperature and holding time depend on the chosen pressure, and *vice versa*, but pressure retains the largest overall effect on leachability.

8.3 Optimisation Strategies and Practical Implications

The research provided a comprehensive framework for optimizing the HPHT sintering process to achieve desired PDC properties. The developed models, including linear regression, CCD and multiple regression, are valuable tools for predicting leach rate using sintering parameters. Dominance analysis clarified the hierarchy of parameter

importance, showing pressure as the main factor to manipulate for controlling leachability.

- **Targeted Leachability:** The dominance of pressure and the interactions of temperature and holding time are established. By considering these factors, the results of this study demonstrated a pathway for achieving targeted leachability. Manufacturers can now leverage this understanding to tailor the sintering process by selecting parameters within the lower end of the optimal sintering window for high-leachability applications, or employing higher pressures and optimised holding times, as predicted by the multiple regression model in Chapter 6, to minimise leachability when wear resistance is important.
- **Balancing Competing Properties:** The research revealed the trade-off between leachability and wear resistance. While lower pressures may enhance leachability, they can also compromise the mechanical integrity of the PDC. Therefore, a careful balance must be achieved.
- **Cost-Effectiveness:** By focusing on precise pressure control, manufacturers can minimise the need for excessive temperatures or prolonged holding times, potentially reducing energy consumption and processing time.
- ***In situ* Pressure Calibration:** The novel *in situ* pressure calibration method developed in this research (Chapter 5) provides a valuable tool for ensuring accurate pressure control during PDC sintering. This method offers advantages over conventional techniques by providing a continuous calibration curve that is directly relevant to the material and conditions of interest.

8.4 Limitations

While this research provided significant insights into the optimisation of PDC sintering, it is important to acknowledge the limitations:

- **Specific Parameter Range:** The study focused on a specific range of sintering pressures, temperatures and holding times. Extrapolating the findings beyond this range should be done with caution, as the relationships between parameters and leachability may change. The models developed were most accurate within the tested range.

- **Material:** The research was conducted on a specific PDC material system. The findings may not be directly applicable to PDCs with different diamond grain sizes, cobalt content, or binder compositions.
- **Simplified Models:** While the statistical models provided valuable insights, they are simplifications of complex real-world phenomena. Other factors not included in the models, such as cooling rate or minor variations in starting materials, could also influence PDC properties.
- **Physical, Microstructural and Mechanical Property Testing:** Microscopy techniques such as STEM and TEM as well as tests such as hardness, fracture toughness and transverse rapture strength in addition to the tests already done can assist in better understanding the wear behaviour of the samples.

8.5 Future Research Directions

This research could be expanded for future investigations:

- **Expanding Parameter Range:** Future studies could explore a wider range of sintering pressures, temperatures and holding times to further develop understanding of their effects on PDC microstructures and properties and to develop more comprehensive predictive models.
- **Investigating Other Parameters:** Future research could investigate other sintering parameters, such as heating and cooling rates. This would lead to a more complete understanding of the sintering process.
- **Exploring Different Materials:** Applying the methodologies developed in this research to different PDC materials, including different binders would be valuable.
- **Advanced Microstructural Characterisation:** Employing advanced characterisation techniques, such as three-dimensional tomography, could provide a more detailed understanding of the pore network and cobalt distribution in leached PDCs.
- **Incorporating Microstructural Features into Models:** Developing more sophisticated models that directly incorporate microstructural features, such as

porosity, grain size and phase distribution, could enhance the accuracy of predictions and provide deeper insights into the underlying mechanisms.

- ***In situ* Monitoring of Sintering:** Further development of *in situ* monitoring techniques, such as real-time pressure and temperature measurements during sintering, could provide valuable data for process optimisation and control.
- **Investigating Different Leaching Agents:** Exploring the use of different leaching agents and their effects on PDC microstructures and properties could lead to further improvements in leachability and performance.
- **Investigating microscopy techniques such as STEM and TEM as well as tests such as hardness, fracture toughness and transverse rapture strength** could help improve the unexplained variation in the results.

Chapter 9: Overall Conclusions

9.1 Summary of the research

This research investigated the relationships between sintering parameters and the resulting properties of PDCs manufactured by HPHT sintering. The parameters studied were pressure, temperature, and holding time, while the properties examined were microstructure, leachability, and wear resistance. The overarching goal was to develop a comprehensive framework for optimising the sintering process to produce PDCs with tailored properties for specific applications. To achieve this, a multi-faceted approach was employed, combining novel experimental techniques with advanced statistical modelling. This included the development of an *in situ* pressure calibration method, an investigation into the influence of thermocouple placement on temperature measurement accuracy and the application of regression analysis, central composite design (CCD), multiple regression analysis, and dominance analysis (DA) to quantify the effects and interactions of the sintering parameters.

9.2 Main Findings and Contributions

The research yielded several key findings that significantly contribute to the understanding of HPHT sintering of PDCs:

1. **Accurate Process Parameter Control is Important:** The study demonstrated that precise control of pressure, temperature and holding time is essential for achieving desired PDC properties.
    - ***In situ* Pressure Calibration (Chapter 5):** A novel *in situ* pressure calibration method was developed and validated, offering a more accurate and material-specific approach than conventional fixed-point methods. This method, which is based on the *in situ* volume change of the PDC sample during sintering, provided a foundation for the subsequent investigations.
    - **Temperature Measurement Accuracy (Chapter 5):** The research indicated the difficulties of accurate temperature measurement in a cubic press and demonstrated the significant effect of thermocouple placement on the measured temperature. Placing the thermocouple closer to the sample (inside the heater) was shown to be crucial for

obtaining reliable temperature readings and, consequently, to achieve optimal PDC microstructures and wear resistance.

2. **Individual and Combined Effects of Sintering Parameters:** Each sintering parameter was shown to have a distinct effect on PDC properties, with interdependencies.
    - **Holding Time (Chapter 6):** Longer holding times promoted densification, leading to reduced porosity and decreased leachability. A polynomial regression model ($Y = 0.002X^2 - 0.124X + 6.778$) accurately captured the relationship between holding time and leach rate within the tested range.
    - **Temperature (Chapter 6):** Increased sintering temperature also reduced leachability, mainly due to enhanced densification, altered pore morphology and potential changes in cobalt distribution. A linear regression model ($Y = -0.009X + 21.113$) effectively described the relationship between temperature and leach rate.
    - **Pressure (Chapter 6):** Pressure emerged as the most dominant factor affecting leachability. Higher pressures consistently led to reduced cobalt pool size, increased diamond contiguity, enhanced densification, lower leach rates and improved wear resistance. A linear model ($Y = -1.047X + 11.139$) derived from CCD modelling accurately described the relationship between pressure and leach rate within the investigated range.
3. **Interaction and Hierarchy of Importance:** The research revealed an interaction between the sintering parameters, particularly a significant interaction between holding time and temperature.
    - **Multiple Regression Analysis (Chapter 7):** A multiple regression model ($Y = –1.02X1 – 0.02X2 – 2.11X3 + 0.01X1X2 + 56.72$) was developed, quantifying the combined effects of pressure *(X1)*, temperature *(X2)* and holding time *(X3)*, as well as their interactions, on leach rate. This model explained 86.14% of the variance in leach rate, indicating the significant role of these parameters and their interactions.

- **Dominance Analysis (Chapter 7):** Dominance analysis (DA) established a hierarchy of parameter importance: pressure > temperature > holding time. While holding time had a minimal independent effect, it acted as a suppressor variable, amplifying the effects of pressure and temperature on leachability.

9.3 Significance and Implications

This research provided an advance in the understanding of HPHT sintering of PDCs. These findings have a significant effect on the theoretical understanding of sintering mechanisms. They also have a significant effect on the practical optimization of PDC manufacturing:

- **Enhanced Process Control:** The developed models provide a framework for controlling the sintering process to achieve desired PDC properties, particularly leachability.
- **Tailored Properties:** By manipulating the sintering parameters, especially pressure, manufacturers can tailor the microstructure and leachability of PDCs to meet the specific requirements of different drilling and cutting applications.
- **Improved Efficiency and Cost-Effectiveness:** The research findings, particularly the dominance of pressure, show that optimising pressure control offers the most significant potential for improving the efficiency and cost-effectiveness of PDC production.

References

[1] H. Huang, B. Zhao, W. Wei, Z. Si, K. Huang, Effect of cobalt content on the performance of polycrystalline diamond compacts, Int J Refract Metals Hard Mater 92 (2020) 105312. https://doi.org/10.1016/j.ijrmhm.2020.105312.

[2] S. Zhao, X. Cui, J. Hao, R. Mao, S. Hou, F. Lan, L. Li, L. Deng, H. Li, S. Gao, An advanced investigation of polycrystalline diamond compact's degradation mechanism during granite turning, Int J Refract Metals Hard Mater 120 (2024) 106615. https://doi.org/10.1016/j.ijrmhm.2024.106615.

[3] M. Jivanji, R.P. Forbes, H. Sithebe, J.E. Westraadt, Effect of ZrB2 additions on the thermal stability of polycrystalline diamond, Int J Refract Metals Hard Mater 113 (2023) 106202. https://doi.org/10.1016/j.ijrmhm.2023.106202.

[4] W. Dai, S. Zhang, J. Tu, X. Wang, C. Zhao, B. Liu, Grain size dependence of wear resistance of polycrystalline diamond compact, Ceram Int 49 (2023) 37396–37406. https://doi.org/10.1016/j.ceramint.2023.09.064.

[5] J.E. Westraadt, I. Sigalas, J.H. Neethling, Characterisation of thermally degraded polycrystalline diamond, Int J Refract Metals Hard Mater 48 (2015) 286–292. https://doi.org/10.1016/j.ijrmhm.2014.08.008.

[6] X. Wang, J. Tu, W. Dai, P. Zhu, Q. Tao, F. Ning, B. Liu, Enhanced mechanical properties of fine-grained polycrystalline diamond compact doping with nano-vanadium carbide, Int J Refract Metals Hard Mater 114 (2023) 106248. https://doi.org/10.1016/j.ijrmhm.2023.106248.

[7] D.E. Scott, The History and Impact of Synthetic Diamond Cutters and Diamond Enhanced Inserts on the Oil and Gas Industry, Canadian Energy Research Institute, Canada, 2000.

[8] G. Bruton, R. Crockett Malcolm Taylor, D. DenBoer Jeff Lund Provo, U. Craig Fleming Robert Ford Gary Garcia Allen White, M. Teel, R. von Flatern, E. Wilshusen, PDC Bit Technology for the 21st Century, SPE Annual Technical Conference and Exhibition, Amsterdam, 2014.

[9] R.M. German, Sintering window and sintering mechanism for diamond, Int J Refract Metals Hard Mater 117 (2023) 106401. https://doi.org/10.1016/j.ijrmhm.2023.106401.

[10] A. Dourfaye, W.W. King, Thermally stable polycrystalline diamond compact, US060547 A1, Patent, 2010.

[11] T.A. Scott, The influence of microstructure on the mechanical properties of polycrystalline diamond: a literature review, Advances in Applied Ceramics, 117 (2018) 161–176. https://doi.org/10.1080/17436753.2017.1389462.

[12] F. Bellin, A. Dourfaye, W. King, M. Thigpen, The current state of PDC bit technology Part 1 of 3: Development and application of polycrystalline diamond compact bits have overcome complex challenges from the difficulty of reliably mounting PDC cutters in bit bodies to accelerated thermal wear, J Pet Technol, 69(02), 2017, 53–55. SPE-186034-JPT. doi: https://doi.org/10.2118/186034-JPT.

[13] K. Davis, R. Frazier, J. Fischer, Sonochemical leaching of polycrystalline diamond, US0169419 A1, Patent, 2007.

[14] Naidoo K., Liversage J.H., Scott D.E., Sithebe H.S.L., Kaiser B.A., Fish M.L., Polycrystalline diamond element, US0061149 A1, Patent, 2012.

[15] K. Naidoo, G.J. Davies, J.L. Myburgh, Method of making polycrystalline diamond material, US0291443 A1, Patent, 2013.

[16] C.S. Montross, K. Naidoo, Polycrystalline diamond material, US0326963 A1, Patent, 2013.

[17] K. Naidoo, Polycrystalline diamond material, US0333300 A1, Patent, 2013.

[18] D.L. Decker, W.A. Bassett, L. Merrill, H.T. Hall, J.D. Barnett, High Pressure Calibration: A Critical Review, J Phys Chem Ref Data 1 (1972) 773–836. https://doi.org/10.1063/1.3253105.

[19] G. Li, M.Z. Rahim, W. Pan, C. Wen, S. Ding, The manufacturing and the application of polycrystalline diamond tools – A comprehensive review, J Manuf Process 56 (2020) 400–416. https://doi.org/10.1016/j.jmapro.2020.05.010.

[20] J. Gu, K. Huang, Role of cobalt of polycrystalline diamond compact (PDC) in drilling process, Diam Relat Mater 66 (2016) 98–101. https://doi.org/10.1016/j.diamond.2016.03.025.

[21] S.Z. Zhao, X.W. Cui, J.L. Hao, R.Q. Mao, S. Hou, F.L. Lan, L.H. Li, L.F. Deng, H. Li, S. Gao, An advanced investigation of polycrystalline diamond compact's degradation mechanism during granite turning, Int. J. Refract. Met. Hard Mater. 120 (2024) 106615.

[22] K. Naidoo, J.H. Liversage, D.E. Scott, H.S.L. Sithebe, B.A. Kaiser, M.L. Fish, Polycrystalline diamond element, US0061149A1, Patent, 2012.

[23] M. Yahiaoui, L. Gerbaud, J.Y. Paris, J. Denape, A. Dourfaye, A study on PDC drill bits quality, Wear 298–299 (2013) 32–41. https://doi.org/10.1016/j.wear.2012.12.026.

[24] M. Yahiaouia, L. Gerbaudb, J.Y. Parisa, J. Denapea, A. Dourfaye, A study on PDC drill bits quality, Wear 298 (2012) 32–41.

[25] J.S. Li, W. Yue, W.B. Qin, Q.Z. Mao, B. Gao, Y.S. Li, Effect of quenching processes on microstructures and tribological behaviors of polycrystalline diamond compact (PCD/WC-Co) in annealing treatment, Diamond Relat. Mater. 79 (2017) 79–87.

[26] Q.S. Bai, Y.X. Yao, P. Bex, G. Zhang, Study on wear mechanisms and grain effects of PCD tool in machining laminated flooring, Int. J. Refract. Met. Hard Mater. 22 (2004) 111–115.

[27] F.J. Li, W. Liu, D. Gao, Y. Li, Study on super impact resistant polycrystalline diamond compacts with homogeneous PCD/WC-Co interlayer, Int. J. Refract. Met. Hard Mater. 119 (2024) 106558.

[28] J.E. Westraadt, Thermal degradation of diamond compacts: A TEM investigation, Nelson Mandela University, PhD, 2011.

[29] E.G. Minnaar, Characterisation of Ultra-High Pressure Polycrystalline Diamond, Nelson Mandela University, PhD, 2019.

[30] S.I. Petrov, Fracture in polycrystalline diamond. Investigating cracking and toughness behaviour using a miniature double torsion technique, University of Cambridge, PhD, 2019.

[31] H.L.E. Mehan R.L., Thermal degradation of sintered diamond compacts, J Mater Sci 24 (1989) 942–950.

[32] R.M. German, P. Suri, S.J. Park, Review: Liquid phase sintering, J Mater Sci 44 (2009) 1–39. https://doi.org/10.1007/s10853-008-3008-0.

[33] K. Tank, R.D. Achilles, Abrasive compacts, US20100043302, Patent, 2010.

[34] F.R. Corrigan, H.S. Marek, Method for producing abrasive compact with improved properties, US6132675, Patent, 2000.

[35] S. Liu, L. Han, Y. Zou, P. Zhu, B. Liu, Polycrystalline diamond compact with enhanced thermal stability, J Mater Sci Technol 33 (2017) 1386–1391. https://doi.org/10.1016/j.jmst.2017.03.014.

[36] L.W.F. Katzman H., Sintered diamond compacts with a cobalt binder, Science (1979) 172 (1971) 1132–1134.

[37] D. McNamara, P. Alveen, D. Carolan, N. Murphy, A. Ivanković, Fracture toughness evaluation of polycrystalline diamond as a function of microstructure, J. Eng Fract Mech 143 (2015) 1–16. https://doi.org/10.1016/j.engfracmech.2015.06.028

[38] M. Yahiaoui, J.Y. Paris, K. Delbé, J. Denape, L. Gerbaud, C. Colin, O. Ther, A. Dourfaye, Quality and wear behavior of graded polycrystalline diamond compact cutters, Int J Refract Metals Hard Mater 56 (2016) 87–95. https://doi.org/10.1016/j.ijrmhm.2015.12.009.

[39] J. Fan, T. Lin, F. Hu, Y. Yu, M. Ibrahim, R. Zheng, S. Huang, J. Ma, Effect of sintering temperature on microstructure and mechanical properties of zirconia-toughened alumina machinable dental ceramics, Ceram Int 43 (2017) 3647–3653. https://doi.org/10.1016/j.ceramint.2016.11.204.

[40] Y. Li, Y. Zu, G. Chen, X. Fu, W. Zhou, Effect of sintering temperature on microstructure and mechanical properties of Ti2AlNb-based composites, Journal of Materials Research and Technology 29 (2024) 4854–4862. https://doi.org/10.1016/j.jmrt.2024.02.202.

[41] B. Leszczyńska-Madej, D. Garbiec, M. Madej, Effect of sintering temperature on microstructure and selected properties of spark plasma sintered Al-SiC composites, Vacuum 164 (2019) 250–255. https://doi.org/10.1016/j.vacuum.2019.03.033.

[42] D. Yang, Y. Zhang, X. Song, Y. Chen, Z. Shen, C. Yang, Effects of sintering temperature and holding time on porosity and shrinkage of glass tubes, Ceram Int 42 (2016) 5906–5910. https://doi.org/10.1016/j.ceramint.2015.12.138.

[43] Y. Pan, H. Li, Y. Liu, Y. Liu, K. Hu, N. Wang, Z. Lu, J. Liang, S. He, Effect of Holding Time During Sintering on Microstructure and Properties of 3D Printed Alumina Ceramics, Front Mater 7 (2020) 55. https://doi.org/10.3389/fmats.2020.00054.

[44] X. Zhang, G. Chen, C. Fu, W. Cai, R. Gao, F. Wang, Effects of sintering temperature and holding time on the microstructure and electric properties of $Ba(Zr_{0.3}Ti_{0.7})O_3$ ceramics, Processing and Application of Ceramics 12 (2018) 45–55. https://doi.org/10.2298/PAC1801045Z.

[45] Y. Hu, Y. Li, J. Lou, H. He, X. Zhang, Effects of Sintering Temperature and Holding Time on Densification and Mechanical Properties of MIM HK30 Stainless Steel, International Journal of Metallurgy and Metal Physics Citation 3 (2018) 22.

[46] D. Liu, Y. Gao, J. Liu, Y. Wang, L. An, Effect of holding time on the microstructure and properties of flash-sintered Y_2O_3-doped ZrO_2, Ceram Int 42 (2016) 17442–17446. https://doi.org/10.1016/j.ceramint.2016.08.048.

[47] S. Du, L. Xu, X. Zhang, P. Hu, W. Han, Effect of sintering temperature and holding time on the microstructure and mechanical properties of ZrB2-SiCw composites, Mater Chem Phys 116 (2009) 76–80. https://doi.org/10.1016/j.matchemphys.2009.02.039.

[48] R.L. Ladi, C.E. Wells, B.K. Kataria, S.W. Almond, Chemical agents for leaching polycrystalline diamond compacts, US8435324, Patent, 2013.

[49] R.L. Ladi, C.E. Wells, B.K. Kataria, S.W. Almond., Chemical agents for leaching polycrystalline diamond elements, US0152064 A1, Patent, 2012.

[50] R. Gou, X. Luo, K. Li, C. Kang, J. Chen, PCD after cobalt leaching reinforced by high temperature annealing: Tribological properties and graphitization evolution, Diam Relat Mater 125 (2022) 108988. https://doi.org/10.1016/j.diamond.2022.108988.

[51] J. Shamburger, Method and apparatus for selectively leaching portions of PCD cutters through templates formed in mechanical shields placed over the cutters, US20100011673, Patent, 2010.

[52] B. Bhushan, Principles and Applications of Tribology, John Wiley and Sons, New York, USA, 1999.

[53] S. Masethe, PDC wear testing, Springs, Report, 2014.

[54] F.G. Marro, A. Mestra, E. Jiménez-Piqué, S. Ozbayraktar, L. Llanes, Damage induced by monotonic and cyclic spherical indentation in polycrystalline diamond (PCD), Int. J. Refract. Met. Hard Mater. 49 (2015) 292–301.

[55] M. Yahiaoui, L. Gerbaud, J.Y. Paris, J. Denape, A. Dourfaye, A study on PDC drill bits quality, Wear 298–299 (2013) 32–41. https://doi.org/10.1016/j.wear.2012.12.026.

[56] J.E. Westraadt, N. Dubrovinskaia, J.H. Neethling, I. Sigalas, Thermally stable polycrystalline diamond sintered with calcium carbonate, Diam Relat Mater 16 (2007) 1929–1935. https://doi.org/10.1016/j.diamond.2007.08.011.

[57] G. Udupa, S.S. Rao, K.V. Gangadharan, Functionally Graded Composite Materials: An Overview, Procedia Materials Science 5 (2014) 1291–1299. https://doi.org/10.1016/j.mspro.2014.07.442.

[58] R. Gou, X. Luo, G. Xu, C. Kang, J. Chen, J. Zhang, S. Long, Improvement of ambient temperature tribological properties of polycrystalline diamond compact treated by cobalt removal, Diam Relat Mater 119 (2021) 108567. https://doi.org/10.1016/j.diamond.2021.108567.

[59] M. Akhaishi, H. Kanda, Y. Sato, N. Setaka, T. Ohsawa, O. Fukunaga, Sintering behaviour of the diamond-cobalt system at high temperature and pressure, Journal of Materials Science 17 (2005) 193–198.

[60] Francis K., Effect of carbide additives on the structure and behaviour of polycrystalline diamond, PhD, University of Pretoria, 2017.

[61] T.P. Lin, M. Hood, G.A. Cooper, X. Li, Wear and failure mechanisms of polycrystalline diamond compact bits, Int. J. Mach Tools Manuf, 34 (1994) 405-414. https://doi.org/10.1016/0890-6955(94)90008-2.

[62] B.M.D. Morrison, C.R. Jonker, R.W. Nilen, Polycrystalline Diamond Abrasive Compacts, US8231698B2, Patent, 2012.

[63] T.J. Shin, J.O. Oh, K.H. Oh, D.N. Lee, The mechanism of abnormal grain growth in polycrystalline diamond during high pressure-high temperature sintering, Diam Relat Mater 13 (2004) 488–494. https://doi.org/10.1016/j.diamond.2003.11.091.

[64] S. Yamaoka, S. Kumar, H. Kanda, M. Akaishi, Formation of diamond from CaCO in a reduced C-O-H fluid at HP-HT, Report, 2002.

[65] Childerhouse, R. M'Saoubi, L.F.P. Franca, P. Crawforth, M. Jackson, Machining performance and wear behaviour of polycrystalline diamond and coated carbide tools during milling of titanium alloy Ti-54M, Wear. 523 (2023) 204791.

[66] Lin T.P., Hood M., Cooper G.A., Li X., Wear and failure mechanisms of Polycrystalline diamond compact bits, Wear 156 (1992) 133–150.

[67] E.G. Minnaar, Characterisation of Ultra-High Pressure Polycrystalline Diamond, Nelson Mandela University, PhD, 2019.

[68] S. Ono, High-pressure phase transition of bismuth, High Press Res 38 (2018) 414–421. https://doi.org/10.1080/08957959.2018.1541456.

[69] X. Liu, J. Chen, J. Tang, Q. He, S. Li, F. Peng, D. He, L. Zhang, Y. Fei, A large volume cubic press with a pressure-generating capability up to about 10GPa, High Press Res 32 (2012) 239–254. https://doi.org/10.1080/08957959.2012.657634.

[70] S. Wang, D. He, W. Wang, L. Lei, Pressure calibration for the cubic press by differential thermal analysis and the high-pressure fusion curve of aluminum, Int J High Press Res, 29(4) (2009) 806–814. https://doi.org/10.1080/08957950903335521.

[71] A. McKie, M. Herrmann, I. Sigalas, K. Sempf, R. Nilen, Suppression of abnormal grain growth in fine grained polycrystalline diamond materials (PCD), Int J Refract Metals Hard Mater 41 (2013) 66–72. https://doi.org/10.1016/j.ijrmhm.2013.02.004.

[72] V. Kanyanta, S. Ozbayraktar, K. Maweja, Effect of manufacturing parameters on polycrystalline diamond compact cutting tool stress-state, Int J Refract Metals Hard Mater 45 (2014) 147–152. https://doi.org/10.1016/j.ijrmhm.2014.03.009.

[73] J. Li, C. Hadidiacos, H.K. Mao, Y. Fei, R.J. Hemley, Behavior of thermocouples under high pressure in a multi-anvil apparatus, High Press Res 23 (2003) 389–401. https://doi.org/10.1080/0895795031000088269.

[74] D.L. Decker, W.A. Bassett, L. Merrill, H.T. Hall, J.D. Barnett, High Pressure Calibration: A Critical Review, J Phys Chem Ref Data 1 (1972) 773–836. https://doi.org/10.1063/1.3253105.

[75] O. Ongrai, J. V. Pearce, G. Machin, S.J. Sweeney, Comparative study of Pt/Pd and Pt-Rh/Pt thermocouples, in: Int J Thermophys, 2010: 1506–1516. https://doi.org/10.1007/s10765-010-0782-0.

[76] K.F. Nimon, F.L. Oswald, Understanding the Results of Multiple Linear Regression: Beyond Standardized Regression Coefficients, Organ Res Methods 16 (2013) 650–674. https://doi.org/10.1177/1094428113493929.

[77] A. Javaid, A. Mohammed, A. Ghaithan, A regression-based model for prediction of flowmeters calibration cost in oil and gas industry, Flow Meas and Inst 86 (2022) 102191. https://doi.org/10.1016/j.flowmeasinst.2022.102191.

[78] L.L. Nathans, F.L. Oswald, K. Nimon, Interpreting Multiple Linear Regression: A Guidebook of Variable Importance, Practical Assessment, Research, and Evaluation 17 (2012) 9. https://doi.org/10.7275/5fex-b874.

[79] S. Hadi A, Regression Analysis by Example, Fourth Edition, John Wiley and Sons, Canada, 2006.

[80] J.H. Smid, C.D.M. van der Swaluw-Dekker, J. Ueckert, E. de Vries, A. Pielaat, Bayesian global regression model relating product characteristics of intermediate moisture food products to heat inactivation parameters for Salmonella Napoli and Eurotium herbariorum mould spores, Int J Food Microbiol 370 (2022) 109638. https://doi.org/10.1016/j.ijfoodmicro.2022.109638.

[81] K. Nimon, M. Lewis, R. Kane, R.M. Haynes, An R package to compute commonality coefficients in the multiple regression case: An introduction to the package and a practical example, Behav Res Methods 40 (2008) 457–466. https://doi.org/10.3758/BRM.40.2.457.

[82] A. Pritam, R.R. Dash, R.K. Mallik, Predictive modeling and multi objective optimization of Al 6063 for engraving depth and surface roughness using grey relational and regression analysis, Mater Today Proc 47(16) (2021) 5885–5896. https://doi.org/10.1016/j.matpr.2021.07.271.

[83] A. Atabati, H. Adab, G. Zolfaghari, M. Nasrabadi, Modeling groundwater nitrate concentrations using spatial and non-spatial regression models in a semi-arid environment, J Water Sci Eng, 15(3) (2022) 220–230. https://doi.org/10.1016/j.wse.2022.05.

[84] D.V. Budescu, Dominance Analysis: A New Approach to the Problem of Relative Importance of Predictors in Multiple Regression, Psychol Bull 114 (1993) 542–551.

[85] U. Grömping, Relative Importance for Linear Regression in R: The Package relaimpo, J Stat Softw, 17(1) (2006) 1–27. doi:10.18637/jss.v017.i01.

[86] S. Tang, Inferential Procedures for Dominance Analysis Measures in Multiple Regression, University of Wisconsin-Milwaukee, 2014. https://dc.uwm.edu/etd/645 (Date accessed: 8 March 2024).

[87] R. Azen, D.V. Budescu, The Dominance Analysis Approach for Comparing Predictors in Multiple Regression, Psychol Methods 8 (2003) 129–148. https://doi.org/10.1037/1082-989X.8.2.129.

[88] W. Luo, R Azen, Determining Predictor Importance in Hierarchical Linear Models Using Dominance Analysis, J Educ Behav Stat 38 (2013) 3–31. https://doi.org/10.3102/1076998612458319.

[89] L.P. Cancado, Determining Predictor Importance in Multilevel Models for Longitudinal Data: An Extension of Dominance Analysis, University of Wisconsin-Milwaukee, PhD, 2018.

[90] R.B. Darlington, A.F. Hayes, Regression Analysis and Linear Models, second ed., Guilford Press, New York, 2017. www.guilford.com/MSS.

[91] R.A. Johnson, D.W. Wichern, Applied Multivariate Statistical Analysis, Sixth ed., Pearson, New Jersey, 2007.

[92] S. Chatterjee, J.S. Simonoff, Handbook of Regression Analysis., First ed., John Wiley & Sons , New Jersey, 2013.

[93] J.F. Hair, W.C. Black, B.J. Babin, R.E. Anderson, Multivariate data analysis, Seventh ed., Pearson, London, 214AD.

[94] C. Wolf, H. Best, Regression Analysis and Casual Inference, Second ed., Sage, Los Angels, 2014.

[95] A.C. Rencher, G.B. Schaalje, Linear Models in Statistics, Second ed., John Wiley & Sons, New Jersey, 2008.

[96] T. Courville, B. Thompson, Use of Structure Coefficients in Published Multiple Regression Articles: β is not Enough, Educ Psychol Meas 61 (2001) 229–248. https://doi.org/10.1177/0013164401612006.

[97] M. Njeri, J. Allen, G. Jennings, Assessing the application of β-weights and structure coefficients in published hospitality and tourism research, Journal of Global Hospitality and Tourism 2 (2023) 10–31. https://doi.org/10.5038/2771-5957.2.1.1018.

[98] B.B. Baltes, C.P. Parker, L.M. Young, J.W. Huff, R. Altmann, The practical utility of importance measures in assessing the relative importance of work-related perceptions and organizational characteristics on work-related outcomes, Organ Res Methods 7 (2004) 326–340. https://doi.org/10.1177/1094428104266014.

[99] M.T. Braun, P.D. Converse, F.L. Oswald, The accuracy of dominance analysis as a metric to assess relative importance: The joint impact of sampling error variance and measurement unreliability, Journal of Applied Psychology 104 (2019) 593–602. https://doi.org/10.1037/apl0000361.

[100] J.S. Knibbe, S.M. Luginbühl, R. Stoevelaar, W. van der Plas, D.M. van Harlingen, N. Rai, E.S. Steenstra, R. van de Geer, W. van Westrenen, Calibration of a multi-anvil high-pressure apparatus to simulate planetary interior conditions, EPJ Tech Instrum 5(1) (2018) 6. https://doi.org/10.1140/epjti/s40485-018-0047-z.

[101] X.Q. Liu, Improved Liu estimator in a linear regression model, J Stat Plan Inference 141 (2011) 189–196. https://doi.org/10.1016/j.jspi.2010.05.030.

[102] M.R. Steenbergen, Regression analysis: A Primer for the Social Sciences, Political Science - All Faculty Scholarship, Syracuse University, 2016. https://surface.syr.edu/psc/8.

[103] S.K. Prion, K.A. Haerling, Making Sense of Methods and Measurements: Simple Linear Regression, Clin Simul Nurs 48 (2020) 94–95. https://doi.org/10.1016/j.ecns.2020.07.004.

[104] C.P. Dhakal, Interpreting the Basic Outputs (SPSS) of Multiple Linear Regression, Int J Sci Res 7(4) (2018) 31–34. https://doi.org/10.21275/4061901.

[105] M.R. Schwarz, Multianvil calibration and education: A four probe method to measure the entire force-versus-pressure curve in a single run - Performed as an interdisciplinary lab-course for students, J Phys Conf Ser, 215 (2010) 012193. https://doi.org/10.1088/1742-6596/215/1/012193

[106] D. Walker, J. Li, Castable solid pressure media for multianvil devices, J. Matter Radiat Extremes, 5(1) (2020) 018201. https://doi.org/10.1063/1.5129534.

[107] D. McNamara, D. Carolan, P. Alveen, N. Murphy, A. Ivanković, Effect of loading rate on the fracture toughness and failure mechanisms of polycrystalline diamond (PCD), Int. J. Refract. Met. Hard Mater. 60 (2016) 1–10.

[108] V. Stutzmann, A. Dewaele, J. Bouchet, F. Bottin, M. Mezouar, High-pressure melting curve of titanium, Phys Rev B Condens Matter Mater Phys 92(22) (2015) 22411092. https://doi.org/10.1103/PhysRevB.92.224110.

[109] M. Abbasi, D.I. Kim, J.H. Shim, W.S. Jung, Effects of alloyed aluminum and titanium on the oxidation behavior of INCONEL 740 superalloy, J Alloys Compd 658 (2016) 210–221. https://doi.org/10.1016/j.jallcom.2015.10.198.

[110] Y. Li, Y. Zeng, Z.J. Chen, L.Y. Liu, H.L. Liu, Y.X. Yang, Failure characteristics and service life prediction of polycrystalline diamond compact (PDC) cutter under cyclic impact loading, 1 Geoenergy Sci. Eng. 231 (2023) 212339

[111] H.S.L. Sithebe, K. Naidoo, polycrystalline diamond (PCD) Materials, WO2008096314, Patent, 2008.

[112] D. Brandon, W.D. Kaplan, Microstructural Characterization of Materials, 2nd ed., 2nd ed., John Wiley & Sons, Chichester, UK, 2008.

[113] W. Soboyejo, Mechanical Properties of Engineered Materials, Marcel Dekker, New York, USA, 2003.

[114] J.F. Shackelford, Introduction to Materials Science for Engineers, Prentice Hall, New Jersey, USA, 2005.

[115] J.N. Boland, X.S. Li, Microstructural Characterisation and Wear Behaviour of Diamond Composite Materials, Materials 3 (2010) 1390–1419.

[116] X. Sha, B. Feng, W. Yue, C. Wang, Grain size dependent tribological behaviours of 700 °C annealed polycrystalline diamond, Int J Refract Metals Hard Mater 94 (2021) 105406. https://doi.org/10.1016/j.ijrmhm.2020.105406.

[117] J. Yu, Q. Zhao, S. Huang, Y. Zhao, Y. Zhou, J. Lu, L. Dong, Y. Zhang, Effect of sintering temperature on microstructure and properties of graphene nanoplatelets reinforced TC21 composites prepared by spark plasma sintering, J Alloys Compd 879 (2021). https://doi.org/10.1016/j.jallcom.2021.160346.

[118] X. Yuan, X. Qu, H. Yin, Z. Feng, M. Tang, Z. Yan, Z. Tan, Effects of sintering temperature on densification, microstructure and mechanical properties of al-based alloy by high-velocity compaction, Metals (Basel) 11 (2021) 1–11. https://doi.org/10.3390/met11020218.

[119] A.D. Timoshenko, A.G. Doroshenko, S. V. Parkhomenko, I.O. Vorona, O.S. Kryzhanovska, N.A. Safronova, O.O. Vovk, V. V. Tolmachev, V.N. Baumer, I. Matolínová, R.P. Yavetskiy, Effect of the sintering temperature on microstructure and optical properties of reactive sintered ceramics, Optical Materials: X 13 (2022) 100131. https://doi.org/10.1016/j.omx.2021.100131.

[120] W. Hong-tao, Z. Shi, Study on mechanism of thermal damage on PCD compacts induced by induction heating, J Mater Sci Technol 13(9), 2005, 787-792.

[121] J. Gu, K. Huang, Role of cobalt of polycrystalline diamond compact (PDC) in drilling process, Diam Relat Mater 66 (2016) 98–101. https://doi.org/10.1016/j.diamond.2016.03.025.

[122] R. Gou, X. Luo, K. Li, C. Kang, J. Chen, PCD after cobalt leaching reinforced by high temperature annealing: Tribological properties and graphitization evolution, Diam Relat Mater 125 (2022) 108988. https://doi.org/10.1016/j.diamond.2022.108988.

[123] C. Liu, Z. Kou, D. He, Y. Chen, K. Wang, B. Hui, R. Zhang, Y. Wang, Effect of removing internal residual metallic phases on wear resistance of polycrystalline diamond compacts, Int J Refract Metals Hard Mater 31 (2012) 187–191. https://doi.org/10.1016/j.ijrmhm.2011.10.014.

[124] M.H. Kutner, C. Nachtsheim, J. Neter, W. Li, Applied linear statistical models, 4th ed., McGraw-Hill, 2004.

[125] T. Catalina, J. Virgone, E. Blanco, Development and validation of regression models to predict monthly heating demand for residential buildings, Energy Build 40 (2008) 1825–1832. https://doi.org/10.1016/j.enbuild.2008.04.001.

[126] N. Fumo, M.A. Rafe Biswas, Regression analysis for prediction of residential energy consumption, Renewable and Sustainable Energy Reviews 47 (2015) 332–343. https://doi.org/10.1016/j.rser.2015.03.035.

[127] J.E. Miller, Interpreting the substantive significance of multivariable regression coefficients, Rutgers University, Report, 2010.

[128] K.F. Nimon, L.R. Zientek, B. Thompson, Investigating bias in squared regression structure coefficients, Front Psychol 6 (2015) 949. https://doi.org/10.3389/fpsyg.2015.00949.

[129] S.J.L Kang, Sintering, Densification, Grain Growth and Microstructure, Elsevier Butterworth-Heinemann, Massachusetts, USA, 2005.

[130] Z. Chu, C. Jia, J. Liu, R. Ding, G. Yuan, Effects of sintering time on microstructure and properties of alumina foam ceramics, J Ceram Sci Technol, 8 (2017) 499–504. https://doi.org/10.4416/JCST2017-00028.

[131] M. Akaishi, T. Ohsawa, S.Y. Amaoka, Synthesis of Fine-Grained Polycrystalline Diamond Compact and Its Microstructure, J Am Ceram Soc, 74(1), 1991, 5–10.

[132] H.M. Patil, S.S. Sirsikar, N.N. Gholap, Product Design and Development: Phases and Approach, (2017). www.ijert.org.

[133] M. Sandberg, Design for manufacturing: Methods and applications using knowledge engineering, PhD, Department of Production Engineering, School of Industrial Engineering and Management, Royal Institute of Technology, Stockholm, 2007.

[134] T. Hill, Manufacturing Strategy: Text and Cases, Third Edition, McGraw-Hill, New York, 2000.

[135] A. Mizumoto, Calculating the relative importance of multiple regression predictor variables using dominance analysis and random forests, Kansai University, Report, 2018.

[136] S. Pandey, W. Elliott, Suppressor Variables in Social Work Research: Ways to Identify in Multiple Regression Models, J Soc Social Work Res 1 (2010) 28–40. https://doi.org/10.5243/jsswr.2010.2.

[137] P.W. Bridgman, Freezing Parameters and Compressions of Twenty-One Substances to 50,000 kg/cm², Proe Amer Acad Arts Sci, 74 (1940) 1-10.

[138] J.C. Haygarth, I.C. Getting, G.C. Kennedy, Determination of Pressure for the Barium I–II Transition with Single-Stage Piston-Cylinder Apparatus, J Appl Phys, 38(12) (1967) 4557–4564.

[139] H.G. Drickamer, Solids Under Pressure, Turnbull, Solid State Physics, vol 17, Academic Press Inc., New York, 1965.

[140] V.G. Tyuterev, N. Vast, First-principles study of pressure-induced phase transitions in BeO, Comput Mater Sci, 38(2) (2006) 350-353.

[141] J.L. Murray, The Pt-Ti (Platinum-Titanium) System, Bull. Alloy Phase Diagrams, 1982, 3(3), p 329-335.

[142] Ozbayraktar, S. 1995. PCD Sintering Model. Element 6 internal report.

[143] Ozbayraktar, S. 1997. Mechanisms of Liquid Phase Sintering of PCD. Element 6 internal report.

[144] Ozbayraktar, S. 2000. Polycrystalline Diamond and Cubic Boron Nitride. In R. Riedel (ed.), Handbook of Ceramic Hard Materials. New York: Wiley-VCH. pp. 512-520.

[145] Walmsley, J.C. 1988. The Microstructure of Ultrahard Material Compacts Studies by Transmission Electron Microscopy. Materials Science and Engineering A, 105-106:549-553.

[146] Walmsley, J.C. & Lang, A.R. 1983. Transmission electron microscopic observations of deformation and microtwinning in a synthetic diamond compact. Journal of Materials Science Letters, 2:785-788.

[147] Brookes, E.J. & Brookes C.A. 1995. Impression Plasticity and Creep in Hard Crystals. In R.C Brandt, C.A Brookes & J.L. Routbort (eds.), Plastic Deformation of Ceramics. US: Springer. pp. 131-147.

[148] Fukunaga, O., Yamaoka, S., Endoh, T., Akaishi, M. & Kanda, H. 1977. Modification of Belt-Like High-Pressure Apparatus. In K.D. Timmerhaus & M.S. Barber (eds.), High-Pressure Science and Technology: Volume 1: Physical Properties and Material Synthesis. Springer Science + Business Media, LCC, pp. 846-852.

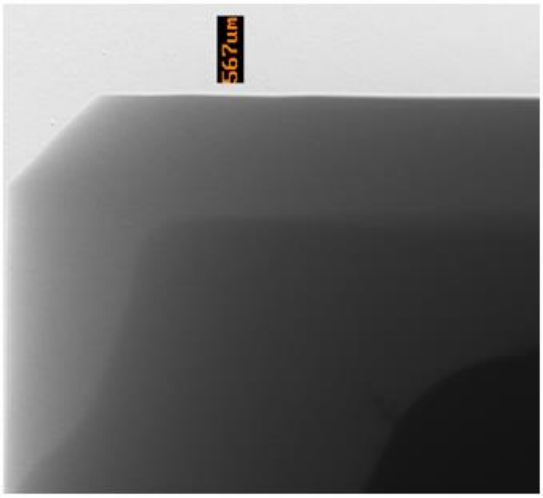
[149] J. Shumburger, Method for selectively leaching portions of Polycrystalline Diamond Compacts in drill bits, US77121553B2, Patent, 2006.

[150] Thermo Fisher Scientific Inc., Phenom desktop scanning electron microscope, Publication No. WP0015-EN-10-2019, Manual, 2019. Retrieved from https://www.thermofisher.com/phenom

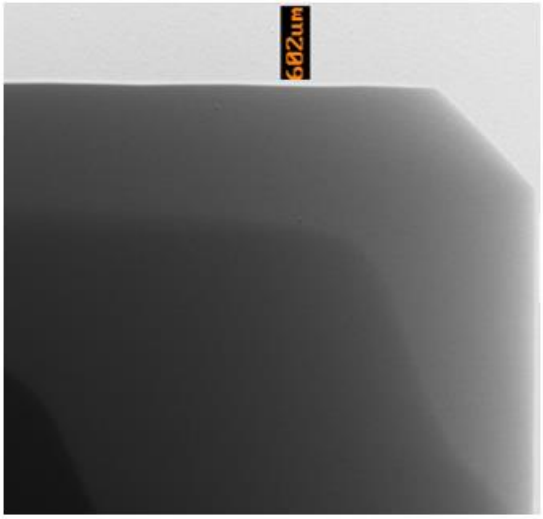
Appendix A: X-ray tomography images.

The X-ray tomography images which were used to take leach depth measurements from the 64 experimental runs, showing: leach depth (light contrast), unleached layer (dark grey contrast) and substrate (dark contrast).

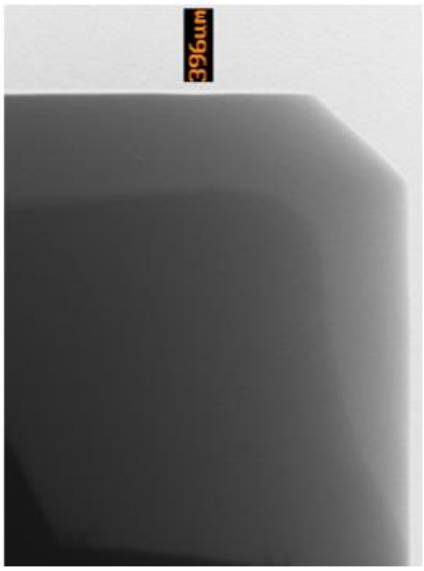
Data point 46:
- Conditions: 6 GPa, 1600°C, 25 minutes.
- Leach depth: 567 µm.



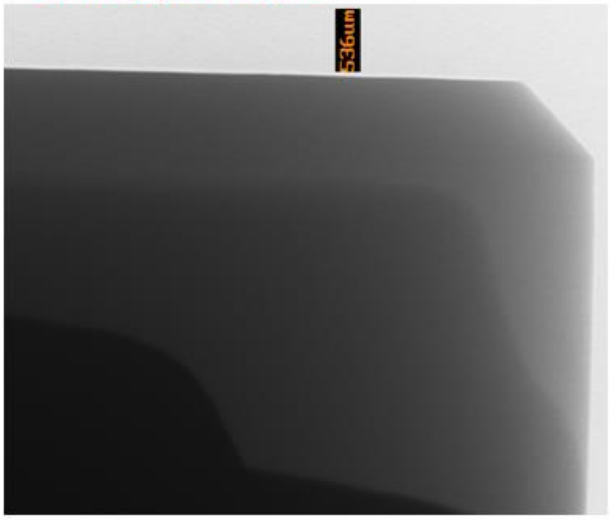
Data point 57:
- Conditions: 6 GPa, 1600°C, 20 minutes.
- Leach depth: 602 µm.



Data point 1:
- Conditions: 6 GPa, 1600°C, 25 minutes.
- Leach depth: 396 µm.



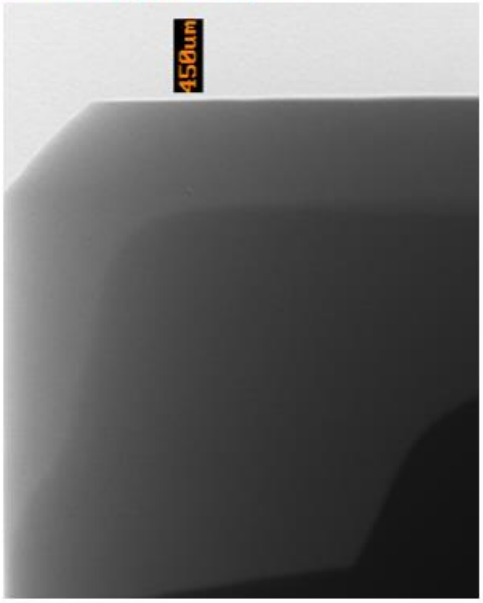
Data point 9:
- Conditions: 5 GPa, 1700°C, 20 minutes.
- Leach depth: 536 µm.



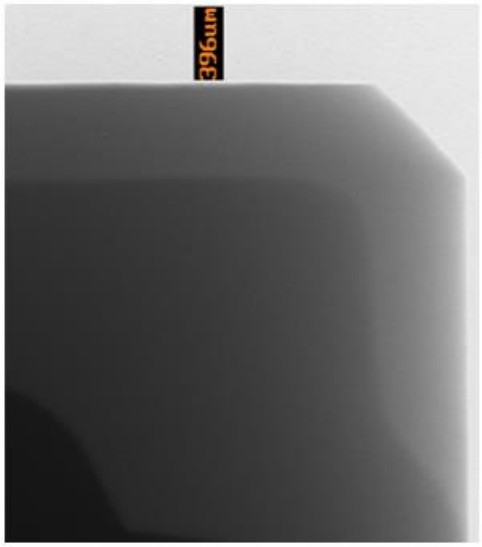
Data point 54:
- Conditions: 7 GPa, 1700°C, 20 minutes.
- Leach depth: 225 µm.



Data point 53:
- Conditions: 6 GPa, 1600°C, 25 minutes.
- Leach depth: 450 µm.



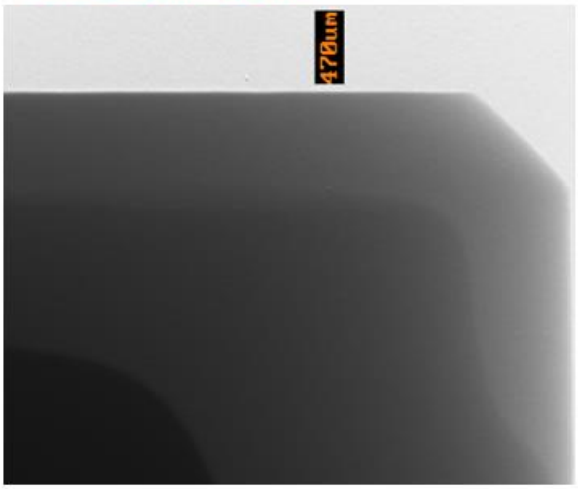
Data point 61:
- Conditions: 7 GPa, 1600°C, 25 minutes.
- Leach depth: 396 µm.



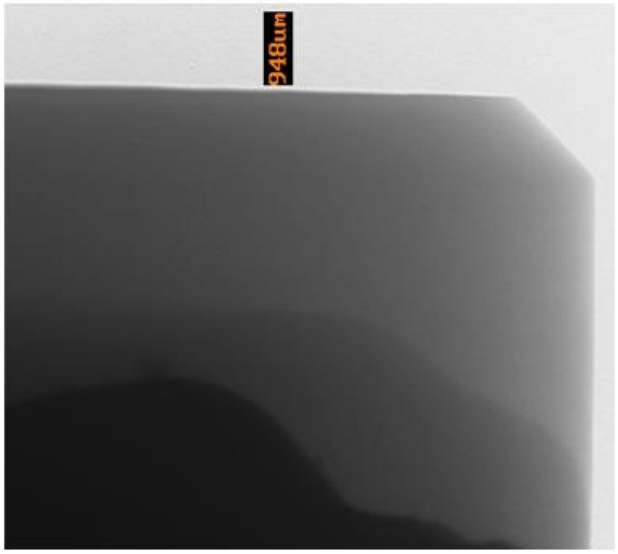
Data point 24:
- Conditions: 5 GPa, 1700°C, 20 minutes.
- Leach depth: 563 µm.



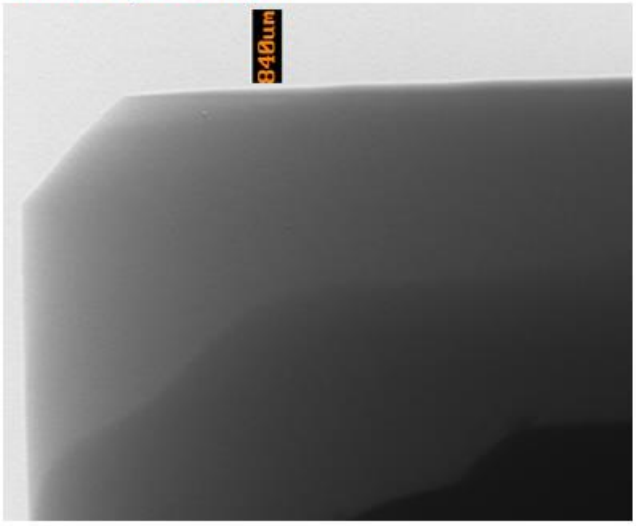
Data point 40:
- Conditions: 5 GPa, 1700°C, 30 minutes.
- Leach depth: 470 µm.



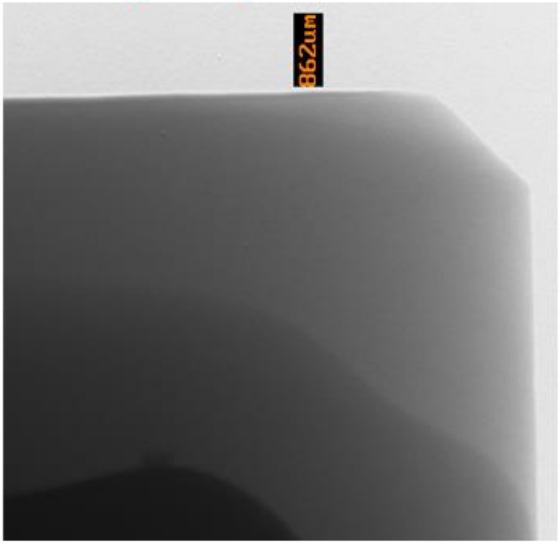
Data point 50:
- Conditions: 5 GPa, 1500°C, 20 minutes.
- Leach depth: 948 µm.



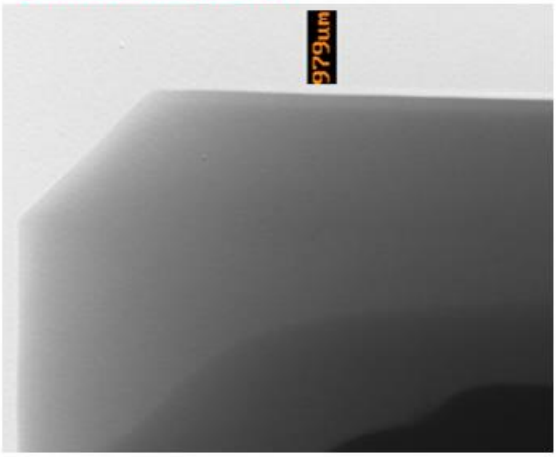
Data point 21:
- Conditions: 5 GPa, 1500°C, 30 minutes.
- Leach depth: 840 µm.



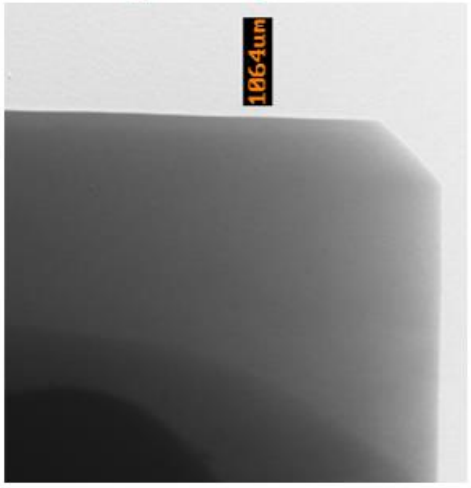
Data point 35:
- Conditions: 5 GPa, 1500°C, 30 minutes.
- Leach depth: 862 µm.



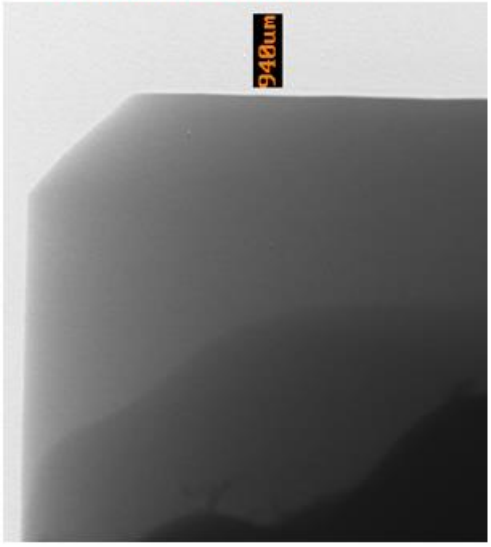
Data point 20:
- Conditions: 5 GPa, 1500°C, 20 minutes.
- Leach depth: 979 µm.



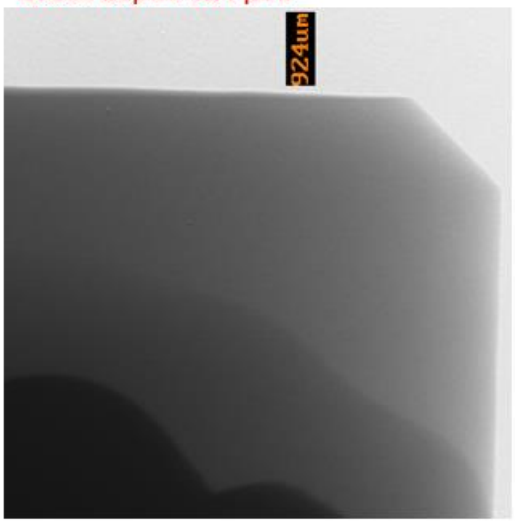
Data point 42:
- Conditions: 5 GPa, 1500°C, 20 minutes.
- Leach depth: 1064 µm.



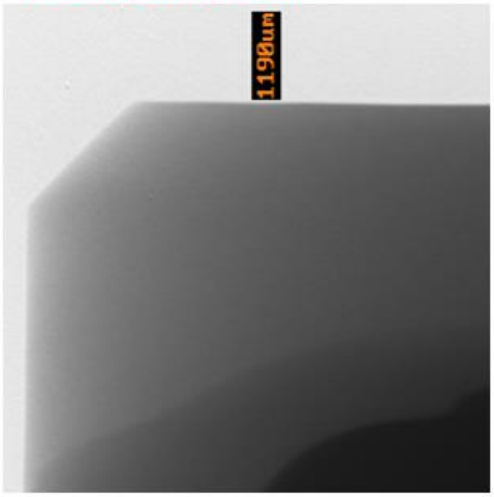
Data point 5:
- Conditions: 5 GPa, 1500°C, 20 minutes.
- Leach depth: 940 µm.



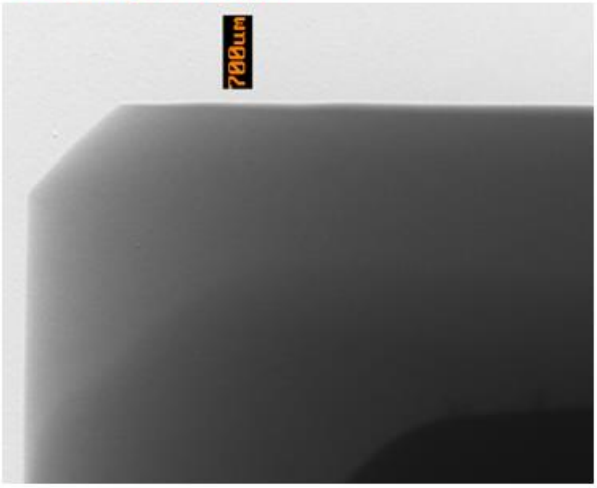
Data point 22:
- Conditions: 7 GPa, 1500°C, 20 minutes.
- Leach depth: 924 µm.



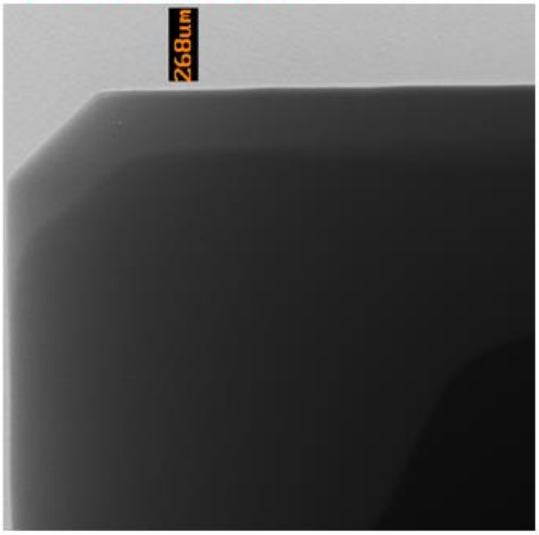
Data point 32:
- Conditions: 5 GPa, 1500°C, 20 minutes.
- Leach depth: 1190 µm.



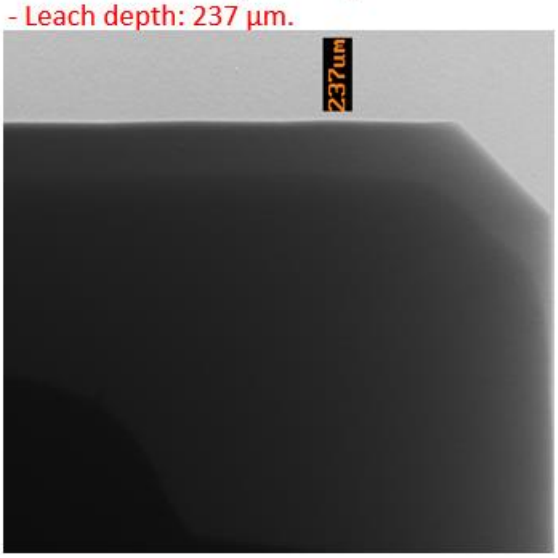
Data point 49:
- Conditions: 5 GPa, 1500°C, 30 minutes.
- Leach depth: 700 µm.



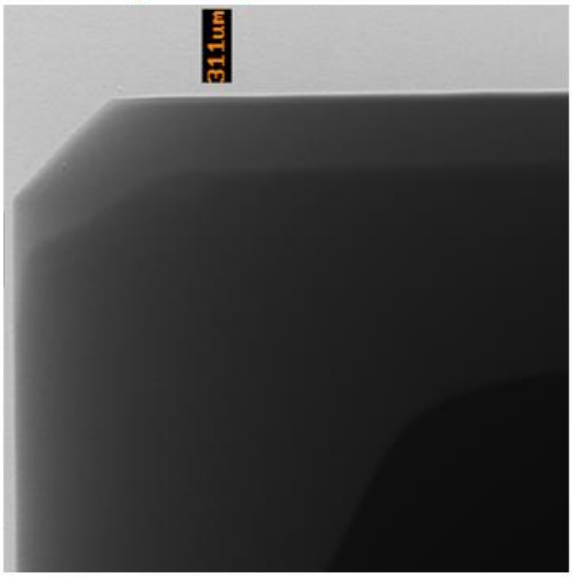
Data point 19:
- Conditions: 7 GPa, 1700°C, 20 minutes.
- Leach depth: 268 µm.



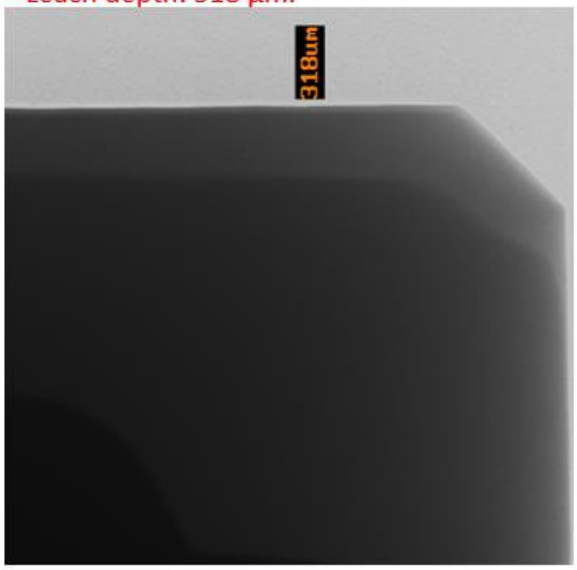
Data point 29:
- Conditions: 7 GPa, 1700°C, 20 minutes.
- Leach depth: 237 µm.



Data point 47:
- Conditions: 7 GPa, 1500°C, 30 minutes.
- Leach depth: 311 µm.



Data point 37:
- Conditions: 7 GPa, 1500°C, 30 minutes.
- Leach depth: 318 µm.



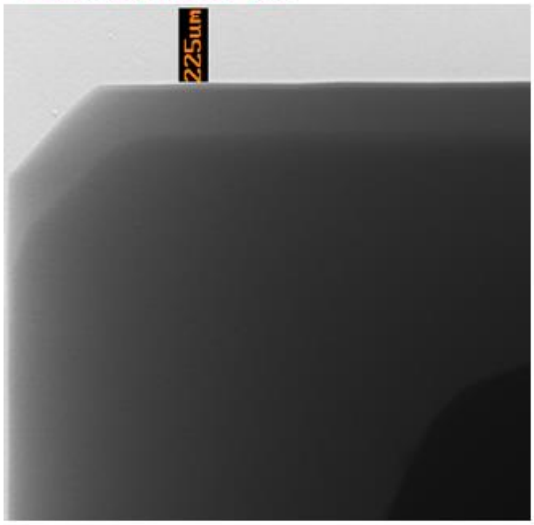
Data point 3:
- Conditions: 7 GPa, 1700°C, 20 minutes.
- Leach depth: 276 µm.



Data point 36:
- Conditions: 7 GPa, 1700°C, 20 minutes.
- Leach depth: 311 µm.



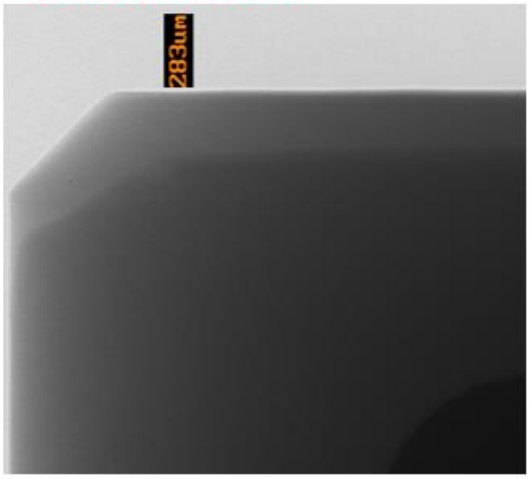
Data point 4:
- Conditions: 7 GPa, 1700°C, 30 minutes.
- Leach depth: 225 µm.



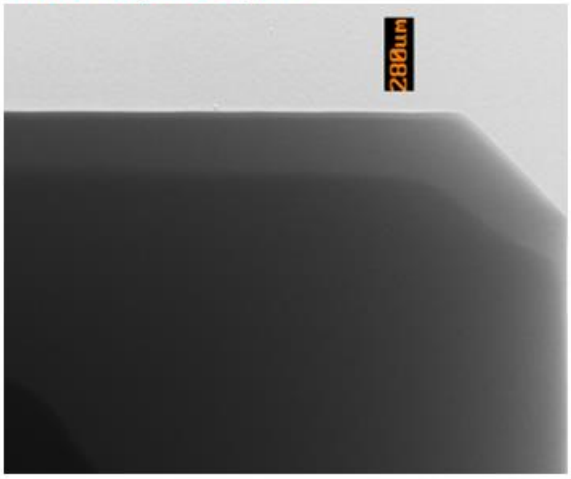
Data point 15:
- Conditions: 7 GPa, 1700°C, 30 minutes.
- Leach depth: 225 µm.



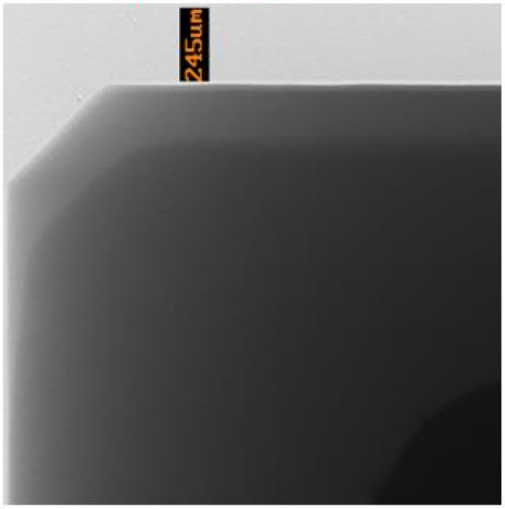
Data point 31:
- Conditions: 7 GPa, 1500°C, 20 minutes.
- Leach depth: 283 µm.



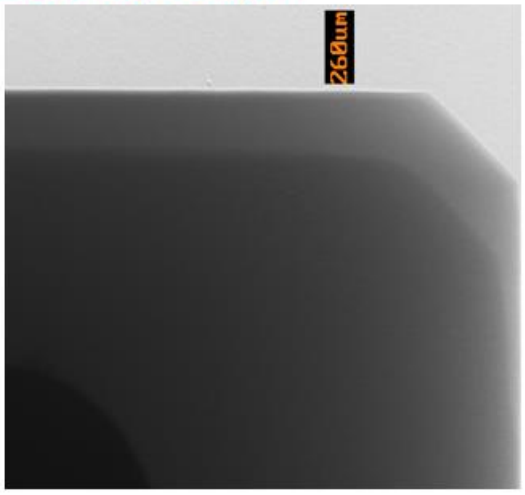
Data point 41:
- Conditions: 7 GPa, 1500°C, 20 minutes.
- Leach depth: 280 µm.



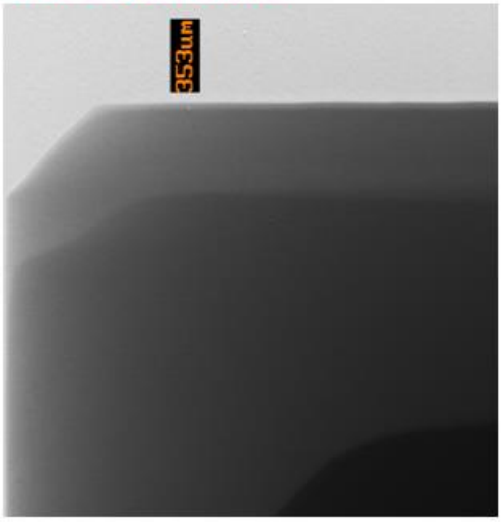
Data point 45:
- Conditions: 7 GPa, 1700°C, 30 minutes.
- Leach depth: 245 µm.



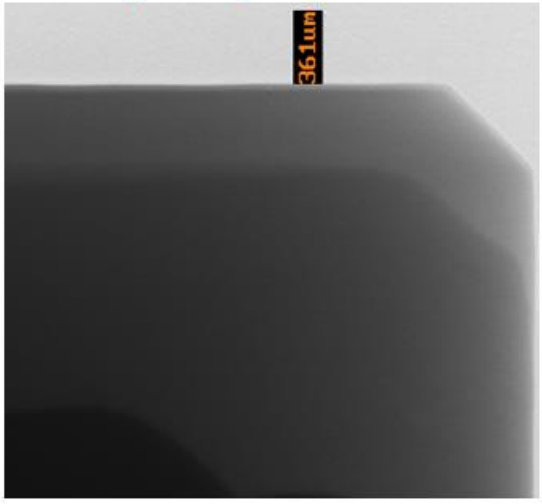
Data point 34:
- Conditions: 7 GPa, 1700°C, 30 minutes.
- Leach depth: 260 µm.



Data point 51:
- Conditions: 7 GPa, 1500°C, 20 minutes.
- Leach depth: 353 µm.



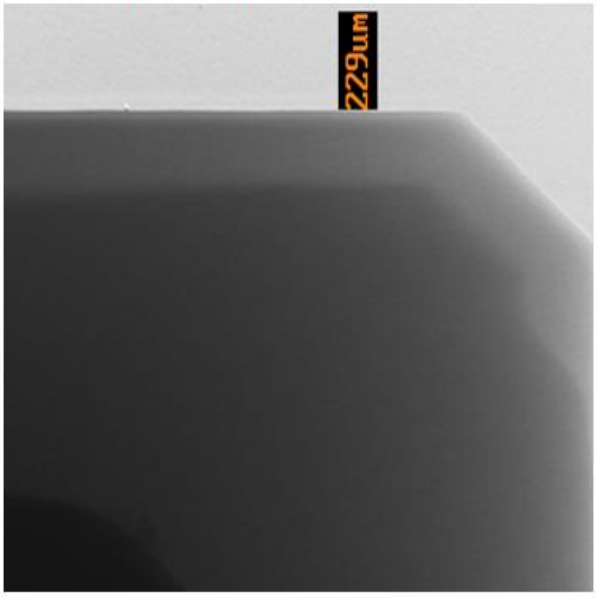
Data point 6:
- Conditions: 7 GPa, 1500°C, 30 minutes.
- Leach depth: 361 µm.



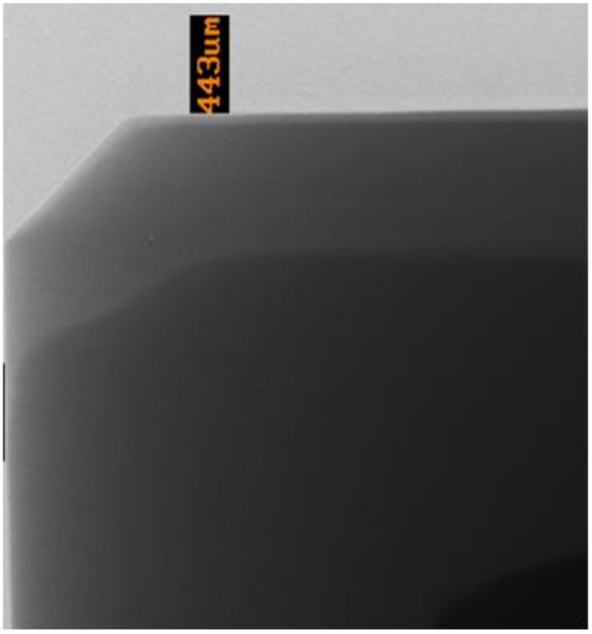
Data point 33:
- Conditions: 7 GPa, 1700°C, 30 minutes.
- Leach depth: 163 µm.



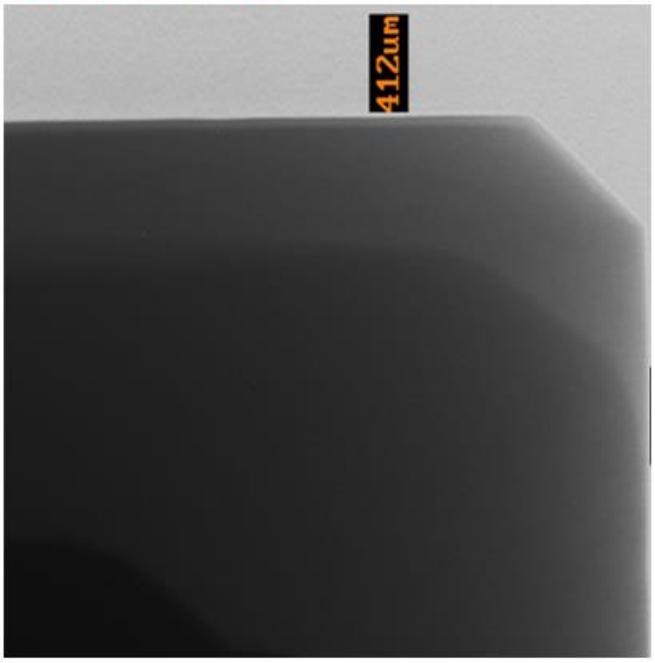
Data point 13:
- Conditions: 7 GPa, 1500°C, 30 minutes.
- Leach depth: 229 µm.



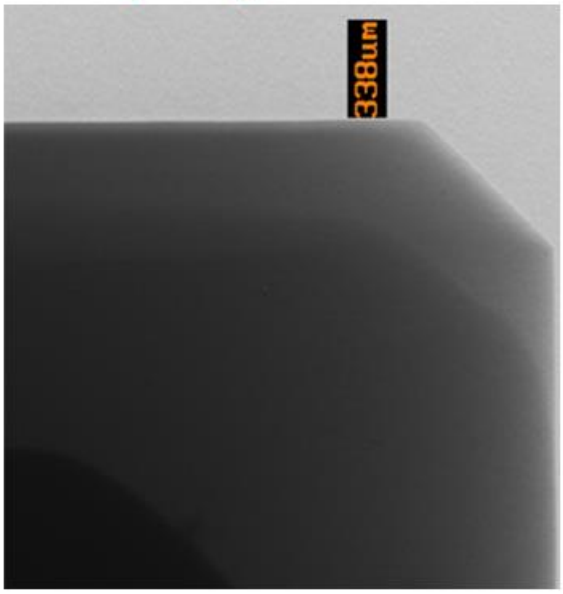
Data point 7:
- Conditions: 6 GPa, 1600°C, 25 minutes.
- Leach depth: 443 µm.



Data point 11:
- Conditions: 7 GPa, 1500°C, 20 minutes.
- Leach depth: 412 µm.



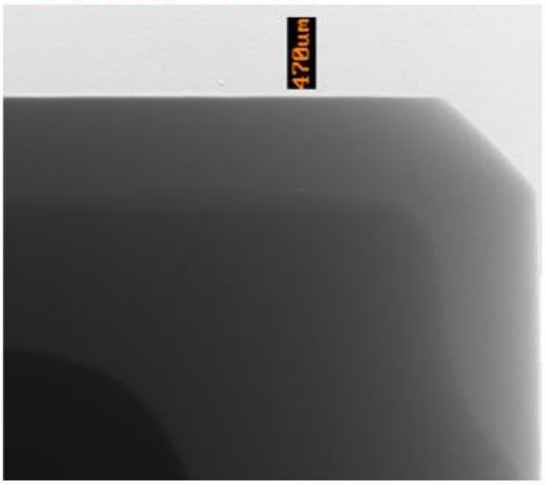
Data point 27:
- Conditions: 7 GPa, 1500°C, 30 minutes.
- Leach depth: 338 µm.



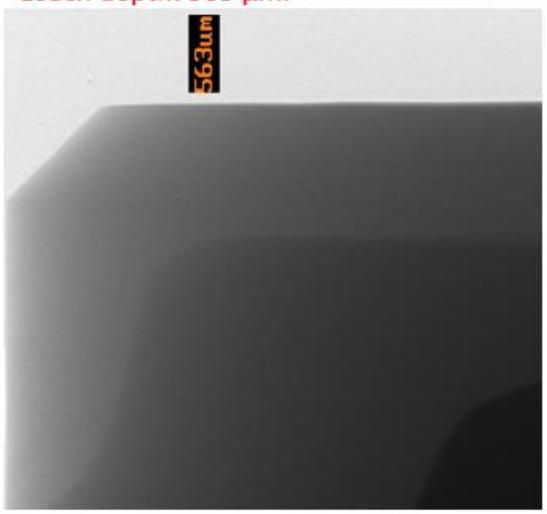
Data point 25:
- Conditions: 6 GPa, 1600°C, 25 minutes.
- Leach depth: 311 µm.



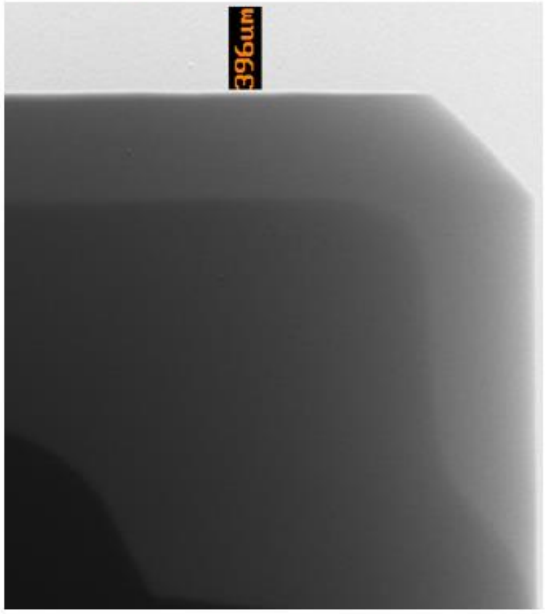
Data point 60:
- Conditions: 6 GPa, 1600°C, 25 minutes.
- Leach depth: 470 µm.



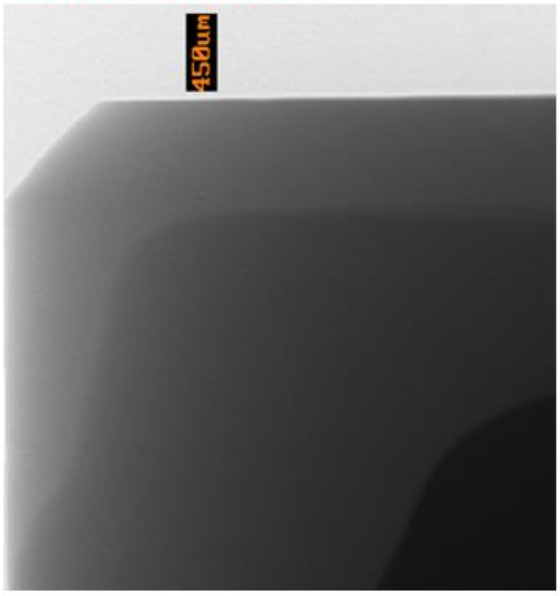
Data point 44:
- Conditions: 5 GPa, 1700°C, 20 minutes.
- Leach depth: 563 µm.



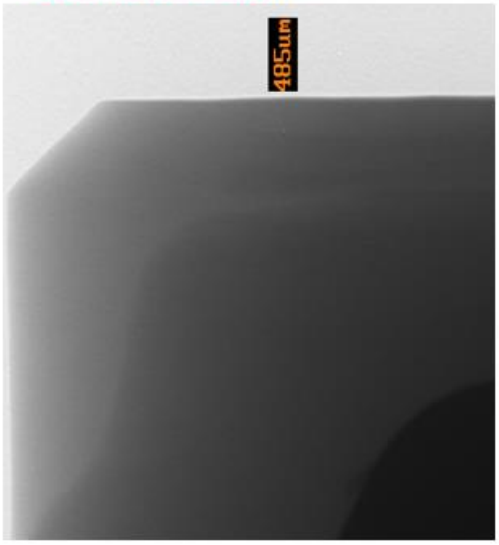
Data point 55:
- Conditions: 6 GPa, 1600°C, 25 minutes.
- Leach depth: 396 µm.



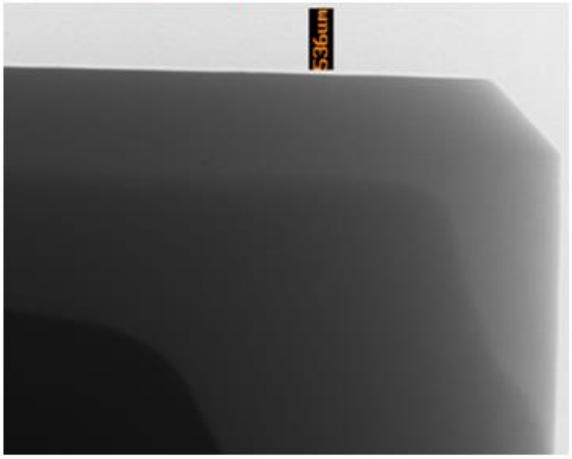
Data point 38:
- Conditions: 6 GPa, 1600°C, 25 minutes.
- Leach depth: 450 µm.



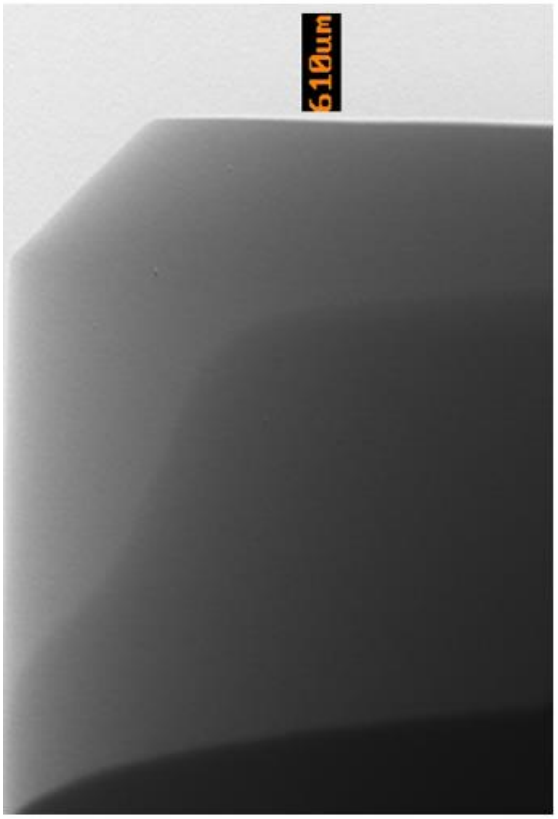
Data point 52:
- Conditions: 5 GPa, 1700°C, 20 minutes
- Leach depth: 485 µm.



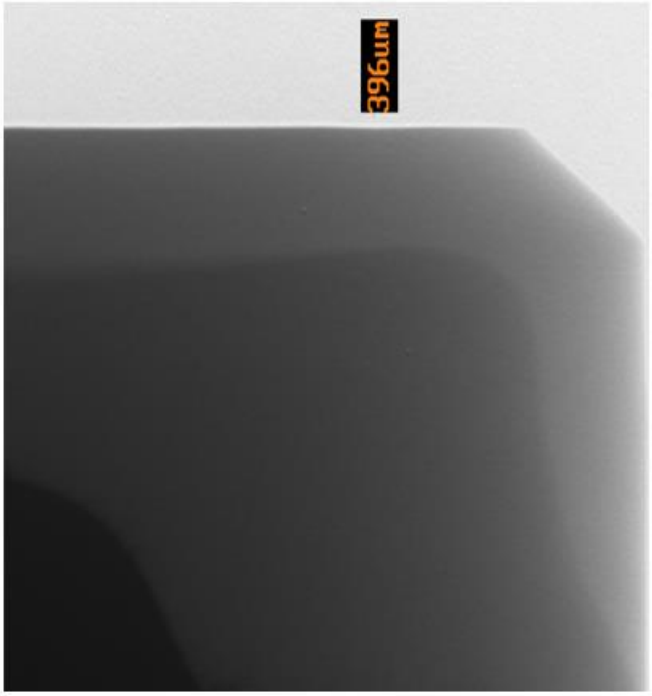
Data point 38:
- Conditions: 6 GPa, 1600°C, 25 minutes.
- Leach depth: 536 µm.



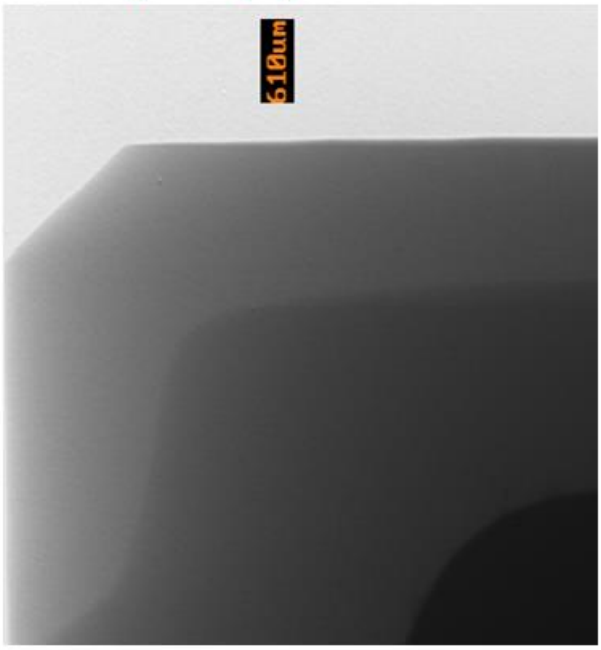
Data point 56:
- Conditions: 5 GPa, 1600°C, 25 minutes.
- Leach depth: 610 µm.



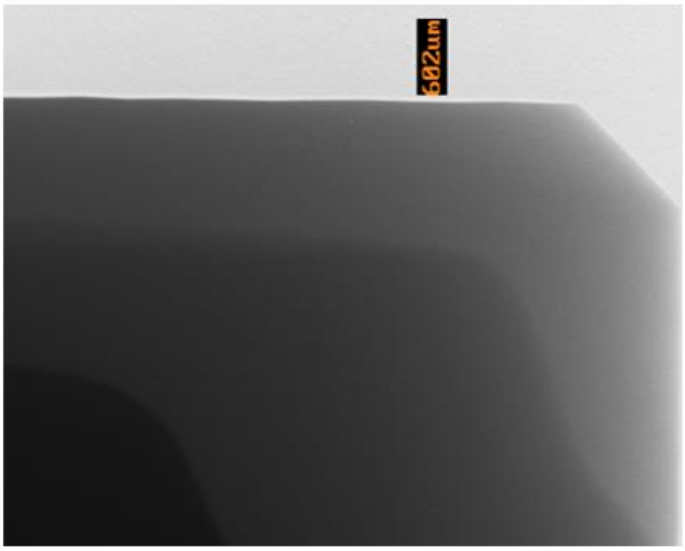
Data point 58:
- Conditions: 6 GPa, 1600°C, 30 minutes.
- Leach depth: 396 µm.



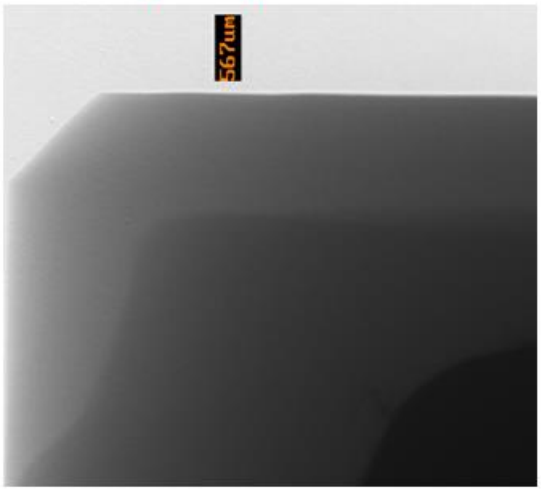
Data point 2:
- Conditions: 5 GPa, 1500°C, 30 minutes.
- Leach depth: 610 µm/h.



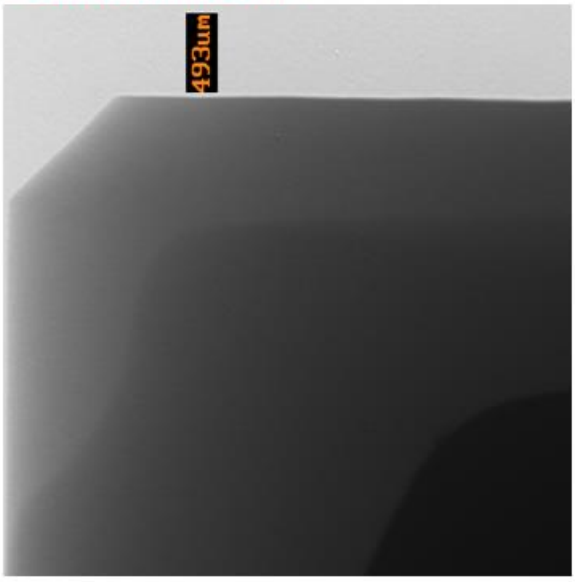
Data point 30:
- Conditions: 5 GPa, 1500°C, 30 minutes.
- Leach depth: 602 µm.



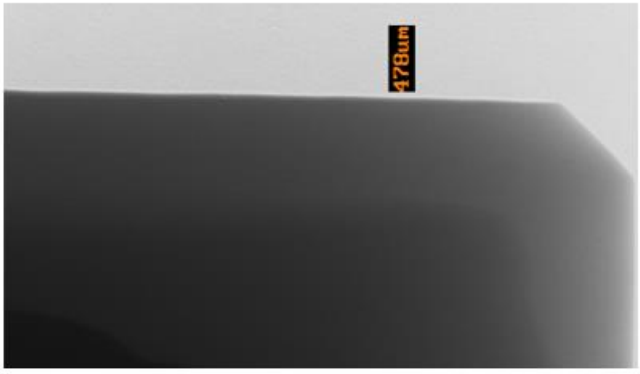
Data point 59:
- Conditions: 6 GPa, 1700°C, 25 minutes.
- Leach depth: 567 µm.



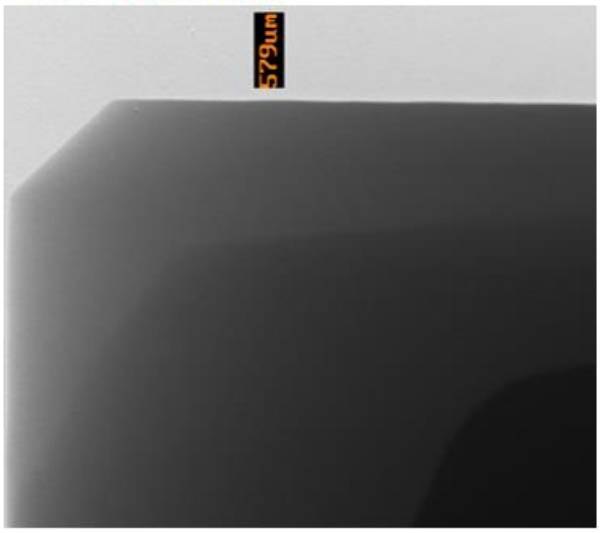
Data point 44:
- Conditions: 5 GPa, 1700°C, 20 minutes.
- Leach depth: 493 µm.



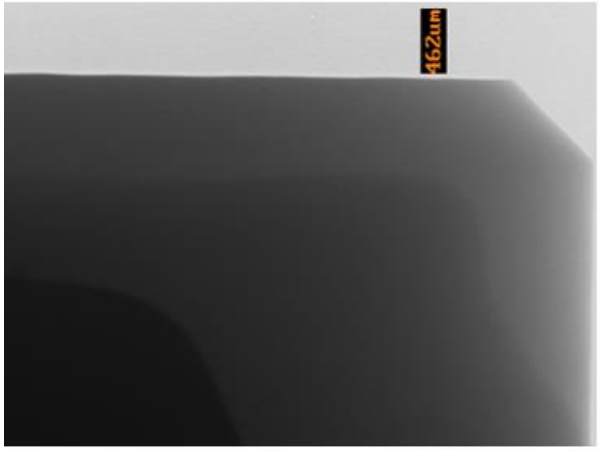
Data point 63:
- Conditions: 6 GPa, 1600°C, 25 minutes.
- Leach depth: 478 µm.



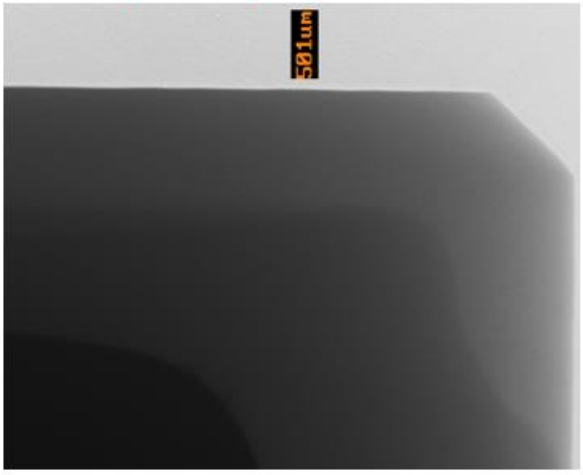
Data point 12:
- Conditions: 5 GPa, 1700°C, 20 minutes.
- Leach depth: 579 µm.



Data point 26:
- Conditions: 6 GPa, 1600°C, 25 minutes.
- Leach depth: 462 µm.



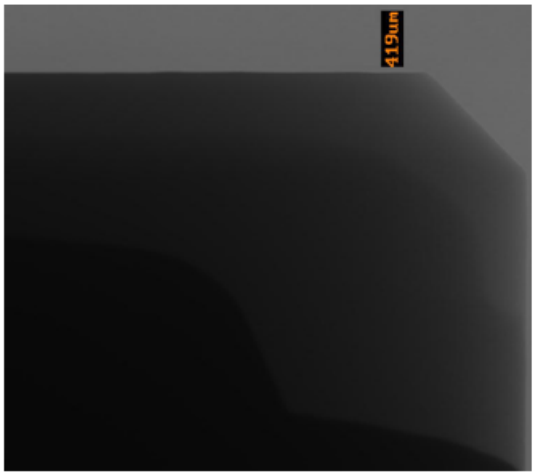
Data point 23:
- Conditions: 6 GPa, 1600°C, 25 minutes.
- Leach depth: 501 µm.



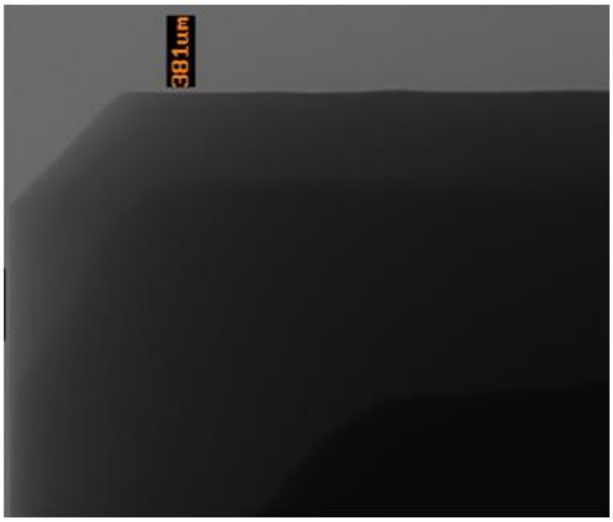
Data point 18:
- Conditions: 5 GPa, 1700°C, 30 minutes.
- Leach depth: 411 µm.



Data point 17:
- Conditions: 6 GPa, 1600°C, 25 minutes.
- Leach depth: 419 µm.



Data point 16:
- Conditions: 6 GPa, 1600°C, 25 minutes.
- Leach depth: 381 µm.



Data point 8:
- Conditions: 6 GPa, 1600°C, 25 minutes.
- Leach depth: 318 µm.



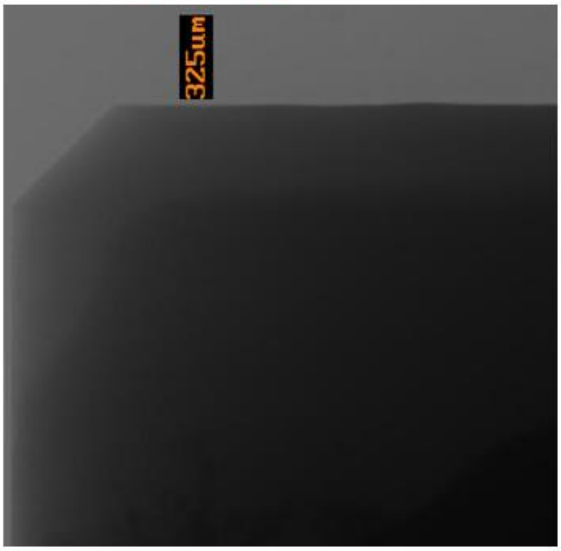
Data point 62:
- Conditions: 6 GPa, 1500°C, 25 minutes.
- Leach depth: 363 µm/h.



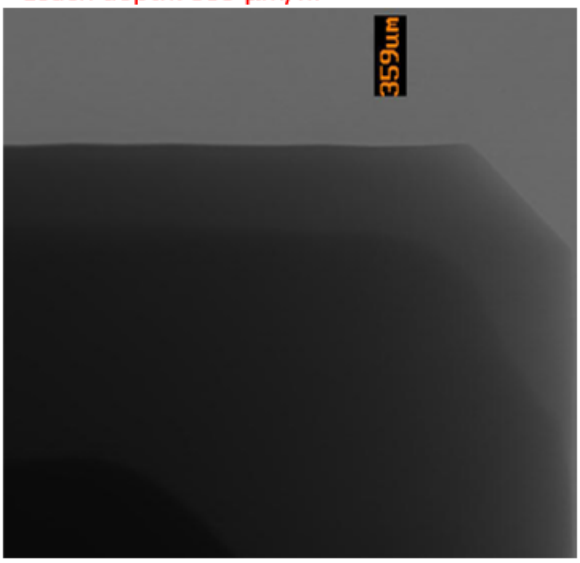
Data point 48:
- Conditions: 6 GPa, 1600°C, 25 minutes.
- Leach depth: 363 µm/h.



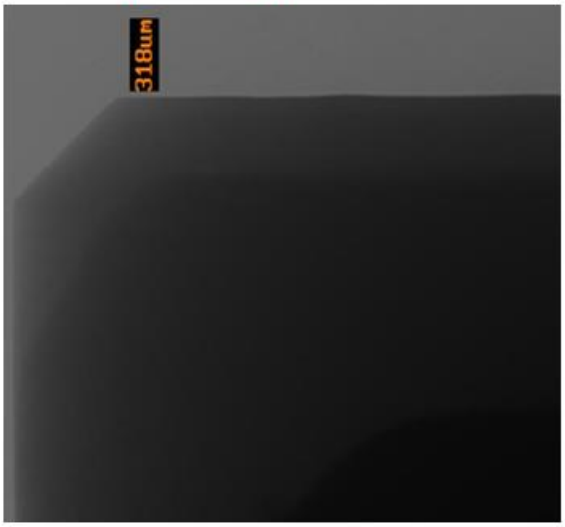
Data point 46:
- Conditions: 5 GPa, 1700°C, 30 minutes.
- Leach depth: 325 µm/h.



Data point 43:
- Conditions: 6 GPa, 1600°C, 25 minutes.
- Leach depth: 359 µm/h.



Data point 10:
- Conditions: 5 GPa, 1700°C, 30 minutes.
- Leach depth: 318 µm/h.



Data point 14:
- Conditions: 6 GPa, 1600°C, 25 minutes.
- Leach depth: 307 µm/h.



Appendix B: Published paper



International Journal of Refractory Metals and Hard Materials 124 (2024) 106854

Contents lists available at ScienceDirect

International Journal of Refractory Metals and Hard Materials

journal homepage: www.elsevier.com/locate/IJRMHM

Relationship between sintering pressure and leach rate of polycrystalline diamond compacts (PDCs) using central composite design (CCD) modelling

A. Ndlovu [a,b,*], L.A. Cornish [b], H.S.L. Sithebe [a]

[a] Element Six (Pty) Ltd, Springs 1559, South Africa
[b] School of Chemical and Metallurgical Engineering, University of the Witwatersrand, Johannesburg, South Africa, and DSI-NRF Centre of Excellence in Strong Materials, hosted by the University of the Witwatersrand, Johannesburg, South Africa

ARTICLE INFO

Keywords:
Sintering pressure
Leach rate
Polycrystalline diamond

ABSTRACT

The effect of sintering pressure on the microstructure, wear resistance and leachability of polycrystalline diamond (PDC) was studied using central composite design (CCD) modelling. Pressure and leachability had an inverse relationship due to reduced cobalt pool size and increased diamond contiguity with higher pressures. X-ray diffraction and X-ray fluorescence confirmed the selective removal of cobalt during leaching. The relationship between pressure and leachability was modelled as linear: $Y = -1.047x + 11.139$, valid within the 5–7 GPa pressure range. For a fixed temperature of 1600 °C, the optimum leach rate was 6.1 μm/h at 5 GPa. This study provided insights into optimizing PDC design and leaching processes for improved performance.

1. Introduction

Polycrystalline diamond compacts (PDCs) are widely used cutting tools due to their exceptional hardness and wear resistance [1–3]. The manufacturing process, which involves sintering diamond powder with a cobalt binder under high pressure and high temperature (HPHT), plays a critical role in defining the final properties of the PDC [4]. The effect of sintering pressure on the microstructure and mechanical properties of PDCs has been extensively studied [5–12]. However, the influence of pressure on the leachability of the cobalt binder, a critical aspect of PDC performance, remains largely unexplored.

Leaching, a well-established industrial practice [13], involves removing a portion of the cobalt binder using strong acids such as hydrochloric acid [13–15]. This process offers significant benefits for PDC performance, particularly in enhancing thermal stability. Studies [16–21] have shown that leaching improves thermal stability by creating a diamond-only layer that facilitates efficient heat dissipation, thereby preventing premature failure due to cobalt induced graphitization or cracking. Understanding the relationship between sintering pressure and leachability is therefore essential for optimizing the design and performance of thermally stable PDCs.

This study aims to investigate the effect of varying sintering pressure on the leachability of PDCs. We will establish a quantitative link between sintering pressure and leachability using central composite design (CCD) modelling. Accurate pressure calibration is fundamental to this study, as it ensures the reliability and robustness of the CCD model. By employing calibrated pressure application, we aim to develop an informative quantitative model that accurately reflects the impact of sintering pressure on PDC leachability. This model will not only enhance our understanding of the interaction between pressure and leachability but also guide the development of optimized leaching processes for improved PDC performance.

2. Experimental procedure

2.1. Pressure calibration

To calibrate a 6 × 32,000KN hinge-type cubic press for diamond sintering, reference diamond samples of sufficient size to be measured with a micrometre were sintered at 1500 °C under controlled loads. The resulting change in sample volume relative to the initial volume, ($\Delta V/V_0$), was accurately measured using the micrometre. Three distinct calibration points were established, linking specific pressure values to corresponding observed volume changes ($\Delta V/V_0$): 0.980 (4 GPa), 0.903 (6 GPa), 0.813 (8 GPa). The established calibration points effectively covered the typical 5–7 GPa pressure range required for diamond sintering, ensuring the calibration's practical relevance.

These calibration points formed the basis of a pressure-volume

* Corresponding author at: Element Six (Pty) Ltd, Springs 1559, South Africa.
E-mail address: fgm.ndlovu@gmail.com (A. Ndlovu).

https://doi.org/10.1016/j.ijrmhm.2024.106854
Received 9 May 2024; Received in revised form 9 July 2024; Accepted 19 August 2024
Available online 22 August 2024
0263-4368/© 2024 The Author(s). Published by Elsevier Ltd. This is an open access article under the CC BY-NC-ND license (http://creativecommons.org/licenses/by-nc-nd/4.0/).

shrinkage relationship (P—V relationship). A linear extrapolation of this relationship was employed to create a calibration curve, allowing for the estimation of sample pressure based on measured relative volume changes during subsequent sintering experiments.

2.2. Temperature monitoring

Temperature monitoring during PDC sintering was achieved using an S-type thermocouple, calibrated with a Memocal 2000, and a data logger for readout. Due to the lack of built-in cold junction compensation in the data logger, a reference junction temperature was used to compensate for this effect. The thermocouple was inserted into a hole drilled in the pyrophyllite block, positioned 0.5 mm from the sample to avoid direct contact and potential heat transfer or damage. The hole diameter was intentionally larger than the thermocouple sheath to facilitate placement and minimize heat conduction along the cable. A high-temperature ceramic tube filled the gap around the thermocouple to enhance thermal contact. Power input (kW) was used to control heat generation, and temperature monitoring provided feedback to ensure the desired sintering temperature was achieved. This feedback loop allowed for adjustments to the power input as needed to maintain the temperature within the setpoints.

2.3. Sintering of PDC

Diamond powder (10 μm average particle size) and cemented carbide substrates (WC-13%Co, 6 μm average particle size) were used as starting materials. The diamond powder was placed onto the substrate and sintered at 5 GPa, 6 GPa, and 7 GPa at a fixed temperature of 1600 °C for 15 min using a 6 × 32,000KN hinge-type cubic press cubic press (Fig. 1).

After sintering, the samples were processed to 16 mm diameter, 13 mm height and 3 mm diamond thickness, with the latter achieved by lapping. A CNC OD grinding machine was used to remove the metal cans and reduce the outer diameter from 18 mm to 16 mm. A CNC height-grinding machine was used to reduce the base of the WC substrate from 15 mm to 13 mm.

Microstructures of the PDC samples were examined using a Zeiss Evo15 scanning electron microscope at an accelerating voltage of 10 keV. Image analysis (ImageJ software) was used to measure the aspect ratio (AR) and Feret diameter (FD) of the cobalt pools (all the Co regions). The AR gave an indication of cobalt pool shape while the FD gave an indication of cobalt pool size. The AR is defined as the ratio of the length to the width of the particle and was derived from the ratio of the major and minor axis of a fitted ellipse. The FD is defined as the distance between two parallel tangents of the particle at different arbitrary angles and was derived from the longest distance between any two parallel points of the particle. The cobalt content and contiguity were calculated from the SEM-BSE micrographs using ImageJ on 16 images for each specimen at 1000× magnification and SIS-pro software. Calculations of the cobalt content and contiguity were done using MathConnex 2000 with MathCad 2000 Professional.

Wear resistance was evaluated using a vertical turning lathe (VTL) test with a 5000 N normal load and 1.8 m/s cutting speed. Wear scar areas were measured using an optical profilometer and ZEN Core software. The amount of wear can be measured in different ways, most of which involve measurement of either mass change or the size of a worn region (wear scar). However, for PDCs, wear scar dimensions are commonly reported as an area of the wear scar since PDC wear scars are large enough to measure and the area of the worn region can be clearly differentiated for materials with different wear resistances.

2.4. Leaching of PDC

The sintered and machined samples were placed in a Teflon container with 0.2 M HCl solution and heated at 110 °C for 96 h. Leach depths were measured using X-ray tomography (XRT, X-TEK XTV160, United Kingdom).

XRD was performed using PANalytical X'Pert^3 to analyse the phases of the leached and un-leached PCD samples. The Reference Intensity Ratio (RIR) method was used to calculate relative phase amounts. RIR is semi-quantitative and was suitable for assessing the relative proportions of cobalt and tungsten phases between un-leached and leached PCD samples. XRF was performed using PANalytical ZETIUM to determine the cobalt to tungsten ratio (Co/W) of the leached and un-leached PCD samples.

2.5. Central composite design (CCD) modelling

All modelling was carried out using central composite design (CCD) on Minitab 19 software. The design matrix is presented in Table 1. The α value is the calculated distance of each individual axial point from the centre in the CCD [23–25]. When α is <1, the axial point is within a cube, and if >1, the axial point is outside the cube. The two-level full factorial usually contains >2-level factors. [23–25]. Two factors were considered in the central composite design: sintering pressure (X_1), and sintering temperature (X_2).

The modelled response function was the leach rate and CCD used a quadratic Eq. [25] to approximate how changes in the process variables affected the leach rate:

$$Y = \beta_0 + \sum_{i=1}^{3} \beta_i X_i + \sum_{i=1}^{3} \beta_{ii} X_i^2 + \sum_{i<j}^{3} \beta_{ij} X_i X_j \quad (1)$$

where Y = estimated response; β_0 = constant, β_i = coefficient for the linear terms, β_{ii} = coefficient for the quadratic terms and β_{ij} = coefficient for the interactive terms. The validity of the model was confirmed using the correlation coefficient (R2), to indicate how well the model equation fitted the data. The accuracy of the model was assessed by calculating the percentage variation using Eq. 2, which estimated how close the modelled data matched the experimental data. Quantifying the accuracy

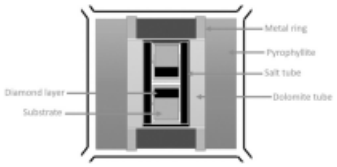


Fig. 1. *Schematic diagram of the cubic press capsule used for sintering* [22].

Table 1
Summary of the central composite design matrix.

Description	
Factors	2
Base runs	13
Base blocks	1
Replicates	1
Total runs	13
Alpha (α)	1.41421
Cubic points	4
Centre points in cube	5
Axial points	4
Centre points in axial	0

of the mathematical model was the most critical process to justify using the model.

$$\%\text{variation} = (|\text{modelled value} - \text{experimental value}|/\text{modelled value}) \times 100 \quad (2)$$

3. Results

Fig. 2 shows the X-ray map of the 6 GPa sample, with diamond surrounding cobalt pools. Some of the cobalt pools also contained tungsten. Table 2 shows the EDX analyses of diamond, cobalt and tungsten.

Fig. 3 shows the microstructures of the diamond layer of the 5 GPa, 6 GPa and 7 GPa samples, showing the cobalt pools between the diamond grains. The larger cobalt pools were elongated while the smaller ones were rounder (Fig. 3). The cobalt pools for the 8 GPa sample were the smallest, while those for the 5 GPa sample were the largest (Fig. 3).

The derived cobalt pool sizes (FD) and shape (AR) are presented in Table 3. The FD of the cobalt pools decreased with increased sintering pressure, as did the AR, as shown in Fig. 3.

Table 4 shows the cobalt content measurements from image analysis, where the cobalt content in the diamond layer decreased with increased pressure.

Table 4 also shows the relationship between contiguity, the calculated amount of diamond-to-diamond contact (diamond neck), and sintering pressure. Better diamond contiguity was achieved after sintering at elevated pressure.

Table 5 shows the wear scar measurements of the samples: the 5 GPa sample had the largest wear scar and the 7 GPa sample had the smallest wear scar. The 6 GPa sample had the lowest standard deviation.

Fig. 4 shows the ANOVA analysis for the measurements of the wear scars. The 5 GPa sample overlapped with the 6 GPa sample, and the 6 GPa sample overlapped with the 7 GPa sample. However, the 5 GPa and 7 GPa samples did not overlap, which was supported by their p-value (probability) of 0.003, which was less than the standard significance value of 0.05, indicating that the bell-curves did not overlap.

Table 6 shows the leach depths measurements after 96 h leaching, where the 5 GPa sample had the highest leach depth and the 7 GPa sample had the lowest leached depth. The 7 GPa sample had lowest standard deviation.

Fig. 5 shows the ANOVA analysis for the average values of the leach depths, showing that the bell-curve for the 7 GPa sample was closer to the 8 GPa sample than the 5 GPa samples, and none overlapped, although the 6 and 7 GPa samples were close. The ANOVA analysis had a p-value of 0.001 for the 5 GPa and 7 GPa samples, indicating that the bell-curves did not overlap.

Fig. 6 shows the relationship between the leach rate and pressure for determining the mathematical model to predict the leachability as function of pressure. The 6 GPa sample had the lowest standard deviation.

Fig. 7 shows that both the leached and un-leached PCD samples contain the cobalt phase (Co_3W), tungsten phase (WC) and diamond (C).

Table 7 shows the RIR quantitative phase analysis indicating the relative amount of cobalt and tungsten phases between un-leached and leached PCD samples.

Table 8 shows the XRF analysis, indicating the cobalt to tungsten (Co_3W) ratio for the leached and un-leached samples.

4. Discussion

4.1. Effect of pressure on as-sintered microstructures

Increased pressure during sintering reduced both average cobalt pool size (Fig. 3, Table 3) and contiguous region size (Fig. 4). This phenomenon can be attributed to enhanced plastic deformation and rearrangement of diamond particles at higher pressures. These processes occur during the cold and hot compaction stages, leading to pore shrinkage and decreased FD of the cobalt pools [10]. Furthermore, smaller pores

Table 2
EDX results of samples pressed at 5 GPa, 6 GPa and 7 GPa.

Sample	Diamond (wt%)	Cobalt (wt%)	Tungsten (wt%)
5 GPa	84.0 ± 1.1	13.7 ± 2.3	2.3 ± 1.1
6 GPa	86.8 ± 1.1	10.5 ± 1.9	2.7 ± 1.4
7 GPa	89.1 ± 0.9	8.8 ± 2.0	2.1 ± 1.2

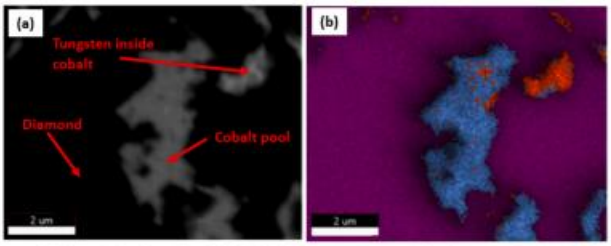


Fig. 2. 6 GPa sample: (a) SEM-BSE image showing diamond (dark), cobalt (medium grey) and tungsten (light) and (b) X-ray map showing cobalt (blue), tungsten (orange) and diamond (purple). (For interpretation of the references to colour in this figure legend, the reader is referred to the web version of this article.)

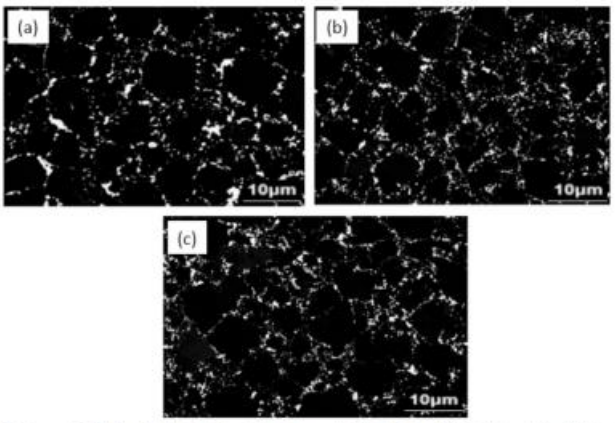


Fig. 3. SEM-BSE images of PDC binder pools at the top of the layer at different pressures: (a) 5 GPa, (b) 6 GPa and (c) 7 GPa, showing cobalt pools (light contrast) and diamond (dark contrast).

Table 3
Average cobalt pool size and shape at different pressures.

Sample	Cobalt pool aspect ratio	Cobalt Pool Feret Diameter (μm)
5 GPa	9.1 ± 2.2	2.36 ± 0.16
6 GPa	7.6 ± 2.1	1.64 ± 0.13
7 GPa	4.9 ± 2.7	1.06 ± 0.09

Table 4
Quantitative image analysis of the 5 GPa, 6 GPa and 7 GPa samples.

Sample	Cobalt (Vol%)	Contiguity (%)
5 GPa	9.2 ± 0.9	61.4 ± 1.8
6 GPa	7.8 ± 0.7	64.3 ± 0.9
7 GPa	6.1 ± 0.8	66.9 ± 1.7

limited cobalt infiltration into the diamond layer, resulting in smaller binder pools (Table 3). This trend is shown by the 7 GPa sample which had the smallest pores before infiltration (Fig. 3), allowing for minimal cobalt infiltration and consequently, the smallest average cobalt pool size (Table 3). This observation aligns with the source of cobalt, originating from the cemented carbide substrate, with the amount reaching the diamond layer being pressure- dependent.

Higher pressure also contributed to a reduction in the contiguous region (Fig. 4) due to the formation of smaller pores at the interface, resulting in fewer open structures within the contiguous region [26]. The availability of open porosity directly affects the extent of cobalt diffusion into the diamond layer. The absence of smaller diamond grains at the interface (Fig. 4) provided space for cobalt infiltration and subsequent dissolution of diamond grains, creating an open structure [26]. This agrees with the 7 GPa sample having the least pre-infiltration porosity, limiting the amount of cobalt that could infiltrate the diamond layer, thus leading to the formation of the smallest cobalt pools. The relationships between pressure, pore size and cobalt infiltration is further supported by Fig. 4 and Table 3, where smaller pore sizes associated with higher pressure had limited cobalt infiltration.

The 5 GPa sample exhibited the highest cobalt content at 9.2 ± 0.9 vol% (Table 4), agreeing with Westraadt et al. [27], who had a similar cobalt content (9.0 ± 1.0 vol%) for a PDC sintered at 5.5 GPa. While Westraadt et al. [27] did not report diamond contiguity for their sample, it is reasonable to expect similar values to the 5 GPa sample in Table 4, given the comparable cobalt content. Additionally, the present findings are consistent with Dai et al. [28], who observed a cobalt content of 10.7 ± 0.1 vol% for a sample sintered at 5.5 GPa. Thus, high pressure reduced pre-infiltration porosity, limiting the amount of cobalt that could infiltrate the diamond layer resulting in reduced cobalt content.

This investigation agreed with previous findings [26,27,30] that cobalt content significantly reduced the wear resistance of polycrystalline diamond composites (PDC). As expected, the sample exhibiting the highest cobalt content (5 GPa) had the lowest contiguity (Table 4) and the poorest wear resistance. This agrees with industrial experience [26,28,29], which shows that both high cobalt content and reduced contiguity are associated with reduced wear resistance. This can be attributed to the role of cobalt as a binder during PDC sintering. Cobalt facilitates the overall sintering process, which involves the dissolution of graphite from the diamond grain surfaces followed by its

Table 5
VTL measurements of the area of the wear scars on the sintered samples.

Pressure	Wear scar area (mm^2)	Minimum	Maximum
5 GPa	12.7 ± 1.5	11.0	14.1
6 GPa	7.4 ± 0.8	6.6	8.2
7 GPa	3.1 ± 1.0	1.9	4.0

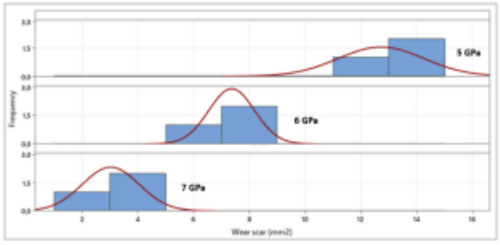


Fig. 4. ANOVA analysis of the wear scar measurements at different pressures.

Table 6
Average leach depth measurements (μm) for 20 measurements.

Pressure	Leach depth (μm)	Minimum	Maximum
5 GPa	744.1 ± 37.8	671.0	811.0
6 GPa	459.4 ± 26.3	420.0	538.0
7 GPa	328.7 ± 13.4	303.0	349.0

reprecipitation as diamond, ultimately forming diamond-to-diamond bonds and diamond intergrowth between the grains (Fig. 3) [4]. This process results in the formation of necks, or new diamond grain connections, between the original diamond grains [4].

4.2. Effect of pressure on wear resistance

The relationship between sintering pressure and wear scar area is presented in Table 5. The wear scar area of the PDC samples decreased significantly from 12.7 mm^2 to 3.1 mm^2 as the sintering pressure increased from 5 GPa to 7 GPa (Table 5). The one-way analysis of variance (ANOVA) of the average wear scar sizes gave a statistically significant difference between the 5 GPa, 6 GPa and 7 GPa (Fig. 4), shown by the p-value (0.003) being lower than the chosen significance level ($\alpha = 0.05$) and the clear separation of standard deviations in Fig. 4. This inverse correlation is attributed to increased diamond-diamond contact points (Table 4) and reduced cobalt pool size (Table 3), resulting in a more wear-resistant structure. However, this increased wear resistance comes at the cost of slower leaching rates (Table 6), as the denser, less porous material hinders acid access to the binder during leaching [13]. Therefore, a trade-off exists between wear resistance and leaching efficiency in PDC manufacturing.

4.3. Leached PCD layer versus un-leached PCD layer

Table 7 showed the RIR values of the changes in the relative amount of the cobalt phase (Co_3W) and tungsten phase (WC) between the un-leached and leached PCD layer samples. The RIR of cobalt phase decreased significantly from 0.9 in the un-leached sample to 0.2 in the leached sample (Table 7). This indicated a substantial reduction of approximately 78% in the relative amount of cobalt phase after the

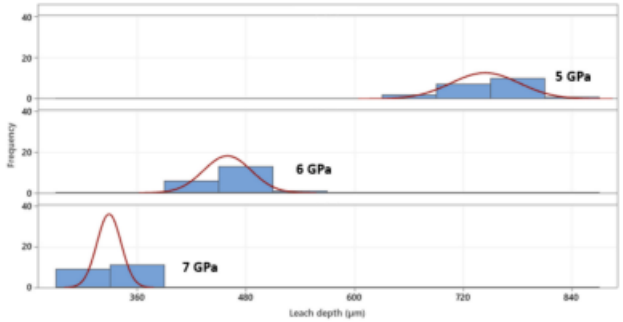


Fig. 5. ANOVA analysis of the leach depth measurements.

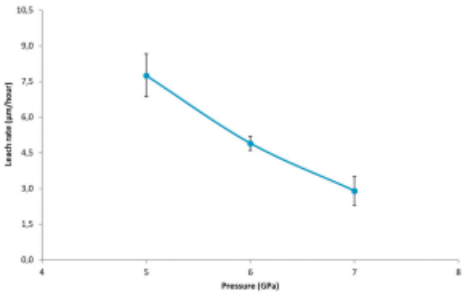


Fig. 6. Relationship between leachability (leach rate) and sintering pressure after 96 h of leaching in HCl acid.

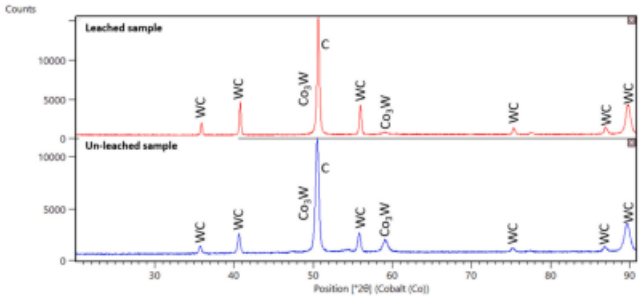


Fig. 7. XRD patterns for the leached and un-leached PCD layer samples.

Table 7
Reference Intensity Ratio (RIR) values for the leached and un-leached PCD layer samples.

RIR	Leached PCD	Un-leached PCD
Cobalt phase (Co_3W)	0.20 ± 0.01	0.91 ± 0.03
Tungsten phase (WC)	1.11 ± 0.02	1.21 ± 0.01

leaching process. This suggested that the leaching process effectively removed a large portion of the cobalt phase. The RIR of the tungsten phase remained relatively constant, decreasing only slightly from 1.2 in the un-leached sample to 1.1 in the leached sample (Table 7). This indicated that the leaching process had a minimal impact on the relative amount of the tungsten phase, suggesting that it is more resistant to the leaching conditions than the cobalt phase. The leaching process appeared to be highly selective, primarily targeting and removing the cobalt phase while leaving the tungsten phase largely unaffected. This selectivity was due to differences in the chemical stability and solubility of the two phases in the HCl leaching environment. The significant reduction in the cobalt phase suggested that it is more susceptible to dissolution under these conditions, while the minimal change in WC indicates its greater resistance to leaching.

Table 7 showed a substantial reduction of approximately 78% in the relative amount of cobalt phase after the leaching process. However, the remaining 22% suggested that a fraction of the cobalt phase was not accessible to the HCl acid during the leaching process. This inaccessible cobalt phase is located within closed pores or cavities within the PCD

Table 8
XRF results showing the cobalt to tungsten ratio (Co/W) between leached and un-leached samples.

Parameter	Leached PCD	Un-leached PCD
Co/W Ratio	0.23 ± 0.01	0.46 ± 0.03

material [8]. These closed pores can act as protective barriers, preventing the acid from reaching and dissolving cobalt encapsulated within them. The presence of closed porosity in PCD is due to coalescence: During sintering, smaller pores can coalesce to form larger pores, some of which may become isolated from the surface and remain closed [8].

Table 8 showed a significant change in the cobalt to tungsten (Co_t/W) ratio following the leaching process. The un-leached PCD sample exhibited a Co_t/W ratio of 0.46, indicating that cobalt comprised 31.6% of the total Co and W content (Table 8). After leaching, this ratio decreased to 0.23, corresponding to a cobalt proportion of 18.6%. This reduction signified a 50% decrease in the relative amount of cobalt in the PCD sample, corroborating the XRD findings and highlighting the effectiveness of the leaching process in removing a substantial portion of the cobalt-containing phase. Both techniques indicated a significant reduction in the amount of cobalt present in the PCD layer after leaching. The minor change in the RIR of WC in the XRD results was also consistent with the XRF data, which showed that the overall tungsten content remained relatively unchanged after leaching. Together, these results suggested that the leaching process primarily removed the Co_3W phase, while leaving the WC phase mostly intact. The combined XRF (Table 8) and XRD (Table 7) results provided strong evidence for the removal of cobalt from the PCD during leaching. The reduction in the Co_t/W ratio and the decrease in the RIR of Co_3W both indicated a significant decrease in the amount of cobalt present in the leached material.

4.4. Effect of pressure on leachability

The leachability of cobalt exhibited negative correlation with pressure (Table 6), due to the influence of cobalt pool size on acid flow pathways. Larger cobalt pools provided wider channels for acid ingress, facilitating cobalt removal. Conversely, smaller pools restricted acid flow, hindering leachability [13]. Among the investigated pressures, 5 GPa had the fastest leachability (Table 6), coinciding with the largest observed cobalt pool size (Fig. 3 and Table 4), highest cobalt content (Fig. 3 and Table 4) and lowest contiguity (Table 4). These findings show that the leachability of the cobalt binder is directly governed by the distribution and accessibility of cobalt within the pools between diamond particles [13]. Physical exposure of the binder to the leaching solution is crucial for the reaction to proceed and the extent of this exposure dictates the leaching rate.

The pores allow acid access, and smaller pores allow smaller acid volumes to pass through them in a given time, and hence reduce leachability (Table 3). Conversely, diamond grains encapsulate some pools, effectively shielding them from the acid solution and making them unreachable. The initial leaching reaction involves chloride anions from the HCl acid interacting with surface-exposed cobalt pools on the PDC. Subsequently, these anions diffuse deeper through the intergranular pores, reacting with additional cobalt to form cobalt chloride, which remains dissolved and is ultimately removed from the system [13,31]. As cobalt is leached from these pools, they transform into pores themselves. Consequently, leachability is further influenced by the diffusion rate of anions and reaction products through these newly formed inter-granular pores. Therefore, the size of the cobalt pools dictates both the rate-limiting step of leaching and the subsequent pore size, which in turn governs acid diffusion and access to the remaining cobalt [13,31]. Smaller pools restrict diffusion and consequently decrease the leaching rate, while larger pools facilitate diffusion and leach rate [13,31].

Leach depth measurements for the 5 GPa and 7 GPa samples exhibited normal distributions (Fig. 5). However, the normality test for the 6 GPa data set was rejected (p-value <0.05), with only one outlier identified (Fig. 5), which skewed the distribution, rendering the 6 GPa data set non-normal. One-way ANOVA identified a statistically significant difference (p-value = 0.001) in the mean leach depths among the pressure groups (Fig. 5), indicating that leach depth decreased with increasing pressure.

Table 9
Mathematical models for the relationship between pressure and leachability.

Mathematical model	K, slope	Fitted equation	Correlation coefficient (R^2)
Exponential	17.167	$Y = 17.167e^{-0.01x}$	0.9607
Linear	−1.047	$Y = -1.047x + 11.139$	0.9847
Logarithmic	−6.221	$Y = -6221\ln(X) + 15.988$	0.9762
Polynomial	0.302	$Y = 0.302x^2 - 4.667x + 21.813$	0.9803
Power	45.745	$Y = 45.745x^{-1.263}$	0.9767

Fig. 6 shows the relationship between the leach rate and pressure. Different models were evaluated using Minitab software by fitting them to Fig. 6 and then assessing their suitability to describe the relationship between leach rate and pressure using the correlation coefficient (R^2). The five mathematical models that fitted Fig. 6 well are presented in Table 9.

The linear model had the highest R^2 value, and the exponential model had the lowest R^2 value. The R^2 value indicated how well the model equation fitted the data: stronger relationships were closer to 1 and weaker relationships were closer to zero. The equation that had the closest to perfect fit for the experimental data (Fig. 6) was the linear model ($R^2 = 0.9847$), implying that 98.47% of the variability in leach rate was explained by the mathematical model. Thus, under the experimental conditions tested, the effect of pressure on the leach rate and pressure can be modelled by:

$$Y = -1.047 \times +11.139 \quad (3)$$

where:

Y = leach rate.

X = sintering pressure.

In Table 7, the slope, K, describes the extent to which sintering pressure affected the leach rate, and the intercept is the value of the leach rate when the sintering pressure is 0 GPa. However, the value of the intercept was neglected because sintering pressure would never be 0 GPa since the typical boundary sintering conditions to sinter a commercial PDC starts from 5 GPa [9]. Also, moving the intercept to zero would have affected the accuracy of the model for prediction within the boundary sintering conditions of 5 GPa – 7 GPa.

To validate Eq. 3 (relationship between leach rate and sintering pressure), samples sintered at 6.8 GPa and 8 GPa were leached for 96 h. These two pressures were chosen because 6.8 GPa was within the sintering boundary conditions tested, whereas 8 GPa was outside. Thus, the 6.8 GPa sample validated the suitability of the model to predict leach rates within the boundary conditions, while the 8 GPa sample validated the suitability of the model to predict leach rates outside the boundary conditions. Pressures <5 GPa were not validated because most commercial products are sintered at or above 5 GPa.

A comparison of modelled and experimental data is presented in Table 10. For the 6.8 GPa sample, the modelled value deviated from the experimental value by 2.4%, indicating good agreement within the established boundary conditions (Eq. 3). Conversely, at 8 GPa, the model over-predicted the experimental value by 62%, indicating a significant limitation in predictive accuracy beyond the defined pressure range (>7 GPa). This agrees with the increased standard deviations of

Table 10
Validation of the modelled data against the experimental data after 96 h of leaching.

Pressure (GPa)	Modelled value (μm/h)	Experimental value (μm/h)	Variation (%)
6.8	4.03	4.12 ± 0.44	2.4
8	2.76	1.05 ± 0.17	61.9

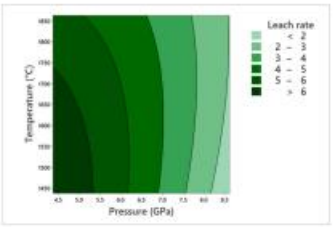


Fig. 8. Contour plot model, showing how sintering conditions affect leachability.

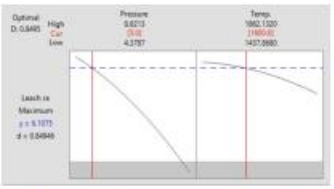


Fig. 9. Response optimization model, showing maximum leachability achievable under the experimental boundary conditions tested, where: high = maximum value of the pressure and temperature, low = lowest value of the pressure and temperature and cur = current value of the pressure and temperature.

the boundary limits in Fig. 6.

Fig. 8 shows the contour plot modelled using central composite design (CCD) with Minitab on the experimental conditions. The plot indicates that higher pressures and higher temperatures would have lower leachability, which agrees with Fig. 6.

A response optimization model was developed using Minitab to investigate the influence of pressure and temperature on leach rate (Fig. 9). The model indicated that pressure exerted a greater influence on leach rate than temperature within the investigated range of 5–7 GPa. The maximum predicted leach rate of 6.1 μm/h was achievable at 5 GPa and 1600 °C. While the model suggests that lower pressures can promote higher leachability, it is important to consider the trade-off between pressure and other factors impacting material properties. As shown in Table 4, lower pressures can also lead to the formation of larger cobalt pools and lower contiguity, which compromises wear resistance. Therefore, an optimal operating pressure needs to be established that balances the desired leach rate and the required mechanical properties.

5. Conclusions

This study investigated the effect of sintering pressure on the microstructure, wear resistance and leachability and found that increased sintering pressure reduced cobalt pool size, increased contiguity, reduced leachability and increased wear resistance. The relationship between sintering pressure and leachability was modelled using CCD modelling within the boundary conditions of 5–7 GPa, to predict PDC leachability, and then estimated the required leach rates for target leach depths. The conclusions were:

- Increased pressure enhances wear resistance but reduces leachability.
- HCl leaching selectively removes cobalt while leaving tungsten unaffected.
- The relationship between pressure and leachability was modelled as linear: $Y = -1.047 \times + 11.139$, valid within the 5–7 GPa pressure range.
- At 1600 °C, the optimum leach rate was 6.1 μm/h within the boundary conditions of 5–7 GPa.

CRediT authorship contribution statement

A. Ndlovu: Writing – original draft, Software, Project administration, Methodology, Investigation, Formal analysis, Data curation. **L.A. Cornish:** Writing – review & editing, Visualization, Validation, Supervision. **H.S.L. Sithebe:** Resources, Project administration, Funding acquisition, Conceptualization.

Declaration of competing interest

The authors declare that they have no known conflict of interests in regard to the manuscript entitled " Relationship between sintering pressure and leach rate of polycrystalline diamond compacts (PDCs) using Central Composite Design (CCD) ".

Data availability

Data will be made available on request.

Acknowledgments

This work was funded by Element Six, South Africa.

References

[1] H. Huang, B. Zhao, W. Wei, Z. Si, K. Huang, Effect of cobalt content on the performance of polycrystalline diamond compacts, Int. J. Refract. Met. Hard Mater. vol. 92 (2020), https://doi.org/10.1016/j.ijrmhm.2020.105312 article no: 105312, Nov.
[2] J. Gu, K. Huang, Role of cobalt of polycrystalline diamond compact (PDC) in drilling process, Diam. Relat. Mater. 66 (2016) 98–101. Jun, https://doi.org/10.1016/j.diamond.2016.03.025.
[3] K. Francis, Effect of Carbide Additives on the Structure and Behaviour of Polycrystalline Diamond, PhD. University of Pretoria, 2017.
[4] J.E. Westraadt, I. Sigalas, J.H. Neethling, Characterization of thermally degraded polycrystalline diamond, Int. J. Refract. Met. Hard Mater. 48 (2015) 286–292, https://doi.org/10.1016/j.ijrmhm.2014.08.008.
[5] V. Kanyanta, S. Ozbayraktar, K. Mawoja, Effect of manufacturing parameters on polycrystalline diamond compact cutting tool stress-state, International journal of refractory metals and hard materials, Int. J. Refract. Met. Hard Mater. 45 (2014) 147–152.
[6] M. Akaishi, T. Ohsawa, S.Y. Amanka, Synthesis of fine-grained polycrystalline diamond compact and its microstructure, J. Am. Ceram. Soc. 74 (1) (1991) 5–10.
[7] S. Middlemiss, Polycrystalline Diamond with Improved Abrasion Resistance, Patent, US0140132A1, 2004.
[8] R.M. German, Liquid Phase Sintering, Springer Science & Business Media, Berlin, Germany, 2013.
[9] J.M. Fuller, PDC cutter with stress diffusing structure, Patent WO2004024752A2 (2009).
[10] S.G. Mtunzi, Characterization of Ultra-High Pressure Polycrystalline Diamond, PhD, Nelson Mandela University, 2018.
[11] Liu S., Han N., Zou Y., Zhu P., and Liu B., "Polycrystalline diamond compact with enhanced thermal stability," J. Mater. Sci. Technol., vol. 33, no. 11, pp. 1366–1369, Nov. 2017, doi: https://doi.org/10.1016/j.jmst.2017.03.014.
[12] Y. Zhang, High pressure and high temperature sintering of fine-grained PCD using bi-layered assembly, High Pressure Res. 29 (2009) 225–234.
[13] K. Davis, R. Frazier, J. Fischer, Sonochemical leaching of polycrystalline diamond, Patent, US0169419 A1, 2007.
[14] K. Naidoo, G.J. Davies, J.L. Myburgh, Method of making polycrystalline diamond material, Patent, US2013029144 3 A1, 2013.

[15] K. Naidoo, J.H. Liversage, D.E. Scott, H.S.L. Sithebe, B.A. Kaiser, M.L. Fish, Polycrystalline diamond element, Patent, US0061146A1, 2012.
[16] C.S. Montross, K. Naidoo, Polycrystalline Diamond Material, Patent, US0326963A1, 2013.
[17] K. Naidoo, Polycrystalline diamond material, Patent, US0333300A1, 2013.
[18] B. Bhushan, Principles and Applications of Tribology, John Wiley and Sons, New York, USA, 1999.
[19] S. Masethe, PDC Wear Testing, Report, Springs, South Africa, 2014.
[20] Randall G.M., Suri P., and Park S. J., "Review: liquid phase sintering," J. Mater. Sci., vol. 44, no. 1, pp. 1–39, Jan. 2009, doi: https://doi.org/10.1007/s10853-008-3008-0.
[21] G. Udupa, S.S. Rao, K.V. Gangadharan, Functionally graded composite materials: an overview, Procedia Mater. Sci. 5 (2014) 1291–1299, https://doi.org/10.1016/j.mspro.2014.07.442.
[22] V. Kanyanta, A. Dormer, N. Murphy, A. Ivankovic, Impact fatigue fracture of polycrystalline diamond compact (PDC) cutters and the effect of microstructure, Int. J. Refract. Met. Hard Mater. 46 (2014) 145–153, https://doi.org/10.1016/j.ijrmhm.2014.06.003.
[23] S. Ibrahim, I. Daut, Y.M. Irwan, M. Irwanto, N. Gomesh, Z. Farhana, Linear regression model in estimating solar radiation, in: Energy Procedia, Elsevier BV, 2012, pp. 1402–1412, https://doi.org/10.1016/j.egypro.2012.05.156.
[24] X.Q. Liu, Improved estimator in a linear regression model, J Stat Plan Inference 141 (1) (2011) 189–196. Jan, https://doi.org/10.1016/j.jspi.2010.05.030.
[25] S.A. Hadi, Regression Analysis by Example, Fourth edition, John Wiley and Sons, Canada, 2006.
[26] Scott T.A. "The influence of microstructure on the mechanical properties of polycrystalline diamond: a literature review," Adv. Appl. Ceram., vol. 117, no. 3, pp. 161–176, Apr. 2018, doi: https://doi.org/10.1080/17436753.2017.1389462.
[27] J.E. Westraadt, Thermal Degradation of Diamond Compacts: A TEM Investigation, PhD, Nelson Mandela University, 2015.
[28] W. Dai, S. Zhang, J. Tu, X. Wang, C. Zhao, B. Liu, Grain size dependence of wear resistance of polycrystalline diamond compact, Ceram. Int. 49 (23) (2023) 37396–37406. Dec, https://doi.org/10.1016/j.ceramint.2023.09.064.
[29] Q.S. Bai, Y.X. Yao, P. Ren, G. Zhang, Study on wear mechanisms and grain effects of PCD tool in machining laminated flooring, Int. J. Refract. Met. Hard Mater. 22 (2–3) (2004) 111–115, https://doi.org/10.1016/j.ijrmhm.2004.01.007.
[30] M. Yahiaoui, L. Gerhard, J.Y. Paris, J. Donze, A. Dourfaye, A study on PDC drill bits quality, Wear 298–299 (1) (2013) 32–41. Feb, https://doi.org/10.1016/j.wear.2012.12.026.
[31] R.L. Ladi, C.E. Wells, B.K. Katuria, S.W. Almond, Chemical agents for leaching polycrystalline diamond elements, Patent US0152064A1 (2012).

Appendix C: Sintering conditions calibration

Data used to plot the derived "sample pressure" (calculated from the Murnaghan EOS, representing the effective pressure required for the observed densification) against the measured *ex situ* relative volume (V/V_0) for the PDC sample.

Applied ram load (KN)	V/V0	P_EOS (GPa)	Predicted P (GPa)	Difference (GPa)
6610	0.96	4.8	4.78	-0.02
8000	0.9	5.9	5.92	0.02
9331	0.83	6.9	6.83	-0.07
10500	0.8	7.8	7.82	0.02